

# 12

# Long-term Climate Change: Projections, Commitments and Irreversibility

## Coordinating Lead Authors:

Matthew Collins (UK), Reto Knutti (Switzerland)

## Lead Authors:

Julie Arblaster (Australia), Jean-Louis Dufresne (France), Thierry Fichefet (Belgium), Pierre Friedlingstein (UK/Belgium), Xuejie Gao (China), William J. Gutowski Jr. (USA), Tim Johns (UK), Gerhard Krinner (France/Germany), Mxolisi Shongwe (South Africa), Claudia Tebaldi (USA), Andrew J. Weaver (Canada), Michael Wehner (USA)

## Contributing Authors:

Myles R. Allen (UK), Tim Andrews (UK), Urs Beyerle (Switzerland), Cecilia M. Bitz (USA), Sandrine Bony (France), Ben B.B. Booth (UK), Harold E. Brooks (USA), Victor Brovkin (Germany), Oliver Browne (UK), Claire Brutel-Vuilmet (France), Mark Cane (USA), Robin Chadwick (UK), Ed Cook (USA), Kerry H. Cook (USA), Michael Eby (Canada), John Fasullo (USA), Erich M. Fischer (Switzerland), Chris E. Forest (USA), Piers Forster (UK), Peter Good (UK), Hugues Goosse (Belgium), Jonathan M. Gregory (UK), Gabriele C. Hegerl (UK/Germany), Paul J. Hezel (Belgium/USA), Kevin I. Hodges (UK), Marika M. Holland (USA), Markus Huber (Switzerland), Philippe Huybrechts (Belgium), Manoj Joshi (UK), Viatcheslav Kharin (Canada), Yochanan Kushnir (USA), David M. Lawrence (USA), Robert W. Lee (UK), Spencer Liddicoat (UK), Christopher Lucas (Australia), Wolfgang Lucht (Germany), Jochem Marotzke (Germany), François Massonnet (Belgium), H. Damon Matthews (Canada), Malte Meinshausen (Germany), Colin Morice (UK), Alexander Otto (UK/Germany), Christina M. Patricola (USA), Gwenaëlle Philippon-Berthier (France), Prabhat (USA), Stefan Rahmstorf (Germany), William J. Riley (USA), Joeri Rogelj (Switzerland/Belgium), Oleg Saenko (Canada), Richard Seager (USA), Jan Sedláček (Switzerland), Len C. Shaffrey (UK), Drew Shindell (USA), Jana Sillmann (Canada), Andrew Slater (USA/Australia), Bjorn Stevens (Germany/USA), Peter A. Stott (UK), Robert Webb (USA), Giuseppe Zappa (UK/Italy), Kirsten Zickfeld (Canada/Germany)

## Review Editors:

Sylvie Joussaume (France), Abdalah Mokssit (Morocco), Karl Taylor (USA), Simon Tett (UK)

## This chapter should be cited as:

Collins, M., R. Knutti, J. Arblaster, J.-L. Dufresne, T. Fichefet, P. Friedlingstein, X. Gao, W.J. Gutowski, T. Johns, G. Krinner, M. Shongwe, C. Tebaldi, A.J. Weaver and M. Wehner, 2013: Long-term Climate Change: Projections, Commitments and Irreversibility. In: *Climate Change 2013: The Physical Science Basis. Contribution of Working Group I to the Fifth Assessment Report of the Intergovernmental Panel on Climate Change* [Stocker, T.F., D. Qin, G.-K. Plattner, M. Tignor, S.K. Allen, J. Boschung, A. Nauels, Y. Xia, V. Bex and P.M. Midgley (eds.)]. Cambridge University Press, Cambridge, United Kingdom and New York, NY, USA.

# Table of Contents

<b>Executive Summary</b> .....	1031
<b>12.1 Introduction</b> .....	1034
<b>12.2 Climate Model Ensembles and Sources of Uncertainty from Emissions to Projections</b> .....	1035
12.2.1 The Coupled Model Intercomparison Project Phase 5 and Other Tools.....	1035
12.2.2 General Concepts: Sources of Uncertainties.....	1035
12.2.3 From Ensembles to Uncertainty Quantification .....	1040
<b>Box 12.1: Methods to Quantify Model Agreement in Maps</b> .....	1041
12.2.4 Joint Projections of Multiple Variables .....	1044
<b>12.3 Projected Changes in Forcing Agents, Including Emissions and Concentrations</b> .....	1044
12.3.1 Description of Scenarios.....	1045
12.3.2 Implementation of Forcings in Coupled Model Intercomparison Project Phase 5 Experiments .....	1047
12.3.3 Synthesis of Projected Global Mean Radiative Forcing for the 21st Century.....	1052
<b>12.4 Projected Climate Change over the 21st Century</b> .....	1054
12.4.1 Time-Evolving Global Quantities.....	1054
12.4.2 Pattern Scaling.....	1058
12.4.3 Changes in Temperature and Energy Budget.....	1062
12.4.4 Changes in Atmospheric Circulation .....	1071
12.4.5 Changes in the Water Cycle .....	1074
12.4.6 Changes in Cryosphere .....	1087
12.4.7 Changes in the Ocean.....	1093
12.4.8 Changes Associated with Carbon Cycle Feedbacks and Vegetation Cover .....	1096
12.4.9 Consistency and Main Differences Between Coupled Model Intercomparison Project Phase 3/Coupled Model Intercomparison Project Phase 5 and Special Report on Emission Scenarios/Representative Concentration Pathways .....	1099
<b>12.5 Climate Change Beyond 2100, Commitment, Stabilization and Irreversibility</b> .....	1102
12.5.1 Representative Concentration Pathway Extensions.....	1102
12.5.2 Climate Change Commitment.....	1102
12.5.3 Forcing and Response, Time Scales of Feedbacks ....	1105
12.5.4 Climate Stabilization and Long-term Climate Targets .....	1107
<b>Box 12.2: Equilibrium Climate Sensitivity and Transient Climate Response</b> .....	1110
12.5.5 Potentially Abrupt or Irreversible Changes .....	1114
<b>References</b> .....	1120

## Frequently Asked Questions

- FAQ 12.1 Why Are So Many Models and Scenarios Used to Project Climate Change?** .....
- FAQ 12.2 How Will the Earth's Water Cycle Change?** .....
- FAQ 12.3 What Would Happen to Future Climate if We Stopped Emissions Today?** .....

## Executive Summary

This chapter assesses long-term projections of climate change for the end of the 21st century and beyond, where the forced signal depends on the scenario and is typically larger than the internal variability of the climate system. Changes are expressed with respect to a baseline period of 1986–2005, unless otherwise stated.

### Scenarios, Ensembles and Uncertainties

**The Coupled Model Intercomparison Project Phase 5 (CMIP5) presents an unprecedented level of information on which to base projections including new Earth System Models with a more complete representation of forcings, new Representative Concentration Pathways (RCP) scenarios and more output available for analysis.** The four RCP scenarios used in CMIP5 lead to a total radiative forcing (RF) at 2100 that spans a wider range than that estimated for the three Special Report on Emission Scenarios (SRES) scenarios (B1, A1B, A2) used in the Fourth Assessment Report (AR4), RCP2.6 being almost 2 W m<sup>-2</sup> lower than SRES B1 by 2100. The magnitude of future aerosol forcing decreases more rapidly in RCP scenarios, reaching lower values than in SRES scenarios through the 21st century. Carbon dioxide (CO<sub>2</sub>) represents about 80 to 90% of the total anthropogenic forcing in all RCP scenarios through the 21st century. The ensemble mean total effective RFs at 2100 for CMIP5 concentration-driven projections are 2.2, 3.8, 4.8 and 7.6 W m<sup>-2</sup> for RCP2.6, RCP4.5, RCP6.0 and RCP8.5 respectively, relative to about 1850, and are close to corresponding Integrated Assessment Model (IAM)-based estimates (2.4, 4.0, 5.2 and 8.0 W m<sup>-2</sup>). {12.2.1, 12.3, Table 12.1, Figures 12.1, 12.2, 12.3, 12.4}

**New experiments and studies have continued to work towards a more complete and rigorous characterization of the uncertainties in long-term projections, but the magnitude of the uncertainties has not changed significantly since AR4.** There is overall consistency between the projections based on CMIP3 and CMIP5, for both large-scale patterns and magnitudes of change. Differences in global temperature projections are largely attributable to a change in scenarios. Model agreement and confidence in projections depend on the variable and spatial and temporal averaging. The well-established stability of large-scale geographical patterns of change during a transient experiment remains valid in the CMIP5 models, thus justifying pattern scaling to approximate changes across time and scenarios under such experiments. Limitations remain when pattern scaling is applied to strong mitigation scenarios, to scenarios where localized forcing (e.g., aerosols) are significant and vary in time and for variables other than average temperature and precipitation. {12.2.2, 12.2.3, 12.4.2, 12.4.9, Figures 12.10, 12.39, 12.40, 12.41}

### Projections of Temperature Change

**Global mean temperatures will continue to rise over the 21st century if greenhouse gas (GHG) emissions continue unabated.** Under the assumptions of the concentration-driven RCPs, global mean surface temperatures for 2081–2100, relative to 1986–2005 will likely<sup>1</sup> be in the 5 to 95% range of the CMIP5 models; 0.3°C to 1.7°C (RCP2.6), 1.1°C to 2.6°C (RCP4.5), 1.4°C to 3.1°C (RCP6.0), 2.6°C to 4.8°C (RCP8.5). Global temperatures averaged over the period 2081–2100 are projected to likely exceed 1.5°C above 1850–1900 for RCP4.5, RCP6.0 and RCP8.5 (*high confidence*), are likely to exceed 2°C above 1850–1900 for RCP6.0 and RCP8.5 (*high confidence*) and are more likely than not to exceed 2°C for RCP4.5 (*medium confidence*). Temperature change above 2°C under RCP2.6 is unlikely (*medium confidence*). Warming above 4°C by 2081–2100 is unlikely in all RCPs (*high confidence*) except for RCP8.5, where it is about as likely as not (*medium confidence*). {12.4.1, Tables 12.2, 12.3, Figures 12.5, 12.8}

**Temperature change will not be regionally uniform.** There is very high confidence<sup>2</sup> that globally averaged changes over land will exceed changes over the ocean at the end of the 21st century by a factor that is likely in the range 1.4 to 1.7. In the absence of a strong reduction in the Atlantic Meridional Overturning, the Arctic region is projected to warm most (*very high confidence*). This polar amplification is not found in Antarctic regions due to deep ocean mixing, ocean heat uptake and the persistence of the Antarctic ice sheet. Projected regional surface air temperature increase has minima in the North Atlantic and Southern Oceans in all scenarios. One model exhibits marked cooling in 2081–2100 over large parts of the Northern Hemisphere (NH), and a few models indicate slight cooling locally in the North Atlantic. Atmospheric zonal mean temperatures show warming throughout the troposphere, especially in the upper troposphere and northern high latitudes, and cooling in the stratosphere. {12.4.2, 12.4.3, Table 12.2, Figures 12.9, 12.10, 12.11, 12.12}

**It is virtually certain that, in most places, there will be more hot and fewer cold temperature extremes as global mean temperatures increase.** These changes are expected for events defined as extremes on both daily and seasonal time scales. Increases in the frequency, duration and magnitude of hot extremes along with heat stress are expected; however, occasional cold winter extremes will continue to occur. Twenty-year return values of low temperature events are projected to increase at a rate greater than winter mean temperatures in most regions, with the largest changes in the return values of low temperatures at high latitudes. Twenty-year return values for high temperature events are projected to increase at a rate similar to or greater than the rate of increase of summer mean temperatures in most regions. Under RCP8.5 it is likely that, in most land regions, a current 20-year high temperature event will occur more frequently by the end of the 21st

<sup>1</sup> In this Report, the following terms have been used to indicate the assessed likelihood of an outcome or a result: Virtually certain 99–100% probability, Very likely 90–100%, Likely 66–100%, About as likely as not 33–66%, Unlikely 0–33%, Very unlikely 0–10%, Exceptionally unlikely 0–1%. Additional terms (Extremely likely: 95–100%, More likely than not >50–100%, and Extremely unlikely 0–5%) may also be used when appropriate. Assessed likelihood is typeset in italics, e.g., *very likely* (see Section 1.4 and Box TS.1 for more details).

<sup>2</sup> In this Report, the following summary terms are used to describe the available evidence: limited, medium, or robust; and for the degree of agreement: low, medium, or high. A level of confidence is expressed using five qualifiers: very low, low, medium, high, and very high, and typeset in italics, e.g., *medium confidence*. For a given evidence and agreement statement, different confidence levels can be assigned, but increasing levels of evidence and degrees of agreement are correlated with increasing confidence (see Section 1.4 and Box TS.1 for more details).

century (at least doubling its frequency, but in many regions becoming an annual or 2-year event) and a current 20-year low temperature event will become exceedingly rare. {12.4.3, Figures 12.13, 12.14}

### Changes in Atmospheric Circulation

**Mean sea level pressure is projected to decrease in high latitudes and increase in the mid-latitudes as global temperatures rise. In the tropics, the Hadley and Walker Circulations are likely to slow down.** Poleward shifts in the mid-latitude jets of about 1 to 2 degrees latitude are *likely* at the end of the 21st century under RCP8.5 in both hemispheres (*medium confidence*), with weaker shifts in the NH. In austral summer, the additional influence of stratospheric ozone recovery in the Southern Hemisphere opposes changes due to GHGs there, though the net response varies strongly across models and scenarios. Substantial uncertainty and thus *low confidence* remains in projecting changes in NH storm tracks, especially for the North Atlantic basin. The Hadley Cell is *likely* to widen, which translates to broader tropical regions and a poleward encroachment of subtropical dry zones. In the stratosphere, the Brewer–Dobson circulation is *likely* to strengthen. {12.4.4, Figures 12.18, 12.19, 12.20}

### Changes in the Water Cycle

**It is virtually certain that, in the long term, global precipitation will increase with increased global mean surface temperature.** Global mean precipitation will increase at a rate per degree Celsius smaller than that of atmospheric water vapour. It will *likely* increase by 1 to 3% °C<sup>-1</sup> for scenarios other than RCP2.6. For RCP2.6 the range of sensitivities in the CMIP5 models is 0.5 to 4% °C<sup>-1</sup> at the end of the 21st century. {12.4.1, Figures 12.6, 12.7}

**Changes in average precipitation in a warmer world will exhibit substantial spatial variation. Some regions will experience increases, other regions will experience decreases and yet others will not experience significant changes at all. There is high confidence that the contrast of annual mean precipitation between dry and wet regions and that the contrast between wet and dry seasons will increase over most of the globe as temperatures increase.** The general pattern of change indicates that high latitude land masses are *likely* to experience greater amounts of precipitation due to the increased specific humidity of the warmer troposphere as well as increased transport of water vapour from the tropics by the end of this century under the RCP8.5 scenario. Many mid-latitude and subtropical arid and semi-arid regions will *likely* experience less precipitation and many moist mid-latitude regions will *likely* experience more precipitation by the end of this century under the RCP8.5 scenario. Globally, for short-duration precipitation events, a shift to more intense individual storms and fewer weak storms is *likely* as temperatures increase. Over most of the mid-latitude land-masses and over wet tropical regions, extreme precipitation events will *very likely* be more intense and more frequent in a warmer world. The global average sensitivity of the 20-year return value of the annual maximum daily precipitation increases ranges from 4% °C<sup>-1</sup> of local temperature increase (average of CMIP3 models) to 5.3% °C<sup>-1</sup> of local temperature increase (average of CMIP5 models) but regionally there are wide variations. {12.4.5, Figures 12.10, 12.22, 12.26, 12.27}

**Annual surface evaporation is projected to increase as global temperatures rise over most of the ocean and is projected to change over land following a similar pattern as precipitation.** Decreases in annual runoff are *likely* in parts of southern Europe, the Middle East, and southern Africa by the end of the 21st century under the RCP8.5 scenario. Increases in annual runoff are *likely* in the high northern latitudes corresponding to large increases in winter and spring precipitation by the end of the 21st century under the RCP8.5 scenario. Regional to global-scale projected decreases in soil moisture and increased risk of agricultural drought are *likely* in presently dry regions and are projected with *medium confidence* by the end of the 21st century under the RCP8.5 scenario. Prominent areas of projected decreases in evaporation include southern Africa and north western Africa along the Mediterranean. Soil moisture drying in the Mediterranean, southwest USA and southern African regions is consistent with projected changes in Hadley Circulation and increased surface temperatures, so surface drying in these regions as global temperatures increase is *likely* with *high confidence* by the end of this century under the RCP8.5 scenario. In regions where surface moistening is projected, changes are generally smaller than natural variability on the 20-year time scale. {12.4.5, Figures 12.23, 12.24, 12.25}

### Changes in Cryosphere

**It is very likely that the Arctic sea ice cover will continue shrinking and thinning year-round in the course of the 21st century as global mean surface temperature rises. At the same time, in the Antarctic, a decrease in sea ice extent and volume is expected, but with low confidence.** Based on the CMIP5 multi-model ensemble, projections of average reductions in Arctic sea ice extent for 2081–2100 compared to 1986–2005 range from 8% for RCP2.6 to 34% for RCP8.5 in February and from 43% for RCP2.6 to 94% for RCP8.5 in September (*medium confidence*). A nearly ice-free Arctic Ocean (sea ice extent less than  $1 \times 10^6$  km<sup>2</sup> for at least 5 consecutive years) in September before mid-century is *likely* under RCP8.5 (*medium confidence*), based on an assessment of a subset of models that most closely reproduce the climatological mean state and 1979–2012 trend of the Arctic sea ice cover. Some climate projections exhibit 5- to 10-year periods of sharp summer Arctic sea ice decline—even steeper than observed over the last decade—and it is *likely* that such instances of rapid ice loss will occur in the future. There is little evidence in global climate models of a tipping point (or critical threshold) in the transition from a perennially ice-covered to a seasonally ice-free Arctic Ocean beyond which further sea ice loss is unstoppable and irreversible. In the Antarctic, the CMIP5 multi-model mean projects a decrease in sea ice extent that ranges from 16% for RCP2.6 to 67% for RCP8.5 in February and from 8% for RCP2.6 to 30% for RCP8.5 in September for 2081–2100 compared to 1986–2005. There is, however, *low confidence* in those values as projections because of the wide inter-model spread and the inability of almost all of the available models to reproduce the mean annual cycle, interannual variability and overall increase of the Antarctic sea ice areal coverage observed during the satellite era. {12.4.6, 12.5.5, Figures 12.28, 12.29, 12.30, 12.31}

**It is very likely that NH snow cover will reduce as global temperatures rise over the coming century. A retreat of permafrost extent with rising global temperatures is virtually certain.** Snow

cover changes result from precipitation and ablation changes, which are sometimes opposite. Projections of the NH spring snow covered area by the end of the 21st century vary between a decrease of 7% (RCP2.6) and a decrease of 25% (RCP8.5), with a pattern that is fairly consistent between models. The projected changes in permafrost are a response not only to warming but also to changes in snow cover, which exerts a control on the underlying soil. By the end of the 21st century, diagnosed near-surface permafrost area is projected to decrease by between 37% (RCP2.6) and 81% (RCP8.5) (*medium confidence*). {12.4.6, Figures 12.32, 12.33}

## Changes in the Ocean

**The global ocean will warm in all RCP scenarios.** The strongest ocean warming is projected for the surface in subtropical and tropical regions. At greater depth the warming is projected to be most pronounced in the Southern Ocean. Best estimates of ocean warming in the top one hundred meters are about 0.6°C (RCP2.6) to 2.0°C (RCP8.5), and about 0.3°C (RCP2.6) to 0.6°C (RCP8.5) at a depth of about 1 km by the end of the 21st century. For RCP4.5 by the end of the 21st century, half of the energy taken up by the ocean is in the uppermost 700 m and 85% is in the uppermost 2000 m. Due to the long time scales of this heat transfer from the surface to depth, ocean warming will continue for centuries, even if GHG emissions are decreased or concentrations kept constant. {12.4.7, 12.5.2–12.5.4, Figure 12.12}

**It is very likely that the Atlantic Meridional Overturning Circulation (AMOC) will weaken over the 21st century but it is very unlikely that the AMOC will undergo an abrupt transition or collapse in the 21st century.** Best estimates and ranges for the reduction from CMIP5 are 11% (1 to 24%) in RCP2.6 and 34% (12 to 54%) in RCP8.5. There is *low confidence* in assessing the evolution of the AMOC beyond the 21st century. {12.4.7, Figure 12.35}

## Carbon Cycle

**When forced with RCP8.5 CO<sub>2</sub> emissions, as opposed to the RCP8.5 CO<sub>2</sub> concentrations, 11 CMIP5 Earth System Models with interactive carbon cycle simulate, on average, a 50 ppm (min to max range –140 to +210 ppm) larger atmospheric CO<sub>2</sub> concentration and 0.2°C (min to max range –0.4 to +0.9°C) larger global surface temperature increase by 2100.** {12.4.8, Figures 12.36, 12.37}

## Long-term Climate Change, Commitment and Irreversibility

**Global temperature equilibrium would be reached only after centuries to millennia if RF were stabilized.** Continuing GHG emissions beyond 2100, as in the RCP8.5 extension, induces a total RF above 12 W m<sup>-2</sup> by 2300. Sustained negative emissions beyond 2100, as in RCP2.6, induce a total RF below 2 W m<sup>-2</sup> by 2300. The projected warming for 2281–2300, relative to 1986–2005, is 0.0°C to 1.2°C for RCP2.6 and 3.0°C to 12.6°C for RCP8.5 (*medium confidence*). In much the same way as the warming to a rapid increase of forcing is delayed, the cooling after a decrease of RF is also delayed. {12.5.1, Figures 12.43, 12.44}

**A large fraction of climate change is largely irreversible on human time scales, unless net anthropogenic CO<sub>2</sub> emissions were strongly negative over a sustained period.** For scenarios

driven by CO<sub>2</sub> alone, global average temperature is projected to remain approximately constant for many centuries following a complete cessation of emissions. The positive commitment from CO<sub>2</sub> may be enhanced by the effect of an abrupt cessation of aerosol emissions, which will cause warming. By contrast, cessation of emission of short-lived GHGs will contribute a cooling. {12.5.3, 12.5.4, Figures 12.44, 12.45, 12.46, FAQ 12.3}

## Equilibrium Climate Sensitivity and Transient Climate Response

**Estimates of the equilibrium climate sensitivity (ECS) based on observed climate change, climate models and feedback analysis, as well as paleoclimate evidence indicate that ECS is likely in the range 1.5°C to 4.5°C with high confidence, extremely unlikely less than 1°C (high confidence) and very unlikely greater than 6°C (medium confidence).** The transient climate response (TCR) is likely in the range 1°C to 2.5°C and extremely unlikely greater than 3°C, based on observed climate change and climate models. {Box 12.2, Figures 1, 2}

## Climate Stabilization

**The principal driver of long-term warming is total emissions of CO<sub>2</sub> and the two quantities are approximately linearly related.** The global mean warming per 1000 PgC (transient climate response to cumulative carbon emissions (TCRE)) is likely between 0.8°C to 2.5°C per 1000 PgC, for cumulative emissions less than about 2000 PgC until the time at which temperatures peak. To limit the warming caused by anthropogenic CO<sub>2</sub> emissions alone to be *likely* less than 2°C relative to the period 1861–1880, total CO<sub>2</sub> emissions from all anthropogenic sources would need to be limited to a cumulative budget of about 1000 PgC since that period. About half [445 to 585 PgC] of this budget was already emitted by 2011. Accounting for projected warming effect of non-CO<sub>2</sub> forcing, a possible release of GHGs from permafrost or methane hydrates, or requiring a higher likelihood of temperatures remaining below 2°C, all imply a lower budget. {12.5.4, Figures 12.45, 12.46, Box 12.2}

**Some aspects of climate will continue to change even if temperatures are stabilized.** Processes related to vegetation change, changes in the ice sheets, deep ocean warming and associated sea level rise and potential feedbacks linking for example ocean and the ice sheets have their own intrinsic long time scales and may result in significant changes hundreds to thousands of years after global temperature is stabilized. {12.5.2 to 12.5.4}

## Abrupt Change

**Several components or phenomena in the climate system could potentially exhibit abrupt or nonlinear changes, and some are known to have done so in the past.** Examples include the AMOC, Arctic sea ice, the Greenland ice sheet, the Amazon forest and monsoonal circulations. For some events, there is information on potential consequences, but in general there is *low confidence* and little consensus on the likelihood of such events over the 21st century. {12.5.5, Table 12.4}

## 12.1 Introduction

Projections of future climate change are not like weather forecasts. It is not possible to make deterministic, definitive predictions of how climate will evolve over the next century and beyond as it is with short-term weather forecasts. It is not even possible to make projections of the frequency of occurrence of all possible outcomes in the way that it might be possible with a calibrated probabilistic medium-range weather forecast. Projections of climate change are uncertain, first because they are dependent primarily on scenarios of future anthropogenic and natural forcings that are uncertain, second because of incomplete understanding and imprecise models of the climate system and finally because of the existence of internal climate variability. The term climate projection tacitly implies these uncertainties and dependencies. Nevertheless, as greenhouse gas (GHG) concentrations continue to rise, we expect to see future changes to the climate system that are greater than those already observed and attributed to human activities. It is possible to understand future climate change using models and to use models to characterize outcomes and uncertainties under specific assumptions about future forcing scenarios.

This chapter assesses climate projections on time scales beyond those covered in Chapter 11, that is, beyond the mid-21st century. Information from a range of different modelling tools is used here; from simple energy balance models, through Earth System Models of Intermediate Complexity (EMICs) to complex dynamical climate and Earth System Models (ESMs). These tools are evaluated in Chapter 9 and, where possible, the evaluation is used in assessing the validity of the projections. This chapter also summarizes some of the information on leading-order measures of the sensitivity of the climate system from other chapters and discusses the relevance of these measures for climate projections, commitments and irreversibility.

Since the AR4 (Meehl et al., 2007b) there have been a number of advances:

- New scenarios of future forcings have been developed to replace the Special Report on Emissions Scenarios (SRES). The Representative Concentration Pathways (RCPs, see Section 12.3) (Moss et al., 2010), have been designed to cover a wide range of possible magnitudes of climate change in models rather than being derived sequentially from storylines of socioeconomic futures. The aim is to provide a range of climate responses while individual socioeconomic scenarios may be derived, scaled and interpolated (some including explicit climate policy). Nevertheless, many studies that have been performed since AR4 have used SRES and, where appropriate, these are assessed. Simplified scenarios of future change, developed strictly for understanding the response of the climate system rather than to represent realistic future outcomes, are also synthesized and the understanding of leading-order measures of climate response such as the equilibrium climate sensitivity (ECS) and the transient climate response (TCR) are assessed.
- New models have been developed with higher spatial resolution, with better representation of processes and with the inclusion of more processes, in particular processes that are important in simulating the carbon cycle of the Earth. In these models, emissions of

GHGs may be specified and these gases may be chemically active in the atmosphere or be exchanged with pools in terrestrial and oceanic systems before ending up as an airborne concentration (see Figure 10.1 of AR4).

- New types of model experiments have been performed, many coordinated by the Coupled Model Intercomparison Project Phase 5 (CMIP5) (Taylor et al., 2012), which exploit the addition of these new processes. Models may be driven by emissions of GHGs, or by their concentrations with different Earth System feedback loops cut. This allows the separate assessment of different feedbacks in the system and of projections of physical climate variables and future emissions.
- Techniques to assess and quantify uncertainties in projections have been further developed but a full probabilistic quantification remains difficult to propose for most quantities, the exception being global, temperature-related measures of the system sensitivity to forcings, such as ECS and TCR. In those few cases, projections are presented in the form of probability density functions (PDFs). We make the distinction between the spread of a multi-model ensemble, an *ad hoc* measure of the possible range of projections and the quantification of uncertainty that combines information from models and observations using statistical algorithms. Just like climate models, different techniques for quantifying uncertainty exist and produce different outcomes. Where possible, different estimates of uncertainty are compared.

Although not an advance, as time has moved on, the baseline period from which climate change is expressed has also moved on (a common baseline period of 1986–2005 is used throughout, consistent with the 2006 start-point for the RCP scenarios). Hence climate change is expressed as a change with respect to a recent period of history, rather than a time before significant anthropogenic influence. It should be borne in mind that some anthropogenically forced climate change had already occurred by the 1986–2005 period (see Chapter 10).

The focus of this chapter is on global and continental/ocean basin-scale features of climate. For many aspects of future climate change, it is possible to discuss generic features of projections and the processes that underpin them for such large scales. Where interesting or unique changes have been investigated at smaller scales, and there is a level of agreement between different studies of those smaller-scale changes, these may also be assessed in this chapter, although where changes are linked to climate phenomena such as El Niño, readers are referred to Chapter 14. Projections of atmospheric composition, chemistry and air quality for the 21st century are assessed in Chapter 11, except for CO<sub>2</sub> which is assessed in this chapter. An innovation for AR5 is Annex I: Atlas of Global and Regional Climate Projections, a collection of global and regional maps of projected climate changes derived from model output. A detailed commentary on each of the maps presented in Annex I is not provided here, but some discussion of generic features is provided.

Projections from regional models driven by boundary conditions from global models are not extensively assessed but may be mentioned in this chapter. More detailed regional information may be found in Chapter 14 and is also now assessed in the Working Group II report, where it can more easily be linked to impacts.

## 12.2 Climate Model Ensembles and Sources of Uncertainty from Emissions to Projections

### 12.2.1 The Coupled Model Intercomparison Project Phase 5 and Other Tools

Many of the figures presented in this chapter and in others draw on data collected as part of CMIP5 (Taylor et al., 2012). The project involves the worldwide coordination of ESM experiments including the coordination of input forcing fields, diagnostic output and the hosting of data in a distributed archive. CMIP5 has been unprecedented in terms of the number of modelling groups and models participating, the number of experiments performed and the number of diagnostics collected. The archive of model simulations began being populated by mid-2011 and continued to grow during the writing of AR5. The production of figures for this chapter draws on a fixed database of simulations and variables that was available on 15 March 2013 (the same as the cut-off date for the acceptance of the publication of papers). Different figures may use different subsets of models and there are unequal numbers of models that have produced output for the different RCP scenarios. Figure 12.1 gives a summary of which output was available from which model for which scenario. Where multiple runs

are performed with exactly the same model but with different initial conditions, we choose only one ensemble member (usually the first but in cases where that was not available, the first available member is chosen) in order not to weight models with more ensemble members than others unduly in the multi-model synthesis. Rather than give an exhaustive account of which models were used to make which figures, this summary information is presented as a guide to readers.

In addition to output from CMIP5, information from a coordinated set of simulations with EMICs is also used (Zickfeld et al., 2013) to investigate long-term climate change beyond 2100. Even more simplified energy balance models or emulation techniques are also used, mostly to estimate responses where ESM experiments are not available (Meinshausen et al., 2011a; Good et al., 2013). An evaluation of the models used for projections is provided in Chapter 9 of this Report.

### 12.2.2 General Concepts: Sources of Uncertainties

The understanding of the sources of uncertainty affecting future climate change projections has not substantially changed since AR4, but many experiments and studies since then have proceeded to explore and characterize those uncertainties further. A full characterization,



**Figure 12.1 |** A summary of the output used to make the CMIP5 figures in this chapter (and some figures in Chapter 11). The climate variable names run along the horizontal axis and use the standard abbreviations in the CMIP5 protocol (Taylor et al., 2012, and online references therein). The climate model names run along the vertical axis. In each box the shading indicates the number of ensemble members available for historical, RCP2.6, RCP4.5, RCP6.0, RCP8.5 and pre-industrial control experiments, although only one ensemble member per model is used in the relevant figures.

## Frequently Asked Questions

**FAQ 12.1 | Why Are So Many Models and Scenarios Used to Project Climate Change?**

*Future climate is partly determined by the magnitude of future emissions of greenhouse gases, aerosols and other natural and man-made forcings. These forcings are external to the climate system, but modify how it behaves. Future climate is shaped by the Earth's response to those forcings, along with internal variability inherent in the climate system. A range of assumptions about the magnitude and pace of future emissions helps scientists develop different emission scenarios, upon which climate model projections are based. Different climate models, meanwhile, provide alternative representations of the Earth's response to those forcings, and of natural climate variability. Together, ensembles of models, simulating the response to a range of different scenarios, map out a range of possible futures, and help us understand their uncertainties.*

Predicting socioeconomic development is arguably even more difficult than predicting the evolution of a physical system. It entails predicting human behaviour, policy choices, technological advances, international competition and cooperation. The common approach is to use scenarios of plausible future socioeconomic development, from which future emissions of greenhouse gases and other forcing agents are derived. It has not, in general, been possible to assign likelihoods to individual forcing scenarios. Rather, a set of alternatives is used to span a range of possibilities. The outcomes from different forcing scenarios provide policymakers with alternatives and a range of possible futures to consider.

Internal fluctuations in climate are spontaneously generated by interactions between components such as the atmosphere and the ocean. In the case of near-term climate change, they may eclipse the effect of external perturbations, like greenhouse gas increases (see Chapter 11). Over the longer term, however, the effect of external forcings is expected to dominate instead. Climate model simulations project that, after a few decades, different scenarios of future anthropogenic greenhouse gases and other forcing agents—and the climate system's response to them—will differently affect the change in mean global temperature (FAQ 12.1, Figure 1, left panel). Therefore, evaluating the consequences of those various scenarios and responses is of paramount importance, especially when policy decisions are considered.

Climate models are built on the basis of the physical principles governing our climate system, and empirical understanding, and represent the complex, interacting processes needed to simulate climate and climate change, both past and future. Analogues from past observations, or extrapolations from recent trends, are inadequate strategies for producing projections, because the future will not necessarily be a simple continuation of what we have seen thus far.

Although it is possible to write down the equations of fluid motion that determine the behaviour of the atmosphere and ocean, it is impossible to solve them without using numerical algorithms through computer model simulation, similarly to how aircraft engineering relies on numerical simulations of similar types of equations. Also, many small-scale physical, biological and chemical processes, such as cloud processes, cannot be described by those equations, either because we lack the computational ability to describe the system at a fine enough resolution to directly simulate these processes or because we still have a partial scientific understanding of the mechanisms driving these processes. Those need instead to be approximated by so-called parameterizations within the climate models, through which a mathematical relation between directly simulated and approximated quantities is established, often on the basis of observed behaviour.

There are various alternative and equally plausible numerical representations, solutions and approximations for modelling the climate system, given the limitations in computing and observations. This diversity is considered a healthy aspect of the climate modelling community, and results in a range of plausible climate change projections at global and regional scales. This range provides a basis for quantifying uncertainty in the projections, but because the number of models is relatively small, and the contribution of model output to public archives is voluntary, the sampling of possible futures is neither systematic nor comprehensive. Also, some inadequacies persist that are common to all models; different models have different strength and weaknesses; it is not yet clear which aspects of the quality of the simulations that can be evaluated through observations should guide our evaluation of future model simulations. *(continued on next page)*

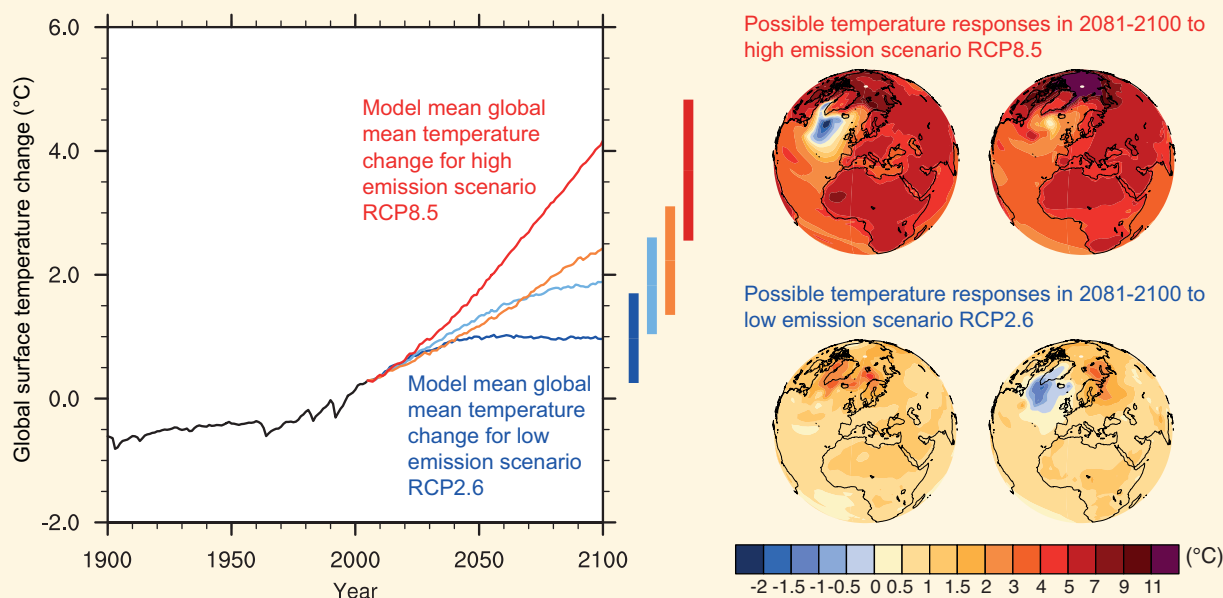
## FAQ 12.1 (continued)

Models of varying complexity are commonly used for different projection problems. A faster model with lower resolution, or a simplified description of some climate processes, may be used in cases where long multi-century simulations are required, or where multiple realizations are needed. Simplified models can adequately represent large-scale average quantities, like global average temperature, but finer details, like regional precipitation, can be simulated only by complex models.

The coordination of model experiments and output by groups such as the Coupled Model Intercomparison Project (CMIP), the World Climate Research Program and its Working Group on Climate Models has seen the science community step up efforts to evaluate the ability of models to simulate past and current climate and to compare future climate change projections. The ‘multi-model’ approach is now a standard technique used by the climate science community to assess projections of a specific climate variable.

FAQ 12.1, Figure 1, right panels, shows the temperature response by the end of the 21st century for two illustrative models and the highest and lowest RCP scenarios. Models agree on large-scale patterns of warming at the surface, for example, that the land is going to warm faster than ocean, and the Arctic will warm faster than the tropics. But they differ both in the magnitude of their global response for the same scenario, and in small scale, regional aspects of their response. The magnitude of Arctic amplification, for instance, varies among different models, and a subset of models show a weaker warming or slight cooling in the North Atlantic as a result of the reduction in deepwater formation and shifts in ocean currents.

There are inevitable uncertainties in future external forcings, and the climate system’s response to them, which are further complicated by internally generated variability. The use of multiple scenarios and models have become a standard choice in order to assess and characterize them, thus allowing us to describe a wide range of possible future evolutions of the Earth’s climate.



**FAQ 12.1, Figure 1 |** Global mean temperature change averaged across all Coupled Model Intercomparison Project Phase 5 (CMIP5) models (relative to 1986–2005) for the four Representative Concentration Pathway (RCP) scenarios: RCP2.6 (dark blue), RCP4.5 (light blue), RCP6.0 (orange) and RCP8.5 (red); 32, 42, 25 and 39 models were used respectively for these 4 scenarios. Likely ranges for global temperature change by the end of the 21st century are indicated by vertical bars. Note that these ranges apply to the difference between two 20-year means, 2081–2100 relative to 1986–2005, which accounts for the bars being centred at a smaller value than the end point of the annual trajectories. For the highest (RCP8.5) and lowest (RCP2.6) scenario, illustrative maps of surface temperature change at the end of the 21st century (2081–2100 relative to 1986–2005) are shown for two CMIP5 models. These models are chosen to show a rather broad range of response, but this particular set is not representative of any measure of model response uncertainty.

qualitative and even more so quantitative, involves much more than a measure of the range of model outcomes, because additional sources of information (e.g., observational constraints, model evaluation, expert judgement) lead us to expect that the uncertainty around the future climate state does not coincide straightforwardly with those ranges. In fact, in this chapter we highlight wherever relevant the distinction between model uncertainty evaluation, which encompasses the understanding that models have intrinsic shortcoming in fully and accurately representing the real system, and cannot all be considered independent of one another (Knutti et al., 2013), and a simpler descriptive quantification, based on the range of outcomes from the ensemble of models.

Uncertainty affecting mid- to long-term projections of climatic changes stems from distinct but possibly interacting sources. Figure 12.2 shows a schematic of the chain from scenarios, through ESMs to projections. Uncertainties affecting near-term projections of which some aspect are also relevant for longer-term projections are discussed in Section 11.3.1.1 and shown in Figure 11.8.

Future anthropogenic emissions of GHGs, aerosol particles and other forcing agents such as land use change are dependent on socioeconomic factors including global geopolitical agreements to control those emissions. Systematic studies that attempt to quantify the likely ranges of anthropogenic emission have been undertaken (Sokolov et al., 2009) but it is more common to use a scenario approach of different but plausible—in the sense of technically feasible—pathways, leading to the concept of *scenario uncertainty*. AR4 made extensive

use of the SRES scenarios (IPCC, 2000) developed using a sequential approach, that is, socioeconomic factors feed into emissions scenarios which are then used either to directly force the climate models or to determine concentrations of GHGs and other agents required to drive these models. This report also assesses outcomes of simulations that use the new RCP scenarios, developed using a parallel process (Moss et al., 2010) whereby different targets in terms of RF at 2100 were selected (2.6, 4.5, 6.0 and 8.5 W m<sup>-2</sup>) and GHG and aerosol emissions consistent with those targets, and their corresponding socioeconomic drivers were developed simultaneously (see Section 12.3). Rather than being identified with one socioeconomic storyline, RCP scenarios are consistent with many possible economic futures (in fact, different combinations of GHG and aerosol emissions can lead to the same RCP). Their development was driven by the need to produce scenarios that could be input to climate model simulations more expediently while corresponding socioeconomic scenarios would be developed in parallel, and to produce a wide range of model responses that may be scaled and interpolated to estimate the response under other scenarios, involving different measures of adaptation and mitigation.

In terms of the uncertainties related to the RCP emissions scenarios, the following issues can be identified:

- No probabilities or likelihoods have been attached to the alternative RCP scenarios (as was the case for SRES scenarios). Each of them should be considered plausible, as no study has questioned their technical feasibility (see Chapter 1).

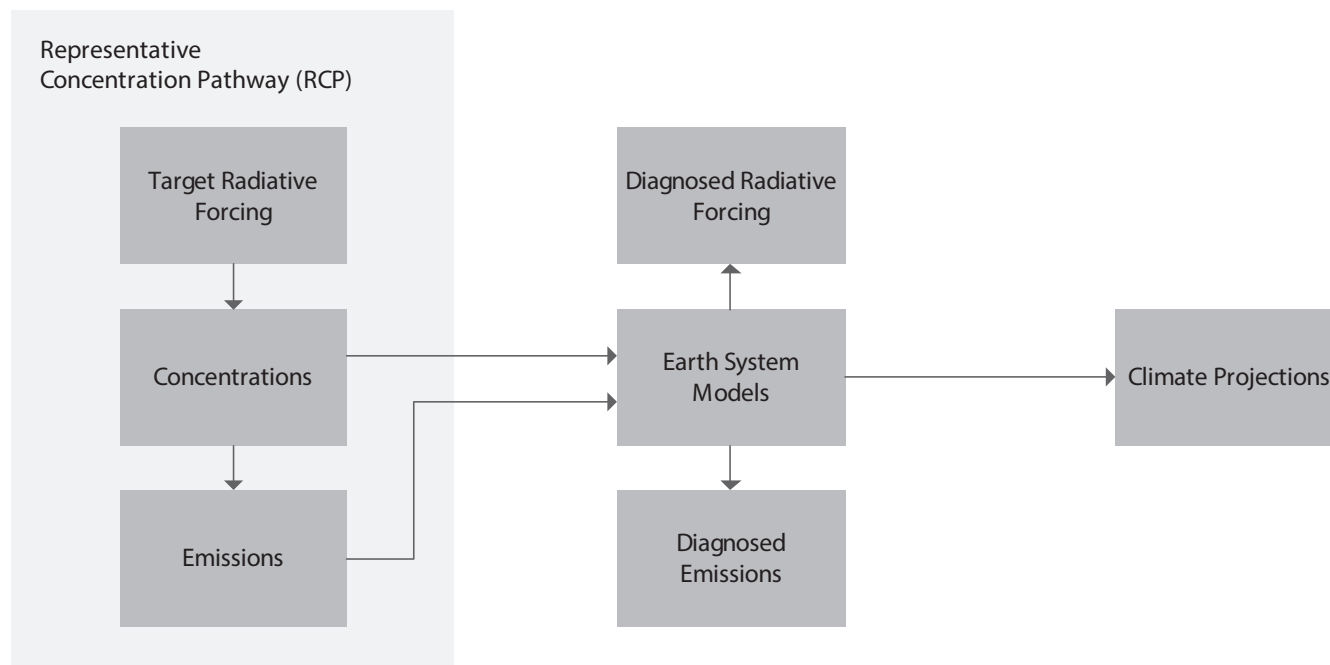


**Figure 12.2 |** Links in the chain from scenarios, through models to climate projections. The Representative Concentration Pathways (RCPs) are designed to sample a range of radiative forcing (RF) of the climate system at 2100. The RCPs are translated into both concentrations and emissions of greenhouse gases using Integrated Assessment Models (IAMs). These are then used as inputs to dynamical Earth System Models (ESMs) in simulations that are either concentration-driven (the majority of projection experiments) or emissions-driven (only for RCP8.5). Aerosols and other forcing factors are implemented in different ways in each ESM. The ESM projections each have a potentially different RF, which may be viewed as an output of the model and which may not correspond to precisely the level of RF indicated by the RCP nomenclature. Similarly, for concentration-driven experiments, the emissions consistent with those concentrations diagnosed from the ESM may be different from those specified in the RCP (diagnosed from the IAM). Different models produce different responses even under the same RF. Uncertainty propagates through the chain and results in a spread of ESM projections. This spread is only one way of assessing uncertainty in projections. Alternative methods, which combine information from simple and complex models and observations through statistical models or expert judgement, are also used to quantify that uncertainty.

- Despite the naming of the RCPs in terms of their target RF at 2100 or at stabilization (Box 1.1), climate models translate concentrations of forcing agents into RF in different ways due to their different structural modelling assumptions. Hence a model simulation of RCP6.0 may not attain exactly a RF of  $6 \text{ W m}^{-2}$ ; more accurately, an RCP6.0 forced model experiment may not attain exactly the same RF as was intended by the specification of the RCP6.0 forcing inputs. Thus in addition to the scenario uncertainty there is RF uncertainty in the way the RCP scenarios are implemented in climate models.
- Some model simulations are concentration-driven (GHG concentrations are specified) whereas some models, which have Earth Systems components, convert emission scenarios into concentrations and are termed emissions-driven. Different ESMs driven by emissions may produce different concentrations of GHGs and aerosols because of differences in the representation and/or parameterization of the processes responsible for the conversion of emissions into concentrations. This aspect may be considered a facet of forcing uncertainty, or may be compounded in the category of model uncertainty, which we discuss below. Also, aerosol loading and land use changes are not dictated intrinsically by the RCP specification. Rather, they are a result of the Integrated Assessment Model that created the emission pathway for a given RCP.

SRES and RCPs account for future changes only in anthropogenic forcings. With regard to solar forcing, the 1985–2005 solar cycle is repeated. Neither projections of future deviations from this solar cycle, nor future volcanic RF and their uncertainties are considered.

Any climate projection is subject to sampling uncertainties that arise because of internal variability. In this chapter, the prediction of, for example, the amplitude or phase of some mode of variability that may be important on long time scales is not addressed (see Sections 11.2 and 11.3). Any climate variable projection derived from a single simulation of an individual climate model will be affected by internal variability (stemming from the chaotic nature of the system), whether it be a variable that involves a long time average (e.g., 20 years), a snapshot in time or some more complex diagnostic such as the variance computed from a time series over many years. No amount of time averaging can reduce internal variability to zero, although for some EMICs and simplified models, which may be used to reproduce the results of more complex model simulations, the representation of internal variability is excluded from the model specification by design. For different variables, and different spatial and time scale averages, the relative importance of internal variability in comparison with other sources of uncertainty will be different. In general, internal variability becomes more important on shorter time scales and for smaller scale variables (see Section 11.3 and Figure 11.2). The concept of signal-to-noise ratio may be used to quantify the relative magnitude of the forced response (signal) versus internal variability (noise). Internal variability may be sampled and estimated explicitly by running ensembles of simulations with slightly different initial conditions, designed explicitly to represent internal variability, or can be estimated on the basis of long control runs where external forcings are held constant. In the case of both multi-model and perturbed physics ensembles (see below), there is an implicit perturbation in the initial state of each run considered, which

means that these ensembles sample both modelling uncertainty and internal variability jointly.

The ability of models to mimic nature is achieved by simplification choices that can vary from model to model in terms of the fundamental numeric and algorithmic structures, forms and values of parameterizations, and number and kinds of coupled processes included. Simplifications and the interactions between parameterized and resolved processes induce ‘errors’ in models, which can have a leading-order impact on projections. It is possible to characterize the choices made when building and running models into structural—indicating the numerical techniques used for solving the dynamical equations, the analytic form of parameterization schemes and the choices of inputs for fixed or varying boundary conditions—and parametric—indicating the choices made in setting the parameters that control the various components of the model. The community of climate modellers has regularly collaborated in producing coordinated experiments forming multi-model ensembles (MMEs), using both global and regional model families, for example, CMIP3/5 (Meehl et al., 2007a), ENSEMBLES (Johns et al., 2011) and Chemistry–Climate Model Validation 1 and 2 (CCM-Val-1 and 2; Eyring et al., 2005), through which structural uncertainty can be at least in part explored by comparing models, and perturbed physics ensembles (PPEs, with e.g., Hadley Centre Coupled Model version 3 (HadCM3; Murphy et al., 2004), Model for Interdisciplinary Research On Climate (MIROC; Yokohata et al., 2012), Community Climate System Model 3 (CCSM3; Jackson et al., 2008; Sanderson, 2011)), through which uncertainties in parameterization choices can be assessed in a given model. As noted below, neither MMEs nor PPEs represent an adequate sample of all the possible choices one could make in building a climate model. Also, current models may exclude some processes that could turn out to be important for projections (e.g., methane clathrate release) or produce a common error in the representation of a particular process. For this reason, it is of critical importance to distinguish two different senses in which the uncertainty terminology is used or misused in the literature (see also Sections 1.4.2, 9.2.2, 9.2.3, 11.2.1 and 11.2.2). A narrow interpretation of the concept of model uncertainty often identifies it with the range of responses of a model ensemble. In this chapter this type of characterization is referred as model range or model spread. A broader concept entails the recognition of a fundamental uncertainty in the representation of the real system that these models can achieve, given their necessary approximations and the limits in the scientific understanding of the real system that they encapsulate. When addressing this aspect and characterizing it, this chapter uses the term model uncertainty.

The relative role of the different sources of uncertainty—model, scenario and internal variability—as one moves from short- to mid- to long-term projections and considers different variables at different spatial scales has to be recognized (see Section 11.3). The three sources exchange relevance as the time horizon, the spatial scale and the variable change. In absolute terms, internal variability is generally estimated, and has been shown in some specific studies (Hu et al., 2012) to remain approximately constant across the forecast horizon, with model ranges and scenario/forcing variability increasing over time. For forecasts of global temperatures after mid-century, scenario and model ranges dominate the amount of variation due to internally generated variability, with scenarios accounting for the largest source

of uncertainty in projections by the end of the century. For global average precipitation projections, scenario uncertainty has a much smaller role even by the end of the 21st century and model range maintains the largest share across all projection horizons. For temperature and precipitation projections at smaller spatial scales, internal variability may remain a significant source of uncertainty up until middle of the 21st century in some regions (Hawkins and Sutton, 2009, 2011; Rowell, 2012; Knutti and Sedláček, 2013). Within single model experiments, the persistently significant role of internally generated variability for regional projections even beyond short- and mid-term horizons has been documented by analyzing relatively large ensembles sampling initial conditions (Deser et al., 2012a, 2012b).

### 12.2.3 From Ensembles to Uncertainty Quantification

Ensembles like CMIP5 do not represent a systematically sampled family of models but rely on self-selection by the modelling groups. This opportunistic nature of MMEs has been discussed, for example, in Tebaldi and Knutti (2007) and Knutti et al. (2010a). These ensembles are therefore not designed to explore uncertainty in a coordinated manner, and the range of their results cannot be straightforwardly interpreted as an exhaustive range of plausible outcomes, even if some studies have shown how they appear to behave as well calibrated probabilistic forecasts for some large-scale quantities (Annan and Hargreaves, 2010). Other studies have argued instead that the tail of distributions is by construction undersampled (Räisänen, 2007). In general, the difficulty in producing quantitative estimates of uncertainty based on multiple model output originates in their peculiarities as a statistical sample, neither random nor systematic, with possible dependencies among the members (Jun et al., 2008; Masson and Knutti, 2011; Pen- nell and Reichler, 2011; Knutti et al., 2013) and of spurious nature, that is, often counting among their members models with different degrees of complexities (different number of processes explicitly represented or parameterized) even within the category of general circulation models.

Agreement between multiple models can be a source of information in an uncertainty assessment or confidence statement. Various methods have been proposed to indicate regions where models agree on the projected changes, agree on no change or disagree. Several of those methods are compared in Box 12.1. Many figures use stippling or hatching to display such information, but it is important to note that confidence cannot be inferred from model agreement alone.

Perturbed physics experiments (PPEs) differ in their output interpretability for they can be, and have been, systematically constructed and as such lend themselves to a more straightforward treatment through statistical modelling (Rougier, 2007; Sanso and Forest, 2009). Uncertain parameters in a single model to whose values the output is known to be sensitive are targeted for perturbations. More often it is the parameters in the atmospheric component of the model that are varied (Collins et al., 2006a; Sanderson et al., 2008), and to date have in fact shown to be the source of the largest uncertainties in large-scale response, but lately, with much larger computing power expense, also parameters within the ocean component have been perturbed (Collins et al., 2007; Brierley et al., 2010). Parameters in the land surface schemes have also been subject to perturbation studies (Fischer et al., 2011; Booth et al., 2012; Lambert et al., 2012). Ranges

of possible values are explored and often statistical models that fit the relationship between parameter values and model output, that is, emulators, are trained on the ensemble and used to predict the outcome for unsampled parameter value combinations, in order to explore the parameter space more thoroughly than would otherwise be computationally affordable (Rougier et al., 2009). The space of a single model simulations (even when filtered through observational constraints) can show a large range of outcomes for a given scenario (Jackson et al., 2008). However, multi-model ensembles and perturbed physics ensembles produce modes and distributions of climate responses that can be different from one another, suggesting that one type of ensemble cannot be used as an analogue for the other (Murphy et al., 2007; Sanderson et al., 2010; Yokohata et al., 2010; Collins et al., 2011).

Many studies have made use of results from these ensembles to characterize uncertainty in future projections, and these will be assessed and their results incorporated when describing specific aspects of future climate responses. PPEs have been uniformly treated across the different studies through the statistical framework of analysis of computer experiments (Sanso et al., 2008; Rougier et al., 2009; Harris et al., 2010) or, more plainly, as a thorough exploration of alternative responses reweighted by observational constraints (Murphy et al., 2004; Piani et al., 2005; Forest et al., 2008; Sexton et al., 2012). In all cases the construction of a probability distribution is facilitated by the systematic nature of the experiments. MMEs have generated a much more diversified treatment (1) according to the choice of applying weights to the different models on the basis of past performance or not (Weigel et al., 2010) and (2) according to the choice between treating the different models and the truth as indistinguishable or treating each model as a version of the truth to which an error has been added (Annan and Hargreaves, 2010; Sanderson and Knutti, 2012). Many studies can be classified according to these two criteria and their combination, but even within each of the four resulting categories different studies produce different estimates of uncertainty, owing to the preponderance of *a priori* assumptions, explicitly in those studies that approach the problem through a Bayesian perspective, or only implicit in the choice of likelihood models, or weighting. This makes the use of probabilistic and other results produced through statistical inference necessarily dependent on agreeing with a particular set of assumptions (Sansom et al., 2013), given the lack of a full exploration of the robustness of probabilistic estimates to varying these assumptions.

In summary, there does not exist at present a single agreed on and robust formal methodology to deliver uncertainty quantification estimates of future changes in all climate variables (see also Section 9.8.3 and Stephenson et al., 2012). As a consequence, in this chapter, statements using the calibrated uncertainty language are a result of the expert judgement of the authors, combining assessed literature results with an evaluation of models demonstrated ability (or lack thereof) in simulating the relevant processes (see Chapter 9) and model consensus (or lack thereof) over future projections. In some cases when a significant relation is detected between model performance and reliability of its future projections, some models (or a particular parametric configuration) may be excluded (e.g., Arctic sea ice; Section 12.4.6.1 and Joshi et al., 2010) but in general it remains an open research question to find significant connections of this kind that justify some form of weighting across the ensemble of models and produce aggregated

### Box 12.1 | Methods to Quantify Model Agreement in Maps

The climate change projections in this report are based on ensembles of climate models. The ensemble mean is a useful quantity to characterize the average response to external forcings, but does not convey any information on the robustness of this response across models, its uncertainty and/or likelihood or its magnitude relative to unforced climate variability. In the IPCC AR4 WGI contribution (IPCC, 2007) several criteria were used to indicate robustness of change, most prominently in Figure SPM.7. In that figure, showing projected precipitation changes, stippling marked regions where at least 90% of the CMIP3 models agreed on the sign of the change. Regions where less than 66% of the models agreed on the sign were masked white. The resulting large white area was often misinterpreted as indicating large uncertainties in the different models' response to external forcings, but recent studies show that, for the most part, the disagreement in sign among models is found where projected changes are small and still within the modelled range of internal variability, that is, where a response to anthropogenic forcings has not yet emerged locally in a statistically significant way (Tebaldi et al., 2011; Power et al., 2012).

A number of methods to indicate model robustness, involving an assessment of the significance of the change when compared to internal variability, have been proposed since AR4. The different methods share the purpose of identifying regions with large, significant or robust changes, regions with small changes, regions where models disagree or a combination of those. They do, however, use different assumptions about the statistical properties of the model ensemble, and therefore different criteria for synthesizing the information from it. Different methods also differ in the way they estimate internal variability. We briefly describe and compare several of these methods here.

**Method (a):** The default method used in Chapters 11, 12 and 14 as well as in the Annex I (hatching only) is shown in Box 12.1, Figure 1a, and is based on relating the climate change signal to internal variability in 20-year means of the models as a reference<sup>3</sup>. Regions where the multi-model mean change exceeds two standard deviations of internal variability and where at least 90% of the models agree on the sign of change are stippled and interpreted as 'large change with high model agreement'. Regions where the model mean is less than one standard deviation of internal variability are hatched and interpreted as 'small signal or low agreement of models'. This can have various reasons: (1) changes in individual models are smaller than internal variability, or (2) although changes in individual models are significant, they disagree about the sign and the multi-model mean change remains small. Using this method, the case where all models scatter widely around zero and the case where all models agree on near zero change therefore are both hatched (e.g., precipitation change over the Amazon region by the end of the 21st century, which the following methods mark as 'inconsistent model response').

**Method (b):** Method (a) does not distinguish the case where all models agree on no change and the case where, for example, half of the models show a significant increase and half a decrease. The distinction may be relevant for many applications and a modification of method (a) is to restrict hatching to regions where there is high agreement among the models that the change will be 'small', thus eliminating the ambiguous interpretation 'small or low agreement' in (a). In contrast to method (a) where the model mean is compared to variability, this case (b) marks regions where at least 80% of the individual models show a change smaller than two standard deviations of variability with hatching. Grid points where many models show significant change but don't agree are no longer hatched (Box 12.1, Figure 1b).

**Method (c):** Knutti and Sedláček (2013) define a dimensionless robustness measure,  $R$ , which is inspired by the signal-to-noise ratio and the ranked probability skill score. It considers the natural variability and agreement on magnitude and sign of change. A value of  $R = 1$  implies perfect model agreement; low or negative values imply poor model agreement (note that by definition  $R$  can assume any negative value). Any level of  $R$  can be chosen for the stippling. For illustration, in Box 12.1, Figure 1c, regions with  $R > 0.8$  are marked with small dots, regions with  $R > 0.9$  with larger dots and are interpreted as 'robust large change'. This yields similar results to method (a) for the end of the century, but with some areas of moderate model robustness ( $R > 0.8$ ) already for the near-term projections, even though the signal is still within the noise. Regions where at least 80% of the models individually show no significant change are hatched and interpreted as 'changes unlikely to emerge from variability'<sup>4</sup>. There is less hatching in this method than in method (a).

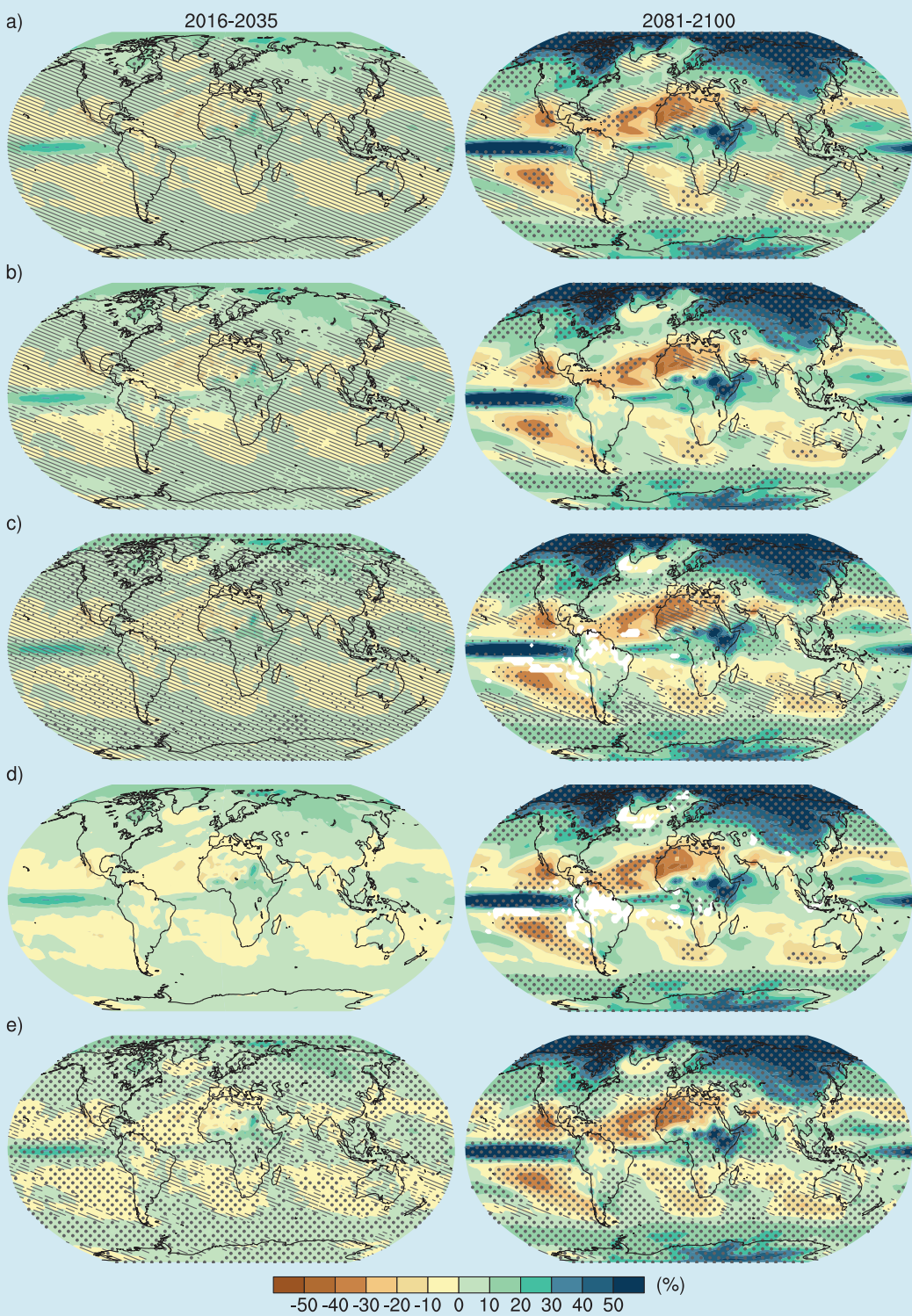
(continued on next page)

<sup>3</sup> The internal variability in this method is estimated using pre-industrial control runs for each of the models which are at least 500 years long. The first 100 years of the pre-industrial are ignored. Variability is calculated for every grid point as the standard deviation of non-overlapping 20-year means, multiplied by the square root of 2 to account for the fact that the variability of a difference in means is of interest. A quadratic fit as a function of time is subtracted from these at every grid point to eliminate model drift. This is by definition the standard deviation of the difference between two independent 20-year averages having the same variance and estimates the variation of that difference that would be expected due to unforced internal variability. The median across all models of that quantity is used.

<sup>4</sup> Variability in methods b–d is estimated from interannual variations in the base period within each model.

Box 12.1 (continued)

## DJF mean precipitation change (RCP8.5)



**Box 12.1, Figure 1 |** Projected change in December to February precipitation for 2016–2035 and 2081–2100, relative to 1986–2005 from CMIP5 models. The choice of the variable and time frames is just for illustration of how the different methods compare in cases with low and high signal-to-noise ratio (left and right column, respectively). The colour maps are identical along each column and only stippling and hatching differ on the basis of the different methods. Different methods for stippling and hatching are shown determined (a) from relating the model mean to internal variability, (b) as in (a) but hatching here indicates high agreement for 'small change', (c) by the robustness measure by Knutti and Sedláček (2013), (d) by the method proposed by Tebaldi et al. (2011) and (e) by the method by Power et al. (2012). Detailed technical explanations for each method are given in the text. 39 models are used in all panels.

*Box 12.1 (continued)*

because it requires 80% of the models to be within variability, not just the model average. Regions where at least 50% of the models show significant change but  $R < 0.5$  are masked as white to indicate ‘models disagreeing on the projected change projections’ (Box 12.1, Figure 1c).

**Method (d):** Tebaldi et al. (2011) start from IPCC AR4 SPM7 but separate lack of model agreement from lack of signal (Box 12.1, Figure 1e). Grid points are stippled and interpreted as ‘robust large change’ when more than 50% of the models show significant change and at least 80% of those agree on the sign of change. Grid points where more than 50% of the models show significant change but less than 80% of those agree on the sign of change are masked as white and interpreted as ‘unreliable’. The results are again similar to the methods above. No hatching was defined in that method (Box 12.1 Figure 1d). (See also Neelin et al., 2006 for a similar approach applied to a specific regional domain.)

**Method (e):** Power et al. (2012) identify three distinct regions using various methods in which projections can be very loosely described as either: ‘statistically significant’, ‘small (relative to temporal variability) or zero, but not statistically significant’ or ‘uncertain’. The emphasis with this approach is to identify robust signals taking the models at face value and to address the questions: (1) What will change? (2) By how much? and (3) What will not change? The underlying consideration here is that statistical testing under the assumption of model independence provides a worthwhile, albeit imperfect, line of evidence that needs to be considered in conjunction with other evidence (e.g., degree of interdependence, ability of models to simulate the past), in order to assess the degree of confidence one has in a projected change.

The examples given here are not exhaustive but illustrate the main ideas. Other methods include simply counting the number of models agreeing on the sign (Christensen et al., 2007), or varying colour hue and saturation to indicate magnitude of change and robustness of change separately (Kaye et al., 2012). In summary, there are a variety of ways to characterize magnitude or significance of change, and agreement between models. There is also a compromise to make between clarity and richness of information. Different methods serve different purposes and a variety of criteria can be justified to highlight specific properties of multi-model ensembles. Clearly only a subset of information regarding robust and uncertain change can be conveyed in a single plot. The methods above convey some important pieces of this information, but obviously more information could be provided if more maps with additional statistics were provided. In fact Annex I provides more explicit information on the range of projected changes evident in the models (e.g., the median, and the upper and lower quartiles). For most of the methods there is a necessity to choose thresholds for the level of agreement that cannot be identified objectively, but could be the result of individual, application-specific evaluations. Note also that all of the above methods measure model agreement in an ensemble of opportunity, and it is impossible to derive a confidence or likelihood statement from the model agreement or model spread alone, without considering consistency with observations, model dependence and the degree to which the relevant processes are understood and reflected in the models (see Section 12.2.3).

The method used by Power et al. (2012) differs from the other methods in that it tests the statistical significance of the ensemble mean rather than a single simulation. As a result, the area where changes are significant increases with an increasing number of models. Already for the period centred on 2025, most of the grid points when using this method show significant change in the ensemble mean whereas in the other methods projections for this time period are classified as changes not exceeding internal variability. The reason is that the former produces a statement about the mean of the distribution being significantly different from zero, equivalent to treating the ensemble as ‘truth plus error’, that is, assuming that the models are independent and randomly distributed around reality. Methods a–d, on the other hand, use an ‘indistinguishable’ interpretation, in which each model and reality are drawn from the same distribution. In that case, the stippling and hatching characterize the likelihood of a single member being significant or not, rather than the ensemble mean. There is some debate in the literature on how the multi-model ensembles should be interpreted statistically. This and past IPCC reports treat the model spread as some measure of uncertainty, irrespective of the number of models, which implies an ‘indistinguishable’ interpretation. For a detailed discussion readers are referred to the literature (Tebaldi and Knutti, 2007; Annan and Hargreaves, 2010; Knutti et al., 2010a, 2010b; Annan and Hargreaves, 2011a; Sanderson and Knutti, 2012).

future projections that are significantly different from straightforward one model—one vote (Knutti, 2010) ensemble results. Therefore, most of the analyses performed for this chapter make use of all available models in the ensembles, with equal weight given to each of them unless otherwise stated.

#### 12.2.4 Joint Projections of Multiple Variables

While many of the key processes relevant to the simulation of single variables are understood, studies are only starting to focus on assessing projections of joint variables, especially when extremes or variability in the individual quantities are of concern. A few studies have addressed projected changes in joint variables, for example, by combining mean temperature and precipitation (Williams et al., 2007; Tebaldi and Lobell, 2008; Tebaldi and Sanso, 2009; Watterson, 2011; Watterson and Whetton, 2011a; Sexton et al., 2012), linking soil moisture, precipitation and temperature mean and variability (Seneviratne et al., 2006; Fischer and Schär, 2009; Koster et al., 2009b, 2009c), combining temperature and humidity (Diffenbaugh et al., 2007; Fischer and Schär, 2010; Willett and Sherwood, 2012), linking summertime temperature and soil moisture to prior winter snowpack (Hall et al., 2008) or linking precipitation change to circulation, moisture and moist static energy budget changes (Neelin et al., 2003; Chou and Neelin, 2004; Chou et al., 2006, 2009). Models may have difficulties simulating all relevant interactions between atmosphere and land surface and the water cycle that determine the joint response, observations to evaluate models are often limited (Seneviratne et al., 2010), and model uncertainties are therefore large (Koster et al., 2006; Boé and Terray, 2008; Notaro, 2008; Fischer et al., 2011). In some cases, correlations between, for example, temperature and precipitation or accumulated precipitation and temperature have found to be too strong in climate models (Trenberth and Shea, 2005; Hirschi et al., 2011). The situation is further complicated by the fact that model biases in one variable affect other variables. The standard method for model projections is to subtract model biases derived from control integrations (assuming that the bias remains constant in a future scenario integration). Several studies note that this may be problematic when a consistent treatment of biases in multiple variables is required (Christensen et al., 2008; Buser et al., 2009), but there is no consensus at this stage for a methodology addressing this problem (Ho et al., 2012). More generally the existence of structural errors in models according to which an unavoidable discrepancy (Rougier, 2007) between their simulations and reality cannot be avoided is relevant here, as well as for univariate projections. In the recent literature an estimate of this discrepancy has been proposed through the use of MMEs, using each model in turn as a surrogate for reality, and measuring the distance between it and the other models of the ensemble. Some summary statistic of these measures is then used to estimate the distance between models and the real world (Sexton and Murphy, 2012; Sexton et al., 2012; Sanderson, 2013). Statistical frameworks to deal with multivariate projections are challenging even for just two variables, as they have to address a trade-off between modelling the joint behavior at scales that are relevant for impacts—that is, fine spatial and temporal scales, often requiring complex spatio-temporal models—and maintaining computational feasibility. In one instance (Tebaldi and Sanso, 2009) scales were investigated at the seasonal and sub-continental level, and projections of the forced response of temperature and precipitation at those scales did not show

significant correlations, likely because of the heterogeneity of the relation between the variables within those large averaged regions and seasons. In Sexton et al. (2012) the spatial scale focussed on regions of Great Britain and correlation emerged as more significant, for example, between summer temperatures and precipitation amounts. Fischer and Knutti (2013) estimated strong relationships between variables making up impact relevant indices (e.g., temperature and humidity) and showed how in some cases, uncertainties across models are larger for a combined variable than if the uncertainties in the individual underlying variables were treated independently (e.g., wildfires), whereas in other cases the uncertainties in the combined variables are smaller than in the individual ones (e.g., heat stress for humans).

Even while recognizing the need for joint multivariate projections, the above limitations at this stage prevent a quantitative assessment for most cases. A few robust qualitative relationships nonetheless emerge from the literature and these are assessed, where appropriate, in the rest of the chapter. For applications that are sensitive to relationships between variables, but still choose to use the multi-model framework to determine possible ranges for projections, sampling from univariate ranges may lead to unrealistic results when significant correlations exist. IPCC assessments often show model averages as best estimates, but such averages can underestimate spatial variability, and more in general they neither represent any of the actual model states (Knutti et al., 2010a) nor do they necessarily represent the joint best estimate in a multivariate sense. Impact studies usually need temporally and spatially coherent multivariate input from climate model simulations. In those cases, using each climate model output individually and feeding it into the impact model, rather than trying to summarise a multivariate distribution from the MME and sample from it, is likely to be more consistent, assuming that the climate model itself correctly captures the spatial covariance, the temporal co-evolution and the relevant feedbacks.

### 12.3 Projected Changes in Forcing Agents, Including Emissions and Concentrations

The experiments that form the basis of global future projections discussed in this chapter are extensions of the simulations of the observational record discussed in Chapters 9 and 10. The scenarios assessed in AR5, introduced in Chapter 1, include four new scenarios designed to explore a wide range of future climate characterized by representative trajectories of well-mixed greenhouse gas (WMGHG) concentrations and other anthropogenic forcing agents. These are described further in Section 12.3.1. The implementation of forcing agents in model projections, including natural and anthropogenic aerosols, ozone and land use change are discussed in Section 12.3.2, with a strong focus on CMIP5 experiments. Global mean emissions, concentrations and RFs applicable to the historical record simulations assessed in Chapters 8, 9 and 10, and the future scenario simulations assessed here, are listed in Annex II. Global mean RF for the 21st century consistent with these scenarios, derived from CMIP5 and other climate model studies, is discussed in Section 12.3.3.

### 12.3.1 Description of Scenarios

Long-term climate change projections reflect how human activities or natural effects could alter the climate over decades and centuries. In this context, defined scenarios are important, as using specific time series of emissions, land use, atmospheric concentrations or RF across multiple models allows for coherent climate model intercomparisons and synthesis. Some scenarios present a simple stylized future (not accompanied by a socioeconomic storyline) and are used for process understanding. More comprehensive scenarios are produced by Integrated Assessment Models (IAMs) as internally consistent sets of emissions and socioeconomic assumptions (e.g., regarding population and socioeconomic development) with the aim of presenting several plausible future worlds (see Section 1.5.2 and Box 1.1). In general it is these scenarios that are used for policy relevant climate change, impact, adaptation and mitigation analysis. It is beyond the scope of this report to consider the full range of currently published scenarios and their implications for mitigation policy and climate targets—that is covered by the Working Group III contribution to the AR5. Here, we focus on the RCP scenarios used within the CMIP5 intercomparison exercise (Taylor et al. 2012) along with the SRES scenarios (IPCC, 2000) developed for the IPCC Third Assessment Report (TAR) but still widely used by the climate community.

#### 12.3.1.1 Stylized Concentration Scenarios

A 1% per annum compound increase of atmospheric CO<sub>2</sub> concentration until a doubling or a quadrupling of its initial value has been widely used since the second phase of CMIP (Meehl et al., 2000) and the Second Assessment Report (Kattenberg et al., 1996). This stylized scenario is a useful benchmark for comparing coupled model climate sensitivity, climate feedback and transient climate response, but is not used directly for future projections. The exponential increase of CO<sub>2</sub> concentration induces approximately a linear increase in RF due to a 'saturation effect' of the strong absorbing bands (Augustsson and Ramanathan, 1977; Hansen et al., 1988; Myhre et al., 1998). Thus, a linear ramp function in forcing results from these stylized pathways, adding to their suitability for comparative diagnostics of the models' climate feedbacks and inertia. The CMIP5 intercomparison project again includes such a stylized pathway, in which the CO<sub>2</sub> concentration reaches twice the initial concentration after 70 years and four times the initial concentration after 140 years. The corresponding RFs are 3.7 W m<sup>-2</sup> (Ramaswamy et al., 2001) and 7.4 W m<sup>-2</sup> respectively with a range of ±20% accounting for uncertainties in radiative transfer calculations and rapid adjustments (see Section 8.3.2.1), placing them within the range of the RFs at the end of the 21st century for the future scenarios presented below. The CMIP5 project also includes a second stylized experiment in which the CO<sub>2</sub> concentration is quadrupled instantaneously, which allows a distinction between effective RFs and longer-term climate feedbacks (Gregory et al., 2004).

#### 12.3.1.2 The Socioeconomic Driven Scenarios from the Special Report on Emission Scenarios

The climate change projections undertaken as part of CMIP3 and discussed in AR4 were based primarily on the SRES A2, A1B and B1 scenarios (IPCC, 2000). These scenarios were developed using IAMs and

resulted from specific socioeconomic scenarios, that is, from storylines about future demographic and economic development, regionalization, energy production and use, technology, agriculture, forestry, and land use. All SRES scenarios assumed that no climate mitigation policy would be undertaken. Based on these SRES scenarios, global climate models were then forced with corresponding WMGHG and aerosol concentrations, although the degree to which models implemented these forcings differed (Meehl et al., 2007b, Table 10.1). The resulting climate projections, together with the socioeconomic scenarios on which they are based, have been widely used in further analysis by the impact, adaptation and vulnerability research communities.

#### 12.3.1.3 The New Concentration Driven Representative Concentration Pathway Scenarios, and Their Extensions

As introduced in Box 1.1 and mentioned in Section 12.1, a new parallel process for scenario development was proposed in order to facilitate the interactions between the scientific communities working on climate change, adaptation and mitigation (Hibbard et al., 2007; Moss et al., 2008, 2010; van Vuuren et al., 2011). These new scenarios, Representative Concentration Pathways, are referred to as pathways in order to emphasize that they are not definitive scenarios, but rather internally consistent sets of time-dependent forcing projections that could potentially be realized with more than one underlying socioeconomic scenario. The primary products of the RCPs are concentrations but they also provide gas emissions. They are representative in that they are one of several different scenarios, sampling the full range of published scenarios (including mitigation scenarios) at the time they were defined, that have similar RF and emissions characteristics. They are identified by the approximate value of the RF (in W m<sup>-2</sup>) at 2100 or at stabilization after 2100 in their extensions, relative to pre-industrial (Moss et al., 2008; Meinshausen et al., 2011c). RCP2.6 (the lowest of the four, also referred to as RCP3-PD) peaks at 3.0 W m<sup>-2</sup> and then declines to 2.6 W m<sup>-2</sup> in 2100, RCP4.5 (medium-low) and RCP6.0 (medium-high) stabilize after 2100 at 4.2 and 6.0 W m<sup>-2</sup> respectively, while RCP8.5 (highest) reaches 8.3 W m<sup>-2</sup> in 2100 on a rising trajectory (see also Figure 12.3a which takes into account the efficacies of the various anthropogenic forcings). The primary objective of these scenarios is to provide all the input variables necessary to run comprehensive climate models in order to reach a target RF (Figure 12.2). These scenarios were developed using IAMs that provide the time evolution of a large ensemble of anthropogenic forcings (concentration and emission of gas and aerosols, land use changes, etc.) and their individual RF values (Moss et al., 2008, 2010; van Vuuren et al., 2011). Note that due to the substantial uncertainties in RF, these forcing values should be understood as comparative 'labels', not as exact definitions of the forcing that is effective in climate models. This is because concentrations or emissions, rather than the RF itself, are prescribed in the CMIP5 climate model runs. The forcing as manifested in climate models is discussed in Section 12.3.3.

Various steps were necessary to turn the selected 'raw' RCP scenarios from the IAMs into data sets usable by the climate modelling community. First, harmonization with historical data was performed for emissions of reactive gases and aerosols (Lamarque et al., 2010; Granier et al., 2011; Smith et al., 2011), land use (Hurt et al., 2011), and for GHG emissions and concentrations (Meinshausen et al., 2011c). Then

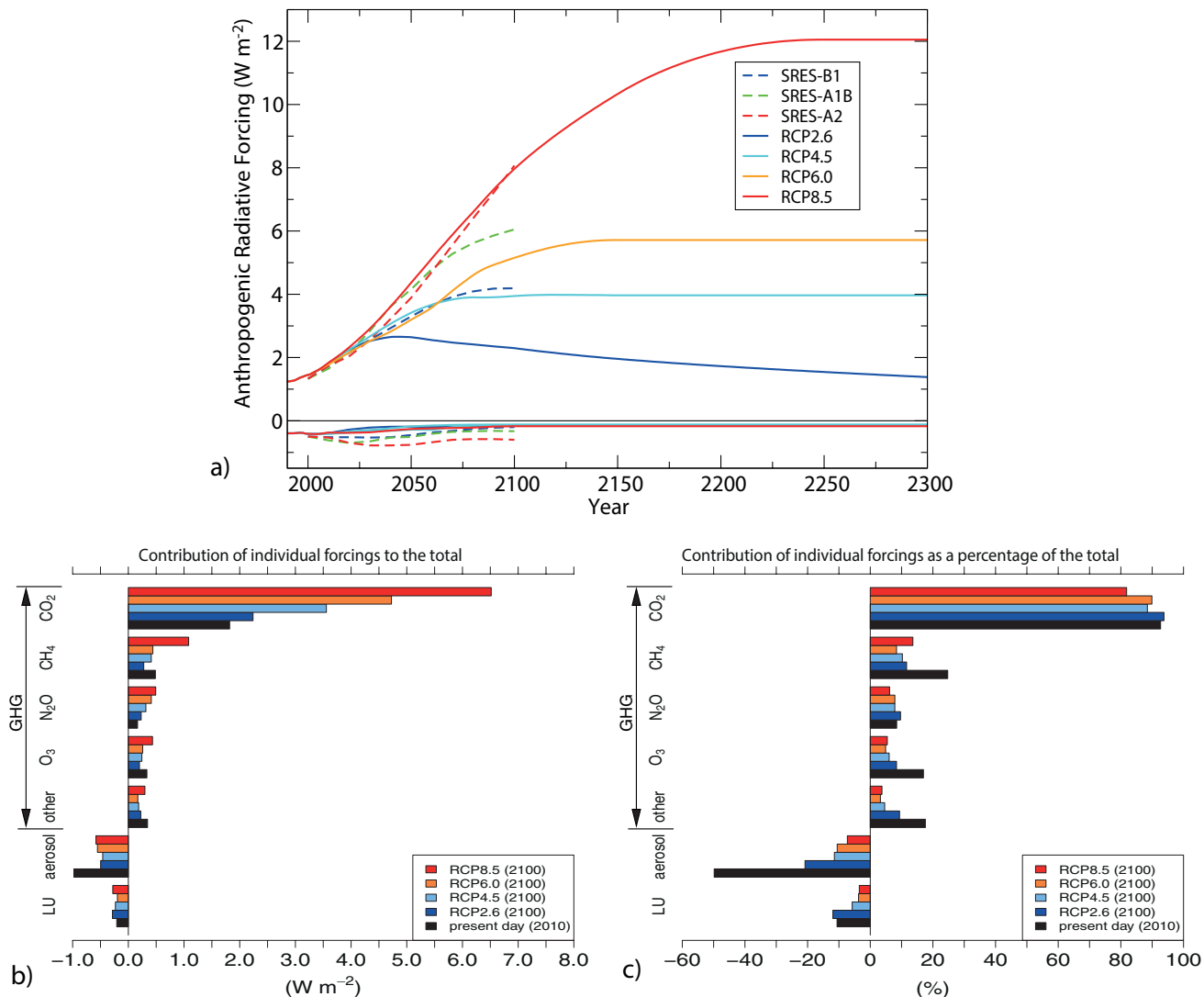


**Figure 12.3 |** (a) Time evolution of the total anthropogenic (positive) and anthropogenic aerosol (negative) radiative forcing (RF) relative to pre-industrial (about 1765) between 2000 and 2300 for RCP scenarios and their extensions (continuous lines), and SRES scenarios (dashed lines) as computed by the Integrated Assessment Models (IAMs) used to develop those scenarios. The four RCP scenarios used in CMIP5 are: RCP2.6 (dark blue), RCP4.5 (light blue), RCP6.0 (orange) and RCP8.5 (red). The three SRES scenarios used in CMIP3 are: B1 (blue, dashed), A1B (green, dashed) and A2 (red, dashed). Positive values correspond to the total anthropogenic RF. Negative values correspond to the forcing from all anthropogenic aerosol–radiation interactions (i.e., direct effects only). The total RF of the SRES and RCP families of scenarios differs in 2000 because the number of forcings represented and our knowledge about them have changed since the TAR. The total RF of the RCP family is computed taking into account the efficacy of the various forcings (Meinshausen et al., 2011a). (b) Contribution of the individual anthropogenic forcings to the total RF in year 2100 for the four RCP scenarios and at present day (year 2010). The individual forcings are gathered into seven groups: carbon dioxide (CO<sub>2</sub>), methane (CH<sub>4</sub>), nitrous oxide (N<sub>2</sub>O), ozone (O<sub>3</sub>), other greenhouse gases, aerosol (all effects unlike in (a), i.e., aerosol–radiation and aerosol–cloud interactions, aerosol deposition on snow) and land use (LU). (c) As in (b), but the individual forcings are relative to the total RF (i.e.,  $RF_x / RF_{tot}$ , in %, with  $RF_x$  individual RFs and  $RF_{tot}$  total RF). Note that the RFs in (b) and (c) are not efficacy adjusted, unlike in (a). The values shown in (a) are summarized in Table All.6.8. The values shown in (b) and (c) have been directly extracted from data files (hosted at <http://tntcat.iiasa.ac.at:8787/RcpDb/>) compiled by the four modelling teams that developed the RCP scenarios and are summarized in Tables All.6.1 to All.6.3 for CO<sub>2</sub>, CH<sub>4</sub> and N<sub>2</sub>O respectively.

atmospheric chemistry runs were performed to estimate ozone and aerosol distributions (Lamarque et al., 2011). Finally, a single carbon cycle model with a representation of carbon–climate feedbacks was used in order to provide consistent values of CO<sub>2</sub> concentration for the CO<sub>2</sub> emission provided by a different IAM for each of the scenarios. This methodology was used to produce consistent data sets across scenarios but does not provide uncertainty estimates for them. After these processing steps, the final RCP data sets comprise land use data, harmonized GHG emissions and concentrations, gridded reactive gas and aerosol emissions, as well as ozone and aerosol abundance fields. These data are used as forcings in individual climate models. The

number and type of forcings included primarily depend on the experiment. For instance, while the CO<sub>2</sub> concentration is prescribed in most experiments, CO<sub>2</sub> emissions are prescribed in some others (see Box 6.4 and Section 12.3.2.1). Which of these forcings are included in individual CMIP5 models, and variations in their implementation, is described in Section 12.3.2.2.

During this development process, the total RF and the RF of individual forcing agents have been estimated by the IAMs and made available via the RCP database (Meinshausen et al., 2011c). Each individual anthropogenic forcing varies from one scenario to another. They have

been aggregated into a few groups in Figure 12.3b and c. The total anthropogenic RF estimated by the IAMs in 2010 is about  $0.15 \text{ W m}^{-2}$  lower than Chapter 8's best estimate of ERF in 2010 ( $2.2 \text{ W m}^{-2}$ ), the difference arising from a revision of the RF due to aerosols and land use in the current assessment compared to AR4. All the other individual forcings are consistent to within  $0.02 \text{ W m}^{-2}$ . The change in  $\text{CO}_2$  concentration is the main cause of difference in the total RF among the scenarios (Figure 12.3b). The relative contribution<sup>5</sup> of  $\text{CO}_2$  to the total anthropogenic forcing is currently (year 2010) about 80 to 90% and does not vary much across the scenarios (Figure 12.3c), as was also the case for SRES scenarios (Ramaswamy et al., 2001). Aerosols have a large negative contribution to the total forcing (about  $-40$  to  $-50\%$  in 2010), but this contribution decreases (in both absolute and relative terms) in the future for all the RCPs scenarios. This means that while anthropogenic aerosols have had a cooling effect in the past, their decrease in all RCP scenarios relative to current levels is expected to have a net warming effect in the future (Levy II et al., 2013; see also Figure 8.20). The 21st century decrease in the magnitude of future aerosol forcing was not as large and as rapid in the SRES scenarios (Figure 12.3a). However, even in the SRES scenarios, aerosol effects were expected to have a diminishing role in the future compared to GHG forcings, mainly because of the accumulation of GHG in the atmosphere (Dufresne et al., 2005). Other forcings do not change much in the future, except  $\text{CH}_4$  which increases in the RCP8.5 scenario. Note that the estimates of all of these individual RFs are subject to many uncertainties (see Sections 7.5, 8.5 and 11.3.6). In this section and in Table AII.6.8, the RF values for RCP scenarios are derived from published equivalent- $\text{CO}_2$  ( $\text{CO}_2\text{eq}$ ) concentration data that aggregates all anthropogenic forcings including GHGs and aerosols. The conversion to RF uses the formula:  $\text{RF} = 3.71/\ln(2) \cdot \ln(\text{CO}_2\text{eq}/278) \text{ W m}^{-2}$ , where  $\text{CO}_2\text{eq}$  is in ppmv.

The four RCPs (Meinshausen et al., 2011c) are based on IAMs up to the end of the 21st century only. In order to investigate longer-term climate change implications, these RCPs were also extended until 2300. The extensions, formally named Extended Concentration Pathways (ECPs) but often simply referred to as RCP extensions, use simple assumptions about GHG and aerosol emissions and concentrations beyond 2100 (such as stabilization or steady decline) and were designed as hypothetical 'what-if' scenarios, not as an outcome of an IAM assuming socioeconomic considerations beyond 2100 (Meinshausen et al., 2011c) (see Box 1.1). In order to continue to investigate a broad range of possible climate futures, RCP2.6 assumes small constant net negative emissions after 2100 and RCP8.5 assumes stabilization with high emissions between 2100 and 2150, then a linear decrease until 2250. The two middle RCPs aim for a smooth stabilization of concentrations by 2150. RCP8.5 stabilizes concentrations only by 2250, with  $\text{CO}_2$  concentrations of approximately 2000 ppmv, nearly seven times the pre-industrial level. As RCP2.6 implies net negative  $\text{CO}_2$  emissions after around 2070 and throughout the extension,  $\text{CO}_2$  concentrations slowly reduce towards 360 ppmv by 2300.

### 12.3.1.4 Comparison of Special Report on Emission Scenarios and Representative Concentration Pathway Scenarios

The four RCP scenarios used in CMIP5 lead to RF values that range from  $2.3$  to  $8.0 \text{ W m}^{-2}$  at 2100, a wider range than that of the three SRES scenarios used in CMIP3 which vary from  $4.2$  to  $8.1 \text{ W m}^{-2}$  at 2100 (see Table AII.6.8 and Figure 12.3). The SRES scenarios do not assume any policy to control climate change, unlike the RCP scenarios. The RF of RCP2.6 is hence lower by  $1.9 \text{ W m}^{-2}$  than the three SRES scenarios and very close to the ENSEMBLES E1 scenario (Johns et al., 2011). RCP4.5 and SRES B1 have similar RF at 2100, and comparable time evolution (within  $0.2 \text{ W m}^{-2}$ ). The RF of SRES A2 is lower than RCP8.5 throughout the 21st century, mainly due to a faster decline in the radiative effect of aerosols in RCP8.5 than SRES A2, but they converge to within  $0.1 \text{ W m}^{-2}$  at 2100. RCP6.0 lies in between SRES B1 and SRES A1B. Results obtained with one General Circulation Model (GCM) (Dufresne et al., 2013) and with a reduced-complexity model (Rogelj et al., 2012) confirm that the differences in temperature responses are consistent with the differences in RFs estimates. RCP2.6, which assumes strong mitigation action, yields a smaller temperature increase than any SRES scenario. The temperature increase with the RCP4.5 and SRES B1 scenarios are close and the temperature increase is larger with RCP8.5 than with SRES A2. The spread of projected global mean temperature for the RCP scenarios (Section 12.4.1) is considerably larger (at both the high and low response ends) than for the three SRES scenarios used in CMIP3 (B1, A1B and A2) as a direct consequence of the larger range of RF across the RCP scenarios compared to that across the three SRES scenarios (see analysis of SRES versus RCP global temperature projections in Section 12.4.9 and Figure 12.40).

### 12.3.2 Implementation of Forcings in Coupled Model Intercomparison Project Phase 5 Experiments

The CMIP5 experimental protocol for long-term transient climate experiments prescribes a common basis for a comprehensive set of anthropogenic forcing agents acting as boundary conditions in three experimental phases—historical, RCPs and ECPs (Taylor et al., 2012). To permit common implementations of this set of forcing agents in CMIP5 models, self-consistent forcing data time series have been computed and provided to participating models (see Sections 9.3.2.2 and 12.3.1.3) comprising emissions or concentrations of GHGs and related compounds, ozone and atmospheric aerosols and their chemical precursors, and land use change.

The forcing agents implemented in Atmosphere–Ocean General Circulation Models (AOGCMs) and ESMs used to make long-term climate projections in CMIP5 are summarized in Table 12.1. The number of CMIP5 models listed here is about double the number of CMIP3 models listed in Table 10.1 of AR4 (Meehl et al., 2007b).

Natural forcings (arising from solar variability and aerosol emissions via volcanic activity) are also specified elements in the CMIP5 experimental protocol, but their future time evolutions are not prescribed

<sup>5</sup> The range of the relative contribution of  $\text{CO}_2$  and aerosols to the total anthropogenic forcing is derived here from the RF values given by the IAMs and the best estimate assessed in Chapter 8.

**Table 12.1** Radiative forcing agents in the CMIP5 multi-model global climate projections. See Table 9.A.1 for descriptions of the models and main model references. Earth System Models (ESMs) are highlighted in bold. Numeric superscripts indicate model-specific references that document forcing implementations. Forcing agents are mostly implemented in close conformance with standard prescriptions (Taylor et al., 2012) and recommended data sets (Lamarque et al., 2010; Cionni et al., 2011; Lamarque et al., 2011; Meinshausen et al., 2011c) provided for CMIP5. Variations in forcing implementations are highlighted with superscripts and expanded in the table footnotes. Entries mean: n.a.: Forcing agent is not included in either the historical or future scenario simulations; Y: Forcing agent included (via prescribed concentrations, distributions or time series data); E: Concentrations of forcing agent calculated interactively driven by prescribed emissions or precursor emissions; Es: Concentrations of forcing agent calculated interactively constrained by prescribed surface concentrations. For a more detailed classification of ozone chemistry and ozone forcing implementations in CMIP5 models see Eyring et al. (2013).

Model	Greenhouse Gases							Forcing Agents							Other			
	CO <sub>2</sub> <sup>ee</sup>	CH <sub>4</sub>	N <sub>2</sub> O	Trop O <sub>3</sub>	Strat O <sub>3</sub>	CFCs	SO <sub>4</sub>	Black carbon	Organic carbon	Nitrate	Cloud albedo effect <sup>ac</sup>	Cloud lifetime effect <sup>ac</sup>	Dust	Volcanic	Sea salt	Land use	Solar	
ACCESS-1.0 <sup>1</sup>	Y <sup>p</sup>	Y	Y	Y <sup>b</sup>	Y <sup>b</sup>	Y	E	E	E	n.a.	Y	Y	Y <sup>pd</sup>	Y <sup>v5</sup>	Y <sup>pd</sup>	n.a.	Y	
ACCESS-1.3 <sup>1</sup>	Y <sup>p</sup>	Y	Y	Y <sup>b</sup>	Y <sup>b</sup>	Y	E	E	E	n.a.	Y	Y	n.a.	Y <sup>v5</sup>	Y <sup>pd</sup>	n.a.	Y	
<b>BCC-CSM1.1<sup>2</sup></b>	Y/E <sup>p</sup>	Y	Y	Y <sup>b</sup>	Y <sup>b</sup>	Y	Y <sup>a</sup>	Y <sup>a</sup>	Y <sup>a</sup>	n.a.	n.a.	Y <sup>a</sup>	Y <sup>a</sup>	Y <sup>v0</sup>	Y <sup>a</sup>	n.a.	Y	
<b>BCC-CSM1.1(m)<sup>2</sup></b>	Y/E <sup>p</sup>	Y	Y	Y <sup>b</sup>	Y <sup>b</sup>	Y	Y <sup>a</sup>	Y <sup>a</sup>	Y <sup>a</sup>	n.a.	n.a.	Y <sup>a</sup>	Y <sup>a</sup>	Y <sup>v0</sup>	Y <sup>a</sup>	n.a.	Y	
<b>BNU-ESM</b>	Y/E <sup>p</sup>	Y	Y	Y <sup>a</sup>	Y <sup>a</sup>	Y	Y <sup>a</sup>	Y <sup>a</sup>	Y <sup>a</sup>	n.a.	n.a.	Y <sup>a</sup>	Y <sup>a</sup>	Y <sup>v0</sup>	Y <sup>a</sup>	n.a.	Y	
CanCM4	Y	Y	Y	Y <sup>b</sup>	Y <sup>b</sup>	Y	E	E	E	n.a.	Y <sup>so</sup>	n.a.	Y <sup>pd</sup>	Y/E <sup>std0</sup>	Y <sup>pd</sup>	n.a.	Y	
<b>CanESM2</b>	Y/E <sup>p</sup>	Y	Y	Y <sup>b</sup>	Y <sup>b</sup>	Y	E	E	E	n.a.	Y <sup>so</sup>	n.a.	Y <sup>pd</sup>	Y/E <sup>std0</sup>	Y <sup>pd</sup>	Y <sup>cr</sup>	Y	
CCSM4 <sup>3</sup>	Y <sup>p</sup>	Y	Y	Y <sup>a</sup>	Y <sup>a</sup>	Y	Y <sup>a</sup>	Y <sup>a</sup>	Y <sup>a</sup>	n.a.	n.a.	Y <sup>a</sup>	Y <sup>a</sup>	Y <sup>v0</sup>	Y <sup>a</sup>	Y	Y	
<b>CESM1(BGC)<sup>4</sup></b>	Y/E <sup>p</sup>	Y	Y	Y <sup>a</sup>	Y <sup>a</sup>	Y	Y <sup>a</sup>	Y <sup>a</sup>	Y <sup>a</sup>	n.a.	n.a.	Y <sup>a</sup>	Y <sup>a</sup>	Y <sup>v0</sup>	Y <sup>a</sup>	Y	Y	
CESM1(CAM5) <sup>5</sup>	Y <sup>p</sup>	Y	Y	Y <sup>a</sup>	Y <sup>a</sup>	Y	E	E	E	n.a.	Y	Y	E	Y <sup>v0</sup>	E	Y	Y	
CESM1(CAM5.1,FV2) <sup>5</sup>	Y <sup>p</sup>	Y	Y	Y <sup>a</sup>	Y <sup>a</sup>	Y	E	E	E	n.a.	Y	Y	E	Y <sup>v0</sup>	E	Y	Y	
CESM1(FASTCHEM)	Y <sup>a</sup>	Y	Y	E	E	Y	E	Y <sup>a</sup>	Y <sup>a</sup>	n.a.	n.a.	Y <sup>a</sup>	Y <sup>a</sup>	Y <sup>v0</sup>	Y <sup>a</sup>	Y	Y	
CESM1(WACCM) <sup>6</sup>	Es <sup>p</sup>	Es	E/E <sup>op</sup>	E/E <sup>op</sup>	Es	Y	Y	Y	Y	n.a.	n.a.	Y <sup>a</sup>	Y <sup>a</sup>	Y <sup>v0</sup>	Y <sup>a</sup>	Y	Y	
<b>CMCC-CESM<sup>7</sup></b>	Y	Y	Y	Y <sup>b</sup>	Y <sup>b</sup>	Y <sup>b</sup>	n.a.	n.a.	n.a.	n.a.	Y <sup>so</sup>	n.a.	Y <sup>fk</sup>	n.a.	Y <sup>fk</sup>	n.a.	Y <sup>or</sup>	
CMCC-CM	Y	Y	Y	Y <sup>b</sup>	Y <sup>b</sup>	Y <sup>b</sup>	n.a.	n.a.	n.a.	n.a.	Y <sup>so</sup>	n.a.	Y <sup>fk</sup>	n.a.	Y <sup>fk</sup>	n.a.	Y <sup>or</sup>	
CMCC-CMS	Y	Y	Y	Y <sup>b</sup>	Y <sup>b</sup>	Y <sup>b</sup>	n.a.	n.a.	n.a.	n.a.	Y <sup>so</sup>	n.a.	Y <sup>fk</sup>	n.a.	Y <sup>fk</sup>	n.a.	Y <sup>or</sup>	
CNRM-CM5 <sup>8</sup>	Y	Y	Y <sup>c</sup>	Y <sup>c</sup>	Y <sup>c</sup>	Y <sup>e</sup>	Y <sup>e</sup>	Y <sup>e</sup>	Y <sup>e</sup>	n.a.	Y <sup>so<sub>ik</sub></sup>	n.a.	Y <sup>e</sup>	Y <sup>v1</sup>	Y <sup>e</sup>	n.a.	Y	
CSIRO-Mk3.6.0 <sup>9</sup>	Y	Y	Y	Y <sup>b</sup>	Y <sup>b</sup>	Y <sup>b</sup>	n.a.	n.a.	n.a.	n.a.	Y <sup>so</sup>	n.a.	Y <sup>fk</sup>	Y <sup>v0</sup>	Y <sup>pd</sup>	n.a.	Y	
EC-EARTH <sup>10</sup>	Y	Y	Y <sup>b</sup>	Y <sup>b</sup>	Y <sup>a</sup>	Y <sup>a</sup>	Y <sup>a</sup>	Y <sup>a</sup>	Y <sup>a</sup>	n.a.	n.a.	Y <sup>a</sup>	Y <sup>a</sup>	Y <sup>v1</sup>	Y <sup>a</sup>	Y	Y	
FGOALS-g2 <sup>11</sup>	Y	Y	Y	Y <sup>b</sup>	Y <sup>b</sup>	Y <sup>a</sup>	Y <sup>a</sup>	Y <sup>a</sup>	Y <sup>a</sup>	n.a.	Y	Y	n.a.	Y <sup>a</sup>	n.a.	Y	Y	
<b>FGOALS-g2<sup>12</sup></b>	Y/E	Y	Y	Y <sup>b</sup>	Y <sup>b</sup>	Y <sup>b</sup>	Y <sup>a</sup>	Y <sup>a</sup>	Y <sup>a</sup>	n.a.	n.a.	Y <sup>a</sup>	Y <sup>a</sup>	Y <sup>v0</sup>	Y <sup>a</sup>	n.a.	Y	
<b>FIO-ESM</b>	Y/E	Y	Y	Y <sup>a</sup>	Y <sup>a</sup>	Y	Y <sup>a</sup>	Y <sup>a</sup>	Y <sup>a</sup>	n.a.	n.a.	Y <sup>a</sup>	Y <sup>a</sup>	Y <sup>v0</sup>	Y <sup>a</sup>	n.a.	Y	
GFDL-CM3 <sup>13</sup>	Y <sup>p</sup>	Y/E <sup>rc</sup>	E	E	E	Y/E <sup>rc</sup>	E	E	E	n.a./E <sup>rc</sup>	Y	Y	E <sup>pd</sup>	Y/E <sup>std0</sup>	E <sup>pd</sup>	Y	Y	
<b>GFDL-ESM2G</b>	Y/E <sup>p</sup>	Y	Y	Y <sup>b</sup>	Y <sup>b</sup>	Y	Y	Y <sup>a</sup>	Y <sup>a</sup>	n.a.	n.a.	Y <sup>fk</sup>	Y <sup>fk</sup>	Y	Y	Y	Y	
<b>GFDL-ESM2M</b>	Y/E <sup>p</sup>	Y	Y	Y <sup>b</sup>	Y <sup>b</sup>	Y	Y <sup>a</sup>	Y <sup>a</sup>	Y <sup>a</sup>	n.a.	n.a.	Y <sup>fk</sup>	Y <sup>fk</sup>	Y	Y	Y	Y	
GISS-E2-p1 <sup>14</sup>	Y	Y	Y	Y <sup>d</sup>	Y <sup>d</sup>	Y	Y	Y	Y	n.a.	n.a.	Y <sup>fk</sup>	Y <sup>fk</sup>	Y	Y	Y <sup>or</sup>	Y <sup>or</sup>	
GISS-E2-p2 <sup>14</sup>	Y	Y	Es/E <sup>Hf</sup>	Es	E	E	E	E	E	n.a.	Y <sup>pd</sup>	Y <sup>pd</sup>	Y <sup>pd</sup>	Y <sup>pd</sup>	Y	Y	Y <sup>or</sup>	Y <sup>or</sup>

(continued on next page)

Table 12.1 (continued)

Model	Greenhouse Gases										Forcing Agents						Other	
	CO <sub>2</sub> <sup>ee</sup>	CH <sub>4</sub>	N <sub>2</sub> O	Trop O <sub>3</sub>	Strat O <sub>3</sub>	CFCs	SO <sub>4</sub>	Black carbon	Organic carbon	Nitrate	Cloud albedo effect	Cloud lifetime effect <sup>ac</sup>	Dust	Volcanic	Sea salt	Land use	Solar	
GISS-E2-p3 <sup>14</sup>	Y	Es/E <sup>nf</sup>	Es	E	E	E <sub>SE</sub> E <sup>nf</sup>	E	E	E	n.a.	n.a.	n.a.	Y <sup>pd</sup>	Y <sup>v4</sup>	Y <sup>pd</sup>	Y	Y <sup>cr</sup>	
HadCM3	Y <sup>p</sup>	Y	Y	Y <sub>b</sub>	Y <sub>b</sub>	Y <sup>b</sup>	Y	E	n.a.	n.a.	Y <sub>50</sub>	n.a.	n.a.	Y <sup>v2</sup>	n.a.	n.a.	Y	
HadGEM2-AO <sup>15</sup>	Y <sup>p</sup>	Y	Y	Y	Y <sub>b</sub>	Y <sup>b</sup>	Y	E	E	n.a.	Y	Y	Y <sup>pd</sup>	Y <sup>v2</sup>	Y <sup>pd</sup>	Y	Y	
HadGEM2-CC <sup>16,17</sup>	Y <sup>p</sup>	Y	Y	Y <sub>b</sub>	Y <sup>b</sup>	Y <sup>b</sup>	Y	E	E	n.a.	Y	Y	Y <sup>pd</sup>	Y <sup>v2</sup>	Y <sup>pd</sup>	Y	Y	
HadGEM2-ES <sup>16</sup>	Y/E <sup>p</sup>	Es	Y	E	Y <sup>b</sup>	Y <sup>b</sup>	Y	E	E	n.a.	Y	Y	Y <sup>pd</sup>	Y <sup>v2</sup>	Y <sup>pd</sup>	Y	Y	
INM-CM4	Y/E	Y	Y	Y <sub>b</sub>	Y <sup>b</sup>	Y <sup>b</sup>	n.a.	Y <sup>fc</sup>	n.a.	n.a.	Y <sub>50</sub>	n.a.	n.a.	Y <sup>v0</sup>	n.a.	n.a.	Y	
IPSL-CM5A-LR <sup>18</sup>	Y/E <sup>p</sup>	Y	Y	Y <sup>e</sup>	Y <sup>e</sup>	Y <sup>e</sup>	Y	Y <sup>e</sup>	Y <sup>e</sup>	n.a.	Y	n.a.	Y <sup>e</sup>	Y <sup>v1</sup>	Y <sup>e</sup>	Y	Y	
IPSL-CM5A-MR <sup>18</sup>	Y/E <sup>p</sup>	Y	Y	Y <sup>e</sup>	Y <sup>e</sup>	Y <sup>e</sup>	Y	Y <sup>e</sup>	Y <sup>e</sup>	n.a.	Y	n.a.	Y <sup>e</sup>	Y <sup>v1</sup>	Y <sup>e</sup>	Y	Y	
IPSL-CM5B-LR <sup>18</sup>	Y <sup>p</sup>	Y	Y	Y <sup>e</sup>	Y <sup>e</sup>	Y <sup>e</sup>	Y	Y <sup>e</sup>	Y <sup>e</sup>	n.a.	Y	n.a.	Y <sup>e</sup>	Y <sup>v1</sup>	Y <sup>e</sup>	Y	Y	
MIROC-ESM <sup>19</sup>	Y/E <sup>p</sup>	Y	Y	Y <sup>f</sup>	Y <sup>f</sup>	Y <sup>f</sup>	Y	E	E	n.a.	Y <sup>fc</sup>	n.a.	Y <sup>pd</sup>	Y <sup>v3</sup>	Y <sup>pd</sup>	Y	Y	
MIROC-ESM-CHEM <sup>19</sup>	Y <sup>p</sup>	Y	Y	E	E	Y	E	E	E	n.a.	Y <sup>fc</sup>	n.a.	Y <sup>pd</sup>	Y <sup>v3</sup>	Y <sup>pd</sup>	Y	Y	
MIROC4-h20	Y <sup>p</sup>	Y	Y	Y <sup>g</sup>	Y <sup>g</sup>	Y <sup>g</sup>	Y	E	E	n.a.	Y	n.a.	Y <sup>pd</sup>	Y <sup>v3</sup>	Y <sup>pd</sup>	Y	Y	
MIROC5 <sup>20</sup>	Y <sup>p</sup>	Y	Y	Y <sup>f</sup>	Y <sup>f</sup>	Y <sup>f</sup>	Y	E	E	n.a.	Y <sup>fc</sup>	n.a.	Y <sup>pd</sup>	Y <sup>v3</sup>	Y <sup>pd</sup>	Y	Y	
MPI-ESM-LR	Y/E <sup>p</sup>	Y	Y	Y <sup>b</sup>	Y <sup>b</sup>	Y <sup>b</sup>	Y	Y <sup>h</sup>	Y <sup>h</sup>	n.a.	Y <sup>h</sup>	n.a.	Y <sup>v0</sup>	Y <sup>v1</sup>	Y <sup>v0</sup>	Y	Y <sup>cr</sup>	
MPI-ESM-MR	Y <sup>p</sup>	Y	Y	Y <sup>b</sup>	Y <sup>b</sup>	Y <sup>b</sup>	Y	Y <sup>h</sup>	Y <sup>h</sup>	n.a.	Y <sup>h</sup>	n.a.	Y <sup>v0</sup>	Y <sup>v1</sup>	Y <sup>v0</sup>	Y	Y <sup>cr</sup>	
MPI-ESM-P	Y <sup>p</sup>	Y	Y	Y <sup>b</sup>	Y <sup>b</sup>	Y <sup>b</sup>	Y	Y <sup>h</sup>	Y <sup>h</sup>	n.a.	Y <sup>h</sup>	n.a.	Y <sup>v0</sup>	Y <sup>v1</sup>	Y <sup>v0</sup>	Y	Y <sup>cr</sup>	
MRI-CGCM3 <sup>21</sup>	Y	Y	Y	Y <sup>b</sup>	Y <sup>b</sup>	Y <sup>b</sup>	Y	E	E	n.a.	Y <sup>h</sup>	n.a.	Y <sup>pd</sup>	E <sup>v0</sup>	E <sup>pd</sup>	Y	Y	
MRI-ESM <sup>22</sup>	E	Y	Y	E	E	E	Es	E	E	n.a.	Y <sup>h</sup>	n.a.	Y <sup>pd</sup>	E <sup>v0</sup>	E <sup>pd</sup>	Y	Y	
NorESM1-M <sup>23</sup>	Y <sup>p</sup>	Y	Y	Y <sup>a</sup>	Y <sup>a</sup>	Y <sup>a</sup>	Y	E	E	n.a.	Y	n.a.	Y <sup>pd</sup>	Y <sup>stn1</sup>	E <sup>pd</sup>	Y	Y	
NorESM1-ME <sup>23</sup>	Y/E <sup>p</sup>	Y	Y	Y <sup>a</sup>	Y <sup>a</sup>	Y <sup>a</sup>	Y	E	E	n.a.	Y	n.a.	Y <sup>pd</sup>	Y <sup>stn1</sup>	E <sup>pd</sup>	Y	Y	

Notes:

Model-specific references relating to forcing implementations:

- 1 Dix et al. (2013)
- 2 Wu et al. (2013); Xin et al. (2013a, 2013b)
- 3 Meehl et al. (2012); Gent et al. (2011)
- 4 Long et al. (2013); Meehl et al. (2012)
- 5 Meehl et al. (2013)
- 6 Calvo et al. (2012); Meehl et al. (2012)
- 7 Cagnazzo et al. (2013)
- 8 Voldoire et al. (2013)
- 9 Rorstan et al. (2012)
- 10 Hazeleger et al. (2013)
- 11 Li et al. (2013c)
- 12 Bao et al. (2013)
- 13 Levy II et al. (2013)
- 14 Stindell et al. (2013a). GISS-E2-R and GISS-E2-H model variants are forced similarly and both represented here as GISS-E2. Both R and H model versions have three variants; in physics version 1 (p1) aerosols and ozone are specified from pre-computed transient aerosol and ozone fields, in physics version 2 (p2) aerosols and atmospheric chemistry are calculated online as a function of atmospheric state and transient emissions inventories, while in physics version 3 (p3) atmospheric composition is calculated as for p2 but the aerosol impacts on clouds and hence the aerosol indirect effect is calculated interactively. In p1 and p2 variants the aerosol indirect effect is parameterized following Hansen et al. (2005b).
- 15 HadGEM2-AO is forced in a similar way to HadGEM2-ES and HadGEM2-CC following Jones et al. (2011), but tropospheric ozone, stratospheric ozone and land cover are prescribed.
- 16 Jones et al. (2011)
- 17 Heldman et al. (2012)
- 18 Dufresne et al. (2013)
- 19 Watanabe et al. (2011)
- 20 Komuro et al. (2012)
- 21 Yukimoto et al. (2012)
- 22 Adachi et al. (2013)
- 23 Iversen et al. (2013); Killekäg et al. (2013); Tipputra et al. (2013)

(continued on next page)

Table 12.1 (continued)

Additional notes:	
<sup>e</sup> Separate entries for $\text{CO}_2$ denote 'concentration-driven' and 'emissions-driven' experiments as indicated.	
<sup>f</sup> 'Cloud albedo effect' and 'Cloud lifetime effect' are classical terms (as used in AR4) to describe indirect effects of radiative forcing associated with aerosols. They relate to the revised terminologies defined in Chapter 7 and used in AR5: 'Radiative forcing from aerosol–cloud interactions (RFaci)' and 'Effective radiative forcing from aerosol–cloud interactions (ERFaci)'. RFaci equates to cloud albedo effect, while ERFaci is the effective forcing resulting from cloud albedo effect plus cloud lifetime effect, including all rapid adjustments to cloud lifetime and thermodynamics (Section 7.1.3, Figure 7.3).	
<sup>g</sup> Physiological forcing effect of $\text{CO}_2$ , via plant stomatal response and evapotranspiration (Betts et al., 2007) included.	
<sup>h</sup> Separate entries denote different treatments used for radiation and chemistry respectively.	
<sup>i</sup> Separate entries denote treatment for historical and future (RCPs) respectively.	
<sup>j</sup> Three-dimensional tropospheric ozone, stratospheric ozone, methane, and/or aerosol distributions specified as monthly 10-year mean concentrations, computed off-line using CAM-Chem – a modified version of CAM3.5 with interactive chemistry – driven with specified emissions for the historical period (Lamarque et al., 2010) and RCPs (Lamarque et al., 2011) with sea surface temperature and sea ice boundary conditions based on CCSM3's projections for the closest corresponding AR4 scenarios.	
<sup>k</sup> Ozone prescribed using the original or slightly modified IGAC/SPARC ozone data set (Cionni et al., 2011); in some models this data set is modified to add a future solar cycle and in some models tropospheric ozone is zonally averaged.	
<sup>l</sup> Linearized 2D ozone chemistry scheme (Cariolle and Teyssede, 2007) including transport and photochemistry, reactive to stratospheric chlorine concentrations but not tropospheric chemical emissions.	
<sup>m</sup> Ozone prescribed using the data set described in Hansen et al. (2007), with historical tropospheric ozone being calculated by a CCM and stratospheric ozone taken from Randel and Wu (2007) in the past. Tropospheric ozone is held constant from 1990 onwards, while stratospheric ozone is constant from 1997 to 2003 and then returned linearly to its 1979 value over the period 2004 to 2050.	
<sup>n</sup> For IPSL-CM5 model versions, ozone and aerosol concentrations are calculated semi-offline with the atmospheric general circulation model including interactive chemistry and aerosol, following the four RCPs in the future (Dufresne et al., 2013; Szopa et al., 2013). The same aerosol concentration fields (but not ozone) are also prescribed for the CNRM-CM5 model.	
<sup>o</sup> Radiative effects of aerosols on ice clouds are represented.	
<sup>p</sup> Prognostic or diagnostic scheme for dust/sea salt aerosol with emissions/concentrations determined by the model state rather than externally prescribed.	
<sup>q</sup> Fixed prescribed climatology of dust/sea salt aerosol concentrations with no year-to-year variability.	
<sup>r</sup> Explosive volcanic aerosol returns rapidly in future to zero (or near-zero) background, like that in the pre-industrial control experiment.	
<sup>s</sup> Explosive volcanic aerosol returns rapidly in future to constant (average volcano) background, the same as in the pre-industrial control experiment.	
<sup>t</sup> Explosive volcanic aerosol returns slowly in future (over several decades) to constant (average volcano) background like that in the pre-industrial control experiment.	
<sup>u</sup> Explosive volcanic aerosol returns slowly in future to near-zero background, below that in the pre-industrial control experiment.	
<sup>v</sup> Explosive volcanic aerosol returns slowly in future (over several decades) to constant (average volcano) background, the same as in the pre-industrial control experiment.	
<sup>w</sup> Explosive volcanic aerosol returns rapidly in future to near-zero background, below that in the pre-industrial control experiment.	
<sup>x</sup> Land use change represented via crop change only.	
<sup>y</sup> Realistic time-varying orbital parameters for solar forcing (in historical period only for GISS-E2).	

very precisely. A repeated 11-year cycle for total solar irradiance (Lean and Rind, 2009) is suggested for future projections but the periodicity is not specified precisely as solar cycles vary in length. Some models include the effect of orbital variations as well, but most do not. For volcanic eruptions, no specific CMIP5 prescription is given for future emissions or concentration data, the general recommendation being that volcanic aerosols should either be omitted entirely both from the control experiment and future projections or the same background volcanic aerosols should be prescribed in both. This provides a consistent framework for model intercomparison given a lack of knowledge of when future large eruptions will occur. In general models have adhered to this guidance, but there are variations in the background volcanic aerosol levels chosen (zero or an average volcano background in general) and some cases, for example, Australian Community Climate and Earth System Simulator (ACCESS)1.0 and ACCESS1.3 (Dix et al., 2013), where the background volcanic aerosol in future differs significantly from that in the control experiment, with a small effect on future RF.

For the other natural aerosols (dust, sea-salt, etc.), no emission or concentration data are recommended. The emissions are potentially computed interactively by the models themselves and may change with climate, or prescribed from separate model simulations carried out in the implementation of CMIP5 experiments, or simply held constant. Natural aerosols (mineral dust and sea salt) are in a few cases prescribed with no year-to-year variation (giving no transient forcing effect), in some cases prescribed from data sets computed off-line as described above, and in other cases calculated interactively via prognostic or diagnostic calculations. The degree to which natural aerosol emissions are interactive is effectively greater in some such models than others, however, as mineral dust emissions are more constrained when land vegetation cover is specified (e.g., as in Commonwealth Scientific and Industrial Research Organisation (CSIRO)-Mk3.6.0) (Rotstayn et al., 2012) than when vegetation is allowed to evolve dynamically (e.g., as in Hadley Centre new Global Environmental Model 2-ES (HadGEM2-ES)) (Jones et al., 2011) (Table 9.A.1).

### 12.3.2.1 'Emissions-Driven' versus 'Concentration Driven' Experiments

A novel feature within the CMIP5 experimental design is that experiments with prescribed anthropogenic emissions are included in addition to classical experiments with prescribed concentration pathways for WMGHGs (Taylor et al., 2012). The essential features of these two classes of experiment are described in Box 6.4. The CMIP5 protocol includes experiments in which 'ESMs' (models possessing at least a carbon cycle, allowing for interactive calculation of atmospheric CO<sub>2</sub> or compatible emissions) and AOGCMs (that do not possess such an interactive carbon cycle) are both forced with WMGHG concentration pathways to derive a range of climate responses consistent with those pathways from the two types of model. The range of climate responses including climate–carbon cycle feedbacks can additionally be explored in ESMs driven with emissions rather than concentrations, analogous to Coupled Climate Carbon Cycle Model Intercomparison Project (C<sup>4</sup>MIP) experiments (Friedlingstein et al., 2006)—see Box 6.4. Results from the two types of experiment cannot be compared directly, but they provide complementary information. Uncertainties in the forward

climate response driven with specified emissions or concentrations can be derived from all participating models, while concentration-driven ESM experiments also permit a policy-relevant diagnosis of the range of anthropogenic carbon emissions compatible with the imposed concentration pathways (Hibbard et al., 2007; Moss et al., 2010).

WMGHG forcing implementations in CMIP5 concentration-driven experiments conform closely in almost all cases to the standard protocol (Table 12.1; CO<sub>2</sub>, CH<sub>4</sub>, N<sub>2</sub>O, chlorofluorocarbons (CFCs)), imposing an effective control over the RF due to WMGHGs across the multi-model ensemble, apart from the model spread arising from radiative transfer codes (Collins et al., 2006b; Meehl et al., 2007b). The ability of ESMs to determine their own WMGHG concentrations in emissions-driven experiments means that RF due to WMGHGs is less tightly controlled in such experiments. Even in concentration-driven experiments, many models implement some emissions-driven forcing agents (more often aerosols, but also ozone in some cases), leading to a potentially greater spread in both the concentrations and hence RF of those emissions-driven agents.

### 12.3.2.2 Variations Between Model Forcing Implementations

Apart from the distinction between concentration-driven and emissions-driven protocols, a number of variations are present in the implementation of forcing agents listed in Table 12.1, which generally arise due to constraining characteristics of the model formulations, various computational efficiency considerations or local implementation decisions. In a number of models, off-line modelling using an aerosol chemistry climate model has been used to convert emissions into concentrations compatible with the specific model formulation or characteristics. As a result, although detailed prescriptions are given for the forcing agents in CMIP5 experiments in emissions terms, individual modelling approaches lead to considerable variations in their implementations and consequential RFs. This was also the case in the ENSEMBLES multi-model projections, in which similar forcing agents to CMIP5 models were applied but again with variations in the implementation of aerosol, ozone and land use forcings, prescribing the SRES A1B and E1 scenarios in a concentration-driven protocol (Johns et al., 2011) akin to the CMIP5 protocol.

Methane, nitrous oxide and CFCs (typically with some aggregation of the multiple gases) are generally prescribed in CMIP5 models as well-mixed concentrations following the forcing data time series provided for the given scenarios. In a number of models (CESM1(WACCM), GFDL-CM3, GISS-E2-p2, GISS-E2-p3, HadGEM2-ES and MRI-ESM1) the three-dimensional concentrations in the atmosphere of some species evolve interactively driven by the full emissions/sinks cycle (in some cases constrained by prescribed concentrations at the surface, e.g., HadGEM2-ES for methane). In cases where the full emissions/sinks cycle is modelled, the radiation scheme is usually passed the time-varying 3-D concentrations, but some models prescribe different concentrations for the purpose of radiation.

Eyring et al. (2013) document, in greater detail than Table 12.1, the implementations of tropospheric and stratospheric ozone in CMIP5 models, including their ozone chemistry schemes and modifications applied to reference data sets in models driven by concentrations. In

most models that prescribe ozone, concentrations are based on the original or slightly modified CMIP5 standard ozone data set computed as part of the International Global Atmospheric Chemistry/Stratospheric Processes and their Role in Climate (IGAC/SPARC) activity (Cionni et al., 2011). In the stratosphere, this data set is based on observations of the past (Randel and Wu, 2007) continued into the future with the multi-model mean of 13 chemistry–climate models (CCMs) projections following the SRES A1B (IPCC, 2000) and SRES A1 adjusted halogen scenario (WMO, 2007). The stratospheric zonal mean ozone field is merged with a 3-D tropospheric ozone time series generated as the mean of two CCMs (Goddard Institute of Space Studies-Physical Understanding of Composition-Climate Interactions and Impacts (GISS-PUCCINI), Shindell et al., 2006; CAM3.5, Lamarque et al., 2010) in the past and continued by one CCM (CAM3.5) in the future. Some CMIP5 models (MIROC-ESM, MIROC4h, MIROC5 and GISS-E2-p1) prescribe ozone concentrations using different data sets but again following just one GHG scenario in the future for the projection of stratospheric ozone. In other models (e.g., Institut Pierre Simon Laplace (IPSL)-CM5, CCSM4) ozone is again prescribed, but supplied as concentrations from off-line computations using a related CCM. Some models determine ozone interactively from specified emissions via on-line atmospheric chemistry (CESM1(FASTCHEM), CESM1(WACCM), CNRM-CM5, GFDL-CM3, GISS-E2-p2, GISS-E2-p3, MIROC-ESM-CHEM, MRI-ESM1; and HadGEM2-ES for tropospheric ozone only). Computing ozone concentrations interactively allows the fast coupling between chemistry and climate to be captured, but modelling of chemistry processes is sometimes simplified (CNRM-CM5, CESM(FASTCHEM)) in comparison with full complexity CCMs to reduce the computational cost. Compared to CMIP3, in which all models prescribed ozone and around half of them used a fixed ozone climatology, this leads to substantial improvement to ozone forcings in CMIP5, although differences remain among the models with interactive chemistry.

For atmospheric aerosols, either aerosol precursor emissions-driven or concentration-driven forcings are applied depending on individual model characteristics (see Sections 7.3 and 7.4 for an assessment of aerosols processes including aerosol–radiation and aerosol–cloud interactions). A larger fraction of models in CMIP5 than CMIP3 prescribe aerosol precursor emissions rather than concentrations. Many still prescribe concentrations pre-computed either using a directly related aerosol CCM or from output of another, complex, emissions-driven aerosol chemistry model within the CMIP5 process. As for ozone, aerosol concentrations provided from off-line simulations help to reduce the computational burden of the projections themselves. For several of the concentration-driven models (CCSM4, IPSL-CM5A variants, MPI-ESM-LR, MPI-ESM-MR), additional emissions-driven simulations have been undertaken to tailor the prescribed concentrations closely to the model’s individual aerosol–climate characteristics. Lamarque et al. (2010, 2011) provided the recommended CMIP5 aerosols data set which has been used in several of the models driven by concentrations. Compared with the CMIP3 models, a much larger fraction of CMIP5 models now incorporate black and organic carbon aerosol forcings. Also, a larger fraction of CMIP5 than CMIP3 models now includes a range of processes that combine in the effective RF from aerosol–cloud interactions (ERFaci; see Section 7.1.3 and Figure 7.3). Previously such processes were generally termed aerosol indirect effects, usually separated into cloud albedo (or first indirect) effect and cloud

lifetime (or second indirect) effect. Many CMIP5 models only include the interaction between sulphate aerosol and cloud, and the majority of them only model the effect of aerosols on cloud albedo rather than cloud lifetime (Table 12.1). No CMIP5 models represent urban aerosol pollution explicitly so that is not listed in Table 12.1 (see Section 11.3.5.2 for discussion of future air quality). Only one model (GISS-E2) explicitly includes nitrate aerosol as a separate forcing, though it is also included within the total aerosol mixture in the Max Planck Institute-Earth System Model (MPI-ESM) model versions.

Land use change is typically applied by blending anthropogenic land surface disturbance via crop and pasture fraction changes with underlying land cover maps of natural vegetation, but model variations in the underlying land cover maps and biome modelling mean that the land use forcing agent is impossible to impose in a completely common way at present (Pitman et al., 2009). Most CMIP5 models represent crop and pasture disturbance separately, while some (Canadian Earth System Model (CanESM2), MIROC4h, MIROC5) represent crop but not pasture. Some models (e.g., HadGEM2-ES, MIROC-ESM and MPI-ESM versions) allow a dynamical representation of natural vegetation changes alongside anthropogenic disturbance (see also Sections 9.4.4.3 and 9.4.4.4).

Treatment of the CO<sub>2</sub> emissions associated with land cover changes is also model dependent. Some models do not account for land cover changes at all, some simulate the biophysical effects but are still forced externally by land cover change induced CO<sub>2</sub> emissions (in emissions-driven simulations), while the most advanced ESMs simulate both biophysical effects of land cover changes and their associated CO<sub>2</sub> emissions.

### 12.3.3 Synthesis of Projected Global Mean Radiative Forcing for the 21st Century

Quantification of future global mean RF is of interest as it is directly related to changes in the global energy balance of the climate system and resultant climate change. Chapter 8 discusses RF concepts and methods for computing it that form the basis of analysis directly from the output of model projections.

We assess three related estimates of projected global mean forcing and its range through the 21st century in the context of forcing estimated for the recent past (Figure 12.4). The estimates used are: the total forcings for the defined RCP scenarios, harmonized to RF in the past (Meinshausen et al., 2011a; Meinshausen et al., 2011c); the total effective radiative forcing (ERF) estimated from CMIP5 models through the 21st century for the four RCP experiments (Forster et al., 2013); and that estimated from models in the Atmospheric Chemistry and Climate Model Intercomparison Project (ACCMIP; Lamarque et al., 2013—see Section 8.2.2) for RCP time-slice experiments (Shindell et al., 2013b). Methodological differences mean that whereas CMIP5 estimates include both natural and anthropogenic forcings based entirely on ERF, ACCMIP estimates anthropogenic composition forcing only (neglecting forcing changes due to natural, i.e., solar and volcanic, and land use factors) based on a combination of ERF for aerosols and RF for WMGHG (see Section 8.5.3). Note also that total forcing for the defined RCP scenarios is based on Meinshausen et al. (2011c)

but combining total anthropogenic ERF (allowing for efficacies of the various anthropogenic forcings as in Figure 12.3) with natural (solar and volcanic) RF.

The CMIP5 multi-model ensemble mean ERF at 2100 (relative to an 1850–1869 base period) is 2.2, 3.8, 4.8 and 7.6 W m<sup>-2</sup> respectively for RCP2.6, RCP4.5, RCP6.0 and RCP8.5 concentration-driven projections, with a 1- $\sigma$  range based on annual mean data for year 2100 of about  $\pm 0.5$  to 1.0 W m<sup>-2</sup> depending on scenario (lowest for RCP2.6 and highest for RCP8.5). The CMIP5-based ERF estimates are close to the total forcing at 2100 (relative to an 1850–1859 base period) of 2.4, 4.0, 5.2 and 8.0 W m<sup>-2</sup> as defined for the four RCPs.

The spread in ERF indicated from CMIP5 model results with specified GHG concentration pathways is broadly consistent with that found for

CMIP3 models for the A1B scenario using the corresponding method (Forster and Taylor, 2006). As for CMIP3 models, part of the forcing spread in CMIP5 models (Forster et al., 2013) is consistent with differences in GHG forcings arising from the radiative transfer codes (Collins et al., 2006b). Aerosol forcing implementations in CMIP5 models also vary considerably, however (Section 12.3.2), leading to a spread in aerosol concentrations and forcings which contributes to the overall model spread. A further small source of spread in CMIP5 results possibly arises from an underlying ambiguity in the CMIP5 experimental design regarding the volcanic forcing offset between the historical experiment versus the pre-industrial control experiment. Most models implement zero volcanic forcing in the control experiment but some use constant negative forcing equal to the time-mean of historical volcanic forcing (see Table 12.1 and Section 12.3.2). The effect of this volcanic forcing offset persists into the future projections.

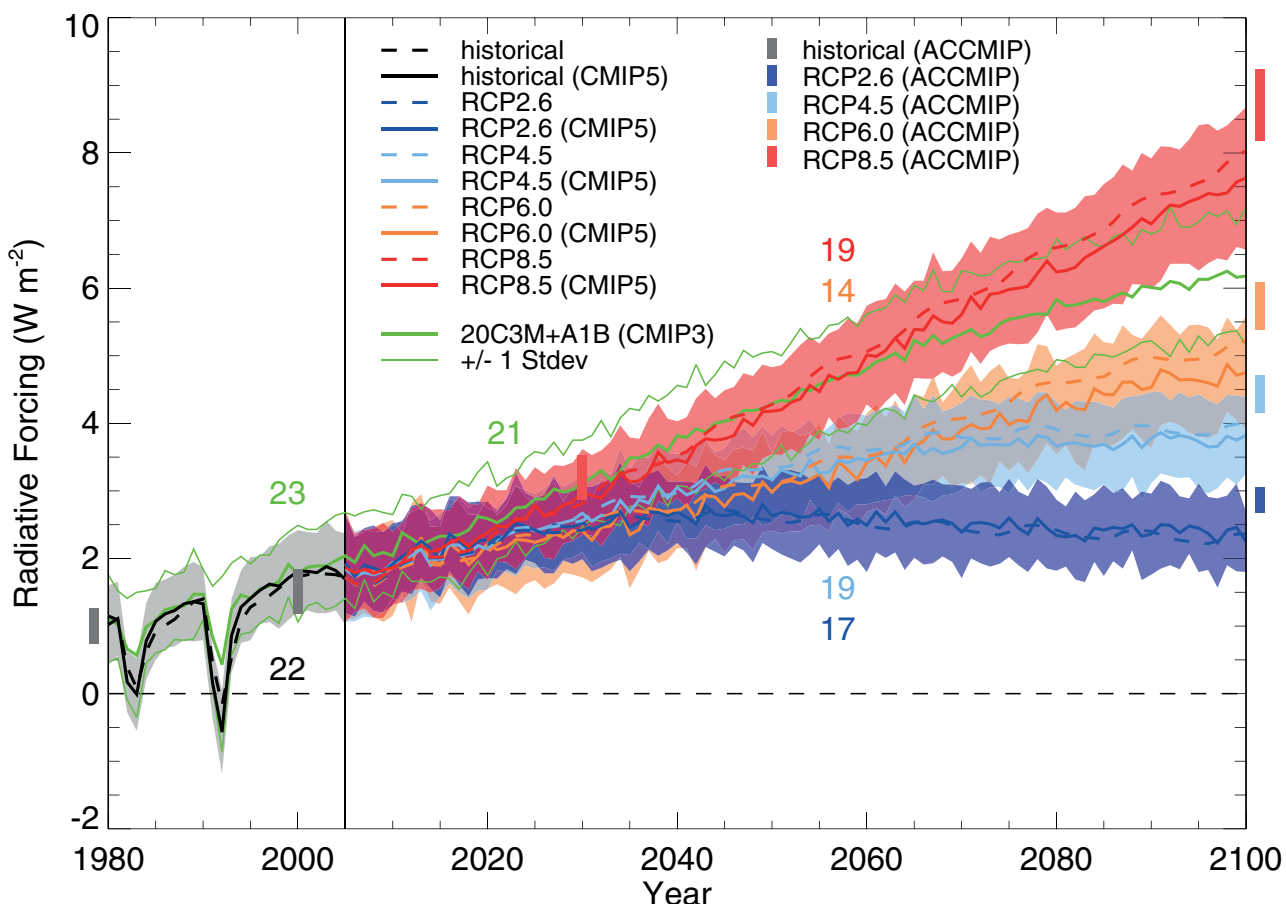


**Figure 12.4 |** Global mean radiative forcing (RF, W m<sup>-2</sup>) between 1980 and 2100 estimated by alternative methods. The baseline is circa 1850 but dependent on the methods. Dashed lines indicate the total anthropogenic plus natural (solar and volcanic) RF for the RCP scenarios as defined by Meinshausen et al. (2011c), taking into account the efficacies of the various anthropogenic forcings (Meinshausen et al., 2011a), normalized by the mean between 1850 and 1859. Solid lines are multi-model mean effective radiative forcing (ERF) realized in a subset of CMIP5 models for the concentration-driven historical experiment and RCP scenarios, normalized either with respect to the 1850–1869 base period or with respect to the pre-industrial control simulation (Forster et al., 2013). (The subset of CMIP5 models included is defined by Table 1 of Forster et al. (2013) but omitting the FGOALS-s2 (Flexible Global Ocean-Atmosphere-Land System) model, the historical and RCP simulations of which were subsequently withdrawn from the CMIP5 archive.) This CMIP5-based estimate assumes each model has an invariant climate feedback parameter, calculated from abrupt 4  $\times$  CO<sub>2</sub> experiments using the method of Gregory et al. (2004). Each individual CMIP5 model's forcing estimate is an average over all available ensemble members, and a 1- $\sigma$  inter-model range around the multi-model mean is shaded in light colour. Grey or coloured vertical bars illustrate the 1- $\sigma$  range (68% confidence interval) of anthropogenic composition forcing (excluding natural and land use change forcings, based on ERF for aerosols combined with RF for WMGHG) estimated in ACCMIP models (Shindell et al., 2013b) for time slice experiments at 1980, 2000, 2030 (RCP8.5 only) and 2100 (all RCPs). The ACCMIP ranges plotted have been converted from the 5 to 95% ranges given in Shindell et al. (2013b) (Table 8) to a 1- $\sigma$  range. Note that the ACCMIP bars at 1980 and 2100 are shifted slightly to aid clarity. The mean ERF diagnosed from 21 CMIP3 models for the SRES A1B scenario, as in Forster and Taylor (2006), is also shown (thick green line) with a 1- $\sigma$  range (thinner green lines). The number of models included in CMIP3 and CMIP5 ensemble means is shown colour coded. (See Tables All.6.8 to All.6.10. Note that the CMIP5 model ranges given in Table All.6.10 are based on decadal averages and therefore differ slightly from the ranges based on annual data shown in this figure.)

ACCMIP projected forcing at 2030 (for RCP8.5) and 2100 (all RCPs) is systematically higher than corresponding CMIP5 ERF, although with some overlap between  $1\sigma$  ranges. CMIP5 and ACCMIP comprise different sets of models and they are related in many but not all cases (Section 8.2.2). Confining analysis to a subset of closely related models also gives higher forcing estimates from ACCMIP compared to CMIP5 so the discrepancy in multi-model ensemble mean forcings appears unrelated to the different model samples associated with the two methods of estimation. The discrepancy is thought to originate mostly from differences in the underlying methodologies used to estimate RF, but is not yet well understood (see also Section 8.5.3).

There is *high confidence* in projections from ACCMIP models (Shindell et al., 2013b) based on the GISS-E2 CMIP5 simulations (Shindell et al., 2013a) and an earlier study with a version of the HadGEM2-ES model related to that used in CMIP5 (Bellouin et al., 2011), consistent with understanding of the processes controlling nitrate formation (Adams et al., 2001), that nitrate aerosols (which provide a negative forcing) will increase substantially over the 21st century under the RCPs (Section 8.5.3, Figure 8.20). The magnitude of total aerosol-related forcing (also negative in sign) will therefore tend to be underestimated in the CMIP5 multi-model mean ERF, as nitrate aerosol has been omitted as a forcing from almost all CMIP5 models.

Natural RF variations are, by their nature, difficult to project reliably (see Section 8.4). There is *very high confidence* that Industrial Era natural forcing has been a small fraction of the (positive) anthropogenic forcing except for brief periods following large volcanic eruptions (Sections 8.5.1 and 8.5.2). Based on that assessment and the assumption that variability in natural forcing remains of a similar magnitude and character to that over the Industrial Era, total anthropogenic forcing relative to pre-industrial, for any of the RCP scenarios through the 21st century, is *very likely* to be greater in magnitude than changes in natural (solar plus volcanic) forcing on decadal time scales.

In summary, global mean forcing projections derived from climate models exhibit a substantial range for the given RCP scenarios in concentration-driven experiments, contributing to the projected global mean temperature range (Section 12.4.1). Forcings derived from ACCMIP models for 2100 are systematically higher than those estimated from CMIP5 models for reasons that are not fully understood but are partly due to methodological differences. The multi-model mean estimate of combined anthropogenic plus natural forcing from CMIP5 is consistent with indicative RCP forcing values at 2100 to within 0.2 to 0.4  $\text{W m}^{-2}$ .

## 12.4 Projected Climate Change over the 21st Century

### 12.4.1 Time-Evolving Global Quantities

#### 12.4.1.1 Projected Changes in Global Mean Temperature and Precipitation

A consistent and robust feature across climate models is a continuation of global warming in the 21st century for all the RCP scenarios

(Figure 12.5 showing changes in concentration-driven model simulations). Temperature increases are almost the same for all the RCP scenarios during the first two decades after 2005 (see Figure 11.25). At longer time scales, the warming rate begins to depend more on the specified GHG concentration pathway, being highest ( $>0.3^\circ\text{C}$  per decade) in the highest RCP8.5 and significantly lower in RCP2.6, particularly after about 2050 when global surface temperature response stabilizes (and declines thereafter). The dependence of global temperature rise on GHG forcing at longer time scales has been confirmed by several studies (Meehl et al., 2007b). In the CMIP5 ensemble mean, global warming under RCP2.6 stays below  $2^\circ\text{C}$  above 1850–1900 levels throughout the 21st century, clearly demonstrating the potential of mitigation policies (note that to translate the anomalies in Figure 12.5 into anomalies with respect to that period, an assumed  $0.61^\circ\text{C}$  of observed warming since 1850–1900, as discussed in Section 2.4.3, should be added). This is in agreement with previous studies of aggressive mitigation scenarios (Johns et al., 2011; Meehl et al., 2012). Note, however, that some individual ensemble members do show warming exceeding  $2^\circ\text{C}$  above 1850–1900 (see Table 12.3). As for the other pathways, global warming exceeds  $2^\circ\text{C}$  within the 21st century under RCP4.5, RCP6.0 and RCP8.5, in qualitative agreement with previous studies using the SRES A1B and A2 scenarios (Joshi et al., 2011). Global mean temperature increase exceeds  $4^\circ\text{C}$  under RCP8.5 by 2100. The CMIP5 concentration-driven global temperature projections are broadly similar to CMIP3 SRES scenarios discussed in AR4 (Meehl et al., 2007b) and Section 12.4.9, although the overall range of the former is larger primarily because of the low-emission mitigation pathway RCP2.6 (Knutti and Sedláček, 2013).

The multi-model global mean temperature changes under different RCPs are summarized in Table 12.2. The relationship between cumulative anthropogenic carbon emissions and global temperature is assessed in Section 12.5 and only concentration-driven models are

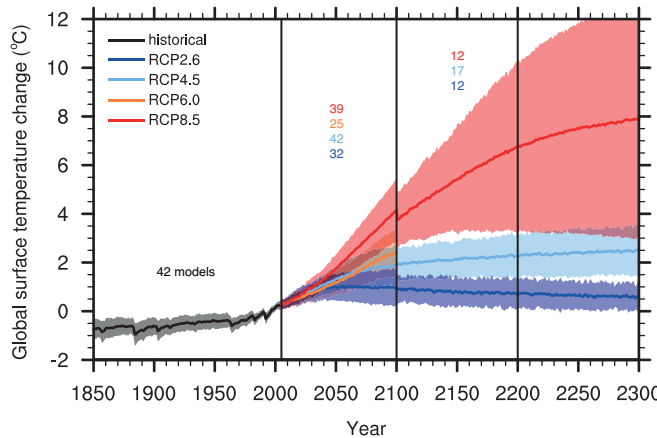


**Figure 12.5 |** Time series of global annual mean surface air temperature anomalies (relative to 1986–2005) from CMIP5 concentration-driven experiments. Projections are shown for each RCP for the multi-model mean (solid lines) and the 5 to 95% range ( $\pm 1.64$  standard deviation) across the distribution of individual models (shading). Discontinuities at 2100 are due to different numbers of models performing the extension runs beyond the 21st century and have no physical meaning. Only one ensemble member is used from each model and numbers in the figure indicate the number of different models contributing to the different time periods. No ranges are given for the RCP6.0 projections beyond 2100 as only two models are available.

**Table 12.2** | CMIP5 annual mean surface air temperature anomalies ( $^{\circ}\text{C}$ ) from the 1986–2005 reference period for selected time periods, regions and RCPs. The multi-model mean  $\pm 1$  standard deviation ranges across the individual models are listed and the 5 to 95% ranges from the models' distribution (based on a Gaussian assumption and obtained by multiplying the CMIP5 ensemble standard deviation by 1.64) are given in brackets. Only one ensemble member is used from each model and the number of models differs for each RCP (see Figure 12.5) and becomes significantly smaller after 2100. No ranges are given for the RCP6.0 projections beyond 2100 as only two models are available. Using Hadley Centre/Climate Research Unit gridded surface temperature data set 4 (HadCRUT4) and its uncertainty estimate (5 to 95% confidence interval), the observed warming to the 1986–2005 reference period (see Section 2.4.3) is  $0.61^{\circ}\text{C} \pm 0.06^{\circ}\text{C}$  (1850–1900),  $0.30^{\circ}\text{C} \pm 0.03^{\circ}\text{C}$  (1961–1990),  $0.11^{\circ}\text{C} \pm 0.02^{\circ}\text{C}$  (1980–1999). Decadal values are provided in Table AII.7.5, but note that percentiles of the CMIP5 distributions cannot directly be interpreted in terms of calibrated language.

	RCP2.6 ( $\Delta T$ in $^{\circ}\text{C}$ )	RCP4.5 ( $\Delta T$ in $^{\circ}\text{C}$ )	RCP6.0 ( $\Delta T$ in $^{\circ}\text{C}$ )	RCP8.5 ( $\Delta T$ in $^{\circ}\text{C}$ )	
Global:	2046–2065	$1.0 \pm 0.3$ (0.4, 1.6)	$1.4 \pm 0.3$ (0.9, 2.0)	$1.3 \pm 0.3$ (0.8, 1.8)	$2.0 \pm 0.4$ (1.4, 2.6)
	2081–2100	$1.0 \pm 0.4$ (0.3, 1.7)	$1.8 \pm 0.5$ (1.1, 2.6)	$2.2 \pm 0.5$ (1.4, 3.1)	$3.7 \pm 0.7$ (2.6, 4.8)
	2181–2200	$0.7 \pm 0.4$ (0.1, 1.3)	$2.3 \pm 0.5$ (1.4, 3.1)	$3.7 \pm 0.7$ (-,-)	$6.5 \pm 2.0$ (3.3, 9.8)
	2281–2300	$0.6 \pm 0.3$ (0.0, 1.2)	$2.5 \pm 0.6$ (1.5, 3.5)	$4.2 \pm 1.0$ (-,-)	$7.8 \pm 2.9$ (3.0, 12.6)
Land: 2081–2100		$1.2 \pm 0.6$ (0.3, 2.2)	$2.4 \pm 0.6$ (1.3, 3.4)	$3.0 \pm 0.7$ (1.8, 4.1)	$4.8 \pm 0.9$ (3.4, 6.2)
Ocean: 2081–2100		$0.8 \pm 0.4$ (0.2, 1.4)	$1.5 \pm 0.4$ (0.9, 2.2)	$1.9 \pm 0.4$ (1.1, 2.6)	$3.1 \pm 0.6$ (2.1, 4.0)
Tropics: 2081–2100		$0.9 \pm 0.3$ (0.3, 1.4)	$1.6 \pm 0.4$ (0.9, 2.3)	$2.0 \pm 0.4$ (1.3, 2.7)	$3.3 \pm 0.6$ (2.2, 4.4)
Polar: Arctic: 2081–2100		$2.2 \pm 1.7$ (-0.5, 5.0)	$4.2 \pm 1.6$ (1.6, 6.9)	$5.2 \pm 1.9$ (2.1, 8.3)	$8.3 \pm 1.9$ (5.2, 11.4)
Polar: Antarctic: 2081–2100		$0.8 \pm 0.6$ (-0.2, 1.8)	$1.5 \pm 0.7$ (0.3, 2.7)	$1.7 \pm 0.9$ (0.2, 3.2)	$3.1 \pm 1.2$ (1.1, 5.1)

included here. Warming in 2046–2065 is slightly larger under RCP4.5 compared to RCP6.0, consistent with its greater total anthropogenic forcing at that time (see Table A.II.6.12). For all other periods the magnitude of global temperature change increases from RCP2.6 to RCP8.5. Beyond 2100, RCP2.6 shows a decreasing trend whereas under all other RCPs warming continues to increase. Also shown in Table 12.2 are projected changes at 2081–2100 averaged over land and ocean separately as well as area-weighted averages over the Tropics ( $30^{\circ}\text{S}$  to  $30^{\circ}\text{N}$ ), Arctic ( $67.5^{\circ}\text{N}$  to  $90^{\circ}\text{N}$ ) and Antarctic ( $90^{\circ}\text{S}$  to  $55^{\circ}\text{S}$ ) regions. Surface air temperatures over land warm more than over the ocean, and northern polar regions warm more than the tropics. The excess of land mass in the Northern Hemisphere (NH) in comparison with the Southern Hemisphere (SH), coupled with the greater uptake of heat by the Southern Ocean in comparison with northern ocean basins means that the NH generally warms more than the SH. Arctic warming is much greater than in the Antarctic, due to the presence of the Antarctic ice sheet and differences in local responses in snow and ice. Mechanisms behind these features of warming are discussed in Section 12.4.3. Maps and time series of regional temperature changes are displayed in Annex I and regional averages are discussed in Section 14.8.1.

Global annual multi-model mean temperature changes above 1850–1900 are listed in Table 12.3 for the 2081–2100 period (assuming  $0.61^{\circ}\text{C}$  warming since 1850–1900 as discussed in Section 2.4.3) along with the percentage of 2081–2100 projections from the CMIP5 models exceeding policy-relevant temperature levels under each RCP. These complement a similar discussion for the near-term projections in Table 11.3 which are based on the CMIP5 ensemble as well as evidence (discussed in Sections 10.3.1, 11.3.2.1.1 and 11.3.6.3) that some CMIP5 models have a higher sensitivity to GHGs and a larger response to other anthropogenic forcings (dominated by the effects of aerosols) than the real world (*medium confidence*). The percentage calculations for the long-term projections in Table 12.3 are based solely on the CMIP5 ensemble, using one ensemble member for each model. For these long-term projections, the 5 to 95% ranges of the CMIP5 model ensemble are considered the *likely* range, an assessment based on the fact that the 5 to 95% range of CMIP5 models'

TCR coincides with the assessed *likely* range of the TCR (see Section 12.4.1.2 below and Box 12.2). Based on this assessment, global mean temperatures averaged in the period 2081–2100 are projected to *likely* exceed  $1.5^{\circ}\text{C}$  above 1850–1900 for RCP4.5, RCP6.0 and RCP8.5 (*high confidence*). They are also *likely* to exceed  $2^{\circ}\text{C}$  above 1850–1900 for RCP6.0 and RCP8.5 (*high confidence*) and *more likely than not* to exceed  $2^{\circ}\text{C}$  for RCP4.5 (*medium confidence*). Temperature change above  $2^{\circ}\text{C}$  under RCP2.6 is *unlikely* but is assessed only with *medium confidence* as some CMIP5 ensemble members do produce a global mean temperature change above  $2^{\circ}\text{C}$ . Warming above  $4^{\circ}\text{C}$  by 2081–2100 is *unlikely* in all RCPs (*high confidence*) except RCP8.5. Under the latter, the  $4^{\circ}\text{C}$  global temperature level is exceeded in more than half of ensemble members, and is assessed to be *about as likely as not* (*medium confidence*). Note that the likelihoods of exceeding specific temperature levels show some sensitivity to the choice of reference period (see Section 11.3.6.3).

CMIP5 models on average project a gradual increase in global precipitation over the 21st century: change exceeds  $0.05 \text{ mm day}^{-1}$  (~2% of global precipitation) and  $0.15 \text{ mm day}^{-1}$  (~5% of global precipitation) by 2100 in RCP2.6 and RCP8.5, respectively. The relationship between global precipitation and global temperature is approximately linear (Figure 12.6). The precipitation sensitivity, that is, the change of global precipitation with temperature, is about 1 to 3%  $^{\circ}\text{C}^{-1}$  in most models, tending to be highest for RCP2.6 and RCP4.5 (Figure 12.7; note that only global values are discussed in this section, ocean and land changes are discussed in Section 12.4.5.2). These behaviours are consistent with previous studies, including CMIP3 model projections for SRES scenarios and AR4 constant composition commitment experiments (Meehl et al., 2007b), and ENSEMBLES multi-model results for SRES A1B and E1 scenarios (Johns et al., 2011).

The processes that govern global precipitation changes are now well understood and have been presented in Section 7.6. They are briefly summarized here and used to interpret the long-term projected changes. The precipitation sensitivity (about 1 to 3%  $^{\circ}\text{C}^{-1}$ ) is very different from the water vapour sensitivity (~7%  $^{\circ}\text{C}^{-1}$ ) as the main physical

**Table 12.3 |** CMIP5 global annual mean temperature changes above 1850–1900 for the 2081–2100 period of each RCP scenario (mean,  $\pm 1$  standard deviation and 5 to 95% ranges based on a Gaussian assumption and obtained by multiplying the CMIP5 ensemble standard deviation by 1.64), assuming 0.61°C warming has occurred prior to 1986–2005 (second column). For a number of temperature levels (1°C, 1.5°C, 2°C, 3°C and 4°C), the proportion of CMIP5 model projections for 2081–2100 above those levels under each RCP scenario are listed. Only one ensemble member is used for each model.

	$\Delta T$ (°C) 2081–2100	$\Delta T > +1.0^\circ\text{C}$	$\Delta T > +1.5^\circ\text{C}$	$\Delta T > +2.0^\circ\text{C}$	$\Delta T > +3.0^\circ\text{C}$	$\Delta T > +4.0^\circ\text{C}$
RCP2.6	$1.6 \pm 0.4$ (0.9, 2.3)	94%	56%	22%	0%	0%
RCP4.5	$2.4 \pm 0.5$ (1.7, 3.2)	100%	100%	79%	12%	0%
RCP6.0	$2.8 \pm 0.5$ (2.0, 3.7)	100%	100%	100%	36%	0%
RCP8.5	$4.3 \pm 0.7$ (3.2, 5.4)	100%	100%	100%	100%	62%

laws that drive these changes also differ. Water vapour increases are primarily a consequence of the Clausius–Clapeyron relationship associated with increasing temperatures in the lower troposphere (where most atmospheric water vapour resides). In contrast, future precipitation changes are primarily the result of changes in the energy balance of the atmosphere and the way that these later interact with

circulation, moisture and temperature (Mitchell et al., 1987; Boer, 1993; Vecchi and Soden, 2007; Previdi, 2010; O’Gorman et al., 2012). Indeed, the radiative cooling of the atmosphere is balanced by latent heating (associated with precipitation) and sensible heating. Since AR4, the changes in heat balance and their effects on precipitation have been analyzed in detail for a large variety of forcings, simulations and models (Takahashi, 2009a; Andrews et al., 2010; Bala et al., 2010; Ming et al., 2010; O’Gorman et al., 2012; Bony et al., 2013).

An increase of CO<sub>2</sub> decreases the radiative cooling of the troposphere and reduces precipitation (Andrews et al., 2010; Bala et al., 2010). On longer time scales than the fast hydrological adjustment time scale (Andrews et al., 2010; Bala et al., 2010; Cao et al., 2012; Bony et al., 2013), the increase of CO<sub>2</sub> induces a slow increase of temperature and water vapour, thereby enhancing the radiative cooling of the atmosphere and increasing global precipitation (Allen and Ingram, 2002; Yang et al., 2003; Held and Soden, 2006). Even after the CO<sub>2</sub> forcing stabilizes or begins to decrease, the ocean continues to warm, which then drives up global temperature, evaporation and precipitation. In addition, nonlinear effects also affect precipitation changes (Good et al., 2012). These different effects explain the steepening of the precipitation versus temperature relationship in RCP2.6 and RCP4.5 scenarios (Figure 12.6), as RF stabilizes and/or declines from the mid-century (Figure 12.4). In idealized CO<sub>2</sub> ramp-up/ramp-down experiments, this effect produces an hydrological response overshoot (Wu et al., 2010). An increase of absorbing aerosols warms the atmosphere and reduces precipitation, and the surface temperature response may be too small to compensate this decrease (Andrews et al., 2010; Ming et al., 2010; Shiogama et al., 2010a). Change in scattering aerosols or incoming solar radiation modifies global precipitation mainly via the response of the surface temperature (Andrews et al., 2009; Bala et al., 2010).

The main reasons for the inter-model spread of the precipitation sensitivity estimate among GCMs have not been fully understood. Nevertheless, spread in the changes of the cloud radiative effect has been shown to have an impact (Previdi, 2010), although the effect is less important for precipitation than it is for the climate sensitivity estimate (Lambert and Webb, 2008). The lapse rate plus water vapour feedback and the response of the surface heat flux (Previdi, 2010; O’Gorman et al., 2012), the shortwave absorption by water vapour (Takahashi, 2009b) or by aerosols, have been also identified as important factors.

Global precipitation sensitivity estimates from observations are very sensitive to the data and the time period considered. Some

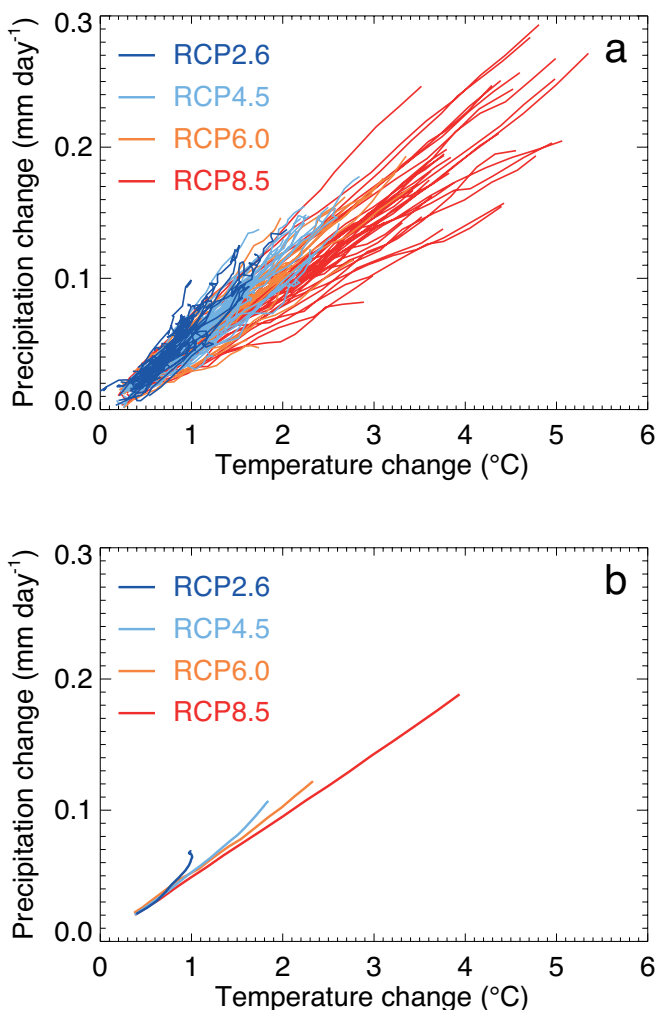


**Figure 12.6 |** Global mean precipitation (mm day<sup>-1</sup>) versus temperature (°C) changes relative to 1986–2005 baseline period in CMIP5 model concentrations-driven projections for the four RCPs for (a) means over decadal periods starting in 2006 and overlapped by 5 years (2006–2015, 2011–2020, up to 2091–2100), each line representing a different model (one ensemble member per model) and (b) corresponding multi-model means for each RCP.

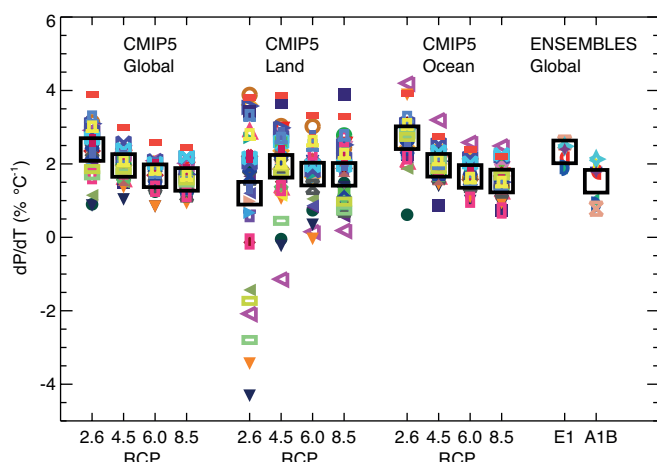


**Figure 12.7 |** Percentage changes over the 21st century in global, land and ocean precipitation per degree Celsius of global warming in CMIP5 model concentration-driven projections for the four RCP scenarios. Annual mean changes are calculated for each year between 2006 and 2100 from one ensemble member per model relative to its mean precipitation and temperature for the 1986–2005 baseline period, and the gradient of a least-squares fit through the annual data is derived. Land and ocean derived values use global mean temperature in the denominator of  $\delta P/\delta T$ . Each coloured symbol represents a different model, the same symbol being used for the same model for different RCPs and larger black squares being the multi-model mean. Also shown for comparison are global mean results for ENSEMBLES model concentrations-driven projections for the E1 and A1B scenarios (Johns et al., 2011), in this case using a least-squares fit derived over the period 2000–2099 and taking percentage changes relative to the 1980–1999 baseline period. Changes of precipitation over land and ocean are discussed in Section 12.4.5.2.

observational studies suggest precipitation sensitivity values higher than model estimates (Wentz et al., 2007; Zhang et al., 2007), although more recent studies suggest consistent values (Adler et al., 2008; Li et al., 2011b).

#### 12.4.1.2 Uncertainties in Global Quantities

Uncertainties in global mean quantities arise from variations in internal natural variability, model response and forcing pathways. Table 12.2 gives two measures of uncertainty in the CMIP5 model projections, the standard deviation and the 5 to 95% range across the ensemble's distribution. Because CMIP5 was not designed to explore fully the uncertainty range in projections (see Section 12.2), neither its standard deviation nor its range can be interpreted directly as an uncertainty statement about the corresponding real quantities, and other techniques and arguments to assess uncertainty in future projections must be considered. Figure 12.8 summarizes the uncertainty ranges in global mean temperature changes at the end of the 21st century under the various scenarios quantified by various methods. Individual CMIP5 models are shown by red crosses. Red bars indicate mean and 5 to 95% percentiles based on assuming a normal distribution for the CMIP5 sample (i.e.,  $\pm 1.64$  standard deviations). Estimates from the simple climate carbon cycle Model for the Assessment of Greenhouse Gas-Induced Climate Change (MAGICC; Meinshausen et al., 2011a; Meinshausen et al., 2011b) calibrated to CMIP (Friedlingstein et al., 2006) carbon cycle models, assuming a PDF for climate sensitivity that corresponds to the assessment of IPCC AR4 (Meehl et al., 2007b, Box 10.2), are given as yellow bars (Rogelj et al., 2012). Note that not all

models have simulated all scenarios. To test the effect of undersampling, and to generate a consistent set of uncertainties across scenarios, a step response method that estimates the total warming as sum of responses to small forcing steps (Good et al., 2011a) is used to emulate 23 CMIP5 models under the different scenarios (those 23 models that supplied the necessary simulations to compute the emulators, i.e., CO<sub>2</sub> step change experiments). This provides means and ranges (5 to 95%) that are comparable across scenarios (blue). See also Section 12.4.9 for a discussion focussed on the differences between CMIP3 and CMIP5 projections of global average temperature changes.

For the CO<sub>2</sub> concentration-driven simulations (Figure 12.8a), the dominant driver of uncertainty in projections of global temperature for the higher RCPs beyond 2050 is the transient climate response (TCR), for RCP2.6, which is closer to equilibrium by the end of the century, it is both the TCR and the equilibrium climate sensitivity (ECS). In a transient situation, the ratio of temperature to forcing is approximately constant and scenario independent (Meehl et al., 2007b, Appendix 10.A.1; Gregory and Forster, 2008; Knutti et al., 2008b; Good et al., 2013). Therefore, the uncertainty in TCR maps directly into the uncertainty in global temperature projections for the RCPs other than RCP2.6. The assessed *likely* range of TCR based on various lines of evidence (see Box 12.2) is similar to the 5 to 95% percentile range of TCR in CMIP5. In addition, the assessed *likely* range of ECS is also consistent with the CMIP5 range (see Box 12.2). There is little evidence that the CMIP5 models are significantly over- or underestimating the RF. The RF uncertainty is small compared to response uncertainty (see Figure 12.4), and is considered by treating the 5 to 95% as a *likely* rather than *very likely* range. Kuhlbrodt and Gregory (2012) suggest that models might be overestimating ocean heat uptake, as previously suggested by Forest et al. (2006), but observationally constrained estimates of TCR are unaffected by that. The ocean heat uptake efficiency does not contribute much to the spread of TCR (Knutti and Tomassini, 2008; Kuhlbrodt and Gregory, 2012).

Therefore, for global mean temperature projections only, the 5 to 95% range (estimated as 1.64 times the sample standard deviation) of the CMIP5 projections can also be interpreted as a *likely* range for future temperature change between about 2050 and 2100. *Confidence* in this assessment is *high* for the end of the century because the warming then is dominated by CO<sub>2</sub> and the TCR. *Confidence* is only *medium* for mid-century when the contributions of RF and initial conditions to the total temperature response uncertainty are larger. The *likely* ranges are an expert assessment, taking into account many lines of evidence, in much the same way as in AR4 (Figure SPM.5), and are not probabilistic. The *likely* ranges for 2046–2065 do not take into account the possible influence of factors that lead to near-term (2016–2035) projections of global mean surface temperature (GMST) that are somewhat cooler than the 5 to 95% model ranges (see Section 11.3.6), because the influence of these factors on longer term projections cannot be quantified. A few recent studies indicate that some of the models with the strongest transient climate response might overestimate the near term warming (Otto et al., 2013; Stott et al., 2013) (see Sections 10.8.1, 11.3.2.1.1), but there is little evidence of whether and how much that affects the long-term warming response. One perturbed physics ensemble combined with observations indicates warming that exceeds the AR4 at the top end but used a relatively short time period of warming

(50 years) to constrain the models' projections (Rowlands et al., 2012) (see Sections 11.3.2.1.1 and 11.3.6.3). GMSTs for 2081–2100 (relative to 1986–2005) for the CO<sub>2</sub> concentration driven RCPs is therefore assessed to *likely* fall in the range 0.3°C to 1.7°C (RCP2.6), 1.1°C to 2.6°C (RCP4.5), 1.4°C to 3.1°C (RCP6.0), and 2.6°C to 4.8°C (RCP8.5) estimated from CMIP5. Beyond 2100, the number of CMIP5 simulations is insufficient to estimate a *likely* range. Uncertainties before 2050 are assessed in Section 11.3.2.1.1. The assessed *likely* range is very similar to the range estimated by the pulse response model, suggesting that the different sample of models for the different RCPs are not strongly affecting the result, and providing further support that this pulse response technique can be used to emulate temperature and ocean heat uptake in Chapter 13 and Section 12.4.9. The results are consistent with the probabilistic results from MAGICC, which for the lower RCPs have a slightly narrower range due to the lack of internal variability in the simple model, and the fact that non-CO<sub>2</sub> forcings are treated more homogeneously than in CMIP5 (Meinshausen et al., 2011a, 2011b). This is particularly pronounced for RCP2.6 where the CMIP5 range is substantially larger, partly due to the larger fraction of non-CO<sub>2</sub> forcings in that scenario.

The uncertainty estimate in AR4 for the SRES scenarios was –40% to +60% around the CMIP3 means (shown here in grey for comparison). That range was asymmetric and wider for the higher scenarios because it included the uncertainty in carbon cycle climate feedbacks. The SRES scenarios are based on the assumption of prescribed emissions, which then translates to uncertainties in concentrations that propagate through to uncertainties in the temperature response. The RCP scenarios assume prescribed concentrations. For scenarios that stabilize (RCP2.6) that approach of constant fractional uncertainty underestimates the uncertainty and is no longer applicable, mainly because internal variability has a larger relative contribution to the total uncertainty (Good et al., 2013; Knutti and Sedláček, 2013). For the RCPs, the carbon cycle climate feedback uncertainty is not included because the simulations are driven by concentrations. Furthermore, there is no clear evidence that distribution of CMIP5 global temperature changes deviates from a normal distribution. For most other variables the shape of the distribution is unclear, and standard deviations are simply used as an indication of model spread, not representing a formal uncertainty assessment.

Simulations with prescribed CO<sub>2</sub> emissions rather than concentrations are only available for RCP8.5 (Figure 12.8b) and from MAGICC. The projected temperature change in 2100 is slightly higher and the uncertainty range is wider as a result of uncertainties in the carbon cycle climate feedbacks. The CMIP5 range is consistent with the uncertainty range given in AR4 for SRES A2 in 2100. Further details about emission versus concentration driven simulations are given in Section 12.4.8.

In summary, the projected changes in global temperature for 2100 in the RCP scenarios are very consistent with those obtained by CMIP3 for SRES in IPCC AR4 (see Section 12.4.9) when taking into account the differences in scenarios. The *likely* uncertainty ranges provided here are similar for RCP4.5 and RCP6.0 but narrower for RCP8.5 compared to AR4. There was no scenario as low as RCP2.6 in AR4. The uncertainties in global temperature projections have not decreased significantly in CMIP5 (Knutti and Sedláček, 2013), but the assessed ranges cannot be

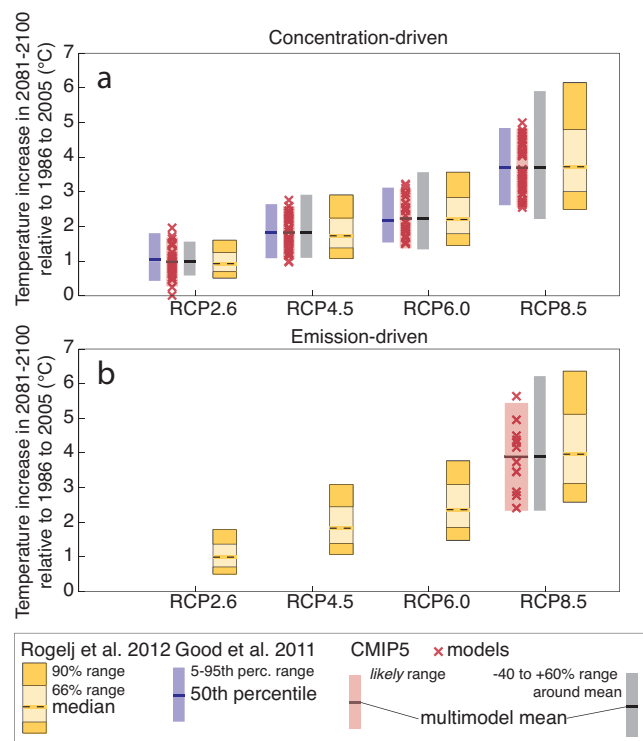


**Figure 12.8 |** Uncertainty estimates for global mean temperature change in 2081–2100 with respect to 1986–2005. Red crosses mark projections from individual CMIP5 models. Red bars indicate mean and 5 to 95% ranges based on CMIP5 (1.64 standard deviations), which are considered as a *likely* range. Blue bars indicate 5 to 95% ranges from the pulse response emulation of 21 models (Good et al., 2011a). Grey bars mark the range from the mean of CMIP5 minus 40% to the mean +60%, assessed as *likely* in AR4 for the SRES scenarios. The yellow bars show the median, 17 to 83% range and 5 to 95% range based on Rogelj et al. (2012). See also Figures 12.39 and 12.40.

compared between AR4 and AR5. The main reason is that uncertainties in carbon cycle feedbacks are not considered in the concentration driven RCPs. In contrast, the *likely* range in AR4 included those. The assessed *likely* ranges are therefore narrower for the high RCPs. The differences in the projected warming are largely attributable to the difference in scenarios (Knutti and Sedláček, 2013), and the change in the future and reference period, rather than to developments in modelling since AR4. A detailed comparison between the SRES and RCP scenarios and the CMIP3 and CMIP5 models is given in Section 12.4.9.

## 12.4.2 Pattern Scaling

### 12.4.2.1 Definition and Use

In this chapter we show geographical patterns of projected changes in climate variables according to specific scenarios and time horizons. Alternative scenarios and projection times can be inferred from those shown by using some established approximation methods. This is especially the case for large-scale regional patterns of average temperature and—with additional caveats—precipitation changes. In fact, 'pattern scaling' is an approximation that has been explicitly suggested in the description of the RCPs (Moss et al., 2010) as a method for deriving impact-relevant regional projections for scenarios that have not been simulated by global and regional climate models. It was first proposed

by Santer et al. (1990) and revisited later by numerous studies (e.g., Huntingford and Cox, 2000). It relies on the existence of robust geographical patterns of change, emerging at the time when the response to external forcings emerges from the noise, and persisting across the length of the simulation, across different scenarios, and even across models, modulated by the corresponding changes in global average temperature. The robustness of temperature change patterns has been amply documented from the original paper onward. An example

is given in Figure 12.9 for surface air temperature from each of the CMIP5 models highlighting both similarities and differences between the responses of different models. The precipitation pattern was shown to scale linearly with global average temperature to a sufficient accuracy in CMIP3 models (Neelin et al., 2006) for this to be useful for projections related to the hydrological cycle. Shiogama et al. (2010b) find similar results with the caution that in the early stages of warming aerosols modify the pattern. A more mixed evaluation can be found in



**Figure 12.9 |** Surface air temperature change in 2081–2100 displayed as anomalies with respect to 1986–2005 for RCP4.5 from one ensemble member of each of the concentration-driven models available in the CMIP5 archive.

Good et al. (2012), where some land areas in the low latitudes exhibit a nonlinear relation to global average temperature, but, largely, average precipitation change over the remaining regions can be well approximated by a grid-point specific linear function of global average temperature change. It is in the latter quantity that the dependence of the evolution of the change in time on the model (e.g., its climate sensitivity) and the forcing (e.g., the emission scenario) is encapsulated.

In analytical terms, it is assumed that the following relation holds:

$$C(t, \xi) = T_g(t) \chi(\xi) + R(t, \xi)$$

where the symbol  $\xi$  identifies the geographic location (model grid point or other spatial coordinates) and possibly the time of year (e.g., a June–July–August average). The index  $t$  runs along the length of the forcing scenario of interest.  $T_g(t)$  indicates global average temperature change at time  $t$  under this scenario;  $\chi(\xi)$  is the time-invariant geographic pattern of change per 1°C global surface temperature change for the variable of interest (which represents the forced component of the change) and  $C(t, \xi)$  is the actual field of change for that variable at the specific time  $t$  under this scenario. The  $R(t, \xi)$  is a residual term and highlights the fact that pattern scaling cannot reconstruct model behaviour with complete accuracy due to both natural variability and because of limitations of the methodology discussed below. This way, regionally and temporally differentiated results under different scenarios or climate sensitivities can be approximated by the product of a spatial pattern, constant over time, scenario and model characteristics, and a time evolving global mean change in temperature. Model and scenario dependence are thus captured through the global mean temperature response, and simple climate models calibrated against fully coupled climate models can be used to simulate the latter, at a great saving in computational cost. The spatial pattern can be estimated through the available coupled model simulations under the assumption that it does not depend on the specific scenario(s) used.

The choice of the pattern in the studies available in the literature can be as simple as the ensemble average field of change (across models and/or across scenarios, for the coupled experiments available), normalized by the corresponding change in global average temperature, choosing a segment of the simulations when the signal has emerged from the noise of natural variability from a baseline of reference (e.g., the last 20 years of the 21st century compared to pre-industrial or current climate) and taking the difference of two multi-decadal means. Similar properties and results have been obtained using more sophisticated multivariate procedures that optimize the variance explained by the pattern (Holden and Edwards, 2010). The validity of this approximation is discussed by Mitchell et al. (1999) and Mitchell (2003). Huntingford and Cox (2000) evaluate the quality of the approximation for numerous variables, showing that the technique performs best for temperature, downward longwave radiation, relative humidity, wind speeds and surface pressure while showing relatively larger limitations for rainfall rate anomalies. Joshi et al. (2013) have recently shown that the accuracy of the approximation, especially across models, is improved by adding a second term, linear in the land–sea surface warming ratio, another quantity that can be easily estimated from existing coupled climate model simulations. There exist of course differences between the patterns generated by different GCMs (documented for example

for CMIP3 in Watterson and Whetton, 2011b), but uncertainty can be characterized, for example, by the inter-model spread in the pattern  $\chi(\xi)$ . Recent applications of the methodology to probabilistic future projections have in fact sought to fully quantify errors introduced by the approximation, on the basis of the available coupled model runs (Harris et al., 2006).

Pattern scaling and its applications have been documented in IPCC WGI Reports before (IPCC, 2001, Section 13.5.2.1; Meehl et al., 2007b, Section 10.3.2). It has been used extensively for regional temperature and precipitation change projections, for example, Murphy et al. (2007), (Watterson, 2008), Giorgi (2008), Harris et al. (2006, 2010), May (2008a), Ruosteenoja et al. (2007), Räisänen and Ruokolainen (2006), Cabré et al. (2010) and impact studies, for example, as described in Dessai et al. (2005) and Fowler et al. (2007b). Recent studies have focussed on patterns linked to warming at certain global average temperature change thresholds (e.g., May, 2008a; Sanderson et al., 2011) and patterns derived under the RCPs (Ishizaki et al., 2012).

There are basic limitations to this approach, besides a degradation of its performance as the regional scale of interest becomes finer and in the presence of regionally specific forcings. Recent work with MIROC3.2 (Shiogama et al., 2010a; Shiogama et al., 2010b) has revealed a dependence of the precipitation sensitivity (global average precipitation change per 1°C of global warming—see Figure 12.6) on the scenario, due to the precipitation being more sensitive to carbon aerosols than WMGHGs. In fact, there are significant differences in black and organic carbon aerosol forcing between the emission scenarios investigated by Shiogama et al. (2010a; 2010b). Levy II et al. (2013) confirm that patterns of precipitation change are spatially correlated with the sources of aerosol emissions, in simulations where the indirect effect is represented. This is a behaviour that is linked to a more general limitation of pattern scaling, which breaks down if aerosol forcing is significant. The effects of aerosols have a regional nature and are thus dependent on the future sources of pollution which are likely to vary geographically in the future and are difficult to predict (May, 2008a). For example, Asian and North American aerosol production are likely to have different time histories and future projections. Schlesinger et al. (2000) extended the methodology of pattern scaling by isolating and recombining patterns derived by dedicated experiments with a coupled climate model where sulphate aerosols were increased for various regions in turn. More recently, in an extension of pattern scaling into a probabilistic treatment of model, scenario and initial condition uncertainties, Frieler et al. (2012) derived joint probability distributions for regionally averaged temperature and precipitation changes as linear functions of global average temperature and additional predictors including regionally specific sulphate aerosol and black carbon emissions.

Pattern scaling is less accurate for strongly mitigated stabilization scenarios. This has been shown recently by May (2012), comparing patterns of temperature change under a scenario limiting global warming since pre-industrial times to 2°C and patterns produced by a scenario that reaches 4.5°C of global average temperature change. The limitations of pattern scaling in approximating changes while the climate system approaches equilibrium have found their explanation in Manabe and Wetherald (1980) and Mitchell et al. (1999). Both studies point out that as the temperatures of the deep oceans reach equilibri-

um (over multiple centuries) the geographical distribution of warming changes as well, for example, showing a larger warming of the high latitudes in the SH than in the earlier periods of the transient response, relative to the global mean warming. More recently, Held et al. (2010) showed how this slow warming pattern is in fact present during the initial transient response of the system as well, albeit with much smaller amplitude. Further, Gillett et al. (2011) show how in a simulation in which emissions cease, regional temperatures and precipitation patterns exhibit ongoing changes, even though global mean temperature remains almost constant. Wu et al. (2010) showed that the global precipitation response shows a nonlinear response to strong mitigation scenarios, with the hydrological cycle continuing to intensify even after atmospheric CO<sub>2</sub> concentration, and thus global average temperature, start decreasing. Regional nonlinear responses to mitigation scenarios of precipitation and sea surface temperatures (SSTs) are shown by Chadwick et al. (2013).

Other areas where pattern scaling shows a lack of robustness are the edges of polar ice caps and sea ice extent, where at an earlier time in the simulation ice melts and regions of sharp gradient surface, while later in the simulation, in the absence of ice, the gradient will become less steep. Different sea ice representations in models also make the location of such regions much less robust across the model ensembles and the scenarios.

Pattern scaling has not been as thoroughly explored for quantities other than average temperature and precipitation. Impact relevant extremes, for example, seem to indicate a critical dependence on the scale at which their changes are evaluated, with studies showing that some aspects of their statistics change in a close-to-linear way with mean temperature (Kharin et al., 2007; Lustenberger et al., 2013) while others have documented the dependence of their changes on moments of their statistical distribution other than the mean (Ballester et al., 2010a), which would make pattern scaling inadequate.

#### 12.4.2.2 Coupled Model Intercomparison Project Phase 5 Patterns Scaled by Global Average Temperature Change

On the basis of CMIP5 simulations, we show geographical patterns (Figure 12.10) of warming and precipitation change and indicate measures of their variability across models and across RCPs. The patterns are scaled to 1°C global mean surface temperature change above the reference period 1986–2005 for 2081–2100 (first row) and for a period of approximate stable temperature, 2181–2200 (thus excluding RCP8.5, which does not stabilize by that time) (second row). Spatial correlation of fields of temperature and precipitation change range from 0.93 to 0.99 when considering ensemble means under different RCPs. The lower values are found when computing correlation between RCP2.6 and the higher RCPs, and may be related to the high mitigation

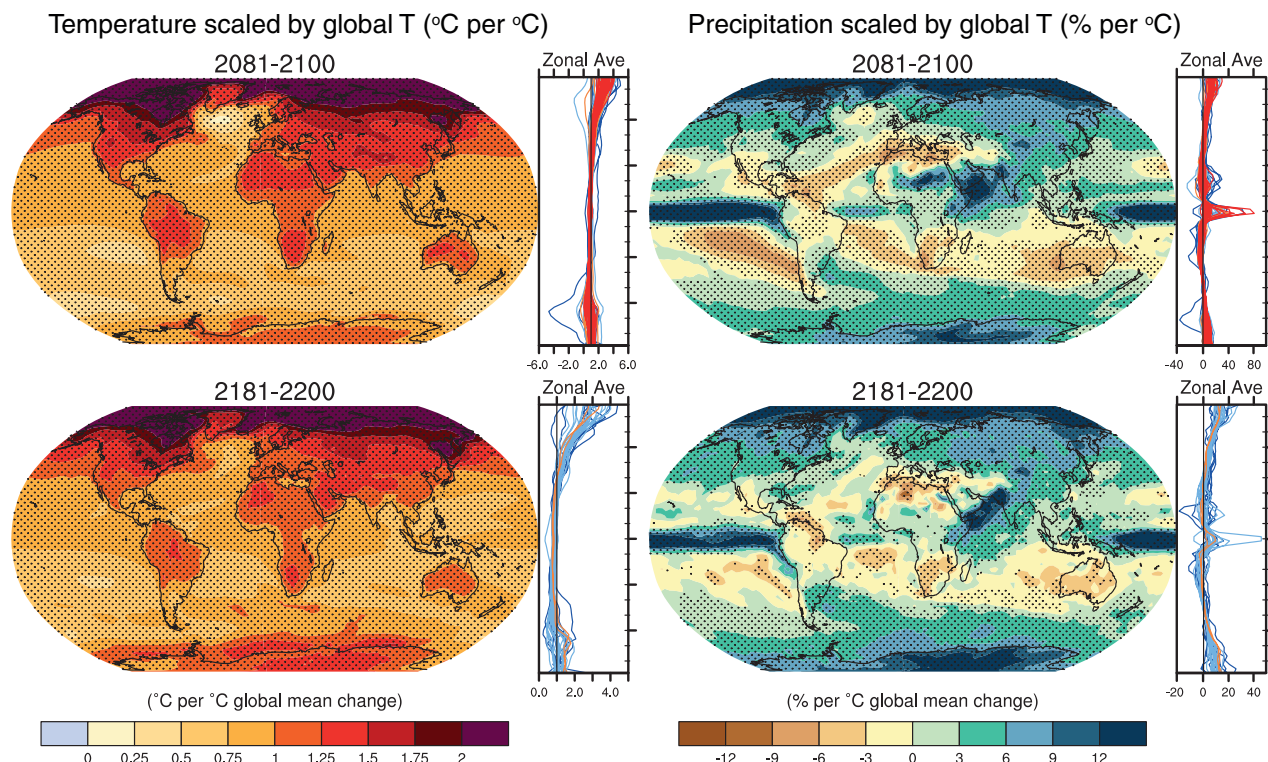


**Figure 12.10 |** Temperature (left) and precipitation (right) change patterns derived from transient simulations from the CMIP5 ensembles, scaled to 1°C of global mean surface temperature change. The patterns have been calculated by computing 20-year averages at the end of the 21st (top) and 22nd (bottom) centuries and over the period 1986–2005 for the available simulations under all RCPs, taking their difference (percentage difference in the case of precipitation) and normalizing it, grid-point by grid-point, by the corresponding value of global average temperature change for each model and scenario. The normalized patterns have then been averaged across models and scenarios. The colour scale represents degrees Celsius (in the case of temperature) and percent (in the case of precipitation) per 1°C of global average temperature change. Stippling indicates where the mean change averaged over all realizations is larger than the 95% percentile of the distribution of models. Zonal means of the geographical patterns are shown for each individual model for RCP2.6 (blue), 4.5 (light blue), 6.0 (orange) and 8.5 (red). RCP8.5 is excluded from the stabilization figures. The RCP2.6 simulation of the FIO-ESM (First Institute of Oceanography) model was excluded because it did not show any warming by the end of the 21st century, thus not complying with the method requirement that the pattern be estimated at a time when the temperature change signal from CO<sub>2</sub> increase has emerged.

enacted under RCP2.6 from early in the 21st century. Pattern correlation varies between 0.91 and 0.98 for temperature and between 0.91 and 0.96 for precipitation when comparing patterns computed by averaging and normalizing changes at the end of the 21st, 22nd and 23rd centuries, with the largest value representing the correlation between the patterns at the end of the 22nd and 23rd centuries, the lowest representing the correlation between the pattern at the end of the 21st and the pattern at the end of the 23rd century. The zonal means shown to the side of each plot represent each model by one line, colour coding the four different scenarios. They show good agreement of models and scenarios over low and mid-latitudes for temperature, but higher spread across models and especially across scenarios for the areas subject to polar amplification, for which the previous discussion about the sensitivity of the patterns to the sea ice edge may be relevant. A comparison of the mean of the lines to their spread indicates overall the presence of a strong mean signal with respect to the spread of the ensemble. Precipitation shows an opposite pattern of inter-model spread, with larger variations in the low latitudes and around the equator, and smaller around the high latitudes. Precipitation has also a lower signal-to-noise ratio (measured as above by comparing the ensemble mean change magnitude to the spread across models and scenarios of these zonal mean averages).

As already mentioned, although we do not explicitly use pattern scaling in the sections that follow, we consider it a useful approximation when the need emerges to interpolate or extrapolate results to different scenarios or time periods, noting the possibility that the scaling may break down at higher levels of global warming, and that the validity of the approximation is limited to broad patterns of change, as opposed to local scales. An important caveat is that pattern scaling only applies to the climate response that is externally forced. The actual response is a combination of forced change and natural variability, which is not and should not be scaled up or down by the application of this technique, which becomes important on small spatial scales and shorter time scales, and whose relative magnitude compared to the forced component also depends on the variable (Hawkins and Sutton, 2009, 2011; Mahlstein et al., 2011; Deser et al., 2012a, 2012b; Mahlstein et al., 2012) (see Section 11.2). One approach to produce projections that include both components is to estimate natural variability separately, scale the forced response and add the two.

12

### 12.4.3 Changes in Temperature and Energy Budget

#### 12.4.3.1 Patterns of Surface Warming: Land–Sea Contrast, Polar Amplification and Sea Surface Temperatures

Patterns of surface air temperature change for various RCPs show widespread warming during the 21st century (Figure 12.11; see Annex I for seasonal patterns). A key feature that has been present throughout the history of coupled modelling is the larger warming over land compared to oceans, which occurs in both transient and equilibrium climate change (e.g., Manabe et al., 1990). The degree to which warming is larger over land than ocean is remarkably constant over time under transient warming due to WMGHGs (Lambert and Chiang, 2007; Boer, 2011; Lambert et al., 2011) suggesting that heat capacity differences between land and ocean do not play a major role in the land–sea warming contrast (Sutton et al., 2007; Joshi et al., 2008,

2013). The phenomenon is predominantly a feature of the surface and lower atmosphere (Joshi et al., 2008). Studies have found it occurs due to contrasts in surface sensible and latent fluxes over land (Sutton et al., 2007), land–ocean contrasts in boundary layer lapse rate changes (Joshi et al., 2008), boundary layer relative humidity and associated low-level cloud cover changes over land (Doutriaux-Boucher et al., 2009; Fasullo, 2010) and soil moisture reductions (Dong et al., 2009; Clark et al., 2010) under climate change. The land–sea warming contrast is also sensitive to aerosol forcing (Allen and Sherwood, 2010; Joshi et al., 2013). Globally averaged warming over land and ocean is identified separately in Table 12.2 for the CMIP5 models and the ratio of land to ocean warming is *likely* in the range of 1.4 to 1.7, consistent with previous studies (Lambert et al., 2011). The CMIP5 multi-model mean ratio is approximately constant from 2020 through to 2100 (based on an update of Joshi et al., 2008 from available CMIP5 models).

Amplified surface warming in Arctic latitudes is also a consistent feature in climate model integrations (e.g., Manabe and Stouffer, 1980). This is often referred to as polar amplification, although numerous studies have shown that under transient forcing, this is primarily an Arctic phenomenon (Manabe et al., 1991; Meehl et al., 2007b). The lack of an amplified transient warming response in high Southern polar latitudes has been associated with deep ocean mixing, strong ocean heat uptake and the persistence of the vast Antarctic ice sheet. In equilibrium simulations, amplified warming occurs in both polar regions.

On an annual average, and depending on the forcing scenario (see Table 12.2), the CMIP5 models show a mean Arctic (67.5°N to 90°N) warming between 2.2 and 2.4 times the global average warming for 2081–2100 compared to 1986–2005. Similar polar amplification factors occurred in earlier coupled model simulations (e.g., Holland and Bitz, 2003; Winton, 2006a). This factor in models is slightly higher than the observed central value, but it is within the uncertainty of the best estimate from observations of the recent past (Bekryaev et al., 2010). The uncertainty is large in the observed factor because station records are short and sparse (Serreze and Francis, 2006) and the forced signal is contaminated by the noise of internal variability. By contrast, model trends in surface air temperature are 2.5 to 5 times higher than observed over Antarctica, but here also the observational estimates have a very large uncertainty, so, for example, the CMIP3 ensemble mean is consistent with observations within error estimates (Monaghan et al., 2008). Moreover, recent work suggests more widespread current West Antarctic surface warming than previously estimated (Bromwich et al., 2013).

The amplified Arctic warming in models has a distinct seasonal character (Manabe and Stouffer, 1980; Rind, 1987; Holland and Bitz, 2003; Lu and Cai, 2009; Kumar et al., 2010). Arctic amplification (defined as the 67.5 N° to 90°N warming compared to the global average warming for 2081–2100 versus 1986–2005) peaks in early winter (November to December) with a CMIP5 RCP4.5 multi-model mean warming for 67.5°N to 90°N exceeding the global average by a factor of more than 4. The warming is smallest in summer when excess heat at the Arctic surface goes into melting ice or is absorbed by the ocean, which has a relatively large thermal inertia. Simulated Arctic warming also has a consistent vertical structure that is largest in the lower troposphere

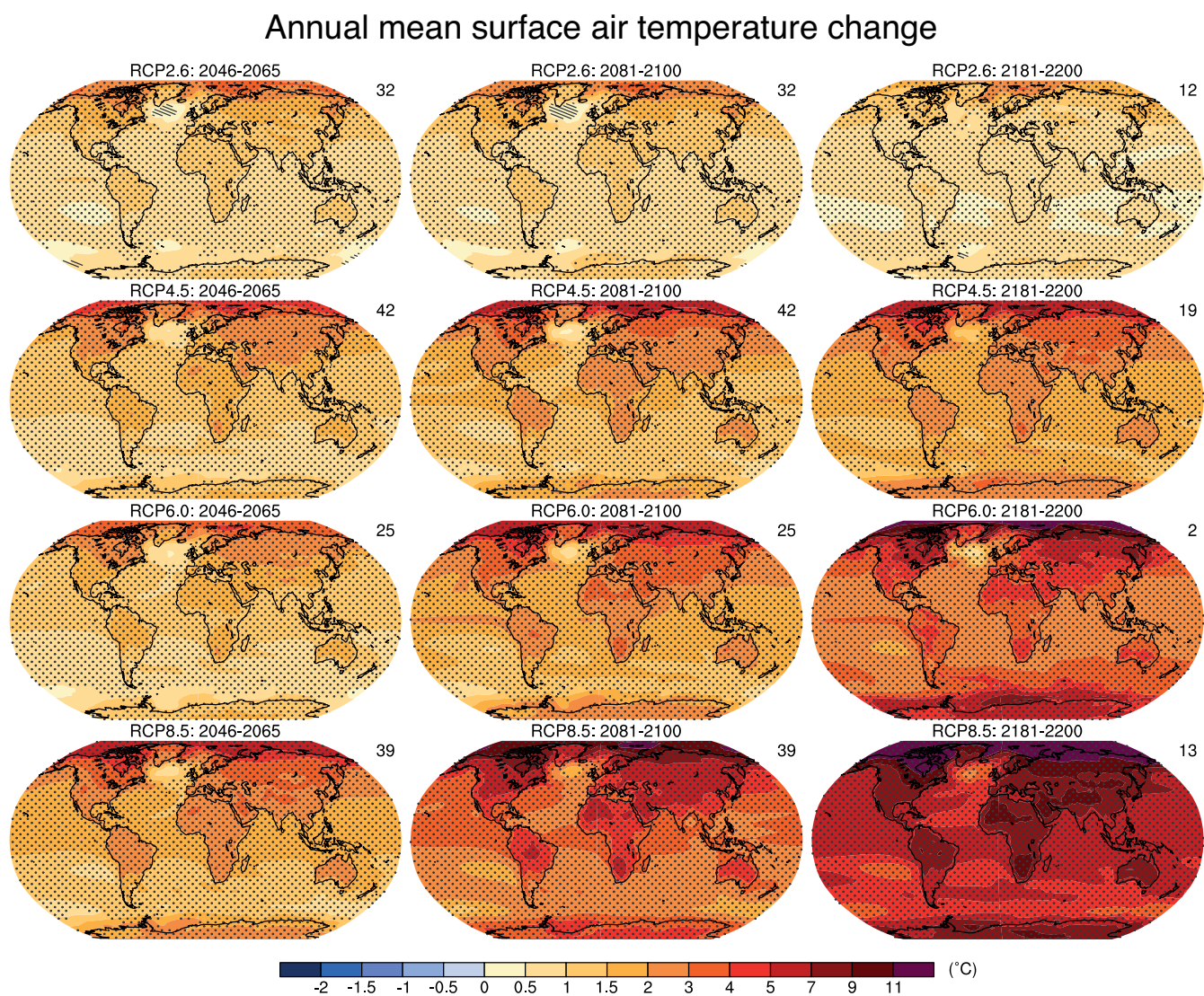


**Figure 12.11 |** Multi-model ensemble average of surface air temperature change (compared to 1986–2005 base period) for 2046–2065, 2081–2100, 2181–2200 for RCP2.6, 4.5, 6.0 and 8.5. Hatching indicates regions where the multi-model mean change is less than one standard deviation of internal variability. Stippling indicates regions where the multi-model mean change is greater than two standard deviations of internal variability and where at least 90% of the models agree on the sign of change (see Box 12.1). The number of CMIP5 models used is indicated in the upper right corner of each panel.

(e.g., Manabe et al., 1991; Kay et al., 2012). This is in agreement with recent observations (Serreze et al., 2009; Screen and Simmonds, 2010) but contrary to an earlier study that suggested a larger warming aloft (Graversen et al., 2008). The discrepancy in observed vertical structure may reflect inadequacies in data sets (Bitz and Fu, 2008; Grant et al., 2008; Thorne, 2008) and sensitivity to the time period used for averaging (see also Box 2.3).

As also discussed in Box 5.1, there are many mechanisms that contribute to Arctic amplification, some of which were identified in early modelling studies (Manabe and Stouffer, 1980). Feedbacks associated with changes in sea ice and snow amplify surface warming near the poles (Hall, 2004; Soden et al., 2008; Graversen and Wang, 2009; Kumar et al., 2010). The longwave radiation changes in the top of the atmosphere associated with surface warming opposes surface warming at all latitudes, but less so in the Arctic (Winton, 2006a; Soden et al., 2008). Rising temperature globally is expected to increase the hori-

12  
zontal latent heat transport by the atmosphere into the Arctic (Flannery, 1984; Alexeev et al., 2005; Cai, 2005; Langen and Alexeev, 2007; Kug et al., 2010), which warms primarily the lower troposphere. On average, CMIP3 models simulate enhanced latent heat transport (Held and Soden, 2006), but north of about 65°N, the sensible heat transport declines enough to more than offset the latent heat transport increase (Hwang et al., 2011). Increased atmospheric heat transport into the Arctic and subsidence warming has been associated with a teleconnection driven by enhanced convection in the tropical western Pacific (Lee et al., 2011). Ocean heat transport plays a role in the simulated Arctic amplification, with both large late 20th century transport (Mahlstein and Knutti, 2011) and increases over the 21st century (Hwang et al., 2011; Bitz et al., 2012) associated with higher amplification. As noted by Held and Soden (2006), Kay et al. (2012), and Alexeev and Jackson (2012), diagnosing the role of various factors in amplified warming is complicated by coupling in the system in which local feedbacks interact with poleward heat transports.

Although models consistently exhibit Arctic amplification as global mean temperatures rise, the multitude of physical processes described above mean that they differ considerably in the magnitude. Previous work has implicated variations across climate models in numerous factors including inversion strength (Boé et al., 2009a), ocean heat transport (Holland and Bitz, 2003; Mahlstein and Knutti, 2011), albedo feedback (Winton, 2006a), longwave radiative feedbacks (Winton, 2006a) and shortwave cloud feedback (Crook et al., 2011; Kay et al., 2012) as playing a role in the across-model scatter in polar amplification. The magnitude of amplification is generally higher in models with less extensive late 20th century sea ice in June, suggesting that the initial ice state influences the 21st century Arctic amplification. The pattern of simulated Arctic warming is also associated with the initial ice state, and in particular with the location of the winter sea ice edge (Holland and Bitz, 2003; Räisänen, 2007; Bracegirdle and Stephenson, 2012). This relationship has been suggested as a constraint on projected Arctic warming (Abe et al., 2011; Bracegirdle and Stephenson, 2012), although, in general, the ability of models to reproduce observed climate and its trends is not a sufficient condition for attributing *high confidence* to the projection of future trends (see Section 9.8).

Minima in surface warming occur in the North Atlantic and Southern Oceans under transient forcing in part due to deep ocean mixed layers in those regions (Manabe et al., 1990; Xie et al., 2010). Trenberth and Fasullo (2010) find that the large biases in the Southern Ocean energy budget in CMIP3 coupled models negatively correlate with equilibrium climate sensitivity (see Section 12.5.3), suggesting that an improved mean state in the Southern Ocean is needed before warming there can be understood. In the equatorial Pacific, warming is enhanced in a narrow band which previous assessments have described as ‘El Niño-like’, as may be expected from the projected decrease in atmospheric tropical circulations (see Section 12.4.4). However, DiNezio et al. (2009) highlight that the tropical Pacific warming in the CMIP3 models is not ‘El Niño-like’ as the pattern of warming and associated teleconnections (Xie et al., 2010; Section 12.4.5.2) is quite distinct from that of an El Niño event. Instead the pattern is of enhanced equatorial warming and is due to a meridional minimum in evaporative damping on the equator (Liu et al., 2005) and ocean dynamical changes that can be decoupled from atmospheric changes (DiNezio et al., 2009) (see also further discussion in Section 12.4.7).

In summary, there is robust evidence over multiple generations of models and *high confidence* in these large-scale warming patterns. In the absence of a strong reduction in the Atlantic Meridional Overturning Circulation (AMOC), there is *very high confidence* that the Arctic region is projected to warm most.

#### 12.4.3.2 Zonal Average Atmospheric Temperature

Zonal temperature changes at the end of the 21st century show warming throughout the troposphere and, depending on the scenario, a mix of warming and cooling in the stratosphere (Figure 12.12). The maximum warming in the tropical upper troposphere is consistent with theoretical explanations and associated with a decline in the moist adiabatic lapse rate of temperature in the tropics as the climate warms (Bony et al., 2006). The northern polar regions also experience large warming in the lower atmosphere, consistent with the mechanisms

discussed in Section 12.4.3.1. The tropospheric patterns are similar to those in the TAR and AR4 with the RCP8.5 changes being up to several degrees warmer in the tropics compared to the A1B changes appearing in the AR4. Similar tropospheric patterns appear in the RCP 2.6 and 4.5 changes, but with reduced magnitudes, suggesting some degree of scaling with forcing change in the troposphere, similar to behaviour discussed in the AR4 and Section 12.4.2. The consistency of tropospheric patterns over multiple generations of models indicates *high confidence* in these projected changes.

In the stratosphere, the models show similar tropical patterns of change, with magnitudes differing according to the degree of climate forcing. Substantial differences appear in polar regions. In the north, RCP8.5 and 4.5 yield cooling, though it is more significant in the RCP8.5 ensemble. In contrast, RCP2.6 shows warming, albeit weak and with little significance. In the southern polar region, RCP 2.6 and 4.5 both show significant warming, and RCP8.5 is the outlier, with significant cooling. The polar stratospheric warming, especially in the SH, is similar to that found by Butchart et al. (2010) and Meehl et al. (2012) in GCM simulations that showed effects of ozone recovery in determining the patterns (Baldwin et al., 2007; Son et al., 2010). Eyring et al. (2013) find behaviour in the CMIP5 ensemble both for models with and without interactive chemistry that supports the contention that the polar stratospheric changes in Figure 12.12 are strongly influenced by ozone recovery. Overall, the stratospheric temperature changes do not exhibit pattern scaling with global temperature change and are dependent on ozone recovery.

Away from the polar stratosphere, there is physical and pattern consistency in temperature changes between different generations of models assessed here and in the TAR and AR4. The consistency is especially clear in the northern high latitudes and, coupled with physical understanding, indicates that some of the greatest warming is *very likely* to occur here. There is also consistency across generations of models in relatively large warming in the tropical upper troposphere. Allen and Sherwood (2008) and Johnson and Xie (2010) have presented dynamic and thermodynamic arguments, respectively, for the physical robustness of the tropical behaviour. However, there remains uncertainty about the magnitude of warming simulated in the tropical upper troposphere because large observational uncertainties and contradictory analyses limit a confident assessment of model accuracy in simulating temperature trends in the tropical upper troposphere (Section 9.4.1.4.2). The combined evidence indicates that relatively large warming in the tropical upper troposphere is *likely*, but with *medium confidence*.

#### 12.4.3.3 Temperature Extremes

As the climate continues to warm, changes in several types of temperature extremes have been observed (Donat et al., 2013), and are expected to continue in the future in concert with global warming (Seneviratne et al., 2012). Extremes occur on multiple time scales, from a single day or a few consecutive days (a heat wave) to monthly and seasonal events. Extreme temperature events are often defined by indices (see Box 2.4 for the common definitions used), for example, percentage of days in a year when maximum temperature is above the 90th percentile of a present day distribution or by long period return values. Although changes in temperature extremes are a very robust

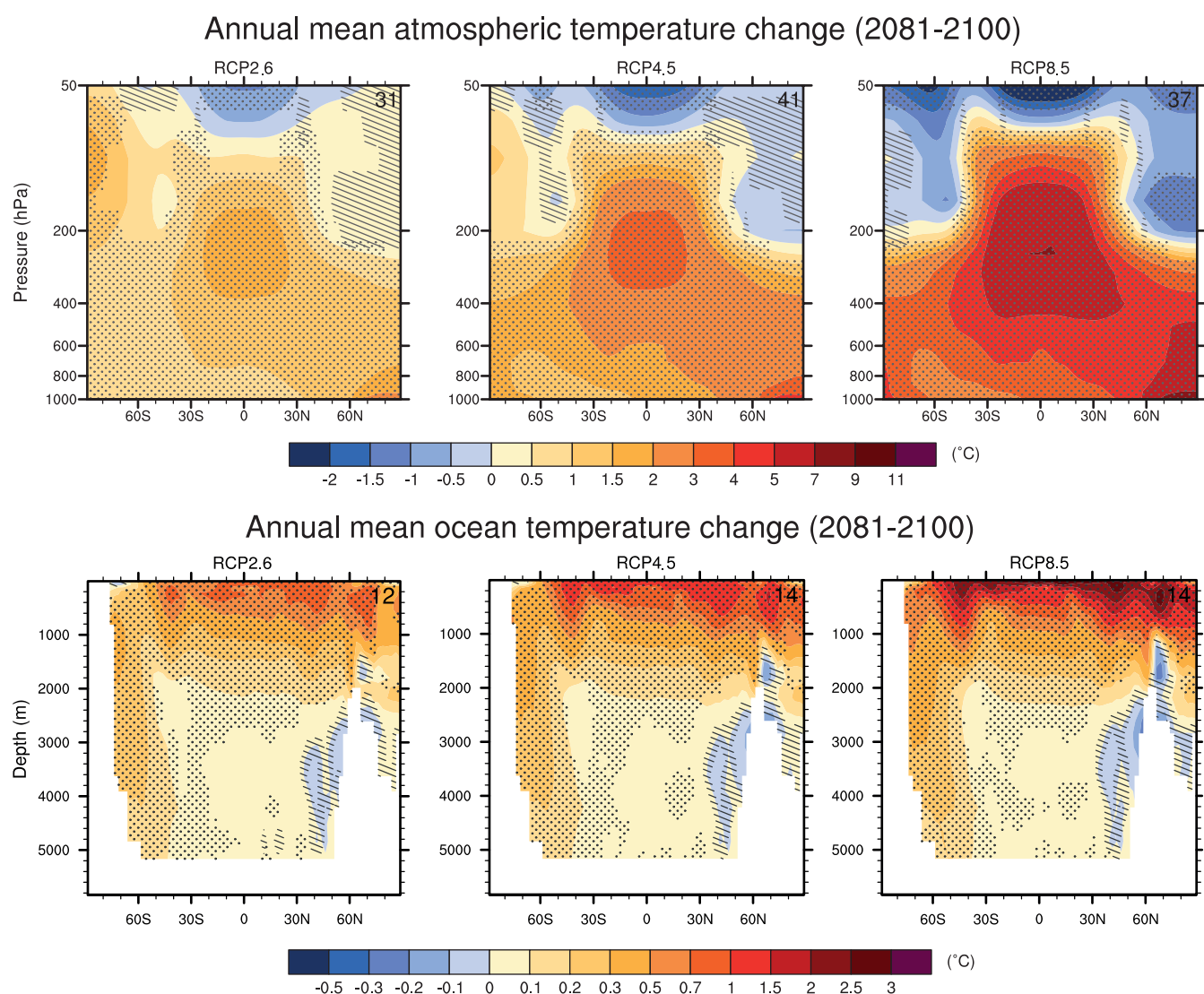


**Figure 12.12** CMIP5 multi-model changes in annual mean zonal mean temperature in the atmosphere and ocean relative to 1986–2005 for 2081–2100 under the RCP2.6 (left), RCP4.5 (centre) and RCP8.5 (right) forcing scenarios. Hatching indicates regions where the multi-model mean change is less than one standard deviation of internal variability. Stippling indicates regions where the multi-model change mean is greater than two standard deviations of internal variability and where at least 90% of the models agree on the sign of change (see Box 12.1).

signature of anthropogenic climate change (Seneviratne et al., 2012), the magnitude of change and consensus among models varies with the characteristics of the event being considered (e.g., time scale, magnitude, duration and spatial extent) as well as the definition used to describe the extreme.

Since the AR4 many advances have been made in establishing global observed records of extremes (Alexander et al., 2006; Perkins et al., 2012; Donat et al., 2013) against which models can be evaluated to give context to future projections (Sillmann and Roeckner, 2008; Alexander and Arblaster, 2009). Numerous regional assessments of future changes in extremes have also been performed and a comprehensive summary of these is given in Seneviratne et al. (2012). Here we summarize the key findings from this report and assess updates since then.

It is *virtually certain* that there will be more hot and fewer cold extremes as global temperature increases (Caesar and Lowe, 2012; Orlowsky

and Seneviratne, 2012; Sillmann et al., 2013), consistent with previous assessments (Solomon et al., 2007; Seneviratne et al., 2012). Figure 12.13 shows multi-model mean changes in the absolute temperature indices of the coldest day of the year and the hottest day of the year and the threshold-based indices of frost days and tropical nights from the CMIP5 ensemble (Sillmann et al., 2013). A robust increase in warm temperature extremes and decrease in cold temperature extremes is found at the end of the 21st century, with the magnitude of the changes increasing with increased anthropogenic forcing. The coldest night of the year undergoes larger increases than the hottest day in the globally averaged time series (Figure 12.13b and d). This tendency is consistent with the CMIP3 model results shown in Figure 12.13, which use different models and the SRES scenarios (see Seneviratne et al. (2012) for earlier CMIP3 results). Similarly, increases in the frequency of warm nights are greater than increases in the frequency of warm days (Sillmann et al., 2013). Regionally, the largest increases in the coldest night are projected in the high latitudes of

the NH under the RCP8.5 scenario (Figure 12.13a). The subtropics and mid-latitudes exhibit the greatest projected changes in the hottest day of the year, whereas changes in tropical nights and the frequency of warm days and warm nights are largest in the tropics (Sillmann et al., 2013). The number of frost days declines in all regions while significant increases in tropical nights are seen in southeastern North America, the Mediterranean and central Asia.

It is *very likely* that, on average, there will be more record high than record cold temperatures in a warmer average climate. For example, Meehl et al. (2009) find that the current ratio of 2 to 1 for record daily high maxima to low minima over the USA becomes approximately 20 to 1 by the mid-21st century and 50 to 1 by late century in their model simulation of the SRES A1B scenario. However, even at the end of the century daily record low minima continue to be broken, if in a small number, consistent with Kodra et al. (2011), who conclude that cold extremes will continue to occur in a warmer climate, even though their frequency will decline.

It is also *very likely* that heat waves, defined as spells of days with temperature above a threshold determined from historical climatology, will occur with a higher frequency and duration, mainly as a direct consequence of the increase in seasonal mean temperatures (Barnett et al., 2006; Ballester et al., 2010a, 2010b; Fischer and Schär, 2010). Changes in the absolute value of temperature extremes are also *very likely* and expected to regionally exceed global temperature increases by far, with substantial changes in hot extremes projected even for moderate ( $<2.5^{\circ}\text{C}$  above present day) average warming levels (Clark et al., 2010; Diffenbaugh and Ashfaq, 2010). These changes often differ from the mean temperature increase, as a result of changes in variability and shape of the temperature distribution (Hegerl et al., 2004; Meehl and Tebaldi, 2004; Clark et al., 2006). For example, summer temperature extremes over central and southern Europe are projected to warm substantially more than the corresponding mean local temperatures as a result of enhanced temperature variability at interannual to intraseasonal time scales (Schär et al., 2004; Clark et al., 2006; Kjellstrom et al., 2007; Vidale et al., 2007; Fischer and Schär, 2009, 2010; Nikulin et al., 2011; Fischer et al., 2012a). Several recent studies have also argued that the probability of occurrence of a Russian heat wave at least as severe as the one in 2010 increases substantially (by a factor of 5 to 10 by the mid-century) along with increasing mean temperatures and enhanced temperature variability (Barriopedro et al., 2011; Dole et al., 2011).

Since the AR4, an increased understanding of mechanisms and feedbacks leading to projected changes in extremes has been gained (Seneviratne et al., 2012). Climate models suggest that hot extremes are amplified by soil moisture-temperature feedbacks (Seneviratne et al., 2006; Diffenbaugh et al., 2007; Lenderink et al., 2007; Vidale et al., 2007; Fischer and Schär, 2009; Fischer et al., 2012a) in northern mid-latitude regions as the climate warms, consistent with previous assessments. Changes in temperature extremes may also be impacted by changes in land-sea contrast, with Watterson et al. (2008) showing an amplification of southern Australian summer warm extremes over the mean due to anomalous temperature advection from warmer continental interiors. The largest increases in the magnitude of warm extremes are simulated over mid-latitude continental areas, consistent

with the drier conditions, and the associated reduction in evaporative cooling from the land surface projected over these areas (Kharin et al., 2007). The representation of the latter constitutes a major source of model uncertainty for projections of the absolute magnitude of temperature extremes (Clark et al., 2010; Fischer et al., 2011).

Winter cold extremes also warm more than the local mean temperature over northern high latitudes (Orlowsky and Seneviratne, 2012; Sillmann et al., 2013) as a result of reduced temperature variability related to declining snow cover (Gregory and Mitchell, 1995; Kjellstrom et al., 2007; Fischer et al., 2011) and decreases in land-sea contrast (de Vries et al., 2012). Changes in atmospheric circulation, induced by remote surface heating can also modify the temperature distribution (Haarsma et al., 2009). Sillmann and Croci-Maspoli (2009) note that cold winter extremes over Europe are in part driven by atmospheric blocking and changes to these blocking patterns in the future lead to changes in the frequency and spatial distribution of cold temperature extremes as global temperatures increase. Occasional cold winters will continue to occur (Räisänen and Ylhäisi, 2011).

Human discomfort, morbidity and mortality during heat waves depend not only on temperature but also specific humidity. Heat stress, defined as the combined effect of temperature and humidity, is expected to increase along with warming temperatures and dominates the local decrease in summer relative humidity due to soil drying (Diffenbaugh et al., 2007; Fischer et al., 2012b; Dunne et al., 2013). Areas with abundant atmospheric moisture availability and high present-day temperatures such as Mediterranean coastal regions are expected to experience the greatest heat stress changes because the heat stress response scales with humidity which thus becomes increasingly important to heat stress at higher temperatures (Fischer and Schär, 2010; Sherwood and Huber, 2010; Willett and Sherwood, 2012). For some regions, simulated heat stress indicators are remarkably robust, because those models with stronger warming simulate a stronger decrease in atmospheric relative humidity (Fischer and Knutti, 2013).

Changes in rare temperature extremes can be assessed using extreme value theory based techniques (Seneviratne et al., 2012). Kharin et al. (2007), in an analysis of CMIP3 models, found large increases in the 20-year return values of the annual maximum and minimum daily averaged surface air temperatures (i.e., the size of an event that would be expected on average once every 20 years, or with a 5% chance every year) with larger changes over land than ocean. Figure 12.14 displays the end of 21st century change in the magnitude of these rare events from the CMIP5 models in the RCP2.6, 4.5 and 8.5 scenarios (Kharin et al., 2013). Comparison to the changes in summer mean temperature shown in Figure AI.5 and A1.7 of Annex I Supplementary Material reveals that rare high temperature events are projected to change at rates similar to or slightly larger than the summertime mean temperature in many land areas. However, in much of Northern Europe 20-year return values of daily high temperatures are projected to increase 2°C or more than JJA mean temperatures under RCP8.5, consistent with previous studies (Sterl et al., 2008; Orlowsky and Seneviratne, 2012). Rare low temperature events are projected to experience significantly larger increases than the mean in most land regions, with a pronounced effect at high latitudes. Twenty-year return values of cold extremes increase significantly more than

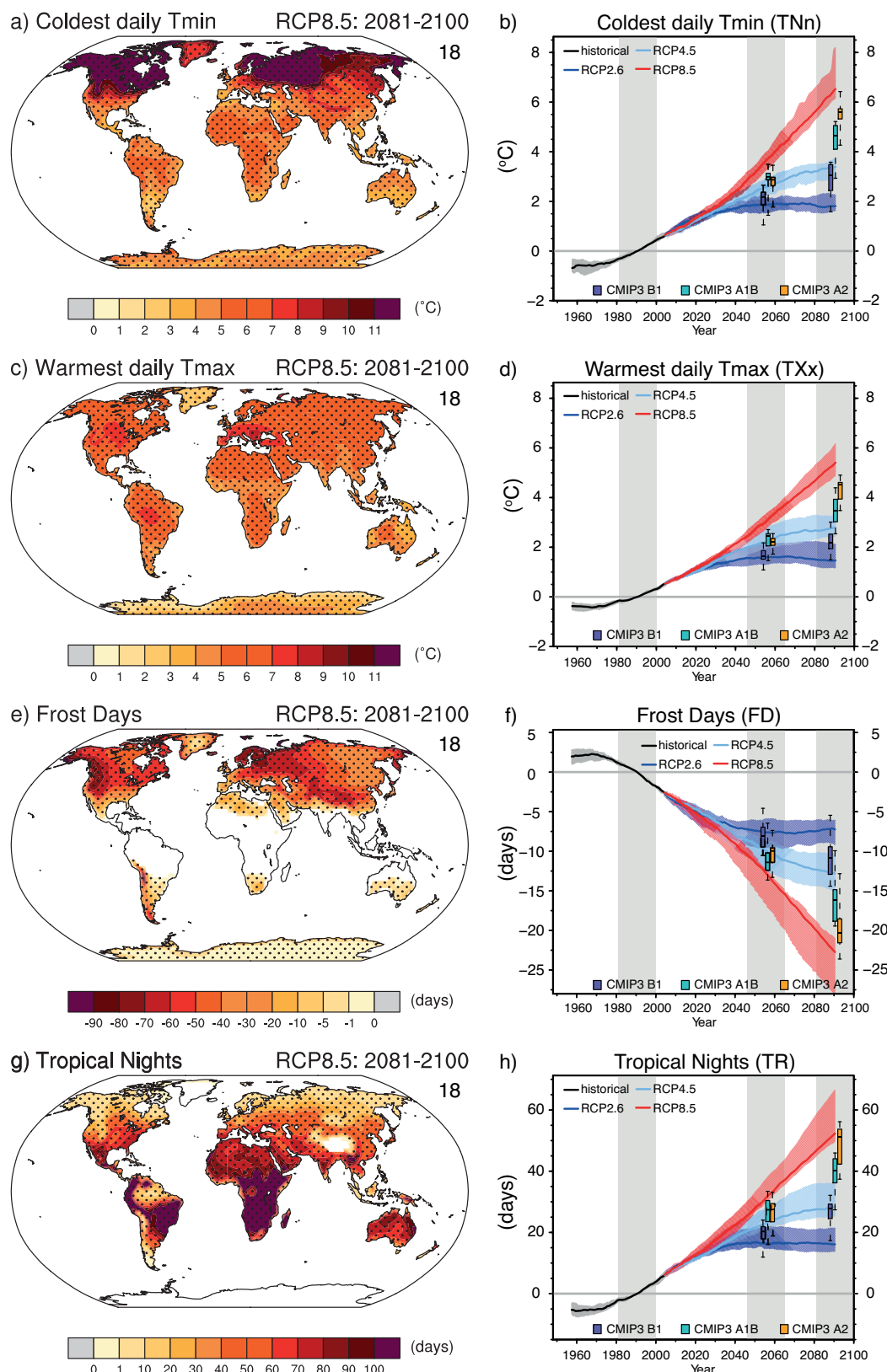


**Figure 12.13 |** CMIP5 multi-model mean geographical changes (relative to a 1981–2000 reference period in common with CMIP3) under RCP8.5 and 20-year smoothed time series for RCP2.6, RCP4.5 and RCP8.5 in the (a, b) annual minimum of daily minimum temperature, (c, d) annual maximum of daily maximum temperature, (e, f) frost days (number of days below 0°C) and (g, h) tropical nights (number of days above 20°C). White areas over land indicate regions where the index is not valid. Shading in the time series represents the interquartile ensemble spread (25th and 75th quantiles). The box-and-whisker plots show the interquartile ensemble spread (box) and outliers (whiskers) for 11 CMIP3 model simulations of the SRES scenarios A2 (orange), A1B (cyan), and B1 (purple) globally averaged over the respective future time periods (2046–2065 and 2081–2100) as anomalies from the 1981–2000 reference period. Stippling indicates grid points with changes that are significant at the 5% level using a Wilcoxon signed-ranked test. (Updated from Sillmann et al. (2013), excluding the FGOALS-s2 model.)

winter mean temperature changes, particularly over parts of North America and Europe. Kharin et al. (2013) concluded from the CMIP5 models that it is *likely* that in most land regions a current 20 year maximum temperature event is projected to become a one-in-two-year event by the end of the 21st century under the RCP4.5 and RCP8.5 scenarios, except for some regions of the high latitudes of the NH where it is *likely* to become a one-in-five-year event (see also Seneviratne et al. (2012) Figure 3.5). Current 20-year minimum temperature events are projected to become exceedingly rare, with return periods *likely* increasing to more than 100 years in almost all locations under RCP8.5 (Kharin et al., 2013). Section 10.6.1.1 notes that a number of detection and attribution studies since SREX suggest that the model changes may tend to be too large for warm extremes and too small for cold extremes and thus these likelihood statements are somewhat less strongly stated than a direct interpretation of model output and

its ranges. The CMIP5 analysis shown in Figure 12.14 reinforces this assessment of large changes in the frequency of rare events, particularly in the RCP8.5 scenario (Kharin et al., 2013).

There is high consensus among models in the sign of the future change in temperature extremes, with recent studies confirming this conclusion from the previous assessments (Tebaldi et al., 2006; Meehl et al., 2007b; Orlowsky and Seneviratne, 2012; Seneviratne et al., 2012; Sillmann et al., 2013). However, the magnitude of the change remains uncertain owing to scenario and model (both structural and parameter) uncertainty (Clark et al., 2010) as well as internal variability. These uncertainties are much larger than corresponding uncertainties in the magnitude of mean temperature change (Barnett et al., 2006; Clark et al., 2006; Fischer and Schär, 2010; Fischer et al., 2011).

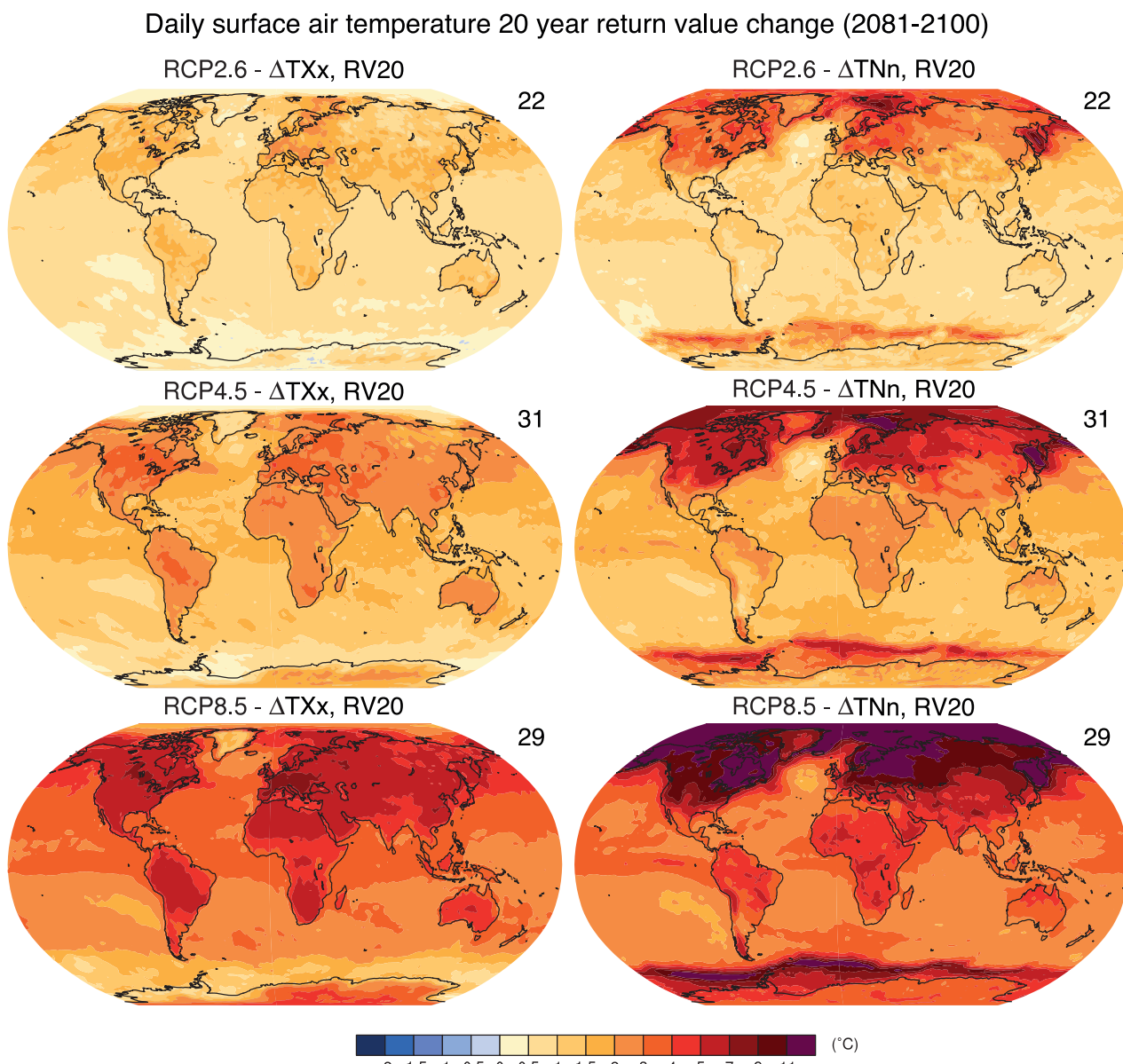


**Figure 12.14 |** The CMIP5 multi-model median change in 20-year return values of annual warm temperature extremes (left-hand panels) and cold temperature extremes (right-hand panels) as simulated by CMIP5 models in 2081–2100 relative to 1986–2005 in the RCP2.6 (top), RCP4.5 (middle) and RCP8.5 (bottom) experiments.

#### 12.4.3.4 Energy Budget

Anthropogenic or natural perturbations to the climate system produce RFs that result in an imbalance in the global energy budget at the top of the atmosphere (TOA) and affect the global mean temperature (Section 12.3.3). The climate responds to a change in RF on multiple time scales and at multiyear time scales the energy imbalance (i.e., the energy heating or cooling the Earth) is very close to the ocean heat uptake due to the much lower thermal inertia of the atmosphere and the continental surfaces (Levitus et al., 2005; Knutti et al., 2008a; Murphy et al., 2009; Hansen et al., 2011). The radiative responses of the fluxes at TOA are generally analysed using the forcing-feedback framework and are presented in Section 9.7.2.

CMIP5 models simulate a small increase of the energy imbalance at the TOA over the 20th century (see Box 3.1, Box 9.2 and Box 13.1). The future evolution of the imbalance is very different depending on the scenario (Figure 12.15a): for RCP8.5 it continues to increase rapidly, much less for RCP6.0, it is almost constant for RCP4.5 and decreases for RCP2.6. This latter negative trend reveals the quasi-stabilization characteristic of RCP2.6. (In a transient scenario simulation, the TOA

imbalance is always less than the RF because of the slow rate of ocean heat uptake.)

The rapid fluctuations that are simulated during the 20th century originate from volcanic eruptions that are prescribed in the models (see Section 12.3.2). These aerosols reflect solar radiation and thus decrease the amount of SW radiation absorbed by the Earth (Figure 12.15c). The minimum of shortwave (SW) radiation absorbed by the Earth during the period 1960–2000 is due mainly to two factors: a sequence of volcanic eruptions and an increase of the reflecting aerosol burden due to human activities (see Sections 7.5, 8.5 and 9.4.6). During the 21st century, the absorbed SW radiation monotonically increases for the RCP8.5 scenario, and increases and subsequently stabilizes for the other scenarios, consistent with what has been previously obtained with CMIP3 models and SRES scenarios (Trenberth and Fasullo, 2009). The two main contributions to the SW changes are the change of clouds (see Section 12.4.3.5) and the change of the cryosphere (see Section 12.4.6) at high latitudes. In the longwave (LW) domain (Figure 12.15b), the net flux at TOA represents the opposite of the flux that is emitted by the Earth's surface and atmosphere toward space, i.e., a negative anomaly represents an increase of the emitted

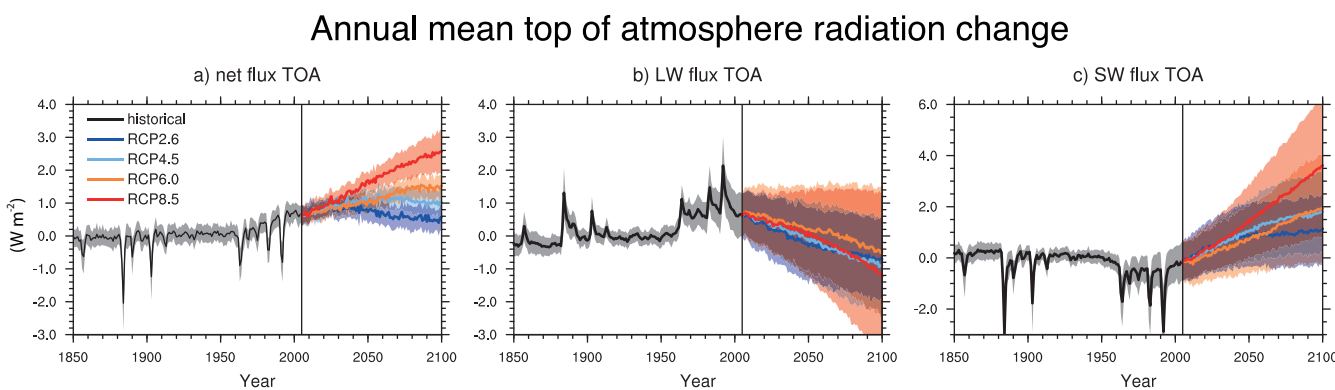


**Figure 12.15 |** Time series of global and annual multi-model mean (a) net total radiation anomaly at the top of the atmosphere (TOA), (b) net longwave radiation anomaly at the TOA and (c) net shortwave radiation anomaly at the TOA from the CMIP5 concentration-driven experiments for the historical period (black) and the four RCP scenarios. All the fluxes are positive downward and units are  $\text{W m}^{-2}$ . The anomalies are calculated relative to the 1900–1950 base period as this is a common period to all model experiments with few volcanic eruptions and relatively small trends. One ensemble member is used for each individual CMIP5 model and the  $\pm$  standard deviation across the distribution of individual models is shaded.

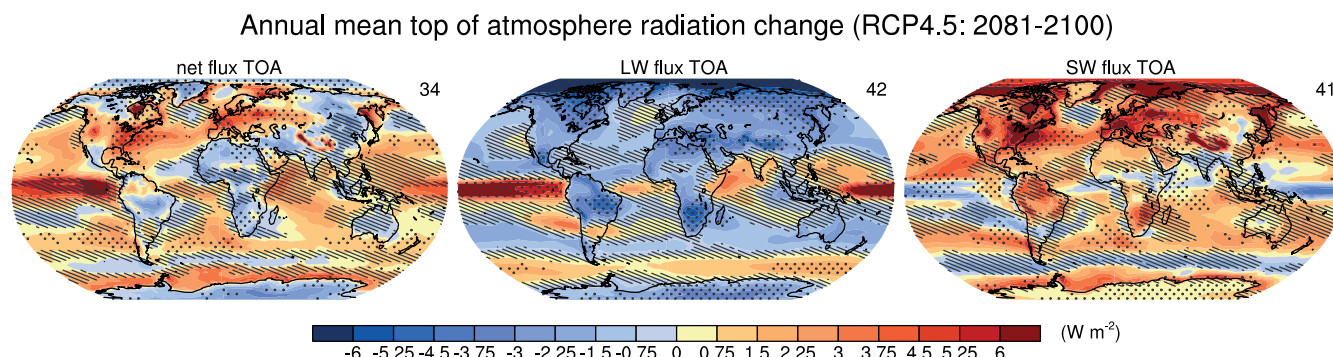


**Figure 12.16 |** Multi-model CMIP5 average changes in annual mean (left) net total radiation anomaly at the top of the atmosphere (TOA), (middle) net longwave radiation anomaly at the TOA and (right) net shortwave radiation anomaly at the TOA for the RCP4.5 scenario averaged over the periods 2081–2100. All fluxes are positive downward, units are  $\text{W m}^{-2}$ . The net radiation anomalies are computed with respect to the 1900–1950 base period. Hatching indicates regions where the multi-model mean change is less than one standard deviation of internal variability. Stippling indicates regions where the multi-model mean change is greater than two standard deviations of internal variability and where at least 90% of models agree on the sign of change (see Box 12.1).

LW radiation. The LW net flux depends mainly on two factors: the surface temperature and the magnitude of the greenhouse effect of the atmosphere. During the 20th century, the rapid fluctuations of LW radiation are driven by volcanic forcings, which decrease the absorbed SW radiation, surface temperature, and the LW radiation emitted by the Earth toward space. During the period 1960–2000, the fast increase of GHG concentrations also decreases the radiation emitted by the Earth. In response to this net heating of the Earth, temperatures warm and thereby increase emitted LW radiation although the change of the temperature vertical profile, water vapour, and cloud properties modulate this response (e.g., Bony et al., 2006; Randall et al., 2007).

#### 12.4.3.5 Clouds

This section provides a summary description of future changes in clouds and their feedbacks on climate. A more general and more precise description and assessment of the role of clouds in the climate system is provided in Chapter 7, in particular Section 7.2 for cloud processes and feedbacks and Section 7.4 for aerosol–cloud interactions. Cloud feedbacks and adjustments are presented in Section 7.2.5 and a synthesis is provided in Section 7.2.6. Clouds are a major component of the climate system and play an important role in climate sensitivity (Cess et al., 1990; Randall et al., 2007), the diurnal temperature range (DTR) over land (Zhou et al., 2009), and land–sea contrast (see Section 12.4.3.1). The observed global mean cloud RF is about  $-20\text{ W m}^{-2}$  (Loeb et al., 2009) (see Section 7.2.1), that is, clouds have a net cooling effect. Current GCMs simulate clouds through various complex parameterizations (see Section 7.2.3), and cloud feedback is a major source of the spread of the climate sensitivity estimate (Soden and Held, 2006; Randall et al., 2007; Dufresne and Bony, 2008) (see Section 9.7.2).

Under future projections the multi-model pattern of total cloud amount shows consistent decreases in the subtropics, in conjunction with a decrease of the relative humidity there, and increases at high latitudes. Another robust pattern is an increase in cloud cover at all latitudes in the vicinity of the tropopause, a signature of the increase of the altitude of high level clouds in convective regions (Wetherald and Manabe, 1988; Meehl et al., 2007b; Soden and Vecchi, 2011; Zelinka et al., 2012). Low-level clouds were identified as a primary cause of inter-model spread in cloud feedbacks in CMIP3 models (Bony and

Dufresne, 2005; Webb et al., 2006; Wyant et al., 2006). Since AR4, these results have been confirmed along with the positive feedbacks due to high level clouds in the CMIP3 or CFMIP models (Zelinka and Hartmann, 2010; Soden and Vecchi, 2011; Webb et al., 2013) and CMIP5 models (Vial et al., 2013). Since AR4, the response of clouds has been partitioned in a direct or ‘rapid’ response of clouds to  $\text{CO}_2$  and a ‘slow’ response of clouds to the surface temperature increase (i.e., the usual feedback response) (Gregory and Webb, 2008). The radiative effect of clouds depends mainly on their fraction, optical depth and temperature. The contribution of these variables to the cloud feedback has been quantified for the multi-model CMIP3 (Soden and Vecchi, 2011) and CFMIP1 database (Zelinka et al., 2012). These findings are consistent with the radiative changes obtained with the CMIP5 models (Figure 12.16) and may be summarized as follows (see Section 7.2.5 for more details).

The dominant contributor to the SW cloud feedback is the change in cloud fraction. The reduction of cloud fraction between  $50^\circ\text{S}$  and  $50^\circ\text{N}$ , except along the equator and the eastern part of the ocean basins (Figure 12.17), contributes to an increase in the absorbed solar radiation (Figure 12.16c). Physical mechanisms and the role of different parameterizations have been proposed to explain this reduction of low-level clouds (Zhang and Bretherton, 2008; Caldwell and Bretherton, 2009; Briant and Bony, 2013; Webb et al., 2013). Poleward of  $50^\circ\text{S}$ , the cloud fraction and the cloud optical depth increases, thereby increasing cloud reflectance. This leads to a decrease of solar absorption around Antarctica where the ocean is nearly ice free in summer (Figure 12.16c). However, there is *low confidence* in this result because GCMs do not reproduce the nearly 100% cloud cover observed there and the negative feedback could be overestimated (Trenberth and Fasullo, 2010) or, at the opposite, underestimated because the cloud optical depth simulated by models is biased high there (Zelinka et al., 2012).

In the LW domain, the tropical high cloud changes exert the dominant effect. A lifting of the cloud top with warming is simulated consistently across models (Meehl et al., 2007b) which leads to a positive feedback whereby the LW emissions from high clouds decrease as they cool (Figure 12.16b). The dominant driver of this effect is the increase of tropopause height and physical explanations have been proposed (Hartmann and Larson, 2002; Lorenz and DeWeaver, 2007; Zelinka

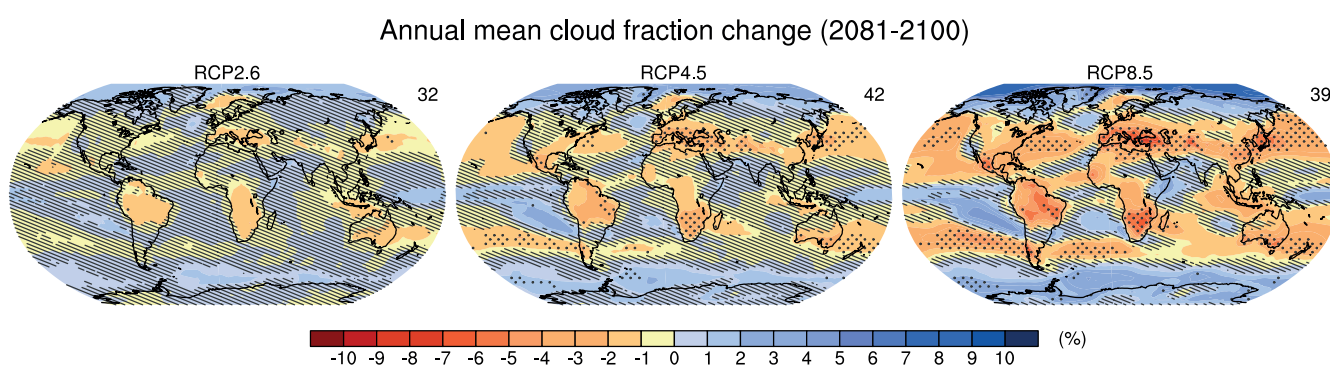


**Figure 12.17 |** CMIP5 multi-model changes in annual mean total cloud fraction (in %) relative to 1986–2005 for 2081–2100 under the RCP2.6 (left), RCP4.5 (centre) and RCP8.5 (right) forcing scenarios. Hatching indicates regions where the multi-model mean change is less than one standard deviation of internal variability. Stippling indicates regions where the multi-model mean change is greater than two standard deviations of internal variability and where 90% of the models agree on the sign of change (see Box 12.1). The number of CMIP5 models used is indicated in the upper right corner of each panel.

and Hartmann, 2010). Although the decrease in cloudiness generally increases outgoing longwave radiation and partly offsets the effect of cloud rising, the net effect is a consistent positive global mean LW cloud feedback across CMIP and CFMIP models. Global mean SW cloud feedbacks range from slightly negative to strongly positive (Soden and Vecchi, 2011; Zelinka et al., 2012), with an inter-model spread in net cloud feedback being mainly attributable to low-level cloud changes.

In summary, both the multi-model mean and the inter-model spread of the cloud fraction and radiative flux changes simulated by the CMIP5 models are consistent with those previously obtained by the CMIP3 models. These include decreases in cloud amount in the subtropics, increases at high latitudes and increases in the altitude of high level clouds in convective regions. Many of these changes have been understood primarily as responses to large-scale circulation changes (see Section 7.2.6).

#### 12.4.4 Changes in Atmospheric Circulation

Projected changes in energy and water cycles couple with changes in atmospheric circulation and mass distribution. Understanding this coupling is necessary to assess physical behaviour underlying projected changes, particularly at regional scales, revealing why changes occur and the realism of the changes. The focus in this section is on atmospheric circulation behaviour that CMIP5 GCMs resolve well. Thus, the section includes discussion of extratropical cyclones but not tropical cyclones: extratropical cyclones are fairly well resolved by most CMIP5 GCMs, whereas tropical cyclones are not, requiring resolutions finer than used by the large majority of CMIP5 GCMs (see Section 9.5.4.3). Detailed discussion of tropical cyclones appears in Section 14.6.1 (see also Section 11.3.2.5.3 for near term changes and Section 3.4.4 in Seneviratne et al. (2012)). Regional detail concerning extratropical storm tracks, including causal processes, appears in Section 14.6.2

(see also Section 11.3.2.4 for near-term changes and Seneviratne et al. (2012) for an assessment of projected changes related to weather and climate extremes).

##### 12.4.4.1 Mean Sea Level Pressure and Upper-Air Winds

Sea level pressure gives an indication of surface changes in atmospheric circulation (Figure 12.18). As in previous assessments, a robust feature of the pattern of change is a decrease in high latitudes and increases in the mid-latitudes, associated with poleward shifts in the SH mid-latitude storm tracks (Section 12.4.4.3) and positive trends in the annular modes (Section 14.5) as well as an expansion of the Hadley Cell (Section 12.4.4.2). Similar patterns of sea level pressure change are found in observed trends over recent decades, suggesting an already detectable change (Gillett and Stott, 2009; Section 10.3.3.4), although the observed patterns are influenced by both natural and anthropogenic forcing as well as internal variability and the relative importance of these influences is likely to change in the future. Internal variability has been found to play a large role in uncertainties of future sea level pressure projections, particularly at higher latitudes (Deser et al., 2012a).

In boreal winter, decreases of sea level pressure over NH high latitudes are slightly weaker in the CMIP5 ensemble compared to previous assessments, consistent with Scaife et al. (2012) and Karpechko and Manzini (2012), who suggest that improvements in the representation of the stratosphere can influence this pattern. In austral summer, the SH projections are impacted by the additional influence of stratospheric ozone recovery (see Section 11.3.2.4.2) which opposes changes due to GHGs. Under the weaker GHG emissions of RCP2.6, decreases in sea level pressure over the SH mid-latitudes and increases over SH high latitudes are consistent with expected changes from ozone recovery (Arblaster et al., 2011; McLandress et al., 2011; Polvani et al., 2011). For

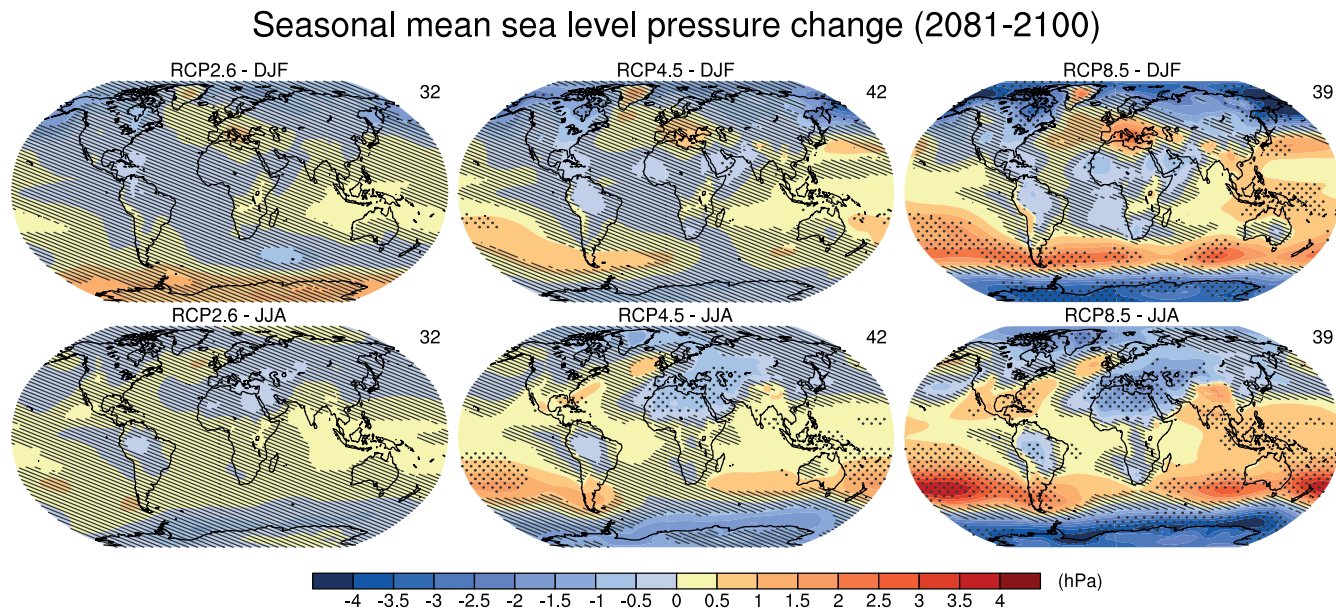


**Figure 12.18 |** CMIP5 multi-model ensemble average of December, January and February (DJF, top row) and June, July and August (JJA, bottom row) mean sea level pressure change (2081–2100 minus 1986–2005) for, from left to right, RCP2.6, 4.5 and 8.5. Hatching indicates regions where the multi-model mean change is less than one standard deviation of internal variability. Stippling indicates regions where the multi-model mean change is greater than two standard deviations of internal variability and where at least 90% of models agree on the sign of change (see Box 12.1).

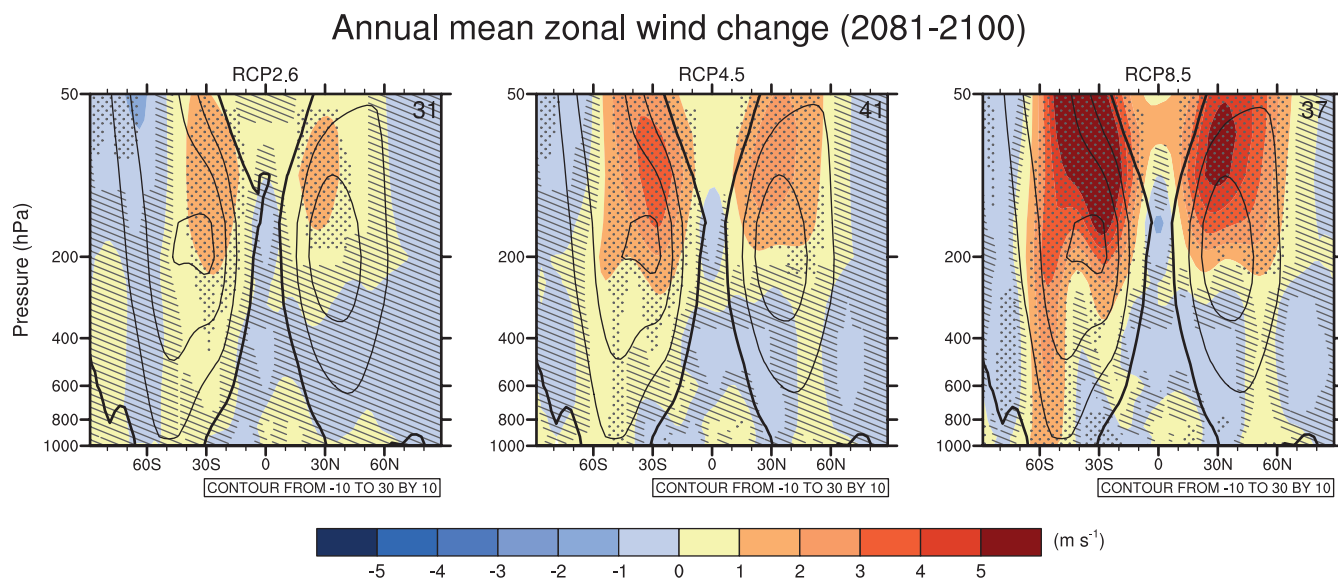


**Figure 12.19 |** Coupled Model Intercomparison Project Phase 5 (CMIP5) multi-model ensemble average of zonal and annual mean wind change (2081–2100 minus 1986–2005) for, from left to right, Representative Concentration Pathway 2.6 (RCP2.6), 4.5 and 8.5. Black contours represent the multi-model average for the 1986–2005 base period. Hatching indicates regions where the multi-model mean change is less than one standard deviation of internal variability. Stippling indicates regions where the multi-model mean change is greater than two standard deviations of internal variability and where at least 90% of models agree on the sign of change (see Box 12.1).

all other RCPs, the magnitude of SH extratropical changes scales with the RF, as found in previous model ensembles (Paeth and Pollinger, 2010; Simpkins and Karpechko, 2012).

Large increases in seasonal sea level pressure are also found in regions of sub-tropical drying such as the Mediterranean and northern Africa in DJF and Australia in JJA. Projected changes in the tropics are less consistent across the models; however, a decrease in the eastern equatorial Pacific and increase over the maritime continent, associated with a weakening of the Walker Circulation (Vecchi and Soden, 2007; Power and Kociuba, 2011b), is found in all RCPs.

Future changes in zonal and annual mean zonal winds (Figure 12.19) are seen throughout the atmosphere with stronger changes in higher RCPs. Large increases in winds are evident in the tropical stratosphere and a poleward shift and intensification of the SH tropospheric jet is seen under RCP4.5 and RCP8.5, associated with an increase in the SH upper tropospheric meridional temperature gradient (Figure 12.12) (Wilcox et al., 2012). In the NH, the response of the tropospheric jet is weaker and complicated by the additional thermal forcing of polar amplification (Woollings, 2008). Barnes and Polvani (2013) evaluate changes in the annual mean mid-latitude jets in the CMIP5 ensemble, finding consistent poleward shifts in both hemispheres under RCP8.5 for the end of the 21st century. In the NH, the poleward shift is  $\sim 1^\circ$ , similar to that found for the CMIP3 ensemble (Woollings and Blackburn, 2012). In the SH, the annual mean mid-latitude jet shifts poleward by  $\sim 2^\circ$  under RCP8.5 at the end of the 21st century in the CMIP5 multi-model mean (Barnes and Polvani, 2013), with a similar shift of  $1.5^\circ$  in the surface westerlies (Swart and Fyfe, 2012). A strengthening of the SH surface westerlies is also found under all RCPs except RCP2.6 (Swart and Fyfe, 2012), with largest changes in the Pacific basin (Bracegirdle et al., 2013). In austral summer, ozone recovery offsets changes in GHGs to some extent, with a weak reversal of the jet

shift found in the multi-model mean under the low emissions scenario of RCP2.6 (Swart and Fyfe, 2012) and weak or poleward shifts in other RCPs (Swart and Fyfe, 2012; Wilcox et al., 2012). Eyring et al. (2013) note the sensitivity of the CMIP5 SH summertime circulation changes to both the strength of the ozone recovery (simulated by some models interactively) and the rate of GHG increases.

Although the poleward shift of the tropospheric jets are robust across models and *likely* under increased GHGs, the dynamical mechanisms behind these projections are still not completely understood and have been explored in both simple and complex models (Chen et al., 2008; Lim and Simmonds, 2009; Butler et al., 2010). The shifts are associated with a strengthening in the upper tropospheric meridional temperature gradient (Wilcox et al., 2012) and hypotheses for associated changes in planetary wave activity and/or synoptic eddy characteristics that impact on the position of the jet have been put forward (Gerber et al., 2012). Equatorward biases in the position of the SH jet (Section 9.5.3.2), while somewhat improved over similar biases in the CMIP3 models (Kidston and Gerber, 2010) still remain, limiting our confidence in the magnitude of future changes.

In summary, poleward shifts in the mid-latitude jets of about 1 to 2 degrees latitude are *likely* at the end of the 21st century under RCP8.5 in both hemispheres (*medium confidence*) with weaker shifts in the NH and under lower emission scenarios. Ozone recovery will *likely* weaken the GHG-induced changes in the SH extratropical circulation in austral summer.

#### 12.4.4.2 Planetary-Scale Overturning Circulations

Large-scale atmospheric overturning circulations and their interaction with other atmospheric mechanisms are significant in determining tropical climate and regional changes in response to enhanced RF. Observed

changes in tropical atmospheric circulation are assessed in Section 2.7.5, while Section 10.3.3 discusses attribution of these observed changes to anthropogenic forcing. Evidence is inconclusive on recent trends in the strength of the Hadley (Stachnik and Schumacher, 2011) and Walker Circulations (Vecchi et al., 2006; Sohn and Park, 2010; Merrifield, 2011; Luo et al., 2012; Tokinaga et al., 2012), though there is *medium confidence* of an anthropogenic influence on the observed widening of the Hadley Circulation (Hu and Fu, 2007; Johanson and Fu, 2009; Davis and Rosenlof, 2012). In the projections, there are indications of a weakening of tropical overturning of air as the climate warms (Held and Soden, 2006; Vecchi and Soden, 2007; Gastineau et al., 2008, 2009; Chou and Chen, 2010; Chadwick et al., 2012; Bony et al., 2013). In the SRES A1B scenario, CMIP3 models show a remarkable agreement in simulating a weakening of the tropical atmospheric overturning circulation (Vecchi and Soden, 2007). CMIP5 models also show a consistent weakening (Chadwick et al., 2012). Along the ascending branches of tropical overturning cells, a reduction in convective mass flux from the boundary layer to the free atmosphere is implied by the differential response to global warming of the boundary-layer moisture content and surface evaporation. This weakening of vertical motion along the ascending regions of both the tropical meridional and near-equatorial zonal cells is associated with an imbalance in the rate of atmospheric moisture increase and that of global mean precipitation (Held and Soden, 2006). A reduction in the compensating climatological subsidence along the downward branches of overturning circulations, where the rate of increase of static stability exceeds radiative cooling, is implied.

Several mechanisms have been suggested for the changes in the intensity of the tropical overturning circulation. The weakening of low-level convective mass flux along ascending regions of tropical overturning cells has been ascribed to changes in the hydrologic cycle (Held and Soden, 2006; Vecchi and Soden, 2007). Advection of dry air from subsidence regions towards the ascending branches of large-scale tropical circulation has been suggested to be a feasible mechanism weakening ascent along the edges of convection regions (Chou et al., 2009). A deepening of the tropical troposphere in response to global warming increases the vertical extent of convection, which has been shown to increase the atmosphere's moist stability and thus also weakening overturning cells (Chou and Chen, 2010). An imbalance between the increase in diabatic heating of the troposphere and in static stability whereby the latter increases more rapidly has also been thought to play a role in weakening tropical ascent (Lu et al., 2008). Mean advection of enhanced vertical stratification under GHG forcing which involves cooling of convective regions and warming of subsidence regions has been shown to slow down tropical cells (Ma et al., 2012). The latest findings using CMIP5 models reveal that an increase in GHGs (particularly CO<sub>2</sub>) contributes significantly to weakening tropical overturning cells by reducing radiative cooling in the upper atmosphere (Bony et al., 2013). SST gradients have also been found to play a role in altering the strength of tropical cells (Tokinaga et al., 2012; Ma and Xie, 2013). Evidence has been provided suggesting that the SH Hadley Cell may strengthen in response to meridional SST gradients featuring reduced warming in the SH subtropical oceans relative to the NH, particularly over the Pacific and Indian Oceans (Ma and Xie, 2013). The north-to-south SST warming gradients are a source of intermodel differences in their projections of changes in the SH Hadley Circulation.

Apart from changes in Hadley Circulation strength, a robust feature in 21st century climate model simulations is an increase in the cell's depth and width (Mitas and Clement, 2006; Frierson et al., 2007; Lu et al., 2007; Lu et al., 2008), with the latter change translating to a broadening of tropical regions (Seidel and Randel, 2007; Seidel et al., 2008) and a poleward displacement of subtropical dry zones (Lu et al., 2007; Scheff and Frierson, 2012). The increase in the cell's depth is consistent with a tropical tropopause rise. The projected increase in the height of the tropical tropopause and the associated increase in meridional temperature gradients close to the tropopause slope have been proposed to be an important mechanism behind the Hadley cell expansion and the poleward displacement of the subtropical westerly jet (Lu et al., 2008; Johanson and Fu, 2009). An increase in subtropical and mid-latitude static stability has been found to be an important factor widening the Hadley Cell by shifting baroclinic eddy activity and the associated eddy-driven jet and subsidence poleward (Mitas and Clement, 2006; Lu et al., 2008). The projected widening of the Hadley Cell is consistent with late 20th century observations, where ~2° to 5° latitude expansion was found (Fu et al., 2006; Johanson and Fu, 2009). The consistency of simulated changes in CMIP3 and CMIP5 models and the consistency of Hadley Cell changes with the projected tropopause rise and increase in subtropical and mid-latitude static stability indicate that a widening and weakening of the NH Hadley Cell by the late 21st century is *likely*.

The zonally asymmetric Walker Circulation is projected to weaken under global warming (Power and Kociuba, 2011a, 2011b), more than the Hadley Circulation (Lu et al., 2007; Vecchi and Soden, 2007). The consistency of the projected Walker Circulation slowdown from CMIP3 to CMIP5 suggests that its change is robust (Ma and Xie, 2013). Almost everywhere around the equatorial belt, changes in the 500 hPa vertical motion oppose the climatological background motion, notably over the maritime continent (Vecchi and Soden, 2007; Shongwe et al., 2011). Around the Indo-Pacific warm pool, in response to a spatially uniform SST warming, the climatological upper tropospheric divergence weakens (Ma and Xie, 2013). Changes in the strength of the Walker Circulation also appear to be linked to differential warming between the Indian and Pacific Ocean warming at low latitudes (Luo et al., 2012). Over the equatorial Pacific Ocean, where mid-tropospheric ascent is projected to strengthen, changes in zonal SST and hence sea level pressure gradients induce low-level westerly wind anomalies that act to weaken the low-level branch of the Pacific Walker Circulation. These projected changes in the tropical Pacific circulation are already occurring (Zhang and Song, 2006). However, the projected weakening of the Pacific Walker Cell does not imply an increase in the frequency and/or magnitude of El Niño events (Collins et al., 2010). The consistency of simulated changes in CMIP3 and CMIP5 models and the consistency of Walker Cell changes with equatorial SST and pressure-gradient changes that are already observed indicate that a weakening of the Walker Cell by the late 21st century is *likely*.

In the upper atmosphere, a robust feature of projected stratospheric circulation change is that the Brewer–Dobson circulation will *likely* strengthen in the 21st century (Butchart et al., 2006, 2010; Li et al., 2008; McLandress and Shepherd, 2009; Shepherd and McLandress, 2011). In a majority of model experiments, the projected changes in the large-scale overturning circulation in the stratosphere feature an

intensification of tropical upward mass flux, which may extend to the upper stratosphere. The proposed driver of the increase in mass flux at the tropical lower stratosphere is the enhanced propagation of wave activity, mainly resolved planetary waves, associated with a positive trend in zonal wind structure (Butchart and Scaife, 2001; Garcia and Randel, 2008). In the 21st century, increases in wave excitation from diabatic heating in the upper tropical troposphere could reinforce the wave forcing on the tropical upwelling branch of the stratospheric mean meridional circulation (Calvo and Garcia, 2009). Parameterized orographic gravity waves that result from strengthening of subtropical westerly jets and cause more waves to propagate into the lower stratosphere also play a role (Sigmond et al., 2004; Butchart et al., 2006). The projected intensification in tropical upwelling is counteracted by enhanced mean extratropical/polar lower stratospheric subsidence. In the NH high latitudes, the enhanced downwelling is associated with an increase in stationary planetary wave activities (McLandress and Shepherd, 2009). The intensification of the stratospheric meridional residual circulation has already been reported in studies focussing on the last decades of the 20th century (Garcia and Randel, 2008; Li et al., 2008; Young et al., 2012). The projected increase in troposphere-to-stratosphere mass exchange rate (Butchart et al., 2006) and stratospheric mixing associated with the strengthening of the Brewer–Dobson circulation will *likely* result in a decrease in the mean age of air in the lower stratosphere. In the mid-latitude lower stratosphere, quasi-horizontal mixing is a significant contributor to reducing the lifetimes of air. There are some suggestions that the changes in stratospheric overturning circulation could lead to a reduction in tropical ozone concentrations and an increase at high latitudes (Jiang et al., 2007) and an increase in the amplitude of the annual cycle of stratospheric ozone (Randel et al., 2007).

#### 12.4.4.3 Extratropical Storms: Tracks and Influences on Planetary-Scale Circulation and Transports

Since the AR4, there has been continued evaluation of changes in extratropical storm tracks under projected warming using both CMIP3 and, more recently, CMIP5 simulations, as well as supporting studies using single models or idealized simulations. CMIP3 analyses use a variety of methods for diagnosing storm tracks, but diagnosis of changes in the tracks appears to be relatively insensitive to methods used (Ulbrich et al., 2013). Analyses of SH storm tracks generally agree with earlier studies, showing that extratropical storm tracks will tend to shift poleward (Bengtsson et al., 2009; Gastineau et al., 2009; Gastineau and Soden, 2009; Perrie et al., 2010; Schuenemann and Cassano, 2010; Chang et al., 2012b). The behaviour is consistent with a *likely* trend in observed storm-track behaviour (see Section 2.7.6). Similar behaviour appears in CMIP5 simulations for the SH (Figure 12.20c, d). In SH winter there is a clear poleward shift in storm tracks of several degrees and a reduction in storm frequency of only a few percent (not shown). The poleward shift at the end of the century is consistent with a poleward shift in the SH of the latitudes with strongest tropospheric jets (Figure 12.19). This appears to coincide with shifts in baroclinic dynamics governing extratropical storms (Frederiksen et al., 2011), though the degree of jet shift appears to be sensitive to bias in a model's contemporary-climate storm tracks (Chang et al., 2012a, 2012b). Although there is thus some uncertainty in the degree of shift, the consistency of behaviour with observation-based trends, consistency

between CMIP5 and CMIP3 projections under a variety of diagnostics and the physical consistency of the storm response with other climatic changes gives *high confidence* that a poleward shift of several degrees in SH storm tracks is *likely* by the end of the 21st century under the RCP8.5 scenario.

In the NH winter (Figure 12.20a, b), the CMIP5 multi-model ensemble shows an overall reduced frequency of storms and less indication of a poleward shift in the tracks. The clearest poleward shift in the NH winter at the end of the 21st century occurs in the Asia-Pacific storm track, where intensification of the westerly jet promotes more intense cyclones in an ensemble of CMIP5 models (Mizuta, 2012). Otherwise, changes in winter storm-track magnitude, as measured by band-pass sea level pressure fluctuations, show only small change relative to interannual and inter-decadal variability by the end of the 21st century in SRES A1B and RCP4.5 simulations for several land areas over the NH (Harvey et al., 2012). Consistency in CMIP3 and CMIP5 changes seen in the SH are absent in the NH (Chang et al., 2012a). Factors identified that affect changes in the North Atlantic basin's storm track include horizontal resolution (Colle et al., 2013) and how models simulate changes in the Atlantic's meridional overturning circulation (Catto et al., 2011; Woollings et al., 2012), the zonal jet and Hadley Circulation (Mizuta, 2012; Zappa et al., 2013) and subtropical upper troposphere temperature (Haarsma et al., 2013). Substantial uncertainty and thus *low confidence* remains in projecting changes in NH winter storm tracks, especially for the North Atlantic basin.

Additional analyses of CMIP3 GCMs have determined other changes in properties of extratropical storms. Most analyses find that the frequency of storms decreases in projected climates (Finnis et al., 2007; Favre and Gershunov, 2009; Dowdy et al., 2013), though the occurrence of strong storms may increase in some regions (Pinto et al., 2007; Bengtsson et al., 2009; Ulbrich et al., 2009; Zappa et al., 2013). Many studies focus on behaviour of specific regions, and results of these studies are detailed in Section 14.6.2.

Changes in extratropical storms in turn may influence other large-scale climatic changes. Kug et al. (2010) in a set of time-slice simulations show that a poleward shift of storm tracks in the NH could enhance polar warming and moistening. The Arctic Oscillation (AO) is sensitive to synoptic eddy vorticity flux, so that projected changes in storm tracks can alter the AO (Choi et al., 2010). The net result is that changes in extratropical storms alter the climate in which they are embedded, so that links between surface warming, extratropical storms and their influence on climate are more complex than simple responses to changes in baroclinicity (O'Gorman, 2010).

#### 12.4.5 Changes in the Water Cycle

The water cycle consists of water stored on the Earth in all its phases, along with the movement of water through the Earth's climate system. In the atmosphere, water occurs primarily as gaseous water vapour, but it also occurs as solid ice and liquid water in clouds. The ocean is primarily liquid water, but is partly covered by ice in polar regions. Terrestrial water in liquid form appears as surface water (lakes, rivers), soil moisture and groundwater. Solid terrestrial water occurs in ice sheets, glaciers, frozen lakes, snow and ice on the surface and permafrost.

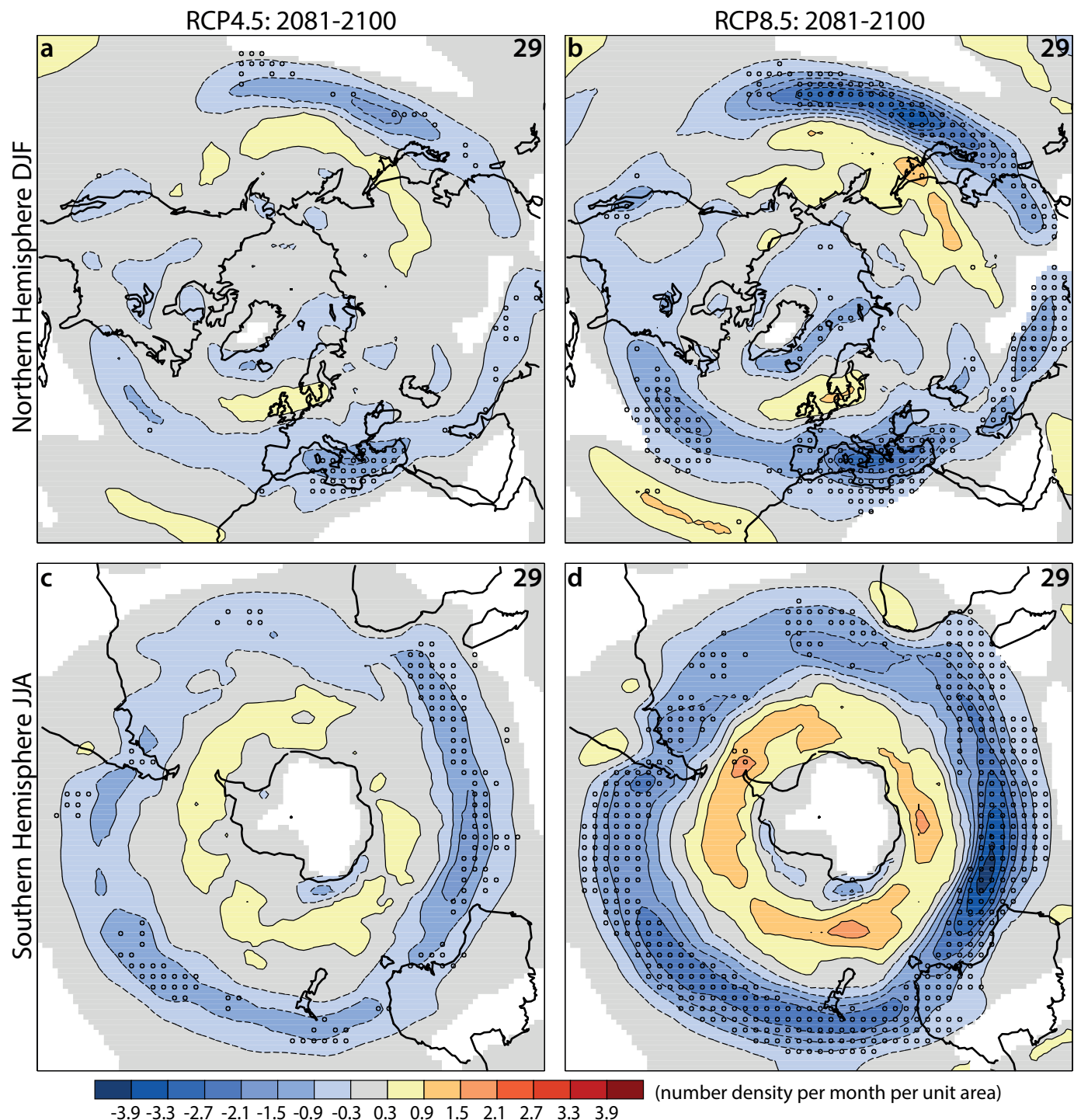


**Figure 12.20 |** Change in winter, extratropical storm track density (2081–2100 – 1986–2005) in CMIP5 multi-model ensembles: (a) RCP4.5 Northern Hemisphere December, January and February (DJF) and (b) RCP8.5 Northern Hemisphere DJF, (c) RCP4.5 Southern Hemisphere June, July and August (JJA) and (d) RCP8.5 Southern Hemisphere JJA. Storm-track computation uses the method of Bengtsson et al. (2006, their Figure 13a) applied to 6-hourly 850 hPa vorticity computed from horizontal winds in the CMIP5 archive. The number of models used appears in the upper right of each panel. DJF panels include data for December 1985 and 2080 and exclude December 2005 and December 2100 for in-season continuity. Stippling marks locations where at least 90% of the models agree on the sign of the change; note that this criterion differs from that used for many other figures in this chapter, due to the small number of models providing sufficient data to estimate internal variability of 20-year means of storm-track statistics. Densities have units (number density per month per unit area), where the unit area is equivalent to a 5° spherical cap ( $\sim 10^6 \text{ km}^2$ ). Locations where the scenario or contemporary-climate ensemble average is below 0.5 density units are left white.

Projections of future changes in the water cycle are inextricably connected to changes in the energy cycle (Section 12.4.3) and atmospheric circulation (Section 12.4.4).

Saturation vapour pressure increases with temperature, but projected future changes in the water cycle are far more complex than projected temperature changes. Some regions of the world will be subject to decreases in hydrologic activity while others will be subject to increases. There are important local seasonal differences among the responses of the water cycle to climate change as well.

At first sight, the water cycles simulated by CMIP3/5 models may appear to be inconsistent, particularly at regional scales. Anthropogenic changes to the water cycle are superimposed on complex naturally varying modes of the climate (such as El Niño-Southern Oscillation (ENSO), AO, Pacific Decadal Oscillation (PDO), etc.) aggravating the differences between model projections. However, by careful consideration of the interaction of the water cycle with changes in other aspects of the climate system, the mechanisms of change are revealed, increasing confidence in projections.

#### 12.4.5.1 Atmospheric Humidity

Atmospheric water vapour is the primary GHG in the atmosphere. Its changes affect all parts of the water cycle. However, the amount of water vapour is dominated by naturally occurring processes and not significantly affected directly by human activities. A common experience from past modelling studies is that relative humidity (RH) remains approximately constant on climatological time scales and planetary space scales, implying a strong constraint by the Clausius–Clapeyron relationship on how specific humidity will change. The AR4 stated that

'a broad-scale, quasi-unchanged RH response [to climate change] is uncontroversial' (Randall et al., 2007). However, underlying this fairly straightforward behaviour are changes in RH that can influence changes in cloud cover and atmospheric convection (Sherwood, 2010). More recent analysis provides further detail and insight on RH changes. Analysis of CMIP3 and CMIP5 models shows near-surface RH decreasing over most land areas as temperatures increase with the notable exception of parts of tropical Africa (O’Gorman and Muller, 2010) (Figure 12.21). The prime contributor to these decreases in RH over land is the larger temperature increases over land than over ocean in the RCP scenarios (Joshi et al., 2008; Fasullo, 2010; O’Gorman and Muller, 2010). The specific humidity of air originating over more slowly warming oceans will be governed by saturation temperatures of oceanic air. As this air moves over land and is warmed, its relative humidity drops as any further moistening of the air over land is insufficient to maintain constant RH, a behaviour Sherwood et al. (2010) term a last-saturation-temperature constraint. The RH decrease over most land areas by the end of the 21st century is consistent with a last-saturation-temperature constraint and with observed behaviour during the first decade of the current century (Section 2.5.5; Simmons et al., 2010). Land–ocean differences in warming are projected to continue through the 21st century, and although the CMIP5 projected changes are small, they are consistent with a last-saturation constraint, indicating with medium confidence that reductions in near-surface RH over many land areas are likely.

#### 12.4.5.2 Patterns of Projected Average Precipitation Changes

Global mean precipitation changes have been presented in Section 12.4.1.1. The processes that govern large-scale changes in precipitation are presented in Section 7.6, and are used here to interpret the

Mean relative humidity change (RCP8.5)

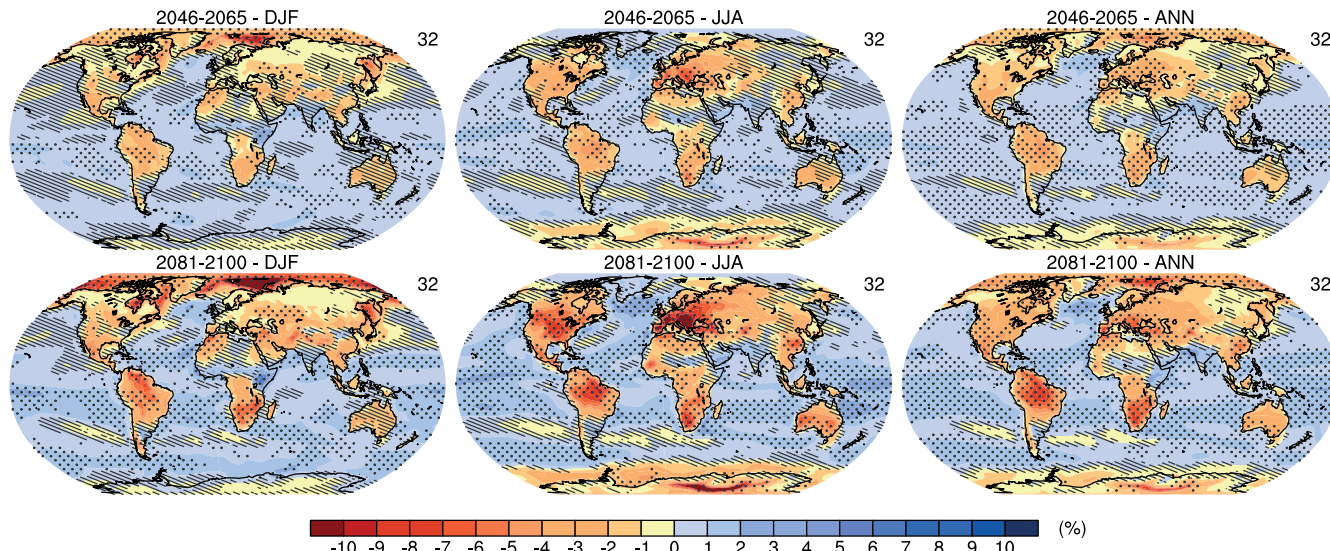


**Figure 12.21 |** Projected changes in near-surface relative humidity from the CMIP5 models under RCP8.5 for the December, January and February (DJF, left), June, July and August (JJA, middle) and annual mean (ANN, right) averages relative to 1986–2005 for the periods 2046–2065 (top row), 2081–2100 (bottom row). The changes are differences in relative humidity percentage (as opposed to a fractional or relative change). Hatching indicates regions where the multi-model mean change is less than one standard deviation of internal variability. Stippling indicates regions where the multi-model mean change is greater than two standard deviations of internal variability and where at least 90% of models agree on the sign of change (see Box 12.1).

projected changes in RCP scenarios. Changes in precipitation extremes are presented in Section 12.4.5.5. Further discussion of regional changes, in particular the monsoon systems, is presented in Chapter 14.

Figure 12.22 shows the CMIP5 multi-model average percentage change in seasonal mean precipitation in the middle of the 21st century, at the end of the 21st century and at the end of the 22nd century for the RCP8.5 scenario relative to the 1986–2005 average. Precipitation changes for all the scenarios are shown in Annex I Supplementary Material and scale approximately with the global mean temperature (Section 12.4.2). In many regions, changes in precipitation exhibit strong seasonal characteristics so that, in regions where the sign of the precipitation changes varies with the season, the annual mean values (Figure 12.10) may hide some of these seasonal changes, resulting in weaker confidence than seasonal mean values (Chou et al., 2013; Huang et al., 2013).

The patterns of multi-model precipitation changes displayed in Figure 12.22 tend to smooth and decrease the spatial contrast of precipitation changes simulated by each model, in particular over regions where model results disagree. Thus the amplitude of the multi-model ensemble mean precipitation response significantly underestimates the median amplitude computed from each individual model (Neelin et al., 2006; Knutti et al., 2010a). The CMIP3/5 multi-model ensemble precipitation projections must be interpreted in the context of uncertainty. Multi-model projections are not probabilistic statements about the likelihood of changes. Maps of multi-model projected changes are smoothly varying but observed changes are and will continue to be much more granular.

To analyze the patterns of projected precipitation changes, a useful framework consists in decomposing them into a part that is related to atmospheric circulation changes and a part that is related mostly to water vapour changes, referred to as dynamical and thermodynamical components, respectively. However, the definition of these two components may differ among studies. At the time of the AR4, the robust changes of the difference between precipitation and evaporation ( $P - E$ ) were interpreted as a wet-get-wetter and dry-get-drier type of response (Mitchell et al., 1987; Chou and Neelin, 2004; Held and Soden, 2006). The theoretical background, which is more relevant over oceans than over land, is that the lower-tropospheric water vapour increase with temperature enhances the moisture transported by the circulation. This leads to additional moisture convergence within the convergence zones and to additional moisture divergence in the descent zones, increasing the contrast in precipitation minus evaporation values between moisture convergence and divergence regions. A weakening of the tropical overturning circulation (see Section 12.4.4.2) partially opposes this thermodynamic response (Chou and Neelin, 2004; Held and Soden, 2006; Vecchi and Soden, 2007; Chou et al., 2009; Seager et al., 2010; Allan, 2012; Bony et al., 2013). At the regional scale the dynamic response may be larger than the thermodynamic response, and this has been analyzed in more detail since the AR4 (Chou et al., 2009; Seager et al., 2010; Xie et al., 2010; Muller and O’Gorman, 2011; Chadwick et al., 2012; Scheff and Frierson, 2012; Bony et al., 2013; Ma and Xie, 2013). Over continents, this simple wet-get-wetter and dry-get-drier type of response fails for some important regions such as the Amazon. At the global scale, the net water vapour

transport from oceans to land increases, and therefore the average  $P - E$  over continents also increases (Liepert and Previdi, 2012).

In the mid and high latitudes, a common feature across generations of climate models is a simulated increased precipitation. The thermodynamical component explains most of the projected increase (Emori and Brown, 2005; Seager et al., 2010). This is consistent with theoretical explanations assuming fixed atmospheric flow patterns but increased water vapour in the lower troposphere (Held and Soden, 2006). In addition to this thermodynamical effect, water transport may be modified by the poleward shift of the storm tracks and by the increase of their intensity (Seager et al., 2010; Wu et al., 2011b), although confidence in such changes in storm tracks may not be high (see Section 12.4.4). On seasonal time scales, the minimum and maximum values of precipitation both increase, with a larger increase of the maximum and therefore an increase of the annual precipitation range (Seager et al., 2010; Chou and Lan, 2012). In particular, the largest changes over northern Eurasia and North America are projected to occur during winter. At high latitudes of the NH, the precipitation increase may lead to an increase of snowfall in the colder regions and a decrease of snowfall in the warmer regions due to the decreased number of freezing days (see Section 12.4.6.2).

Most models simulate a large increase of the annual mean precipitation over the equatorial ocean and an equatorward shift of the Intertropical Convergence Zone (ITCZ), in both summer and winter seasons, that are mainly explained by atmospheric circulation changes (Chou et al., 2009; Seager et al., 2010; Sobel and Camargo, 2011). The changes of the atmospheric circulation have different origins. Along the margins of the convection zones, spatial inhomogeneities, including local convergence feedback or the rate at which air masses from dry regions tend to flow into the convection zone, can yield a considerable sensitivity in precipitation response (Chou et al., 2006; Neelin et al., 2006). Along the equator, atmosphere–ocean interactions yield to a maximum of SST warming and a large precipitation increase there (Xie et al., 2010; Ma and Xie, 2013). Model studies with idealized configurations suggest that tropical precipitation changes should be interpreted as responses to changes of the atmospheric energy budget rather than responses to changes of SST (Kang and Held, 2012). All of these atmospheric circulation changes, and therefore precipitation changes, can differ considerably from model to model. This is the case over both ocean and land. For instance, the spread of model projections in the Sahel region, West Africa, is large in both the CMIP3 and CMIP5 multi-model data base (Roehrig et al., 2013).

In the subtropical dry regions, there is a robust decrease of  $P - E$  that is accounted for by the thermodynamic contribution (Chou and Neelin, 2004; Held and Soden, 2006; Chou et al., 2009; Seager et al., 2010; Bony et al., 2013). Over ocean, the spatial heterogeneity of temperature increase impacts the lower-tropospheric water vapour increase, which impacts both the thermodynamic and the dynamic responses (Xie et al., 2010; Ma and Xie, 2013). In addition, the pattern of precipitation changes in dry regions may be different from that of  $P - E$  because the contribution of evaporation changes can be as large (but of opposite sign) as the moisture transport changes (Chou and Lan, 2012; Scheff and Frierson, 2012; Bony et al., 2013). This is especially the case over the subsidence regions during the warm season over land where the

agreement between models is the smallest (Chou et al., 2009; Allan, 2012). A robust feature is the decline of precipitation on the poleward flanks of the subtropical dry zones as a consequence of the Hadley Cell expansion, with possible additional decrease from a poleward shift of the mid latitude storm tracks (Seager et al., 2010; Scheff and Frierson, 2012). On seasonal time scales, the minimum and the maximum values of precipitation both increase, with a larger increase of the maximum and therefore an increase of the annual precipitation range (Sobel and Camargo, 2011; Chou and Lan, 2012).

Long-term precipitation changes are driven mainly by the increase of the surface temperature, as presented above, but other factors also contribute to them. Recent studies suggest that CO<sub>2</sub> increase has a significant direct influence on atmospheric circulation, and therefore on global and tropical precipitation changes (Andrews et al., 2010; Bala et al., 2010; Cao et al., 2012; Bony et al., 2013). Over the ocean, the positive RF from increased atmospheric CO<sub>2</sub> reduces the radiative cooling

of the troposphere and the large scale rising motion and hence reduces precipitation in the convective regions. Over large landmasses, the direct effect of CO<sub>2</sub> on precipitation is the opposite owing to the small thermal inertia of land surfaces (Andrews et al., 2010; Bala et al., 2010; Cao et al., 2012; Bony et al., 2013). Regional precipitation changes are also influenced by aerosol and ozone (Ramanathan et al., 2001; Allen et al., 2012; Shindell et al., 2013a) through both local and large-scale processes, including changes in the circulation. Stratospheric ozone depletion contributes to the poleward expansion of the Hadley Cell and the related change of precipitation in the SH (Kang et al., 2011) whereas black carbon and tropospheric ozone increases are major contributors in the NH (Allen et al., 2012). Regional precipitation changes depend on regional forcings and on how models simulate their local and remote effects. Based on CMIP3 results, the inter-model spread of the estimate of precipitation changes over land is larger than the inter-scenario spread except in East Asia (Frieler et al., 2012).

### Seasonal mean percentage precipitation change (RCP8.5)

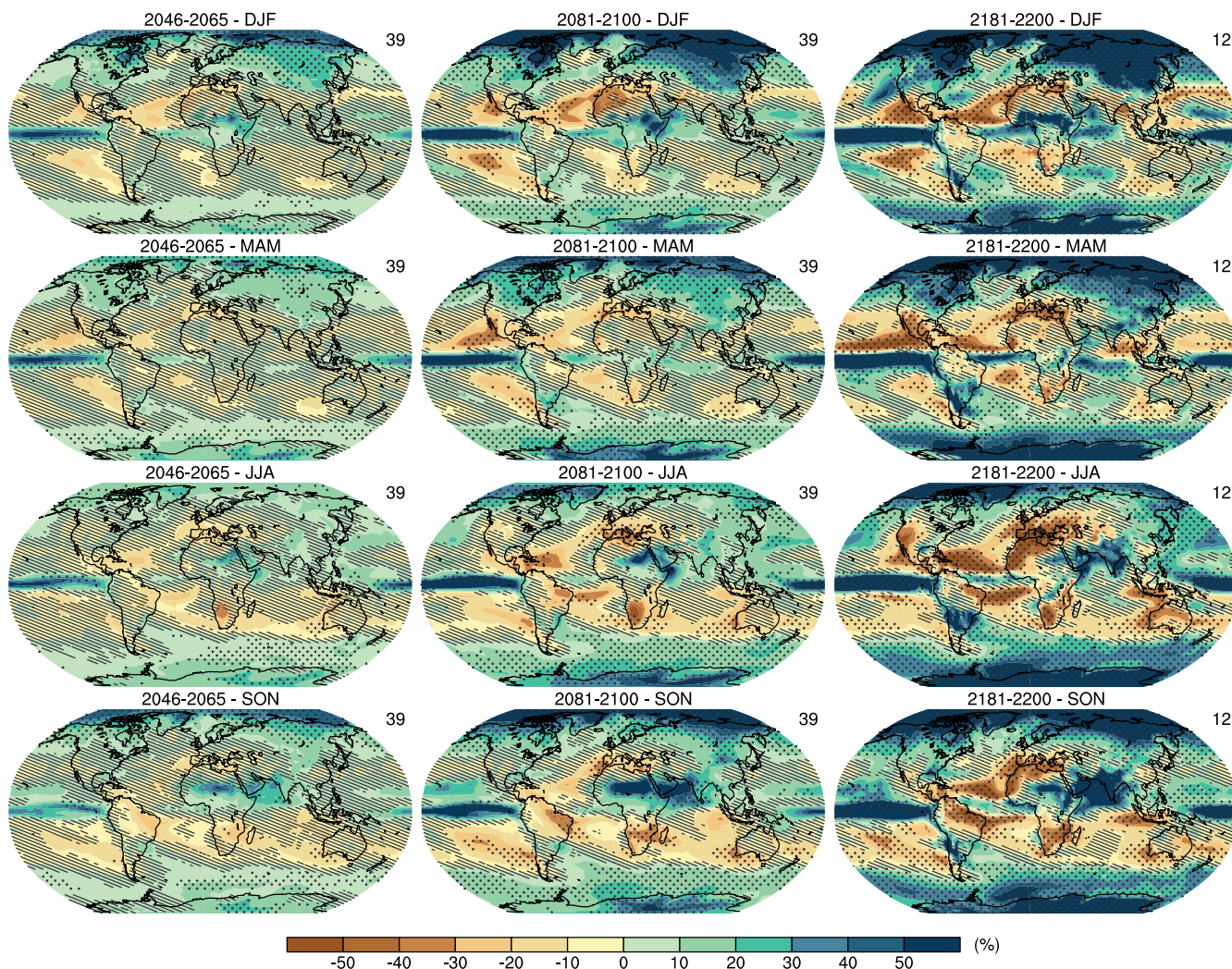


**Figure 12.22 |** Multi-model CMIP5 average percentage change in seasonal mean precipitation relative to the reference period 1986–2005 averaged over the periods 2045–2065, 2081–2100 and 2181–2200 under the RCP8.5 forcing scenario. Hatching indicates regions where the multi-model mean change is less than one standard deviation of internal variability. Stippling indicates regions where the multi-model mean change is greater than two standard deviations of internal variability and where at least 90% of models agree on the sign of change (see Box 12.1).

Projected precipitation changes vary greatly between models, much more so than for temperature projections. Part of this variance is due to genuine differences between the models including their ability to replicate observed precipitation patterns (see Section 9.4.1.1). However, a large part of it is also the result of the small ensemble size from each model (Rowell, 2012). This is especially true for regions of small projected changes located between two regions: one experiencing significant increases while the other experiences significant decreases. Individual climate model realizations will differ in their projection of future precipitation changes in these regions simply owing to their internal variability (Deser et al., 2012b; Deser et al., 2012a). Multi-model projections containing large numbers of realizations would tend to feature small changes in these regions, and hatching in Figure 12.22 indicates regions where the projected multi-model mean change is less than one standard deviation of internal variability (method (a), Box 12.1). Confidence in projections in regions of limited or no change in precipitation may be more difficult to obtain than confidence in regions of large projected changes. However, Power et al. (2012) and Tebaldi et al. (2011) show that for some of the regions featuring small multi-model average projected changes, effective consensus in projections may be better than the metrics reported in AR4 would imply.

Since the AR4, progress has been made in the understanding of the processes that control large scale precipitation changes. There is *high confidence* that the contrast of seasonal mean precipitation between dry and wet regions will increase in a warmer climate over most of the globe although there may be regional exceptions to this general pattern. This response is particularly robust when considering  $P - E$  changes as a function of atmospheric dynamical regimes. However, it is important to note that significant exceptions can occur in specific regions especially along the equator and on the poleward edges of the subtropical dry zone. In these regions, atmospheric circulation changes lead to shifts of the precipitation patterns. There is *high confidence* that the contrast between wet and dry seasons will increase over most of the globe as temperatures increase. Over the mid- and high-latitude regions, projected precipitation increases in winter are larger than in summer. Over most of the subtropical oceans, projected precipitation increases in summer are larger than in winter.

The changes in precipitation shown in Figure 12.22 exhibit patterns that become more pronounced and confidence in them increases as temperatures increase. More generally, the spatial and temporal changes in precipitation between two scenarios or within two periods of a given scenario exhibit the pattern scaling behavior and limitations described in Section 12.4.2. The patterns and the associated multi-model spreads in CMIP5 for the RCP scenarios are very similar to those in CMIP3 for the SRES scenarios discussed in the AR4, with the projections in CMIP5 being slightly more consistent over land than those from CMIP3 (Knutti and Sedláček, 2013). The largest percentage changes are at the high latitudes. By the end of the 21st century, over the large northern land masses, increased precipitation is *likely* under the RCP8.5 scenario in the winter and spring poleward of 50°N. The robustness across scenarios, the magnitude of the projected changes versus natural variability and physical explanations described above yield *high confidence* that the projected changes would be larger than natural 20-year variations (see Box 12.1). In the tropics, precipitation changes exhibit strong regional contrasts, with increased precipitation

over the equatorial Pacific and Indian Oceans and decreases over much of the subtropical ocean. However, decreases are not projected to be larger than natural 20-year variations anywhere until the end of this century under the RCP8.5 scenario. Decreased precipitation in the Mediterranean, Caribbean and Central America, southwestern United States and South Africa is *likely* under the RCP8.5 scenario and is projected with *medium confidence* to be larger than natural variations by the end of the 22nd century in some seasons (Box 12.1). The CMIP3 models' historical simulations of zonal mean precipitation trends were shown to underestimate observed trends (Gillett et al., 2004; Lambert et al., 2005; Zhang et al., 2007; Liepert and Previdi, 2009) (see Section 10.3.2.2). Therefore it is *more likely than not* that the magnitude of the projected future changes in Figure 12.22 based on the multi-model mean is underestimated. Observational uncertainties including limited global coverage and large natural variability, in addition to challenges in precipitation modelling, limit confidence in assessment of climatic changes in precipitation.

#### 12.4.5.3 Soil Moisture

Near-surface soil moisture is the net result of a suite of complex processes (e.g., precipitation evapotranspiration, drainage, overland flow, infiltration), and heterogeneous and difficult-to-characterize aboveground and belowground system properties (e.g., slope, soil texture). As a result, regional to global-scale simulations of soil moisture and drought remain relatively uncertain (Burke and Brown, 2008; Henderson-Sellers et al., 2008). The AR4 (Section 8.2.3.2) discussed the lack of assessments of global-scale models in their ability to simulate soil moisture, and this problem appears to have persisted (Section 9.4.4.2). Furthermore, consistent multi-model projections of total soil moisture are difficult to make owing to substantial differences between climate models in the depth of their soil. However, Koster et al. (2009a) argued that once climatological statistics affecting soil moisture were accounted for, different models tend to agree on soil moisture projections.

The AR4 summarized multi-model projections of 21st century annual mean soil moisture changes as decreasing in the subtropics and Mediterranean region, and increasing in east Africa and central Asia. Dai (2013) found similar changes in an ensemble of 11 CMIP5 GCMs under RCP4.5. Figure 12.23 shows projected changes in surface soil moisture (upper 10 cm) in the CMIP5 ensemble at the end of the 21st century under the RCPs 2.6, 4.5, 6.0 and 8.5. We focus on this new CMIP5 specification because it describes soil moisture at a consistent depth across all CMIP5 models. The broad patterns are moderately consistent across the RCPs, with the changes tending to become stronger as the strength of the forcing change increases. The agreement among CMIP5 models and the consistency with other physical features of climate change indicate *high confidence* in certain regions where surface soils are projected to dry. There is little-to-no confidence anywhere in projections of moister surface soils. Under RCP8.5, with the largest projected change, individual ensemble members (not shown) show consistency across the ensemble for drying in the Mediterranean region, northeast and southwest South America, southern Africa, and southwestern USA. However, ensemble members show disagreement on the sign of change in large regions such as central Asia or the high northern latitudes. The Mediterranean, southwestern USA, northeast South America and southern African drying regions are consistent with

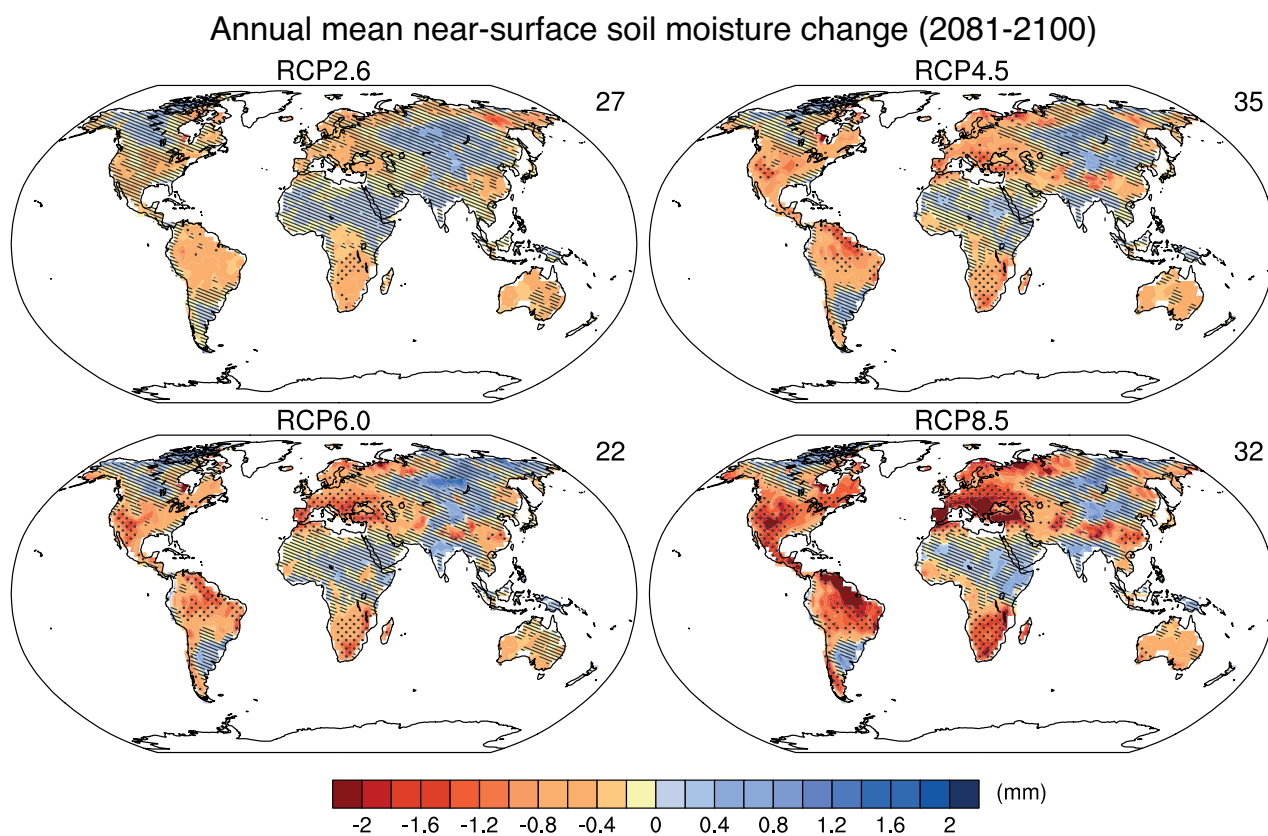


**Figure 12.23** | Change in annual mean soil moisture (mass of water in all phases in the uppermost 10 cm of the soil) (mm) relative to the reference period 1986–2005 projected for 2081–2100 from the CMIP5 ensemble. Hatching indicates regions where the multi-model mean change is less than one standard deviation of internal variability. Stippling indicates regions where the multi-model mean change is greater than two standard deviations of internal variability and where at least 90% of models agree on the sign of change (see Box 12.1). The number of CMIP5 models used is indicated in the upper right corner of each panel.

projected widening of the Hadley Circulation that shifts downwelling, thus inhibiting precipitation in these regions. The large-scale drying in the Mediterranean, southwest USA, and southern Africa appear across generations of projections and climate models and is deemed *likely* as global temperatures rise and will increase the risk of agricultural drought. In addition, an analysis of CMIP3 and CMIP5 projections of soil moisture in five drought-prone regions indicates that the differences in future forcing scenarios are the largest source of uncertainty in such regions rather than differences between model responses (Orlowsky and Seneviratne, 2012).

Other recent assessments include multi-model ensemble approaches, dynamical downscaling, and regional climate models applied around the globe and illustrate the variety of issues influencing soil moisture changes. Analyses of the southwestern USA using CMIP3 models (Christensen and Lettenmaier, 2007; Seager et al., 2007) show consistent projections of drying, primarily due to a decrease in winter precipitation. In contrast, Kellomaki et al. (2010) find that SRES A2 projections for Finland yield decreased snow depth, but soil moisture generally increases, consistent with the general increase in precipitation occurring in high northern latitudes. Kolomyts and Surova (2010), using projections from the CMIP3 models, GISS and HadCM2, under the SRES A2 forcing, show that vegetation type has substantial influence on the development of pronounced drying over the 21st century in Middle Volga Region forests.

Projected changes in soil moisture from the CMIP3/5 models also show substantial seasonal variation. For example, soil moisture changes in the North American midlatitudes, coupled with projected warming, increases the strength of land–atmosphere coupling during spring and summer in 15 GCMs under RCP8.5 (Dirmeyer et al., 2013). For the Cline River watershed in western Canada, Kienzle et al. (2012) find decreases in summer soil moisture content, but annual increases averaging 2.6% by the 2080s using a suite of CMIP3 GCMs simulating B1, A1B and A2 scenarios to drive a regional hydrology model. Hansen et al. (2007), using dynamical downscaling of one GCM running the A2 scenario, find summer soil moisture decreases in Mongolia of up to 6% due to increased potential evaporation in a warming climate and decreased precipitation and decreased precipitation.

Soil moisture projections in high latitude permafrost regions are critically important for assessing future climate feedbacks from trace-gas emissions (Zhuang et al., 2004; Riley et al., 2011) and vegetation changes (Chapin et al., 2005). In addition to changes in precipitation, snow cover and evapotranspiration, future changes in high-latitude soil moisture also will depend on permafrost degradation, thermokarst evolution, rapid changes in drainage (Smith et al., 2005), and changes in plant communities and their water demands. Current understanding of these interacting processes at scales relevant to climate is poor, so that full incorporation in current GCMs is lacking.

#### 12.4.5.4 Runoff and Evaporation

In the AR4, 21st century model-projected runoff consistently showed decreases in southern Europe, the Middle East, and southwestern USA and increases in Southeast Asia, tropical East Africa and at high northern latitudes. The same general features appear in the CMIP5 ensemble of GCMs for all four RCPs shown in Figure 12.24, with the areas of most robust change typically increasing with magnitude of forcing change. However, the robustness of runoff decreases in the southwestern USA is less in the CMIP5 models compared to the AR4. The large decreases in runoff in southern Europe and southern Africa are consistent with changes in the Hadley Circulation and related precipitation decreases and warming-induced evapotranspiration increases. The high northern latitude runoff increases are *likely* under RCP8.5 and consistent with the projected precipitation increases (Figure 12.22). The consistency of changes across different generations of models and different forcing scenarios, together with the physical consistency of change indicates that decreases are also *likely* in runoff in southern Europe, the Middle East, and southern Africa in this scenario.

A number of reports since the AR4 have updated findings from CMIP3 models and analyzed a large set of mechanisms affecting runoff. Several studies have focussed on the Colorado River basin in the United States (Christensen and Lettenmaier, 2007; McCabe and Wolock, 2007; Barnett and Pierce, 2008; Barnett et al., 2008) showing that runoff reductions that do happen under global warming occur through a

combination of evapotranspiration increases and precipitation decreases, with the overall reduction in river flow exacerbated by human water demands on the basin's supply.

A number of CMIP3 analyses have examined trends and seasonal shifts in runoff. For example, Kienzle et al. (2012) studied climate change scenarios over the Cline River watershed in western Canada and projected (1) spring runoff and peak streamflow up to 4 weeks earlier than in 1961–1990; (2) significantly higher streamflow between October and June; and (3) lower streamflow between July and September. For the Mediterranean basin, an ensemble of regional climate models driven by several GCMs using the A1B scenario have a robust decrease in runoff emerging only after 2050 (Sanchez-Gomez et al., 2009).

Annual mean surface evaporation in the models assessed in AR4 showed increases over most of the ocean and increases or decreases over land with largely the same pattern over land as increases and decreases in precipitation. Similar behaviour occurs in an ensemble of CMIP5 models (Figure 12.25). Evaporation increases over most of the ocean and land, with prominent areas of decrease over land occurring in southern Africa and northwestern Africa along the Mediterranean. The areas of decrease correspond to areas with reduced precipitation. There is some uncertainty about storm-track changes over Europe (see Sections 12.4.3 and 14.6.2). However, the consistency of the decreases across different generations of models and different forcing scenarios along with the physical basis for the precipitation decrease

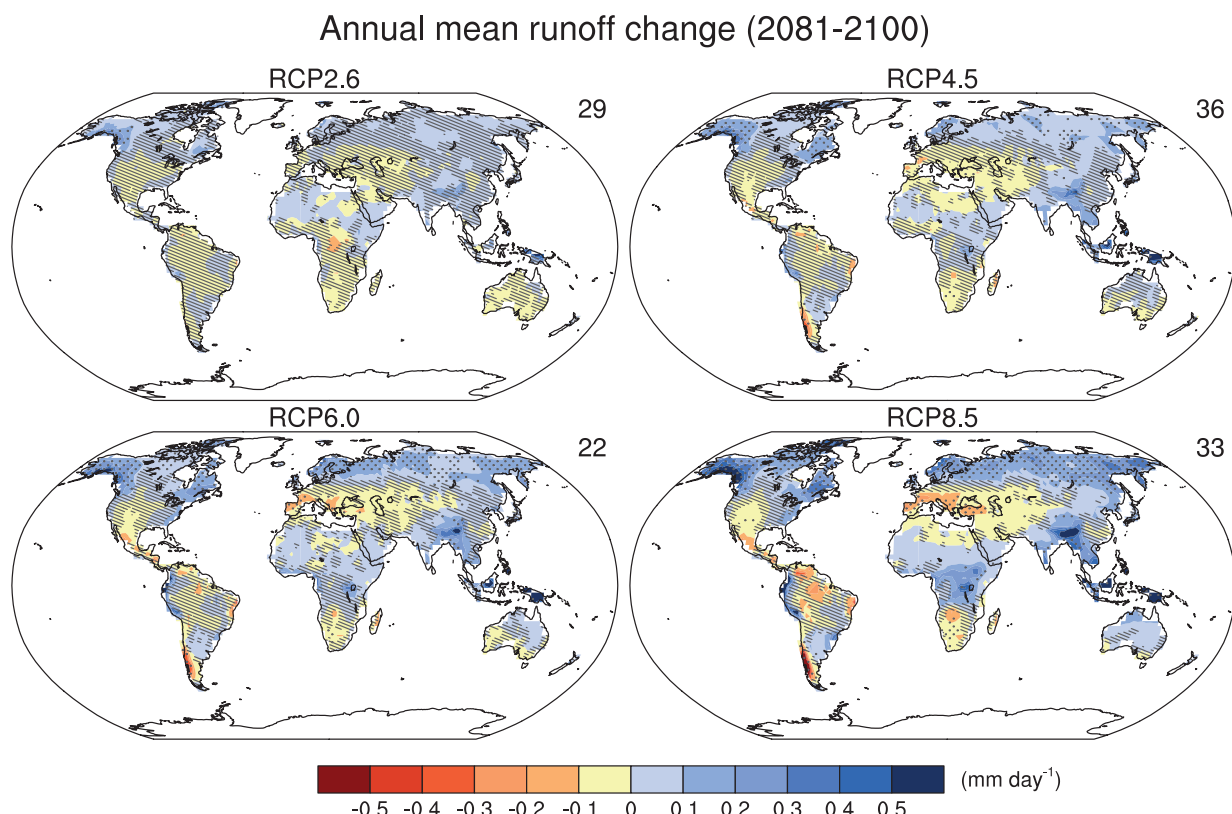


**Figure 12.24 |** Change in annual mean runoff relative to the reference period 1986–2005 projected for 2081–2100 from the CMIP5 ensemble. Hatching indicates regions where the multi-model mean change is less than one standard deviation of internal variability. Stippling indicates regions where the multi-model mean change is greater than two standard deviations of internal variability and where at least 90% of models agree on the sign of change (see Box 12.1). The number of CMIP5 models used is indicated in the upper right corner of each panel.

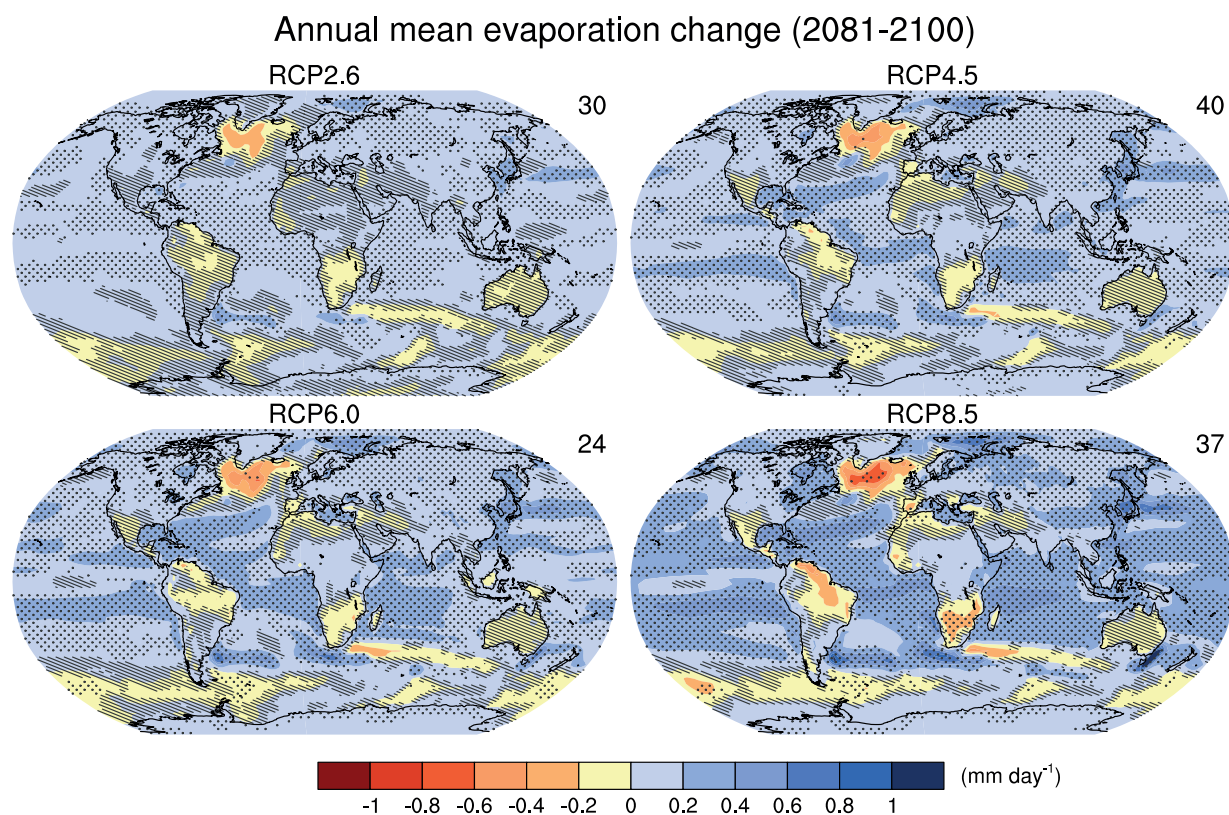


**Figure 12.25 |** Change in annual mean evaporation relative to the reference period 1986–2005 projected for 2081–2100 from the CMIP5 ensemble. Hatching indicates regions where the multi-model mean change is less than one standard deviation of internal variability. Stippling indicates regions where the multi-model mean change is greater than two standard deviations of internal variability and where at least 90% of models agree on the sign of change (see Box 12.1). The number of CMIP5 models used is indicated in the upper right corner of each panel.

indicates that these decreases in annual mean evaporation are *likely* under RCP8.5, but with *medium confidence*. Annual mean evaporation increases over land in the northern high latitudes are consistent with the increase in precipitation and the overall warming that would increase potential evaporation. For the northern high latitudes, the physical consistency and the similar behaviour across multiple generations and forcing scenarios indicates that annual mean evaporation increases there are *likely*, with *high confidence*.

12

Evapotranspiration changes partly reflect changes in precipitation. However, some changes might come from altered biological processes. For example, increased atmospheric CO<sub>2</sub> promotes stomatal closure and reduced transpiration (Betts et al., 2007; Cruz et al., 2010) which can potentially yield increased runoff. There is potential for substantial feedback between vegetation changes and regional water cycles, though the impact of such feedback remains uncertain at this point due to limitations on modelling crop and other vegetation processes in GCMs (e.g., Newlands et al., 2012) and uncertainties in plant response, ecosystem shifts and land management changes.

#### 12.4.5.5 Extreme Events in the Water Cycle

In addition to the changes in the seasonal pattern of mean precipitation described above, the distribution of precipitation events is projected to undergo profound changes (Gutowski et al., 2007; Sun et al., 2007; Boberg et al., 2010). At daily to weekly scales, a shift to more intense

individual storms and fewer weak storms is projected (Seneviratne et al., 2012). At seasonal or longer time scales, increased evapotranspiration over land can lead to more frequent and more intense periods of agricultural drought.

A general relationship between changes in total precipitation and extreme precipitation does not exist (Seneviratne et al., 2012). Two possible mechanisms controlling short-term extreme precipitation amounts are discussed at length in the literature and are similar to the thermodynamic and dynamical mechanisms detailed above for changes in average precipitation.

The first considers that extreme precipitation events occur when most of the available atmospheric water vapour rapidly precipitates out in a single storm. The maximum amount of water vapour in air (saturation) is determined by the Clausius–Clapeyron relationship. As air temperature increases, this saturated amount of water also increases (Allen and Ingram, 2002; Pall et al., 2007; Allan and Soden, 2008; Kendon et al., 2010). Kunkel et al. (2013) examined the CMIP5 model RCP4.5 and 8.5 projections for changes in maximum water vapour concentrations, a principal factor controlling the probable bound on maximum precipitation, concluding that maximum water vapour changes are comparable to mean water vapour changes but that the potential for changes in dynamical factors is less compelling. Such increases in atmospheric water vapour are expected to increase the intensity of individual precipitation events, but have less impact on their frequency. As a result

projected increases in extreme precipitation may be more reliable than similar projections of changes in mean precipitation in some regions (Kendon et al., 2010).

A second mechanism for extreme precipitation put forth by O’Gorman and Schneider (2009a, 2009b) is that such events are controlled by anomalous horizontal moisture flux convergence and associated convective updrafts which would change in a more complicated fashion in a warmer world (Sugiyama et al., 2010). Emori and Brown (2005) showed that the thermodynamic mechanism dominated over the dynamical mechanism nearly everywhere outside the tropical warm pool. However, Utsumi et al. (2011) used gridded observed daily data to find that daily extreme precipitation monotonically increases with temperature only at high latitudes, with the opposite behaviour in the tropics and a mix in the mid-latitudes. Li et al. (2011a) found that both mechanisms contribute to extreme precipitation in a high-resolution aquaplanet model with updrafts as the controlling element in the tropics and air temperature controlling the mid-latitudes consistent with the results by Chou et al. (2012). Using a high-resolution regional model, Berg et al. (2009) found a seasonal dependence in Europe with the Clausius–Clapeyron relationship providing an upper limit to daily precipitation intensity in winter but water availability rather than storage capacity is the controlling factor in summer. Additionally, Lenderink and Van Meijgaard (2008) found that very short (sub-daily) extreme precipitation events increase at a rate twice the amount predicted by Clausius–Clapeyron scaling in a very high-resolution model over Europe suggesting that both mechanisms can interact jointly. Gastineau and Soden (2009) found in the CMIP3 models that the updrafts associated with the most extreme tropical precipitation events actually weaken despite an increase in the frequency of the heaviest rain rates further complicating simple mechanistic explanations. See also Sections 7.6.5 and 11.3.2.5.2.

Projections of changes in future extreme precipitation may be larger at the regional scales than for future mean precipitation, but natural variability is also larger causing a tendency for signal-to-noise ratios to decrease when considering increasingly extreme metrics. However, mechanisms of natural variability still are a large factor in assessing the robustness of projections (Kendon et al., 2008). In addition, large-scale circulation changes, which are uncertain, could dominate over the above mechanisms depending on the rarity and type of events considered. However, analysis of CMIP3 models suggests circulation changes are potentially insufficient to offset the influence of increasing atmospheric water vapour on extreme precipitation change over Europe at least on large spatial scales (Kendon et al., 2010). An additional shift of the storm track has been shown in models with a better representation of the stratosphere, and this is found to lead to an enhanced increase in extreme rainfall over Europe in winter (Scaife et al., 2012).

Similar to temperature extremes (Section 12.4.3.3), the definition of a precipitation extreme depends very much on context and is often used in discussion of particular climate-related impacts (Seneviratne et al. (2012), Box 3.1). Consistently, climate models project future episodes of more intense precipitation in the wet seasons for most of the land areas, especially in the NH and its higher latitudes, and the monsoon regions of the world, and at a global average scale. The actual magnitude of the projected change is dependent on the model used,

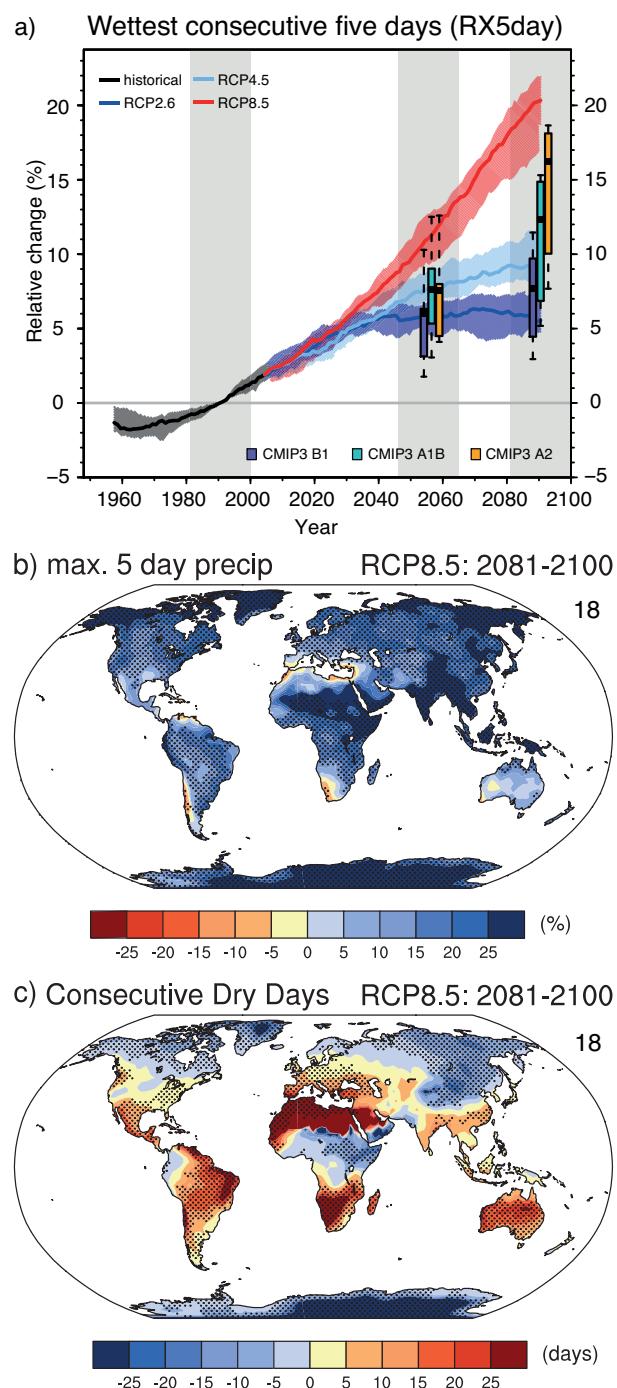


**Figure 12.26 |** (a, b) Projected percent changes (relative to the 1981–2000 reference period in common with CMIP3) from the CMIP5 models in RX5day, the annual maximum five-day precipitation accumulation. (a) Global average percent change over land regions for the RCP2.6, RCP4.5 and RCP8.5 scenarios. Shading in the time series represents the interquartile ensemble spread (25th and 75th quantiles). The box-and-whisker plots show the interquartile ensemble spread (box) and outliers (whiskers) for 11 CMIP3 model simulations of the SRES scenarios A2 (orange), A1B (cyan) and B1 (purple) globally averaged over the respective future time periods (2046–2065 and 2081–2100) as anomalies from the 1981–2000 reference period. (b) Percent change over the 2081–2100 period in the RCP8.5 scenario. (c) Projected change in annual CDD, the maximum number of consecutive dry days when precipitation is less than 1 mm, over the 2081–2100 period in the RCP8.5 scenario (relative to the 1981–2000 reference period) from the CMIP5 models. Stippling indicates gridpoints with changes that are significant at the 5% level using a Wilcoxon signed-ranked test. (Updated from Sillmann et al. (2013), excluding the FGOALS-s2 model.)

## Frequently Asked Questions

**FAQ 12.2 | How Will the Earth's Water Cycle Change?**

The flow and storage of water in the Earth's climate system are highly variable, but changes beyond those due to natural variability are expected by the end of the current century. In a warmer world, there will be net increases in rainfall, surface evaporation and plant transpiration. However, there will be substantial differences in the changes between locations. Some places will experience more precipitation and an accumulation of water on land. In others, the amount of water will decrease, due to regional drying and loss of snow and ice cover.

The water cycle consists of water stored on the Earth in all its phases, along with the movement of water through the Earth's climate system. In the atmosphere, water occurs primarily as a gas—water vapour—but it also occurs as ice and liquid water in clouds. The ocean, of course, is primarily liquid water, but the ocean is also partly covered by ice in polar regions. Terrestrial water in liquid form appears as surface water—such as lakes and rivers—soil moisture and groundwater. Solid terrestrial water occurs in ice sheets, glaciers, snow and ice on the surface and in permafrost and seasonally frozen soil.

Statements about future climate sometimes say that the water cycle will accelerate, but this can be misleading, for strictly speaking, it implies that the cycling of water will occur more and more quickly with time and at all locations. Parts of the world will indeed experience intensification of the water cycle, with larger transports of water and more rapid movement of water into and out of storage reservoirs. However, other parts of the climate system will experience substantial depletion of water, and thus less movement of water. Some stores of water may even vanish.

As the Earth warms, some general features of change will occur simply in response to a warmer climate. Those changes are governed by the amount of energy that global warming adds to the climate system. Ice in all forms will melt more rapidly, and be less pervasive. For example, for some simulations assessed in this report, summer Arctic sea ice disappears before the middle of this century. The atmosphere will have more water vapour, and observations and model results indicate that it already does. By the end of the 21st century, the average amount of water vapour in the atmosphere could increase by 5 to 25%, depending on the amount of human emissions of greenhouse gases and radiatively active particles, such as smoke. Water will evaporate more quickly from the surface. Sea level will rise due to expansion of warming ocean waters and melting land ice flowing into the ocean (see FAQ 13.2).

These general changes are modified by the complexity of the climate system, so that they should not be expected to occur equally in all locations or at the same pace. For example, circulation of water in the atmosphere, on land and in the ocean can change as climate changes, concentrating water in some locations and depleting it in others. The changes also may vary throughout the year: some seasons tend to be wetter than others. Thus, model simulations assessed in this report show that winter precipitation in northern Asia may increase by more than 50%, whereas summer precipitation there is projected to hardly change. Humans also intervene directly in the water cycle, through water management and changes in land use. Changing population distributions and water practices would produce further changes in the water cycle.

Water cycle processes can occur over minutes, hours, days and longer, and over distances from metres to kilometres and greater. Variability on these scales is typically greater than for temperature, so climate changes in precipitation are harder to discern. Despite this complexity, projections of future climate show changes that are common across many models and climate forcing scenarios. Similar changes were reported in the AR4. These results collectively suggest well understood mechanisms of change, even if magnitudes vary with model and forcing. We focus here on changes over land, where changes in the water cycle have their largest impact on human and natural systems.

Projected climate changes from simulations assessed in this report (shown schematically in FAQ 12.2, Figure 1) generally show an increase in precipitation in parts of the deep tropics and polar latitudes that could exceed 50% by the end of the 21st century under the most extreme emissions scenario. In contrast, large areas of the subtropics could have decreases of 30% or more. In the tropics, these changes appear to be governed by increases in atmospheric water vapour and changes in atmospheric circulation that further concentrate water vapour in the tropics and thus promote more tropical rainfall. In the subtropics, these circulation changes simultaneously promote less rainfall despite warming in these regions. Because the subtropics are home to most of the world's deserts, these changes imply increasing aridity in already dry areas, and possible expansion of deserts. (continued on next page)

## FAQ 12.2 (continued)

Increases at higher latitudes are governed by warmer temperatures, which allow more water in the atmosphere and thus, more water that can precipitate. The warmer climate also allows storm systems in the extratropics to transport more water vapour into the higher latitudes, without requiring substantial changes in typical wind strength. As indicated above, high latitude changes are more pronounced during the colder seasons.

Whether land becomes drier or wetter depends partly on precipitation changes, but also on changes in surface evaporation and transpiration from plants (together called evapotranspiration). Because a warmer atmosphere can have more water vapour, it can induce greater evapotranspiration, given sufficient terrestrial water. However, increased carbon dioxide in the atmosphere reduces a plant's tendency to transpire into the atmosphere, partly counteracting the effect of warming.

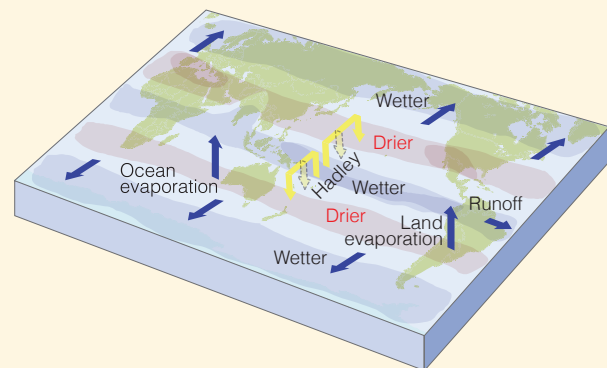
In the tropics, increased evapotranspiration tends to counteract the effects of increased precipitation on soil moisture, whereas in the subtropics, already low amounts of soil moisture allow for little change in evapotranspiration. At higher latitudes, the increased precipitation generally outweighs increased evapotranspiration in projected climates, yielding increased annual mean runoff, but mixed changes in soil moisture. As implied by circulation changes in FAQ 12.2, Figure 1, boundaries of high or low moisture regions may also shift.

A further complicating factor is the character of rainfall. Model projections show rainfall becoming more intense, in part because more moisture will be present in the atmosphere. Thus, for simulations assessed in this report, over much of the land, 1-day precipitation events that currently occur on average every 20 years could occur every 10 years or even more frequently by the end of the 21st century. At the same time, projections also show that precipitation events overall will tend to occur less frequently.

These changes produce two seemingly contradictory effects: more intense downpours, leading to more floods, yet longer dry periods between rain events, leading to more drought.

At high latitudes and at high elevation, further changes occur due to the loss of frozen water. Some of these are resolved by the present generation of global climate models (GCMs), and some changes can only be inferred because they involve features such as glaciers, which typically are not resolved or included in the models. The warmer climate means that snow tends to start accumulating later in the fall, and melt earlier in the spring. Simulations assessed in this report show March to April snow cover in the Northern Hemisphere is projected to decrease by approximately 10 to 30% on average by the end of this century, depending on the greenhouse gas scenario. The earlier spring melt alters the timing of peak springtime flow in rivers receiving snowmelt. As a result, later flow rates will decrease, potentially affecting water resource management. These features appear in GCM simulations.

Loss of permafrost will allow moisture to seep more deeply into the ground, but it will also allow the ground to warm, which could enhance evapotranspiration. However, most current GCMs do not include all the processes needed to simulate well permafrost changes. Studies analysing soils freezing or using GCM output to drive more detailed land models suggest substantial permafrost loss by the end of this century. In addition, even though current GCMs do not explicitly include glacier evolution, we can expect that glaciers will continue to recede, and the volume of water they provide to rivers in the summer may dwindle in some locations as they disappear. Loss of glaciers will also contribute to a reduction in springtime river flow. However, if annual mean precipitation increases—either as snow or rain—then these results do not necessarily mean that annual mean river flow will decrease.



**FAQ 12.2, Figure 1 |** Schematic diagram of projected changes in major components of the water cycle. The blue arrows indicate major types of water movement changes through the Earth's climate system: poleward water transport by extratropical winds, evaporation from the surface and runoff from the land to the oceans. The shaded regions denote areas more likely to become drier or wetter. Yellow arrows indicate an important atmospheric circulation change by the Hadley Circulation, whose upward motion promotes tropical rainfall, while suppressing subtropical rainfall. Model projections indicate that the Hadley Circulation will shift its downward branch poleward in both the Northern and Southern Hemispheres, with associated drying. Wetter conditions are projected at high latitudes, because a warmer atmosphere will allow greater precipitation, with greater movement of water into these regions.

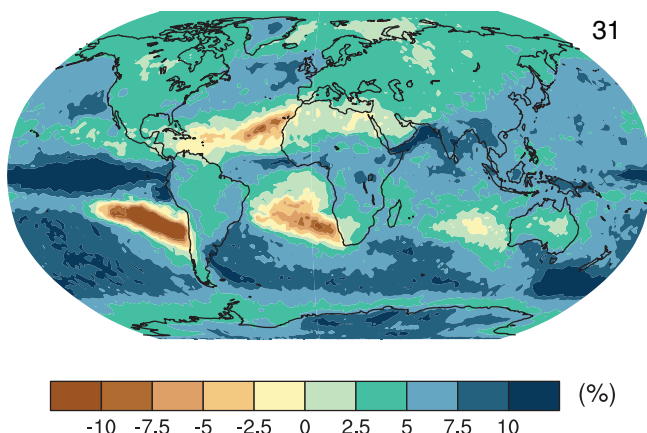
but there is strong agreement across the models over the direction of change (Tebaldi et al., 2006; Goubanova and Li, 2007; Chen and Knutson, 2008; Haugen and Iversen, 2008; May, 2008b; Kysely and Beranová, 2009; Min et al., 2011; Sillmann et al., 2013). Regional details are less robust in terms of the relative magnitude of changes but remain in good accord across models in terms of the sign of the change and the large-scale geographical patterns (Meehl et al., 2005a; CCSP, 2008a). In semi-arid regions of the midlatitudes and subtropics such as the Mediterranean, the southwest USA, southwestern Australia, southern Africa and a large portion of South America, the tendency manifested in the majority of model simulations is for longer dry periods and is consistent with the average decreases shown in Figure 12.22. Figure 12.26 shows projected percent changes in RX5day, the annual maximum of consecutive 5-day precipitation over land regions obtained from the CMIP5 models (Box 2.4, Table 1). Globally averaged end of 21st century changes over land range from 5% (RCP2.6) to 20% (RCP8.5) more precipitation during very wet 5-day periods. Results from the CMIP3 models are shown for comparison (see Section 12.4.9). Locally, the few regions where this index of extreme precipitation decreases in the late 21st century RCP8.5 projection coincide with areas of robust decreases in the mean precipitation of Figure 12.22.

Drought is discussed extensively in the SREX report (Seneviratne et al., 2012) and the conclusions about future drought risk described there based on CMIP3 models are reinforced by the CMIP5 models. As noted in the SREX reports, assessments of changes in drought characteristics with climate change should be made in the context of specific impacts questions. The risk of future agricultural drought episodes is increased in the regions of robust soil moisture decrease described in Section 12.4.5.3 and shown in Figure 12.23. Other measures in the literature of future agricultural drought are largely focussed on the Palmer Drought Severity Index (Wehner et al., 2011; Schwalm et al., 2012; Dai, 2013) and project ‘extreme’ drought as the normal climatological state by the end of the 21st century under the high emission scenarios in many mid-latitude locations. However, this measure of agricultural drought has been criticized as overly sensitive to increased temperatures due to

a simplified soil moisture model (Hoerling et al., 2012). The consecutive dry-day index (CDD) is the length of the longest period of consecutive days with precipitation less than 1 mm (Box 2.4, Table 1). CMIP5 projected changes in CDD over the 2081–2100 period under the RCP8.5 scenario (relative to the 1981–2000 reference period in common with CMIP3) from the CMIP5 models are shown in Figure 12.26c and exhibit patterns similar to projected changes in both precipitation and soil moisture (Sillmann et al., 2013). Substantial increases in this measure of meteorological drought are projected in the Mediterranean, Central America, Brazil, South Africa and Australia while decreases are projected in high northern latitudes.

Truly rare precipitation events can cause very significant impacts. The statistics of these events at the tails of the precipitation distribution are well described by Extreme Value (EV) Theory although there are significant biases in the direct comparison of gridded model output and actual station data (Smith et al., 2009). There is also strong evidence that model resolution plays a key role in replicating EV quantities estimated from gridded observational data, suggesting that high-resolution models may provide somewhat more confidence in projection of changes in rare precipitation events (Fowler et al., 2007a; Wehner et al., 2011). Figure 12.27 shows the late 21st century changes per degree Celsius in local warming in 20-year return values of annual maximum daily precipitation relative to the late 20th century (left) and the associated return periods of late 20th century 20-year return values at the end of the 21st century from the CMIP5 models. Across future emission scenarios, the global average of the CMIP5 multi-model median return value sensitivity is an increase of 5.3% °C<sup>-1</sup> (Kharin et al., 2013). The CMIP5 land average is close to the CMIP3 value of 4% °C<sup>-1</sup> reported by Min et al. (2011) for a subset of CMIP3 models. Corresponding with this change, the global average of return periods of late 20th century 20-year return values is reduced from 20 years to 14 years for a 1°C local warming. Return periods are projected to be reduced by about 10 to 20% °C<sup>-1</sup> over the most of the mid-latitude land masses with larger reductions over wet tropical regions (Kharin et al., 2013). Hence, extreme precipitation events will *very likely* be more intense

Daily precipitation 20-yr RV change per 1°C warming



RP for present day 20-yr RV of daily precipitation under 1°C warming

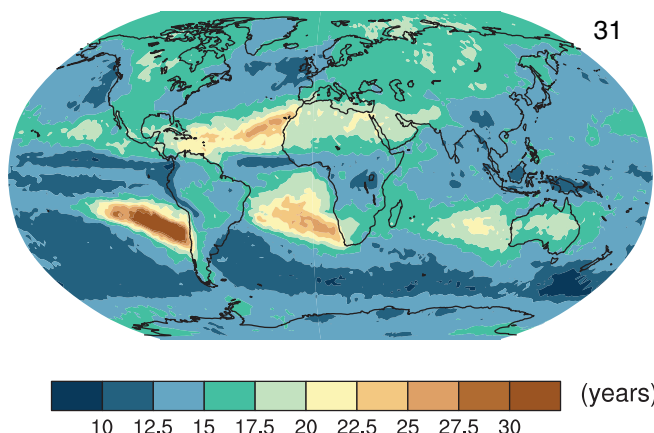


**Figure 12.27 |** (Left) The CMIP5 2081–2100 multi-model ensemble median percent change in 20-year return values of annual maximum daily precipitation per 1°C of local warming relative to the 1986–2005 reference period. (Right) The average 2081–2100 CMIP5 multi-model ensemble median of the return periods (years) of 1986–2005 20-year return values of annual maximum daily precipitation corresponding to 1°C of local warming. Regions of no change would have return periods of 20 years.

and more frequent in these regions in a warmer climate. Reductions in return values (or equivalently, increases in return period) are confined to convergent oceanic regions where circulation changes have reduced the available water vapour.

Severe thunderstorms, associated with large hail, high winds, and tornadoes, are another example of extreme weather associated with the water cycle. The large-scale environments in which they occur are characterized by large Convective Available Potential Energy (CAPE) and deep tropospheric wind shear (Brooks et al., 2003; Brooks, 2009). Del Genio et al. (2007), Trapp et al. (2007, 2009), and Van Klooster and Roeber (2009) found a general increase in the energy and decrease in the shear terms from the late 20th century to the late 21st century over the USA using a variety of regional model simulations embedded in global model SRES scenario simulations. The relative change between these two competing factors would tend to favour more environments that would support severe thunderstorms, providing storms are initiated. Trapp et al. (2009), for example, found an increase in favourable thunderstorm conditions for all regions of the USA east of the Rocky Mountains. Large variability in both the energy and shear terms means that statistical significance is not reached until late in the 21st century under high forcing scenarios. One way of assessing the possibility of a change in the frequency of future thunderstorms is to look at historical records of observed tornado, hail and wind occurrence with respect to the environmental conditions (Brooks, 2013). This indicates that an increase in the fraction of severe thunderstorms containing non-tornadic winds would be consistent with the model projections of increased energy and decreased shear, but there has not been enough research to make a firm conclusion regarding future changes in frequency or magnitude.

Less work has been done on projected changes outside of the USA. Marsh et al. (2009) found that mean energy decreased in the warm season in Europe while it increased in the cool season. Even though the energy decreases in the warm season, the number of days with favourable environments for severe thunderstorms increases because of an increasing number of days with relatively large values of available energy. For Europe, with the Mediterranean Sea and Sahara Desert to the south, questions remain about changes in boundary layer moisture, a main driver of the energy term. Niall and Walsh (2005) examined changes in CAPE, which may be associated with hailstorm occurrence in southeastern Australia using a global model, and found little change under warmer conditions. Leslie et al. (2008) reconsidered the southeastern Australia hail question by nesting models with 1 km horizontal grid spacing and using sophisticated microphysical parameterizations and found an increase in the frequency of large hail by 2050 under the SRES A1B scenario, but with extremely large internal variability in the environments and hail size.

Overall, for all parts of the world studied, the results are suggestive of a trend toward environments favouring more severe thunderstorms, but the small number of analyses precludes any likelihood estimate of this change.

## 12.4.6 Changes in Cryosphere

### 12.4.6.1 Changes in Sea Ice Cover

Based on the analysis of CMIP3 climate change simulations (e.g., Arzel et al., 2006; Zhang and Walsh, 2006), the AR4 concludes that the Arctic and Antarctic sea ice covers are projected to shrink in the 21st century under all SRES scenarios, with a large range of model responses (Meehl et al., 2007b). It also stresses that, in some projections, the Arctic Ocean becomes almost entirely ice-free in late summer during the second half of the 21st century. These conclusions were confirmed by further analyses of the CMIP3 archives (e.g., Stroeve et al., 2007; Bracegirdle et al., 2008; Lefebvre and Goosse, 2008; Boé et al., 2009b; Sen Gupta et al., 2009; Wang and Overland, 2009; Zhang, 2010b; NRC, 2011; Körper et al., 2013). Figures 12.28 and 12.29 and the studies of Maksym et al. (2012), Massonnet et al. (2012), Stroeve et al. (2012) and Wang and Overland (2012) show that the CMIP5 AOGCMs/ESMs as a group also project decreases in sea ice extent through the end of this century in both hemispheres under all RCPs. However, as in the case of CMIP3, the inter-model spread is considerable.

In the NH, in accordance with CMIP3 results, the absolute rate of decrease of the CMIP5 multi-model mean sea ice areal coverage is greatest in September. The reduction in sea ice extent between the time periods 1986–2005 and 2081–2100 for the CMIP5 multi-model average ranges from 8% for RCP2.6 to 34% for RCP8.5 in February and from 43% for RCP2.6 to 94% for RCP8.5 in September. *Medium confidence* is attached to these values as projections of sea ice extent decline in the real world due to errors in the simulation of present-day sea ice extent (mean and trends—see Section 9.4.3) and because of the large spread of model responses. About 90% of the available CMIP5 models reach nearly ice-free conditions (sea ice extent less than  $1 \times 10^6 \text{ km}^2$  for at least 5 consecutive years) during September in the Arctic before 2100 under RCP8.5 (about 45% under RCP4.5). By the end of the 21st century, the decrease in multi-model mean sea ice volume ranges from 29% for RCP2.6 to 73% for RCP8.5 in February and from 54% for RCP2.6 to 96% for RCP8.5 in September. *Medium confidence* is attached to these values as projections of the real world sea ice volume. In February, these percentages are much higher than the corresponding ones for sea ice extent, which is indicative of a substantial sea ice thinning.

A frequent criticism of the CMIP3 models is that, as a group, they strongly underestimate the rapid decline in summer Arctic sea ice extent observed during the past few decades (e.g., Stroeve et al., 2007; Winton, 2011), which suggests that the CMIP3 projections of summer Arctic sea ice areal coverage might be too conservative. As shown in Section 9.4.3 and Figure 12.28b, the magnitude of the CMIP5 multi-model mean trend in September Arctic sea ice extent over the satellite era is more consistent with, but still underestimates, the observed one (see also Massonnet et al., 2012; Stroeve et al., 2012; Wang and Overland, 2012; Overland and Wang, 2013). Owing to the shortness of the observational record, it is difficult to ascertain the relative influence of natural variability on this trend. This hinders the comparison between modelled and observed trends, and hence the estimate of the sensitivity of the September Arctic sea ice extent to global surface temperature change (i.e., the decrease in sea ice extent per degree global

warming) (Kay et al., 2011; Winton, 2011; Mahlstein and Knutti, 2012). This sensitivity may be crucial for determining future sea ice losses. Indeed, a clear relationship exists at longer than decadal time scales in climate change simulations between the annual mean or September mean Arctic sea ice extent and the annual mean global surface temperature change for ice extents larger than  $\sim 1 \times 10^6 \text{ km}^2$  (e.g., Ridley et al., 2007; Zhang, 2010b; NRC, 2011; Winton, 2011; Mahlstein and Knutti, 2012). This relationship is illustrated in Figure 12.30 for both CMIP3 and CMIP5 models. From this figure, it can be seen that the sea ice sensitivity varies significantly from model to model and is generally larger and in better agreement among models in CMIP5.

A complete and detailed explanation for what controls the range of Arctic sea ice responses in models over the 21st century remains elusive, but the Arctic sea ice provides an example where process-based constraints can be used to reduce the spread of model projections

(Overland et al., 2011; Collins et al., 2012; Hodson et al., 2012). For CMIP3 models, results indicate that the changes in Arctic sea ice mass budget over the 21st century are related to the late 20th century mean sea ice thickness distribution (Holland et al., 2010), average sea ice thickness (Bitz, 2008; Hodson et al., 2012), fraction of thin ice cover (Boé et al., 2009b) and oceanic heat transport to the Arctic (Mahlstein and Knutti, 2011). For CMIP5 models, Massonnet et al. (2012) showed that the time needed for the September Arctic sea ice areal coverage to drop below a certain threshold is highly correlated with the September sea ice extent and annual mean sea ice volume averaged over the past several decades (Figure 12.31a, b). The timing of a seasonally ice-free Arctic Ocean or the fraction of remaining sea ice in September at any time during the 21st century were also found to correlate with the past trend in September Arctic sea ice extent and the amplitude of the mean seasonal cycle of sea ice extent (Boé et al., 2009b; Collins et al., 2012; Massonnet et al., 2012) (Figure 12.31c, d). All these empirical

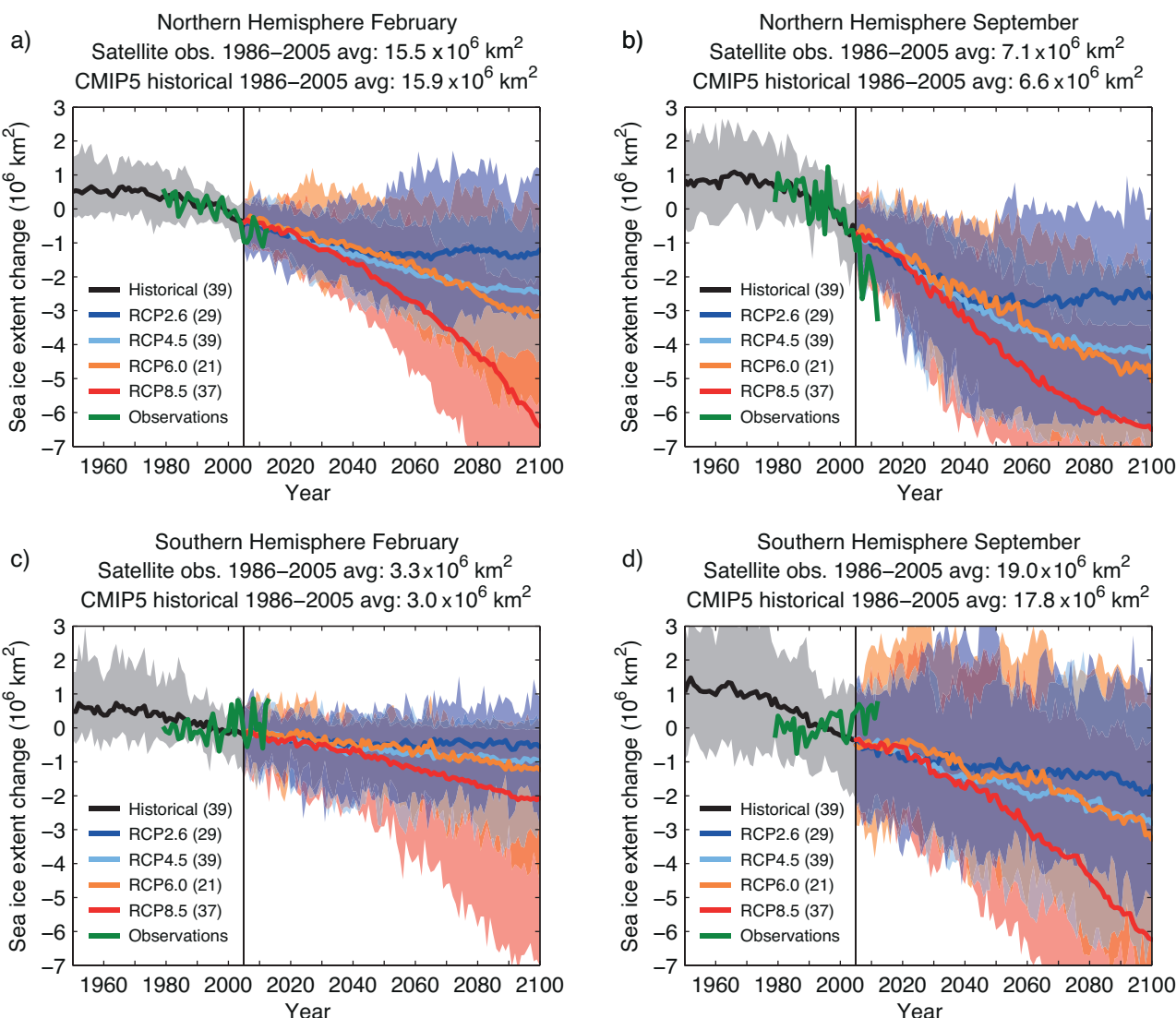


**Figure 12.28 |** Changes in sea ice extent as simulated by CMIP5 models over the second half of the 20th century and the whole 21st century under RCP2.6, RCP4.5, RCP6.0 and RCP8.5 for (a) Northern Hemisphere February, (b) Northern Hemisphere September, (c) Southern Hemisphere February and (d) Southern Hemisphere September. The solid curves show the multi-model means and the shading denotes the 5 to 95% range of the ensemble. The vertical line marks the end of CMIP5 historical climate change simulations. One ensemble member per model is taken into account in the analysis. Sea ice extent is defined as the total ocean area where sea ice concentration exceeds 15% and is calculated on the original model grids. Changes are relative to the reference period 1986–2005. The number of models available for each RCP is given in the legend. Also plotted (solid green curves) are the satellite data of Comiso and Nishio (2008, updated 2012) over 1979–2012.

relationships can be understood on simple physical grounds (see the aforementioned references for details).

These results lend support for weighting/recalibrating the models based on their present-day Arctic sea ice simulations. Today, the optimal approach for constraining sea ice projections from climate models is unclear, although one notes that these methods should have a credible underlying physical basis in order to increase confidence in their results (see Section 12.2). In addition, they should account for

the potentially large imprint of natural variability on both observations and model simulations when these two sources of information are to be compared (see Section 9.8.3). This latter point is particularly critical if the past sea ice trend or sensitivity is used in performance metrics given the relatively short observational period (Kay et al., 2011; Overland et al., 2011; Mahlstein and Knutti, 2012; Massonnet et al., 2012; Stroeve et al., 2012). A number of studies have applied such metrics to the CMIP3 and CMIP5 models. Stroeve et al. (2007) and Stroeve et al. (2012) rejected several CMIP3 and CMIP5 models, respectively, on

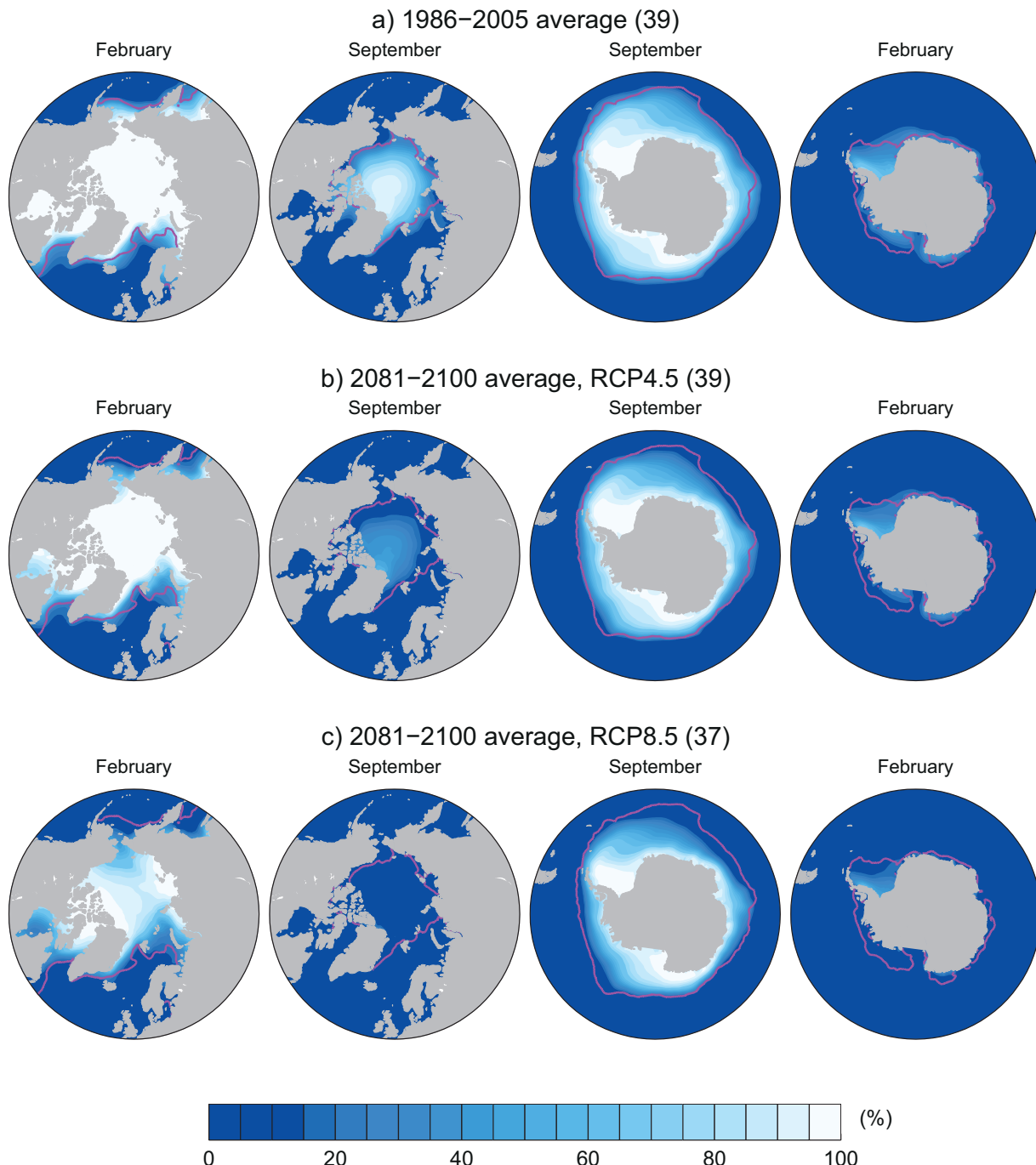


**Figure 12.29** | February and September CMIP5 multi-model mean sea ice concentrations (%) in the Northern and Southern Hemispheres for the periods (a) 1986–2005, (b) 2081–2100 under RCP4.5 and (c) 2081–2100 under RCP8.5. The model sea ice concentrations are interpolated onto a  $1^\circ \times 1^\circ$  regular grid. One ensemble member per model is taken into account in the analysis, and the multi-model mean sea ice concentration is shown where it is larger than 15%. The number of models available for each RCP is given in parentheses. The pink lines indicate the observed 15% sea ice concentration limits averaged over 1986–2005 (Comiso and Nishio, 2008, updated 2012).

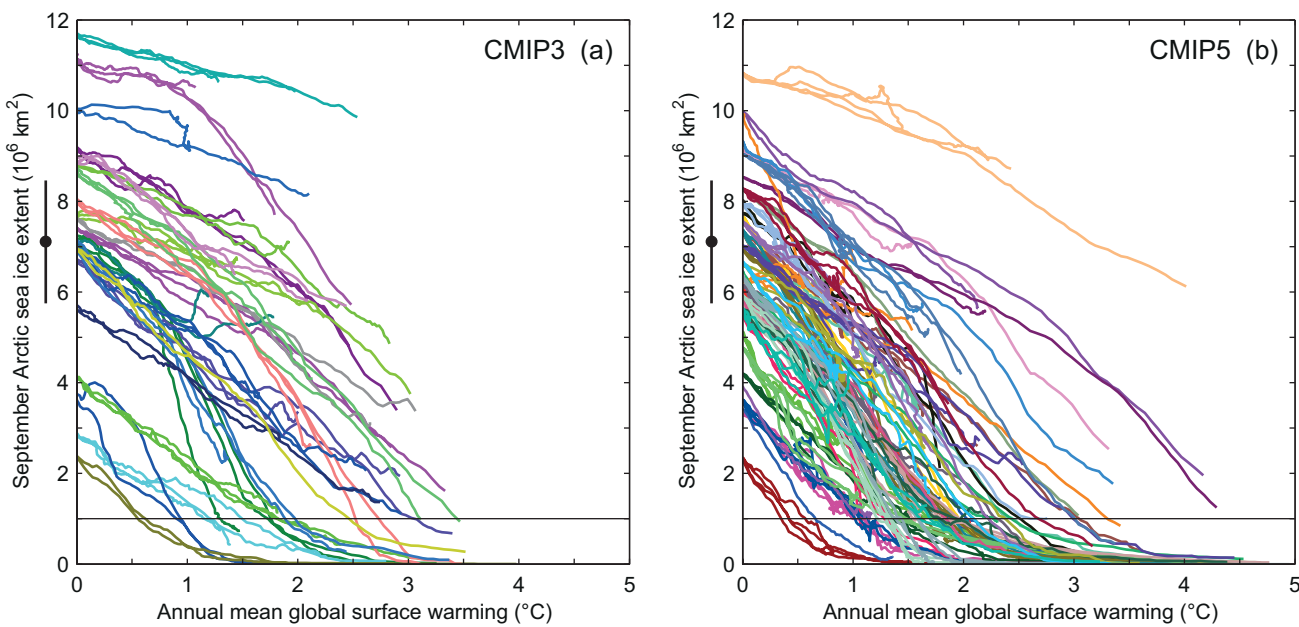


**Figure 12.30** | September Arctic sea ice extent as a function of the annual mean global surface warming relative to the period 1986–2005 for (a) CMIP3 models (all SRES scenarios) and (b) CMIP5 models (all RCPs). The ice extents and global temperatures are computed on a common latitude-longitude grid for CMIP3 and on the original model grids for CMIP5. One ensemble member per model is taken into account in the analysis. A 21-year running mean is applied to the model output. The full black circle and vertical bar on the left-hand side of the y-axis indicate the mean and  $\pm 2$  standard deviations about the mean of the observed September Arctic sea ice extent over 1986–2005, respectively (Comiso and Nishio, 2008, updated 2012). The horizontal line corresponds to a nearly ice-free Arctic Ocean in September.

the basis of their simulated late 20th century mean September Arctic sea ice extent. Wang and Overland (2009) selected a subset of CMIP3 models (and Wang and Overland (2012) did the same for the CMIP5 models) based on their fidelity to the observed mean seasonal cycle of Arctic sea ice extent in the late 20th century and then scaled the chosen models to the recently observed September sea ice extent. Zhang (2010b) retained a number of CMIP3 models based on the regression between summer sea ice loss and Arctic surface temperature change. Boé et al. (2009b) and Mahlstein and Knutti (2012) did not perform a model selection but rather recalibrated the CMIP3 Arctic sea ice projections on available observations of September Arctic sea ice trend and sensitivity to global surface temperature change, respectively. Finally, Massonnet et al. (2012) selected a subset of CMIP5 models on the basis of the four relationships illustrated in Figure 12.31a–d.

12

These various methods all suggest a faster rate of summer Arctic sea ice decline than the multi-model mean. Although they individually provide a reduced range for the year of near disappearance of the September Arctic sea ice compared to the original CMIP3/CMIP5 multi-model ensemble, they lead to different timings (Overland and Wang, 2013). Consequently, the time interval obtained when combining all these studies remains wide: 2020–2100<sup>+</sup> (2100<sup>+</sup> = not before 2100) for the SRES A1B scenario and RCP4.5 (Stroeve et al., 2007, 2012; Boé et al., 2009b; Wang and Overland, 2009, 2012; Zhang, 2010b; Massonnet et al., 2012) and 2020–2060 for RCP8.5 (Massonnet et al., 2012; Wang and Overland, 2012). The method proposed by Massonnet et al. (2012) is applied here to the full set of models that provided the CMIP5 database with sea ice output. The natural variability of each of the four diagnostics shown in Figure 12.31a–d is first estimated by averaging over all available models with more than one ensemble member the diagnostic standard deviations derived from the model

ensemble members. Then, for each model, a  $\pm 2$  standard deviation interval is constructed around the ensemble mean or single realization of the diagnostic considered. A model is retained if, for each diagnostic, either this interval overlaps a  $\pm 20\%$  interval around the observed/reanalysed value of the diagnostic or at least one ensemble member from that model gives a value for the diagnostic that falls within  $\pm 20\%$  of the observational/reanalysed data. The outcome is displayed in Figure 12.31e for RCP8.5. Among the five selected models (ACCESS1.0, ACCESS1.3, GFDL-CM3, IPSL-CM5A-MR, MPI-ESM-MR), four project a nearly ice-free Arctic Ocean in September before 2050 (2080) for RCP8.5 (RCP4.5), the earliest and latest years of near disappearance of the sea ice pack being about 2040 and about 2060 (about 2040 and 2100<sup>+</sup>), respectively. It should be mentioned that Maslowski et al. (2012) projected that it would take only until about 2016 to reach a nearly ice-free Arctic Ocean in summer, based on a linear extrapolation into the future of the recent sea ice volume trend from a hindcast simulation conducted with a regional model of the Arctic sea ice–ocean system. However, such an extrapolation approach is problematic as it ignores the negative feedbacks that can occur when the sea ice cover becomes thin (e.g., Bitz and Roe, 2004; Notz, 2009) and neglects the effect of year-to-year or longer-term variability (Overland and Wang, 2013). Mahlstein and Knutti (2012) encompassed the dependence of sea ice projections on the forcing scenario by determining the annual mean global surface warming threshold for nearly ice-free conditions in September. Their best estimate of  $\sim 2^\circ\text{C}$  above the present derived from both CMIP3 models and observations is consistent with the 1.6 to  $2.1^\circ\text{C}$  range (mean value:  $1.9^\circ\text{C}$ ) obtained from the CMIP5 model subset shown in Figure 12.31e (see also Figure 12.30b). The reduction in September Arctic sea ice extent by the end of the 21st century, averaged over this subset of models, ranges from 56% for RCP2.6 to 100% for RCP8.5.

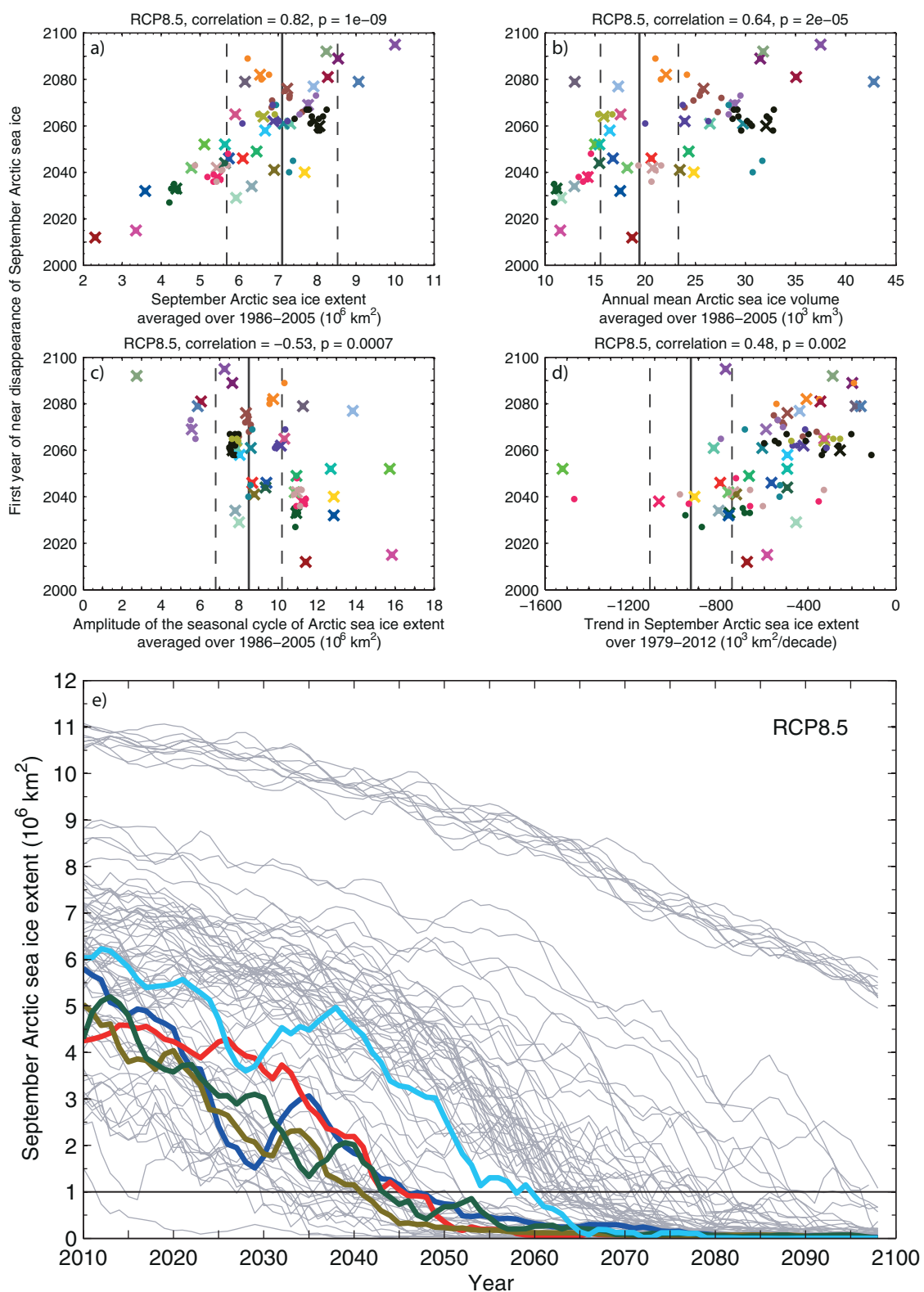


**Figure 12.31 |** (a-d) First year during which the September Arctic sea ice extent falls below  $1 \times 10^6 \text{ km}^2$  in CMIP5 climate projections (37 models, RCP8.5) as a function of (a) the September Arctic sea ice extent averaged over 1986–2005, (b) the annual mean Arctic sea ice volume averaged over 1986–2005, (c) the amplitude of the 1986–2005 mean seasonal cycle of Arctic sea ice extent and (d) the trend in September Arctic sea ice extent over 1979–2012. The sea ice diagnostics displayed are calculated on the original model grids. The correlations and one-tailed p-values are computed from the multi-member means for models with several ensemble members (coloured crosses), but the ensemble members of individual models are also depicted (coloured dots). The vertical solid and dashed lines show the corresponding observations or bias-adjusted PIOMAS (Pan-Arctic Ice-Ocean Modelling and Assimilation System) reanalysis data (a, c and d: Comiso and Nishio, 2008, updated 2012; b: Schweiger et al., 2011) and the  $\pm 20\%$  interval around these data, respectively. (e) Time series of September Arctic sea ice extent (5-year running mean) as simulated by all CMIP5 models and their ensemble members under RCP8.5 (thin curves). The thick, coloured curves correspond to a subset of five CMIP5 models selected on the basis of panels a–d following Massonnet et al. (2012) (see text for details). Note that each of these models provides only one ensemble member for RCP8.5.

In light of all these results, it is *very likely* that the Arctic sea ice cover will continue to shrink and thin all year round during the 21st century as the annual mean global surface temperature rises. It is also *likely* that the Arctic Ocean will become nearly ice-free in September before the middle of the century for high GHG emissions such as those corresponding to RCP8.5 (*medium confidence*). The potential irreversibility of the Arctic sea ice loss and the possibility of an abrupt transition toward an ice-free Arctic Ocean are discussed in Section 12.5.5.7.

In the SH, the decrease in sea ice extent between 1986–2005 and 2081–2100 projected by the CMIP5 models as a group varies from 16% for RCP2.6 to 67% for RCP8.5 in February and from 8% to 30% in September. In contrast with the NH, the absolute rate of decline is greatest in wintertime. Eisenman et al. (2011) argue that this hemispheric asymmetry in the seasonality of sea ice loss is fundamentally related to the geometry of coastlines. For each forcing scenario, the relative changes in multi-model mean February and September Antarctic sea ice volumes by the end of the century are of the same order as the corresponding ones for sea ice extent. About 75% of the available CMIP5 models reach a nearly ice-free state in February within this century under RCP8.5 (about 60% under RCP4.5). For RCP8.5, only small portions of the Weddell and Ross Seas stay ice-covered in February during 2081–2100 in those models that do not project a seasonally ice-free Southern Ocean (see Figure 12.29c). Nonetheless, there is *low confidence* in these Antarctic sea ice projections because of the wide range of model responses and the inability of almost all of the models to reproduce the mean seasonal cycle, interannual variability and overall increase of the Antarctic sea ice areal coverage observed during the satellite era (see Section 9.4.3; Maksym et al., 2012; Turner et al., 2013; Zunz et al., 2013).

#### 12.4.6.2 Changes in Snow Cover and Frozen Ground

Excluding ice sheets and glaciers, analyses of seasonal snow cover changes generally focus on the NH, where the configuration of the continents on the Earth induces a larger maximum seasonal snow cover extent (SCE) and a larger sensitivity of SCE to climate changes. Seasonal snow cover extent and snow water equivalent (SWE) respond to both temperature and precipitation. At the beginning and the end of the snow season, SCE decreases are closely linked to a shortening of the seasonal snow cover duration, while SWE is more sensitive to snowfall amount (Brown and Mote, 2009). Future widespread reductions of SCE, particularly in spring, are simulated by the CMIP3 models (Roesch, 2006; Brown and Mote, 2009) and confirmed by the CMIP5 ensemble (Brutel-Vuilmet et al., 2013). The NH spring (March–April average) snow cover area changes are coherent in the CMIP5 models although there is considerable scatter. Relative to the 1986–2005 reference period, the CMIP5 models simulate a weak decrease of about  $7 \pm 4\%$  (one- $\sigma$  inter-model dispersion) for RCP2.6 during the last two decades of the 21st century, while SCE decreases of about  $13 \pm 4\%$  are simulated for RCP4.5,  $15 \pm 5\%$  for RCP6.0, and  $25 \pm 8\%$  for RCP8.5 (Figure 12.32). There is *medium confidence* in these numbers because of the considerable inter-model scatter mentioned above and because snow processes in global climate models are strongly simplified.

Projections for the change in annual maximum SWE are more mixed. Warming decreases SWE both by reducing the fraction of precipitation

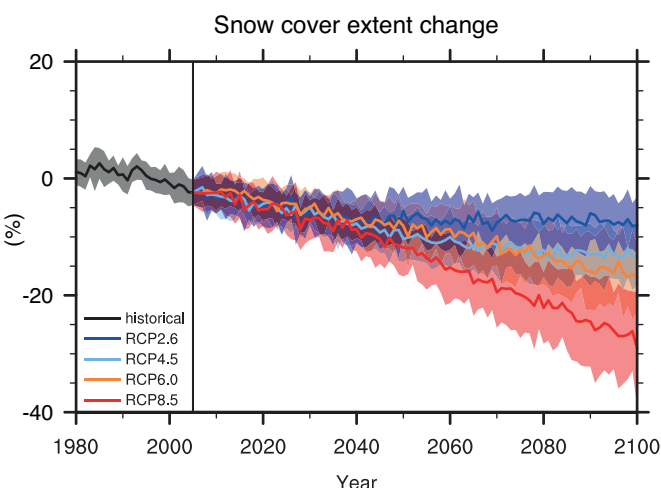


**Figure 12.32 |** Northern Hemisphere spring (March to April average) snow cover extent change (in %) in the CMIP5 ensemble, relative to the simulated extent for the 1986–2005 reference period. Thick lines mark the multi-model average, shading indicates the inter-model spread (one standard deviation). The observed March to April average snow cover extent for the 1986–2005 reference period is  $32.6 \cdot 10^6 \text{ km}^2$  (Brown and Robinson, 2011).

that falls as snow and by increasing snowmelt, but projected increases in precipitation over much of the northern high latitudes during winter months act to increase snow amounts. Whether snow covering the ground will become thicker or thinner depends on the balance between these competing factors. Both in the CMIP3 (Räisänen, 2008) and in the CMIP5 models (Brutel-Vuilmet et al., 2013), annual maximum SWE tends to increase or only marginally decrease in the coldest

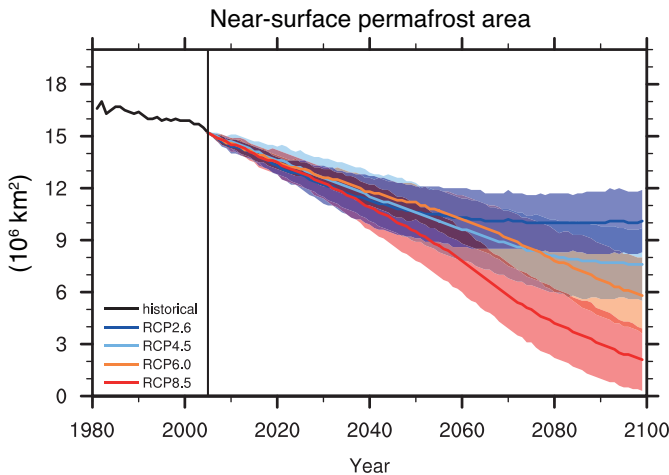


**Figure 12.33 |** Northern Hemisphere near-surface permafrost area, diagnosed for the available CMIP5 models by Slater and Lawrence (2013) following Nelson and Outcalt (1987) and using 20-year average bias-corrected monthly surface air temperatures and snow depths. Thick lines: multi-model average. Shading and thin lines indicate the inter-model spread (one standard deviation). The black line for the historical period is diagnosed from the average of the European Centre for Medium range Weather Forecast (ECMWF) reanalysis of the global atmosphere and surface conditions (ERA), Japanese ReAnalysis (JRA), Modern Era Retrospective-analysis for Research and Applications (MERRA) and Climate Forecast System Reanalysis and Reforecast (CFSRR) reanalyses (Slater and Lawrence, 2013). Estimated present permafrost extent is between 12 and 17 million  $\text{km}^2$  (Zhang et al., 2000).

regions, while annual maximum SWE decreases are strong closer to the southern limit of the seasonally snow-covered area.

It is thus *very likely (high confidence)* that by the end of the 21st century, NH spring snow cover extent will be substantially lower than today if anthropogenic climate forcing is similar to the stronger scenarios considered here. Conversely, there is only *medium confidence* in the latitudinal pattern of annual maximum SWE changes (increase or little change in the coldest regions, stronger decrease further to the South) because annual maximum SWE is influenced by competing factors (earlier melt onset, higher solid precipitation rates in some regions).

The strong projected warming across the northern high latitudes in climate model simulations has implications for frozen ground. Recent projections of the extent of near-surface permafrost (see Glossary) degradation continue to vary widely depending on the underlying climate forcing scenario and model physics, but virtually all of them indicate substantial near-surface permafrost degradation and thaw depth deepening over much of the permafrost area (Saito et al., 2007; Lawrence et al., 2008a, 2012; Koven et al., 2011, 2013; Eliseev et al., 2013; Slater and Lawrence, 2013). Permafrost at greater depths is less directly relevant to the surface energy and water balance, and its degradation naturally occurs much more slowly (Delisle, 2007). Climate models are beginning to represent permafrost physical processes and properties more accurately (Alexeev et al., 2007; Nicolsky et al., 2007; Lawrence et al., 2008a; Rinke et al., 2008; Koven et al., 2009; Gouttevin et al., 2012), but there are large disagreements in the calculation of current frozen soil extent and active layer depth due to differences in the land model physics in the CMIP5 ensemble (Koven et al., 2013). The projected changes in permafrost are a response not only to warming, but also to changes in snow conditions because snow properties and their seasonal evolution exert significant control on soil thermal state (Zhang, 2005; Lawrence and Slater, 2010; Shkolnik et al., 2010; Koven et al., 2013). Applying the surface frost index method (Nelson and Outcalt, 1987) to coupled climate model anomalies from the CMIP5 models (Slater and Lawrence, 2013) yields a reduction of the diagnosed 2080–2099 near-surface permafrost area (continuous plus discontinuous near-surface permafrost) by  $37 \pm 11\%$  (RCP2.6),  $51 \pm 13\%$  (RCP4.5),  $58 \pm 13\%$  (RCP6.0), and  $81 \pm 12\%$  (RCP8.5), compared to the 1986–2005 diagnosed near-surface permafrost area, with *medium confidence* in the numbers as such because of the strongly simplified soil physical processes in current-generation global climate models (Figure 12.33). The uncertainty range given here is the  $1-\sigma$  inter-model dispersion. Applying directly the model output to diagnose permafrost extent and its changes over the 21st century yields similar relative changes (Koven et al., 2013). In summary, based on high agreement across CMIP5 and older model projections, fundamental process understanding, and paleoclimatic evidence (e.g., Vaks et al., 2013), it appears *virtually certain (high confidence)* that near-surface permafrost extent will shrink as global climate warms. However, the amplitude of the projected reductions of near-surface permafrost extent not only depends on the emission scenario and the global climate model response, but also very much on the permafrost-related soil processes taken into account in the models.

## 12.4.7 Changes in the Ocean

### 12.4.7.1 Sea Surface Temperature, Salinity and Ocean Heat Content

Projected increase of SST and heat content over the next two decades is relatively insensitive to the emissions trajectory. However, projected outcomes diverge as the 21st century progresses. When SSTs increase as a result of external forcing, the interior water masses respond to the integrated signal at the surface, which is then propagated down to greater depth (Gleckler et al., 2006; Gregory, 2010). Changes in globally averaged ocean heat content currently account for about 90% of the change in global energy inventory since 1970 (see Box 3.1). Heat is transported within the interior of the ocean by its large-scale general circulation and by smaller-scale mixing processes. Changes in transports lead to redistribution of existing heat content and can cause local cooling even though the global mean heat content is rising (Banks and Gregory, 2006; Lowe and Gregory, 2006; Xie and Vallis, 2012).

Figure 12.12 shows the multi-model mean projections of zonally averaged ocean temperature change under three emission scenarios. The differences in projected ocean temperature changes for different RCPs manifest themselves more markedly as the century progresses. The largest warming is found in the top few hundred metres of the subtropical gyres, similar to the observed pattern of ocean temperature changes (Levitus et al., 2012, see also Section 3.2). Surface warming varies considerably between the emission scenarios ranging from about  $1^{\circ}\text{C}$  (RCP2.6) to more than  $3^{\circ}\text{C}$  in RCP8.5. Mixing and advection processes gradually transfer the additional heat to deeper levels of about 2000 m at the end of the 21st century. Depending on the emission scenario, global ocean warming between  $0.5^{\circ}\text{C}$  (RCP2.6) and  $1.5^{\circ}\text{C}$  (RCP8.5) will reach a depth of about 1 km by the end of the century. The strongest warming signal is found at the surface in subtropical and tropical regions. At depth the warming is most pronounced in the Southern Ocean. From an energy point of view, for RCP4.5 by the end of the 21st century, half of the energy taken up by the ocean is in the uppermost 700 m, and 85% is in the uppermost 2000 m.

In addition to the upper-level warming, the patterns are further characterized by a slight cooling in parts of the northern mid- and high latitudes below 1000 m and a pronounced heat uptake in the deep Southern Ocean at the end of the 21st century. The cooling may be linked to the projected decrease of the strength of the AMOC (see Section 12.4.7.2; 13.4.1; Banks and Gregory, 2006).

The response of ocean temperatures to external forcing comprises mainly two time scales: a relatively fast adjustment of the ocean mixed layer and the slow response of the deep ocean (Hansen et al., 1985; Knutti et al., 2008a; Held et al., 2010). Simulations with coupled ocean–atmosphere GCMs suggest time-scales of several millennia until the deep ocean is in equilibrium with the external forcing (Stouffer, 2004; Hansen et al., 2011; Li et al., 2013a). Thus, the long time-scale of the ocean response to external forcing implies an additional commitment to warming for many centuries when GHG emissions are decreased or concentrations kept constant (see Section 12.5.2). Further assessment of ocean heat uptake and its relationship to projections of sea level rise is presented in Section 13.4.1.

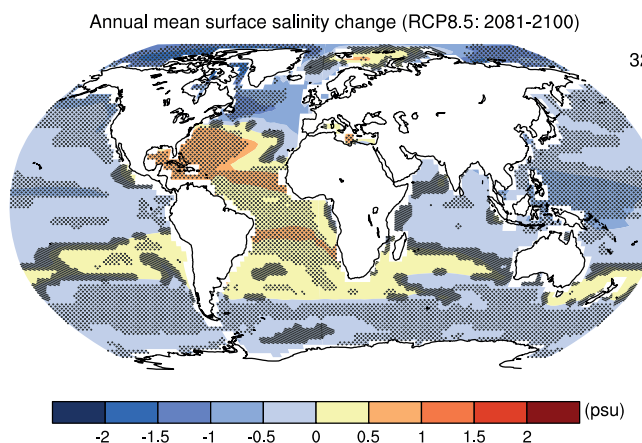


**Figure 12.34 |** Projected sea surface salinity differences 2081–2100 for RCP8.5 relative to 1986–2005 from CMIP5 models. Hatching indicates regions where the multi-model mean change is less than one standard deviation of internal variability. Stippling indicates regions where the multi-model mean change is greater than two standard deviations of internal variability and where at least 90% of the models agree on the sign of change (see Box 12.1). The number of CMIP5 models used is indicated in the upper right corner.

Durack and Wijffels (2010) and Durack et al. (2012) examined trends in global sea surface salinity (SSS) changes over the period 1950–2008. Their analysis revealed strong, spatially coherent trends in SSS over much of the global ocean, with a pattern that bears striking

resemblance to the climatological SSS field and is associated with an intensification of the global water cycle (see Sections 3.3.2.1, 10.4.2 and 12.4.5). The CMIP5 climate model projections available suggest that high SSS subtropical regions that are dominated by net evaporation are typically getting more saline; lower SSS regions at high latitudes are typically getting fresher. They also suggest a continuation of this trend in the Atlantic where subtropical surface waters become more saline as the century progresses (Figure 12.34) (see also Terray et al., 2012). At the same time, the North Pacific is projected to become less saline.

#### 12.4.7.2 Atlantic Meridional Overturning

Almost all climate model projections reveal an increase of high latitude temperature and high latitude precipitation (Meehl et al., 2007b). Both of these effects tend to make the high latitude surface waters lighter and hence increase their stability. As seen in Figure 12.35, all models show a weakening of the AMOC over the course of the 21st century (see Section 12.5.5.2 for further analysis). Projected changes in the strength of the AMOC at high latitudes appear stronger in Geophysical Fluid Dynamics Laboratory (GFDL) CM2.1 when density is used as a vertical coordinate instead of depth (Zhang, 2010a). Once the RF is stabilized, the AMOC recovers, but in some models to less than its pre-industrial level. The recovery may include a significant overshoot (i.e., a weaker circulation may persist) if the anthropogenic RF is eliminated (Wu et al., 2011a). Gregory et al. (2005) found that for all eleven models

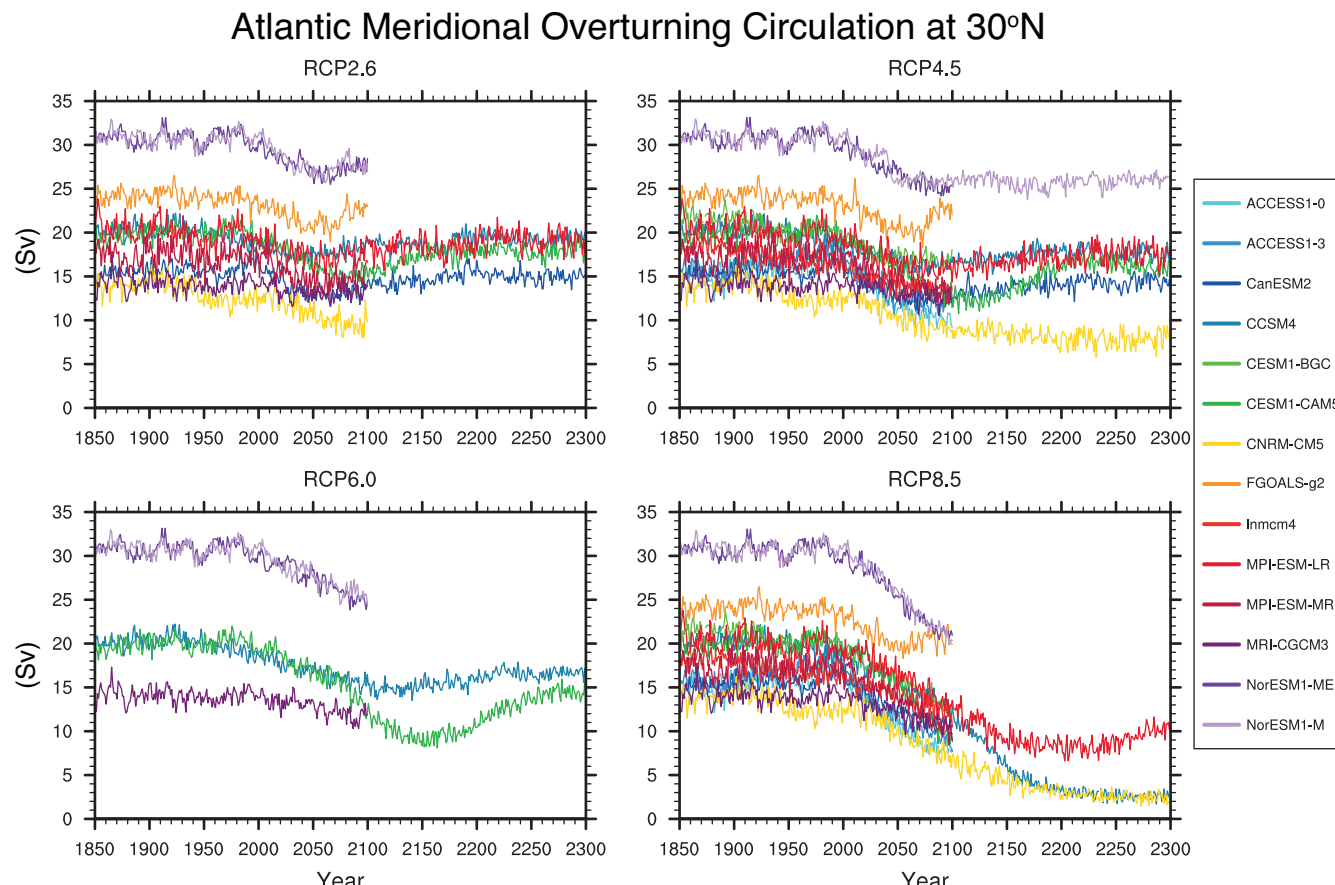


**Figure 12.35 |** Multi-model projections of Atlantic Meridional Overturning Circulation (AMOC) strength at 30°N from 1850 through to the end of the RCP extensions. Results are based on a small number of CMIP5 models available. Curves show results from only the first member of the submitted ensemble of experiments.

analysed (six from CMIP2/3 and five EMICs), the AMOC reduction was caused more by changes in surface heat flux than changes in surface freshwater flux. They further found that models with a stronger AMOC in their control run exhibited a larger weakening (see also Gregory and Tailleux, 2011).

Based on the assessment of the CMIP5 RCP simulations and on our understanding gleaned from analysis of CMIP3 models, observations and our understanding of physical mechanisms, it is *very likely* that the AMOC will weaken over the 21st century. Best estimates and ranges for the reduction from CMIP5 are 11% (1 to 24%) in RCP2.6 and 34% (12 to 54%) in RCP8.5. There is *low confidence* in assessing the evolution of the AMOC beyond the 21st century.

#### 12.4.7.3 Southern Ocean

A dominant and robust feature of the CMIP3 climate projections assessed in AR4 is the weaker surface warming at the end of the 21st century in the Southern Ocean area compared to the global mean. Furthermore, the Antarctic Circumpolar Current (ACC) moves southward in most of the climate projections analysed in response to the simulated southward shift and strengthening of the SH mid-latitude westerlies (Meehl et al., 2007b).

The additional analyses of the CMIP3 model output performed since the release of AR4 confirm and refine the earlier findings. The displacement and intensification of the mid-latitude westerlies contribute to a large warming between 40°S and 60°S from the surface to mid-depths (Fyfe et al., 2007; Sen Gupta et al., 2009). Part of this warming has been attributed to the southward translation of the Southern Ocean current system (Sen Gupta et al., 2009). Moreover, the wind changes influence the surface temperature through modifications of the latent and sensible heat fluxes and force a larger northward Ekman transport of relatively cold polar surface water (Screen et al., 2010). This also leads to a stronger upwelling that brings southward and upward relatively warm and salty deep water, resulting in a subsurface salinity increase at mid-depths south of 50°S (Sen Gupta et al., 2009; Screen et al., 2010).

Overall, CMIP3 climate projections exhibit a decrease in mixed layer depth at southern mid- and high latitudes by the end of the 21st century. This feature is a consequence of the enhanced stratification resulting from surface warming and freshening (Lefebvre and Goosse, 2008; Sen Gupta et al., 2009; Capotondi et al., 2012). Despite large inter-model differences, there is a robust weakening of Antarctic Bottom Water production and its northward outflow, which is consistent with the decrease in surface density and is manifest as a warming signal close to the Antarctic margin that reaches abyssal depths (Sen Gupta et al., 2009).

In the vicinity of the Antarctic ice sheet, CMIP3 models project an average warming of  $\sim 0.5\text{C}^\circ$  at depths of 200–500 m in 2091–2100 compared to 1991–2000 for the SRES A1B scenario, which has the potential to impact the mass balance of ice shelves (Yin et al., 2011). More detailed regional modelling using the SRES A1B scenario indicates that a redirection of the coastal current into the cavities underlying the Filchner-Ronne ice shelf during the second half of the 21st century

might enhance the average basal melting rate there from  $0.2 \text{ m yr}^{-1}$  to almost  $4 \text{ m yr}^{-1}$  (Hellmer et al., 2012; see Section 13.4.4.2).

There are very few published analyses of CMIP5 climate projections focusing on the Southern Ocean. Meijers et al. (2012) found a wide variety of ACC responses to climate warming scenarios across CMIP5 models. Models show a high correlation between the changes in ACC strength and position, with a southward (northward) shift of the ACC core as the ACC gets stronger (weaker). No clear relationship between future changes in wind stress and ACC strength was identified, while the weakening of the ACC transport simulated at the end of the 21st century by many models was found to correlate with the strong decrease in the surface heat and freshwater fluxes in the ACC region (Meijers et al., 2012; Downes and Hogg, 2013). In agreement with the CMIP3 assessment (Sen Gupta et al., 2009), subtropical gyres generally strengthen under RCP4.5 and RCP8.5 and all expand southward, inducing a southward shift of the northern boundary of the ACC at most longitudes in the majority of CMIP5 models (Meijers et al., 2012). As in CMIP3 climate projections, an overall shallowing of the deep mixed layers that develop on the northern edge of the ACC in winter is observed, with larger shallowing simulated by models with deeper mixed layers during 1976–2005 (Sallée et al., 2013a). Sallée et al. (2013b) reported a warming of all mode, intermediate and deep water masses in the Southern Ocean. The largest temperature increase is found in mode and intermediate water layers. Consistently with CMIP3 projections (Downes et al., 2010), these water layers experience a freshening, whereas bottom water becomes slightly saltier. Finally, Sallée et al. (2013b) noted an enhanced upwelling of circumpolar deep water and an increased subduction of intermediate water that are nearly balanced by interior processes (diapycnal fluxes).

A number of studies suggest that oceanic mesoscale eddies might influence the response of the Southern Ocean circulation, meridional heat transport and deep water formation to changes in wind stress and surface buoyancy flux (Böning et al., 2008; Farneti et al., 2010; Downes et al., 2011; Farneti and Gent, 2011; Saenko et al., 2012; Spence et al., 2012). These eddies are not explicitly resolved in climate models and their role in future circulation changes still needs to be precisely quantified. Some of the CMIP5 models have output the meridional overturning due to the Eulerian mean circulation and that induced by parameterized eddies, thus providing a quantitative estimate of the role of the mesoscale circulation in a warming climate. On this basis, Downes and Hogg (2013) found that, under RCP8.5, the strengthening (weakening) of the upper (lower) Eulerian mean meridional overturning cell in the Southern Ocean is significantly correlated with the increased overlying wind stress and surface warming and is partly compensated at best by changes in eddy-induced overturning.

None of the CMIP3 and CMIP5 models include an interactive ice sheet component. When climate–ice sheet interactions are accounted for in an EMIC under a  $4 \times \text{CO}_2$  scenario, the meltwater flux from the Antarctic ice sheet further reduces the surface density close to Antarctica and the rate of Antarctic Bottom Water formation. This ultimately results in a smaller surface warming at high southern latitudes compared to a simulation in which the freshwater flux from the melting ice sheet is not taken into account (Swingedouw et al., 2008). Nevertheless, in this study, this effect becomes significant only after more than one century.

## 12.4.8 Changes Associated with Carbon Cycle Feedbacks and Vegetation Cover

Climate change may affect the global biogeochemical cycles changing the magnitude of the natural sources and sinks of major GHGs. Numerous studies investigated the interactions between climate change and the carbon cycle (e.g., Friedlingstein et al., 2006), methane cycle (e.g., O'Connor et al., 2010), ozone (Cionni et al., 2011) or aerosols (e.g., Carslaw et al., 2010). Many CMIP5 ESMs now include a representation of the carbon cycle as well as atmospheric chemistry, allowing interactive projections of GHGs (mainly CO<sub>2</sub> and O<sub>3</sub>) and aerosols. With such models, projections account for the imposed changes in anthropogenic emissions, but also for changes in natural sources and sinks as they respond to changes in climate and atmospheric composition. If included in ESMs, the impact on projected concentration, RF and hence on climate can be quantified. Climate-induced changes on the carbon cycle are assessed below, while changes in natural emissions of CH<sub>4</sub> are assessed in Chapter 6, changes in atmospheric chemistry in Chapter 11, and climate–aerosol interactions are assessed in Chapter 7.

### 12.4.8.1 Carbon Dioxide

As presented in Section 12.3, the CMIP5 experimental design includes, for the RCP8.5 scenario, experiments driven either by prescribed anthropogenic CO<sub>2</sub> emissions or concentration. The historical and 21st century emission-driven simulations allow evaluating the climate response of the Earth system when atmospheric CO<sub>2</sub> and the climate response are interactively being calculated by the ESMs. In such ESMs, the atmospheric CO<sub>2</sub> is calculated as the difference between the imposed anthropogenic emissions and the sum of land and ocean carbon uptakes. As most of these ESMs account for land use changes and their CO<sub>2</sub> emissions, the only external forcing is fossil fuel CO<sub>2</sub> emissions (along with all non-CO<sub>2</sub> forcings as in the C-driven RCP8.5 simulations). For a given ESM, the emission driven and concentration driven simulations would show different climate projections if the simulated atmospheric CO<sub>2</sub> in the emission driven run is significantly different from the one prescribed for the concentration driven runs. This would happen if the ESMs carbon cycle is different from the one simulated by MAGICC6, the model used to calculate the CMIP5 GHGs concentrations from the emissions for the four RCPs (Meinshausen et al., 2011c). When driven by CO<sub>2</sub> concentration, the ESMs can calculate the fossil fuel CO<sub>2</sub> emissions that would be compatible with the prescribed atmospheric CO<sub>2</sub> trajectory, allowing comparison with the set of CO<sub>2</sub> emissions initially estimated by the IAMs (Arora et al., 2011; Jones et al., 2013) (see Section 6.4.3, Box 6.4).

Figure 12.36 shows the simulated atmospheric CO<sub>2</sub> and global average surface air temperature warming (relative to the 1986–2005 reference period) for the RCP8.5 emission driven simulations from the CMIP5 ESMs, compared to the concentration driven simulations from the same models. Most (seven out of eleven) of the models estimate a larger CO<sub>2</sub> concentration than the prescribed one. By 2100, the multi-model average CO<sub>2</sub> concentration is 985 ± 97 ppm (full range 794 to 1142 ppm), while the CO<sub>2</sub> concentration prescribed for the RCP8.5 is 936 ppm. Figure 12.36 also shows the range of atmospheric CO<sub>2</sub> projections when the MAGICC6 model, used to provide the RCP concentrations, is tuned to emulate combinations of climate sensitivity

uncertainty taken from 19 CMIP3 models and carbon cycle feedbacks uncertainty taken from 10 C<sup>4</sup>MIP models, generating 190 model simulations (Meinshausen et al., 2011c; Meinshausen et al., 2011b). The emulation of the CMIP3/C<sup>4</sup>MIP models shows for the RCP8.5, a range of simulated CO<sub>2</sub> concentrations of 794 to 1149 ppm (90% confidence level), extremely similar to what is obtained with the CMIP5 ESMs, with atmospheric concentration as high as 1150 ppm by 2100, that is, more than 200 ppm above the prescribed CO<sub>2</sub> concentration.

Global warming simulated by the E-driven runs show higher upper ends than when atmospheric CO<sub>2</sub> concentration is prescribed. For the models assessed here, the global surface temperature change (2081–2100 average relative to 1986–2005 average) ranges between 2.6°C and 4.7°C, with a multi-model average of 3.7°C ± 0.7°C for the concentration driven simulations, while the emission driven simulations give a range of 2.5°C to 5.6°C, with a multi-model average of 3.9°C ± 0.9°C, that is, 5% larger than for the concentration driven runs. The models that simulate the largest CO<sub>2</sub> concentration by 2100 have the largest warming amplification in the emission driven simulations, with an additional warming of more than 0.5°C.

The uncertainty on the carbon cycle has been shown to be of comparable magnitude to the uncertainty arising from physical climate processes (Gregory et al., 2009). Huntingford et al. (2009) used a simple model to characterize the relative role of carbon cycle and climate sensitivity uncertainties in contributing to the range of future temperature changes, concluding that the range of carbon cycle processes represent about 40% of the physical feedbacks. Perturbed parameter ensembles systematically explore land carbon cycle parameter uncertainty and illustrate that a wide range of carbon cycle responses are consistent with the same underlying model structures and plausible parameter ranges (Booth et al., 2012; Lambert et al., 2012). Figure 12.37 shows how the comparable range of future climate change (SRES A1B) arises from parametric uncertainty in land carbon cycle and atmospheric feedbacks. The same ensemble shows that the range of atmospheric CO<sub>2</sub> in the land carbon cycle ensemble is wider than the full SRES concentration range (B1 to A1FI scenario).

The CMIP5 ESMs described above do not include the positive feedback arising from the carbon release from high latitudes permafrost thawing under a warming scenario, which could further increase the atmospheric CO<sub>2</sub> concentration and the warming. Two recent studies investigated the climate–permafrost feedback from simulations with models of intermediate complexity (EMICs) that accounts for a permafrost carbon module (MacDougall et al., 2012; Schneider von Deimling et al., 2012). Burke et al. (2012) also estimated carbon loss from permafrost, from a diagnostic of the present-day permafrost carbon store and future soil warming as simulated by CMIP5 models. However, this last study did not quantify the effect on global temperature. Each of these studies found that the range of additional warming due to the permafrost carbon loss is quite large, because of uncertainties in future high latitude soil warming, amount of carbon stored in permafrost soils, vulnerability of freshly thawed organic material, the proportion of soil carbon that might be emitted as carbon dioxide via aerobic decomposition or as methane via anaerobic decomposition (Schneider von Deimling et al., 2012). For the RCP8.5, the additional warming from permafrost ranges between 0.04°C and 0.69°C by 2100 although

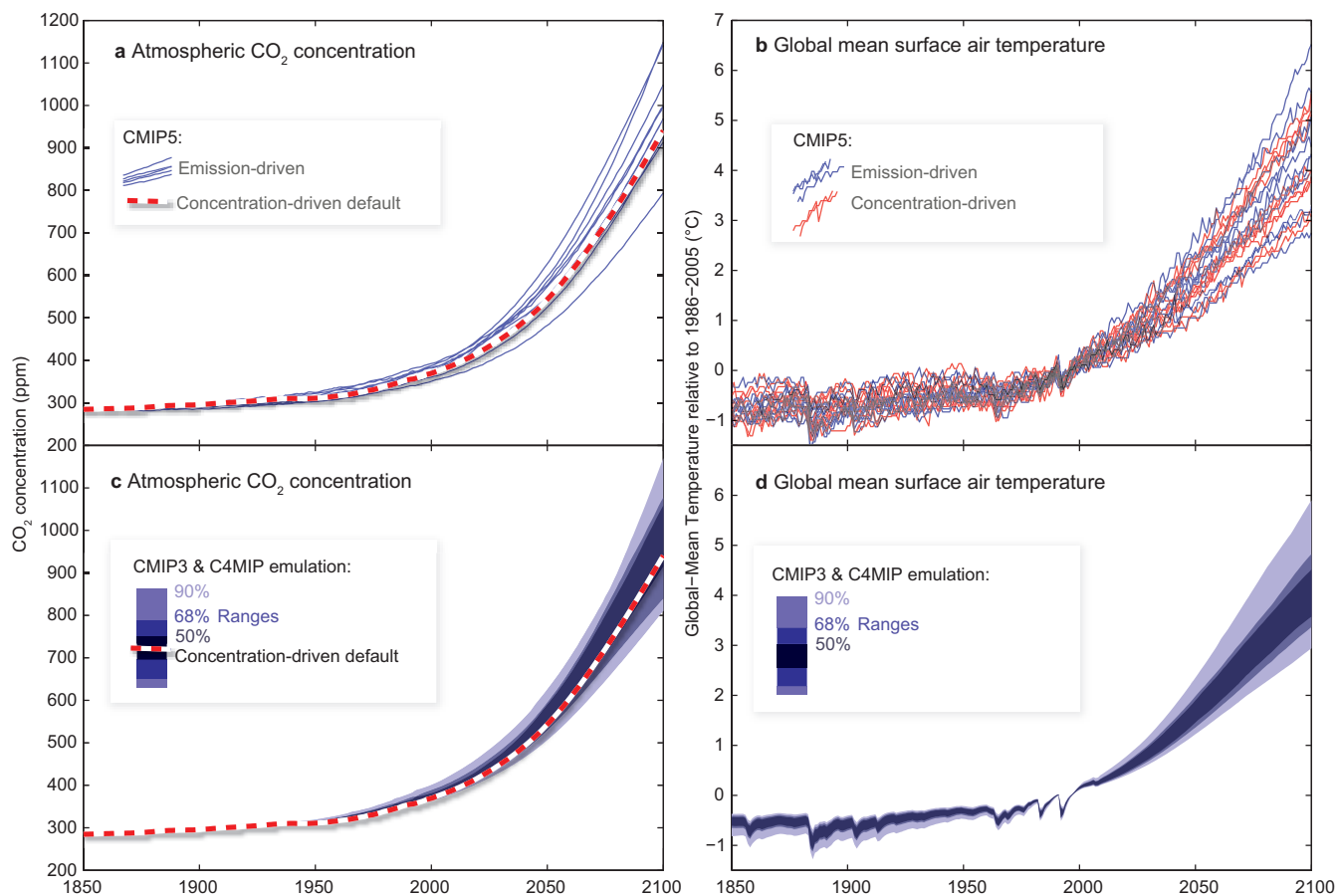


**Figure 12.36** | Simulated changes in (a) atmospheric CO<sub>2</sub> concentration and (b) global averaged surface temperature (°C) as calculated by the CMIP5 Earth System Models (ESMs) for the RCP8.5 scenario when CO<sub>2</sub> emissions are prescribed to the ESMs as external forcing (blue). Also shown (b, in red) is the simulated warming from the same ESMs when directly forced by atmospheric CO<sub>2</sub> concentration (a, red white line). Panels (c) and (d) show the range of CO<sub>2</sub> concentrations and global average surface temperature change simulated by the Model for the Assessment of Greenhouse Gas-Induced Climate Change 6 (MAGICC6) simple climate model when emulating the CMIP3 models climate sensitivity range and the Coupled Climate Carbon Cycle Model Intercomparison Project (C<sup>4</sup>MIP) models carbon cycle feedbacks. The default line in (c) is identical to the one in (a).

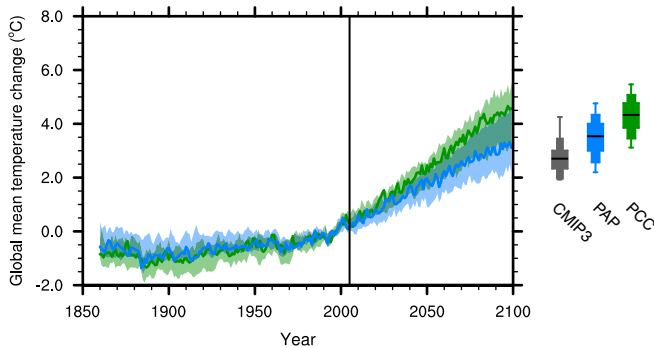


**Figure 12.37** | Uncertainty in global mean temperature from Met Office Hadley Centre climate prediction model 3 (HadCM3) results exploring atmospheric physics and terrestrial carbon cycle parameter perturbations under the SRES A1B scenario (Murphy et al., 2004; Booth et al., 2012). Relative uncertainties in the Perturbed Carbon Cycle (PCC, green plume) and Perturbed Atmospheric Processes (PAP, blue plume) on global mean anomalies of temperature (relative to the 1986–2005 period). The standard simulations from the two ensembles, HadCM3 (blue solid) and HadCM3C (green solid) are also shown. Three bars are shown on the right illustrating the 2100 temperature anomalies associated with the CMIP3/AR4 ensemble (black) the PAP ensemble (blue) and PCC ensemble (green). The ranges indicate the full range, 10th to 90th, 25th to 75th and 50th percentiles.

there is *medium confidence* in these numbers as are the ones on the amount of carbon released (see Section 12.5.5.4) (MacDougall et al., 2012; Schneider von Deimling et al., 2012).

#### 12.4.8.2 Changes in Vegetation Cover

Vegetation cover can also be affected by climate change, with forest cover potentially being decreasing (e.g., in the tropics) or increasing (e.g., in high latitudes). In particular, the Amazon forest has been the subject of several studies, generally agreeing that future climate change would increase the risk tropical Amazon forest being replaced by seasonal forest or even savannah (Huntingford et al., 2008; Jones et al., 2009; Malhi et al., 2009). Increase in atmospheric CO<sub>2</sub> would partly reduce such risk, through increase in water efficiency under elevated CO<sub>2</sub> (Lapola et al., 2009; Malhi et al., 2009). Recent multi-model estimates based on different CMIP3 climate scenarios and different dynamic global vegetation models predict a moderate risk of tropical forest reduction in South America and even lower risk for African and Asian tropical forests (see also Section 12.5.5.6) (Gumpenberger et al., 2010; Huntingford et al., 2013).

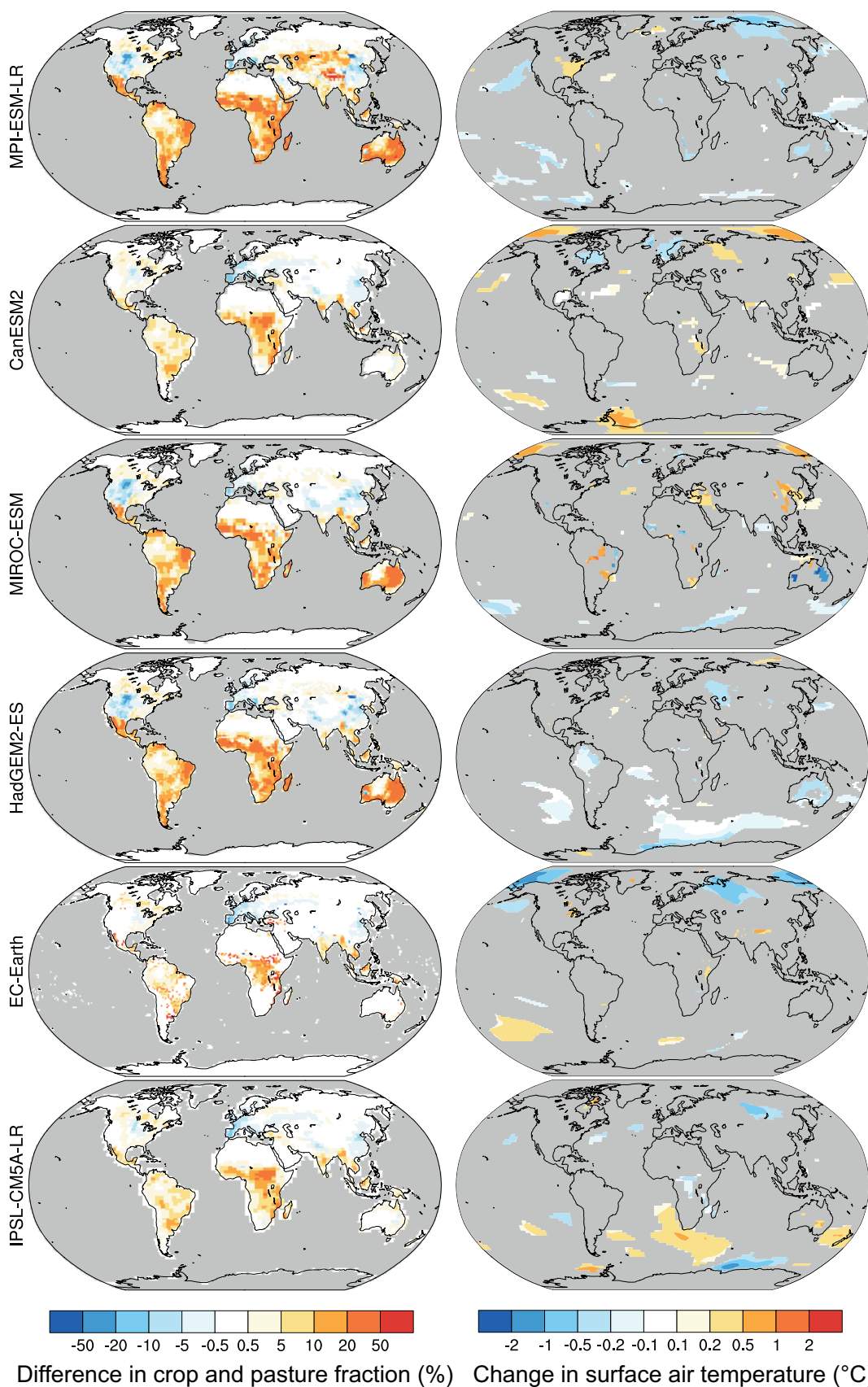


**Figure 12.38 |** Impact of land use change on surface temperature. LUCID-CMIP5 experiments where six ESMs were forced either with or without land use change beyond 2005 under the RCP8.5 scenario. Left maps show changes in total crop and pasture fraction (%) in the RCP8.5 simulations between 2006 and 2100 as implemented in each ESM. Right maps show the differences in surface air temperature (averaged over the 2071–2100 period) between the simulations with and without land use change beyond 2005. Only statistically significant changes ( $p < 0.05$ ) are shown.

ESMs simulations with interactive vegetation confirmed known biophysical feedback associated with large-scale changes in vegetation. In the northern high latitudes, warming-induced vegetation expansion reduces surface albedo, enhancing the warming over these regions (Falloon et al., 2012; Port et al., 2012), with potentially larger amplification due to ocean and sea ice response (Swann et al., 2010). Over tropical forest, reduction of forest coverage would reduce evapotranspiration, also leading to a regional warming (Falloon et al., 2012; Port et al., 2012).

CMIP5 ESMs also include human induced land cover changes (deforestation, reforestation) affecting the climate system through changes in land surface physical properties (Hurt et al., 2011). Future changes in land cover will have an impact on the climate system through biophysical and biogeochemical processes (e.g., Pongratz et al., 2010). Biophysical processes include changes in surface albedo and changes in partitioning between latent and sensible heat, while biogeochemical feedbacks essentially include change in CO<sub>2</sub> sources and sinks but could potentially also include changes in N<sub>2</sub>O or CH<sub>4</sub> emissions. The biophysical response to future land cover changes has been investigated within the SRES scenarios. Using the SRES A2 2100 land cover, Davin et al. (2007) simulated a global cooling of 0.14 K relatively to a simulation with present-day land cover, the cooling being largely driven by change in albedo. Regional analyses have been performed in order to quantify the biophysical impact of biofuels plantation generally finding a local to regional cooling when annual crops are replaced by bioenergy crops, such as sugar cane (Georgescu et al., 2011; Loarie et al., 2011). However, some energy crops require nitrogen inputs for their production, leading inevitably to nitrous oxide (N<sub>2</sub>O) emissions, potentially reducing the direct cooling effect and the benefit of biofuels as an alternative to fossil fuel emissions. Such emission estimates are still uncertain, varying strongly for different crops, management methods, soil types and reference systems (St. Clair et al., 2008; Smeets et al., 2009).

In the context of the Land-Use and Climate, IDentification of robust impacts (LUCID) project (Pitman et al., 2009) ESMs performed additional CMIP5 simulations in order to separate the biophysical from the biogeochemical effects of land use changes in the RCP scenarios. The LUCID-CMIP5 experiments were designed to complement RCP8.5 and RCP2.6 simulations of CMIP5, both of which showing an intensification of land use change over the 21st century. The LUCID-CMIP5 analysis was focussed on a difference in climate and land-atmosphere fluxes between the average of ensemble of simulations with and without land use changes by the end of 21st century (Brovkin et al., 2013). Due to different interpretation of land use classes, areas of crops and pastures were specific for each ESM (Figure 12.38, left). On the global scale, simulated biophysical effects of land use changes projected in the CMIP5 experiments with prescribed CO<sub>2</sub> concentrations were not significant. However, these effects were significant for regions with land use changes >10%. Only three out of six participating models, CanESM2, HadGEM2-ES and MIROC-ESM, reveal statistically significant changes in regional mean annual mean surface air temperature for the RCP8.5 scenario (Figure 12.38, right). However, there is *low confidence* on the overall effect as there is no agreement among the models on the sign of the global average temperature change due to the biophysical effects of land use changes (Brovkin et al., 2013). Changes in land surface albedo, available energy, latent and sensible

heat fluxes were relatively small but significant in most of ESMs for regions with substantial land use changes. The scale of climatic effects reflects a small magnitude of land use changes in both the RCP2.6 and 8.5 scenarios and their limitation mainly to the tropical and subtropical regions where differences between biophysical effects of forests and grasslands are less pronounced than in mid- and high latitudes. LUCID-CMIP5 did not perform similar simulations for the RCP4.5 or RCP6.0 scenarios. As these two scenarios show a global decrease of land use area, one might expect their climatic impact to be different from the one seen in the RC2.6 and RCP8.5.

## 12.4.9 Consistency and Main Differences Between Coupled Model Intercomparison Project Phase 3/ Coupled Model Intercomparison Project Phase 5 and Special Report on Emission Scenarios/ Representative Concentration Pathways

In the experiments collected under CMIP5, both models and scenario have changed with respect to CMIP3 making a comparison with earlier results and the scientific literature they generated (on which some of this chapter's content is still based) complex. The set of models used in AR4 (the CMIP3 models) have been superseded by the new CMIP5 models (Table 12.1; Chapter 9) and the SRES scenarios have been replaced by four RCPs (Section 12.3.1). In addition, the baseline period used to compute anomalies has advanced 6 years, from 1980–1999 to 1986–2005.

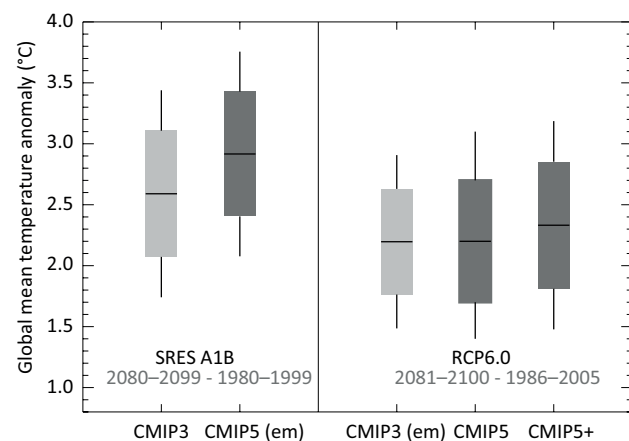


**Figure 12.39 |** Global mean temperature anomalies at the end of the 21st century from General Circulation Model (GCM) experiments and emulators comparing CMIP3/ CMIP5 responses under SRES A1B and RCP6.0. The boxes and whiskers indicate the 5th percentile, mean value – 1 standard deviation, mean, mean value + 1 standard deviation and 95th percentile of the distributions. The first box-and-whiskers on the left is computed directly from the CMIP3 ensemble and corresponds to the numbers quoted in AR4. The emulated SRES A1B projections (second from left) of CMIP5 are obtained by the method of Good et al. (2011a) and are calculated for the period 2080–2099 expressed with respect to the AR4 baseline period of 1980–1999. Because of the method, the subset of CMIP5 that are emulated are restricted to those with pre-industrial control, abrupt 4 × CO<sub>2</sub>, historical, RCP4.5 and RCP8.5 simulations. The emulated RCP6.0 projections of CMIP3 (third from left, see also Figure 12.8) are from Knutti and Sedláček (2013) obtained using the method of Meinshausen et al. (2011b; 2011c) and are calculated for the slightly different future period 2081–2100 to be consistent with the rest of this chapter, and are expressed with respect to the AR5 baseline period of 1986–2005. The box-and-whiskers fourth from the left are a graphical representation of the numbers shown in Table 12.2. The final box-and-whiskers on the right is a combination of CMIP5 model output and emulation of CMIP5 RCP6.0 numbers for those models that did not run RCP6.0.

It would be extremely costly computationally to rerun the full CMIP3 ensemble under the new RCPs and/or the full CMIP5 ensemble under the old SRES scenarios in order to separate model and scenario effects. In the absence of a direct comparison, we rely on simplified modelling frameworks to emulate CMIP3/5 SRES/RCP model behaviour and compare them. Figure 12.39 shows an emulation of the global mean temperature response at the end of the 21st century that one would expect from the CMIP5 models if they were run under SRES A1B. In this case, anomalies are computed with respect to 1980–1999 for direct comparison with the values reported in AR4 (Meehl et al., 2007b) which used that baseline. The method used to emulate the SRES A1B response of the CMIP5 is documented by Good et al. (2011a; 2013). Ensemble-mean A1B RF was computed from CMIP3 projections using the Forster and Taylor (2006) method, scaled to ensure consistency with the forcing required by the method. The simple model is only used to predict the temperature difference between A1B and RCP8.5, and between A1B and RCP4.5 separately for each model. These differences are then added to CMIP5 GCM simulations of RCP8.5 and RCP4.5 respectively, and averaged to give a single A1B estimate. The emulated CMIP5 SRES A1B results show a slightly larger mean response than the actual CMIP3 models, with a similar spread ( $\pm 1$  standard deviation is used in this case). The main reason for this is the slightly larger mean transient climate response (TCR) in the subset of CMIP5 models available in comparison with the AR4 CMIP3 models. An alternative emulation is presented by Knutti and Sedláček (2013) who use the simplified

MAGICC models with parameters chosen to emulate the response of the CMIP3 models to RCP6.0 forcing, with anomalies expressed with respect to the 1986–2005 baseline period (Figure 12.39). They too find a larger mean response in the CMIP5 case but also a larger spread ( $\pm 1$  standard deviation) in CMIP5. Uncertainties in the different approaches to emulating climate model simulations, for example estimating the non-GHG RF, and the small sample sizes of CMIP3 and CMIP5 make it difficult to draw conclusions on the statistical significance of the differences displayed in Figure 12.39, but the same uncertainties lead us to conclude that on the basis of these analyses there appears to be no fundamental difference between the behaviour of the CMIP5 ensemble, in comparison with CMIP3.

Meinshausen et al. (2011a; 2011b) tuned MAGICC6 to emulate 19 GCMs from CMIP3. The results are temperature projections and their uncertainties (based on the empirical distribution of the ensemble) under each of the RCPs, extended to year 2500 (under constant emissions for the lowest RCP and constant concentrations for the remaining three). In the same paper, an ensemble produced by combining carbon cycle parameter calibration to nine CMIP models with the 19 CMIP3 model parameter calibrations is also used to estimate the emissions implied by the various concentration pathways, had the CMIP3 models included a carbon cycle component. Rogelj et al. (2012) used the same tool but performed a fully probabilistic analysis of the SRES and RCP scenarios using a parameter space that is consistent with

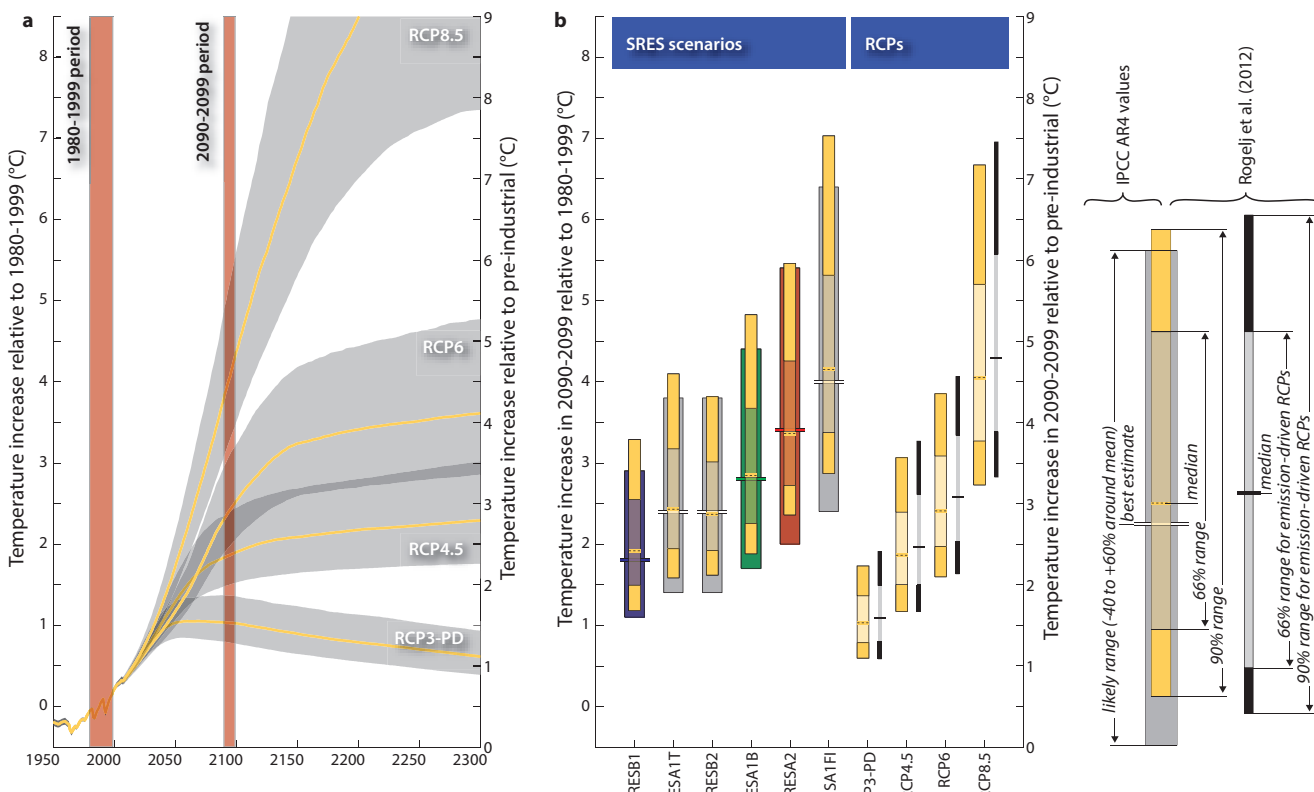


**Figure 12.40 |** Temperature projections for SRES scenarios and the RCPs. (a) Time-evolving temperature distributions (66% range) for the four RCP scenarios computed with the ECS distribution from Rogelj et al. (2012) and a model setup representing closely the carbon-cycle and climate system uncertainty estimates of the AR4 (grey areas). Median paths are drawn in yellow. Red shaded areas indicate time periods referred to in panel b. (b) Ranges of estimated average temperature increase between 2090 and 2099 for SRES scenarios and the RCPs respectively. Note that results are given both relative to 1980–1999 (left scale) and relative to pre-industrial (right scale). Yellow ranges indicate results obtained by Rogelj et al. (2012). Colour-coding of AR4 ranges is chosen to be consistent with AR4 (Meehl et al., 2007b). RCP2.6 is labelled as RCP3-PD here.

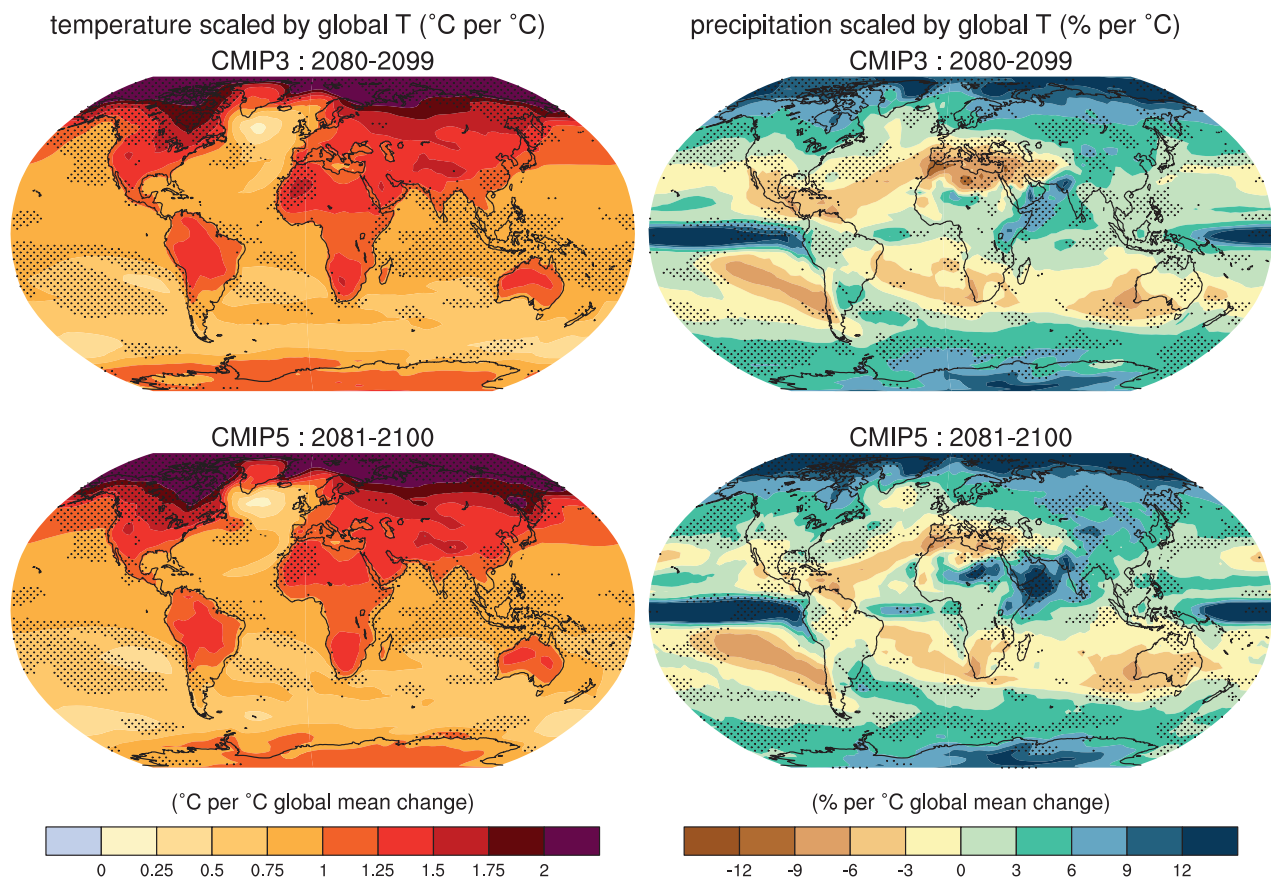


**Figure 12.41** | Patterns of temperature (left column) and percent precipitation change (right column) for the CMIP3 models average (first row) and CMIP5 models average (second row), scaled by the corresponding global average temperature changes. The patterns are computed in both cases by taking the difference between the averages over the last 20 years of the 21st century experiments (2080–2099 for CMIP3 and 2081–2100 for CMIP5) and the last twenty years of the historic experiments (1980–1999 for CMIP3, 1986–2005 for CMIP5) and rescaling each difference by the corresponding change in global average temperature. This is done first for each individual model, and then the results are averaged across models. For the CMIP5 patterns, the RCP2.6 simulation of the FIO-ESM model was excluded because it did not show any warming by the end of the 21st century, thus not complying with the method requirement that the pattern be estimated at a time when the temperature change signal from  $\text{CO}_2$  increase has emerged. Stippling indicates a measure of significance of the difference between the two corresponding patterns obtained by a bootstrap exercise. Two subsets of the pooled set of CMIP3 and CMIP5 ensemble members of the same size as the original ensembles, but without distinguishing CMIP3 from CMIP5 members, were randomly sampled 500 times. For each random sample we compute the corresponding patterns and their difference, then the true difference is compared, grid-point by grid-point, to the distribution of the bootstrapped differences, and only grid-points at which the value of the difference falls in the tails of the bootstrapped distribution (less than the 2.5 percentiles or the 97.5 percentiles) are stippled.

CMIP3/C4MIP but a more general uncertainty characterization for key quantities like equilibrium climate sensitivity, similarly to the approach utilized by Meinshausen et al. (2009). Observational or other historical constraints are also used in this study and the analysis is consistent with the overall assessment of sources and ranges of uncertainties for relevant quantities (equilibrium climate sensitivity above all) from AR4 (Meehl et al., 2007b, Box 10.2). Figure 12.40 summarizes results of this probabilistic comparison for global temperature. The RCPs span a large range of stabilization, mitigation and non-mitigation pathways and the resulting range of temperature changes are larger than those produced under SRES scenarios, which do not consider mitigation options. The SRES results span an interval between just above  $1.0^{\circ}\text{C}$  and  $6.5^{\circ}\text{C}$  when considering the respective *likely* ranges of all scenarios, including B1 as the lowest and A1FI as the highest. Emissions under RCP8.5 are highest and the resulting temperature changes *likely* range from  $4.0^{\circ}\text{C}$  to  $6.1^{\circ}\text{C}$  by 2100. The lowest RCP2.6 assumes significant mitigation and the global temperature change *likely* remains below  $2^{\circ}\text{C}$ .

Similar temperature change projections by the end of the 21st century are obtained under RCP8.5 and SRES A1FI, RCP6 and SRES B2 and RCP4.5 and SRES B1. There remain large differences though in the transient trajectories, with rates of change slower or faster for the different pairs. These differences can be traced back to the interplay of the (negative) short-term effect of sulphate aerosols and the (positive) effect of long-lived GHGs. Impact studies may be sensitive to the differences in these temporal profiles so care should be taken in approximating SRES with RCPs and vice versa.

While simple models can separate the effect of the scenarios and the model response, no studies are currently available that allow an attribution of the CMIP3-CMIP5 differences to changes in the transient climate response, the carbon cycle, and the inclusion of new processes (chemistry, land surface, vegetation). The fact that these sets of CMIP3 and CMIP5 experiments do not include emission-driven runs would suggest that differences in the representation of the carbon cycle are very unlikely to explain differences in the simulations, since the only

effect of changes in the carbon cycle representation would affect the land surface, and thus would have only a minor effect on the climate response at the global scale.

Figure 12.41 shows a comparison of the patterns of warming and precipitation change from CMIP3 (using 23 models and three SRES scenarios) and CMIP5 (using 46 models and four RCPs), utilizing the pattern scaling methodology (Section 12.4.2). The geographic patterns of mean change are very similar across the two ensembles of models, with pattern correlations of 0.98 for temperature and 0.90 for precipitation changes. However there exist significant differences in the absolute values of the patterns, if not in their geographic shapes. A simple bootstrapping exercise that pooled together all models and scenarios and resampled 500 times the same numbers of models/scenarios divided into two groups, but without distinguishing CMIP3 from CMIP5 (and thus SRES from RCPs) allows to compute a measure of significance of the actual differences in the patterns. Stippling in Figure 12.41 marks the large regions where the difference is significant for temperature and precipitation patterns. The temperature pattern from CMIP5 shows significantly larger warming per degree Celsius of global mean temperature change in the NH and less warming per degree Celsius in the SH compared to the corresponding pattern from CMIP3. For precipitation patterns, CMIP5 shows significantly larger increases per degree Celsius in the NH and significantly larger decreases per degree Celsius in the SH compared to CMIP3. Even in this case we do not have studies that allow tracing the source of these differences to specific changes in models' configurations, processes represented or scenarios run.

Knutti and Sedláček (2013) attempt to identify or rule out at least some of these sources. Differences in model projections spread or its counterpart, robustness, between CMIP3 and CMIP5 are discussed, and it is shown that by comparing the behaviour of only a subset of 11 models, contributed to the two CMIPs by the same group of institutions, the robustness of CMIP5 versus that of CMIP3 actually decreases slightly. This would suggest that the enhanced robustness of CMIP5 is not clearly attributable to advances in modelling, and may be a result of the fact that the CMIP5 ensemble contains different versions of the same model that are counted as independent in this measure of robustness.

12

A comparison of CMIP3 and CMIP5 results for extreme indices is provided in Sections 12.4.3.3 and Figure 12.13 for temperature extremes, and Section 12.4.5.5 and Figure 12.26 for extremes in the water cycle.

## 12.5 Climate Change Beyond 2100, Commitment, Stabilization and Irreversibility

This section discusses the long term (century to millennia) climate change based on the RCP scenario extensions and idealized scenarios, the commitment from current atmospheric composition and from past emissions, the concept of cumulative carbon and the resulting constraints on emissions for various temperature targets. The term irreversibility is used in various ways in the literature. This report defines a perturbed state as irreversible on a given time scale if the recovery time scale from this state due to natural processes is significantly

longer than the time it takes for the system to reach this perturbed state (see Glossary), for example, the climate change resulting from the long residence time of a CO<sub>2</sub> perturbation in the atmosphere. These results are discussed in Sections 12.5.2 to 12.5.4. Aspects of irreversibility in the context of abrupt change, multiple steady states and hysteresis are discussed in Section 12.5.5 and in Chapter 13 for ice sheets and sea level rise.

### 12.5.1 Representative Concentration Pathway Extensions

The CMIP5 intercomparison project includes simulations extending the four RCP scenarios to the year 2300 (see Section 12.3.1). This allows exploring the longer-term climate response to idealized GHG and aerosols forcings (Meinshausen et al., 2011c). Continuing GHG emissions beyond 2100 as in the RCP8.5 extension induces a total RF above 12 W m<sup>-2</sup> by 2300, while sustaining negative emissions beyond 2100, as in the RCP2.6 extension, induces a total RF below 2 W m<sup>-2</sup> by 2300. The projected warming for 2281–2300, relative to 1986–2005, is 0.6°C (range 0.0°C to 1.2°C) for RCP2.6, 2.5°C (range 1.5°C to 3.5°C) for RCP4.5, and 7.8°C (range 3.0°C to 12.6°C) for RCP8.5 (*medium confidence*, based on a limited number of CMIP5 simulations) (Figures 12.3 and 12.5, Table 12.2).

EMICs simulations have been performed following the same CMIP5 protocol for the historical simulation and RCP scenarios extended to 2300 (Zickfeld et al., 2013). These scenarios have been prolonged beyond 2300 to investigate longer-term commitment and irreversibility (see below). Up to 2300, projected warming and the reduction of the AMOC as simulated by the EMICs are similar to those simulated by the CMIP5 ESMs (Figures 12.5 and 12.42).

### 12.5.2 Climate Change Commitment

Climate change commitment, the fact that the climate will change further after the forcing or emissions have been eliminated or held constant, has attracted increased attention by scientists and policymakers shortly before the completion of IPCC AR4 (Hansen et al., 2005a; Meehl et al., 2005b, 2006; Wigley, 2005) (see also AR4 Section 10.7.1). However, the argument that the surface response would lag the RF due to the large thermal reservoir of the ocean in fact goes back much longer (Bryan et al., 1982; Hansen et al., 1984, 1985; Siegenthaler and Oeschger, 1984; Schlesinger, 1986; Mitchell et al., 2000; Wetherald et al., 2001). The discussion in this section is framed largely in terms of temperature change, but other changes in the climate system (e.g., precipitation) are closely related to changes in temperature (see Sections 12.4.1.1 and 12.4.2). A summary of how past emissions relate to future warming is also given in FAQ 12.3.

The Earth system has multiple response time scales related to different thermal reservoirs (see also Section 12.5.3). For a step change in forcing (instantaneous increase in the magnitude of the forcing and constant forcing after that), a large fraction of the total of the surface temperature response will be realized within years to a few decades (Brasseur and Roeckner, 2005; Knutti et al., 2008a; Murphy et al., 2009; Hansen et al., 2011). The remaining response, realized over centuries, is controlled by the slow mixing of the energy perturbation into the ocean (Stouffer, 2004). The response time scale depends on the amount of ocean mixing

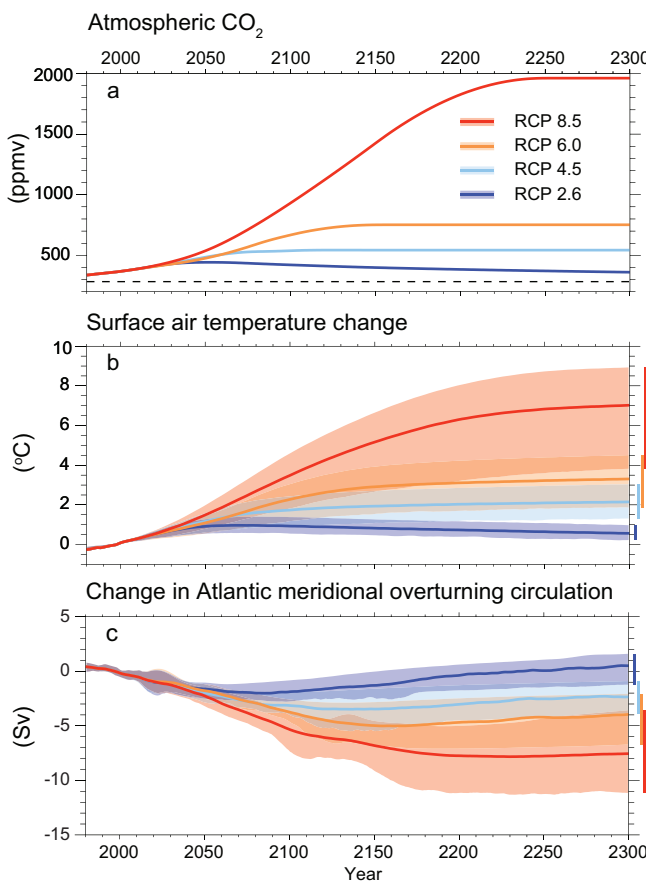


**Figure 12.42** | (a) Atmospheric CO<sub>2</sub>, (b) projected global mean surface temperature change and (c) projected change in the Atlantic meridional overturning circulation, as simulated by EMICs for the four RCPs up to 2300 (Zickfeld et al., 2013). A 10-year smoothing was applied. Shadings and bars denote the minimum to maximum range. The dashed line on (a) indicates the pre-industrial CO<sub>2</sub> concentration.

and the strength of climate feedbacks, and is longer for higher climate sensitivity (Hansen et al., 1985; Knutti et al., 2005). The transient climate response is therefore smaller than the equilibrium response, in particular for high climate sensitivities. This can also be interpreted as the ocean heat uptake being a negative feedback (Dufresne and Bony, 2008; Gregory and Forster, 2008). Delayed responses can also occur due to processes other than ocean warming, for example, vegetation change (Jones et al., 2009) or ice sheet melt that continues long after the forcing has been stabilized (see Section 12.5.3).

Several forms of commitment are often discussed in the literature. The most common is the ‘constant composition commitment’, the warming that would occur after stabilizing all radiative constituents at a given year (for example year 2000) levels. For year 2000 commitment, AOGCMs estimated a most likely value of about 0.6°C for 2100 (relative to 1980–1999, AR4 Section 10.7.1). A present-day composition commitment simulation is not part of CMIP5, so direct comparison with CMIP3 is not possible. However, the available CMIP5 results based on the RCP4.5 extension with constant RF (see Section 12.5.1) are consistent with those numbers, with an additional warming of about 0.5°C 200 years after stabilization of the forcing (Figures 12.5 and 12.42).

A measure of constant composition commitment is the fraction of realized warming which can be estimated as the ratio of the warming at a given time to the long-term equilibrium warming (e.g., Stouffer, 2004; Meehl et al., 2007b, Section 10.7.2; Eby et al., 2009; Solomon et al., 2009). EMIC simulations have been performed with RCPs forcing up to 2300 prolonged until the end of the millennium with a constant forcing set at the value reached by 2300 (Figure 12.43). When the forcing stabilizes, the fraction of realized warming is significantly below unity. However, the fraction of realized warming depends on the history of the forcing. For the RCP4.5 and RCP6.0 extension scenarios with early stabilization, it is about 75% at the time of forcing stabilization; while for RCP8.5, with stabilization occurring later, it is about 85% (see Figure 12.43); but for a 1% yr<sup>-1</sup> CO<sub>2</sub> increase to 2 × CO<sub>2</sub> or 4 × CO<sub>2</sub> and constant forcing thereafter, the fraction of realized warming is much smaller, about 40 to 70% at the time when the forcing is kept constant. The fraction of realized warming rises typically by 10% over the century following the stabilization of forcing. Due to the long time scales in the deep ocean, full equilibrium is reached only after hundreds to thousands of years (Hansen et al., 1985; Gregory et al., 2004; Stouffer, 2004; Meehl et al., 2007b, Section 10.7.2; Knutti et al., 2008a; Danabasoglu and Gent, 2009; Held et al., 2010; Hansen et al., 2011; Li et al., 2013a).

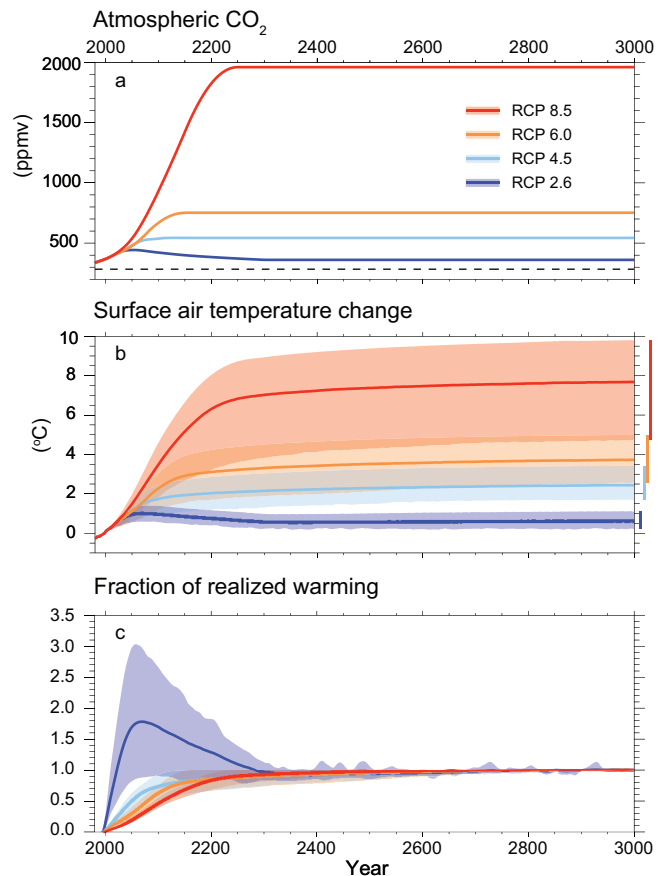


**Figure 12.43** | (a) Atmospheric CO<sub>2</sub>, (b) projected global mean surface temperature change and (c) fraction of realized warming calculated as the ratio of global temperature change at a given time to the change averaged over the 2980–2999 time period, as simulated by Earth System Models of Intermediate Complexity (EMICs) for the 4 RCPs up to 2300 followed by a constant (year 2300 level) radiative forcing up to the year 3000 (Zickfeld et al., 2013). A 10-year smoothing was applied. Shadings and bars denote the minimum to maximum range. The dashed line on (a) indicates the pre-industrial CO<sub>2</sub> concentration.

'Constant emission commitment' is the warming that would result from maintaining annual anthropogenic emissions at the current level. Few studies exist but it is estimated to be about 1°C to 2.5°C by 2100 assuming constant (year 2010) emissions in the future, based on the MAGICC model calibrated to CMIP3 and C4MIP models (Meinshausen et al., 2011a; Meinshausen et al., 2011b) (see FAQ 12.3). Such a scenario is different from non-intervention economic scenarios, and it does not stabilize global temperature, as any plausible emission path after 2100 would cause further warming. It is also different from a constant cumulative emission scenario which implies zero emissions in the future.

Another form of commitment involves climate change when anthropogenic emissions are set to zero ('zero emission commitment'). Results from a variety of models ranging from EMICs (Meehl et al., 2007b; Weaver et al., 2007; Matthews and Caldeira, 2008; Plattner et al., 2008; Eby et al., 2009; Solomon et al., 2009; Friedlingstein et al., 2011) to ESMs (Frölicher and Joos, 2010; Gillett et al., 2011; Gillett et al., 2013) show that abruptly setting CO<sub>2</sub> emissions to zero (keeping other forcings constant if accounted for) results in approximately constant global temperature for several centuries onward. Those results indicate that past emissions commit us to persistent warming for hundreds of years, continuing at about the level of warming that has been realized. On near equilibrium time scales of a few centuries to about a millennium, the temperature response to CO<sub>2</sub> emissions is controlled by climate sensitivity (see Box 12.2) and the cumulative airborne fraction of CO<sub>2</sub> over these time scales. After about a thousand years (i.e., near thermal equilibrium) and cumulative CO<sub>2</sub> emissions less than about 2000 PgC, approximately 20 to 30% of the cumulative anthropogenic carbon emissions still remain in the atmosphere (Montenegro et al., 2007; Plattner et al., 2008; Archer et al., 2009; Frölicher and Joos, 2010; Joos et al., 2013) (see Box 6.1) and maintain a substantial temperature response long after emissions have ceased (Friedlingstein and Solomon, 2005; Hare and Meinshausen, 2006; Weaver et al., 2007; Matthews and Caldeira, 2008; Plattner et al., 2008; Eby et al., 2009; Lowe et al., 2009; Solomon et al., 2009, 2010; Frölicher and Joos, 2010; Zickfeld et al., 2012). In the transient phase, on a 100- to 1000-year time scale, the approximately constant temperature results from a compensation between delayed commitment warming (Meehl et al., 2005b; Wigley, 2005) and the reduction in atmospheric CO<sub>2</sub> resulting from ocean and land carbon uptake as well as from the nonlinear dependence of RF on atmospheric CO<sub>2</sub> (Meehl et al., 2007b; Plattner et al., 2008; Solomon et al., 2009; Solomon et al., 2010). The commitment associated with past emissions depends, as mentioned above, on the value of climate sensitivity and cumulative CO<sub>2</sub> airborne fraction, but it also depends on the choices made for other RF constituents. In a CO<sub>2</sub> only case and for equilibrium climate sensitivities near 3°C, the warming commitment (i.e., the warming relative to the time when emissions are stopped) is near zero or slightly negative. For high climate sensitivities, and in particular if aerosol emissions are eliminated at the same time, the commitment from past emission can be significantly positive, and is a superposition of a fast response to reduced aerosols emissions and a slow response associated with high climate sensitivities (Brasseur and Roeckner, 2005; Hare and Meinshausen, 2006; Armour and Roe, 2011; Knutti and Plattner, 2012; Matthews and Zickfeld, 2012) (see FAQ 12.3). In the real world, the emissions of CO<sub>2</sub> and non-CO<sub>2</sub> forcing agents are of course coupled. All of the above studies support the conclusion that temperatures would decrease only very slowly (if at all),

even for strong reductions or complete elimination of CO<sub>2</sub> emissions, and might even increase temporarily for an abrupt reduction of the short-lived aerosols (FAQ 12.3). The implications of this fact for climate stabilization are discussed in Section 12.5.4.

New EMIC simulations with pre-industrial CO<sub>2</sub> emissions and zero non-CO<sub>2</sub> forcings after 2300 (Zickfeld et al., 2013) confirm this behaviour (Figure 12.44) seen in many earlier studies (see above). Switching off anthropogenic CO<sub>2</sub> emissions in 2300 leads to a continuous slow decline of atmospheric CO<sub>2</sub>, to a significantly slower decline of global temperature and to a continuous increase in ocean thermal expansion

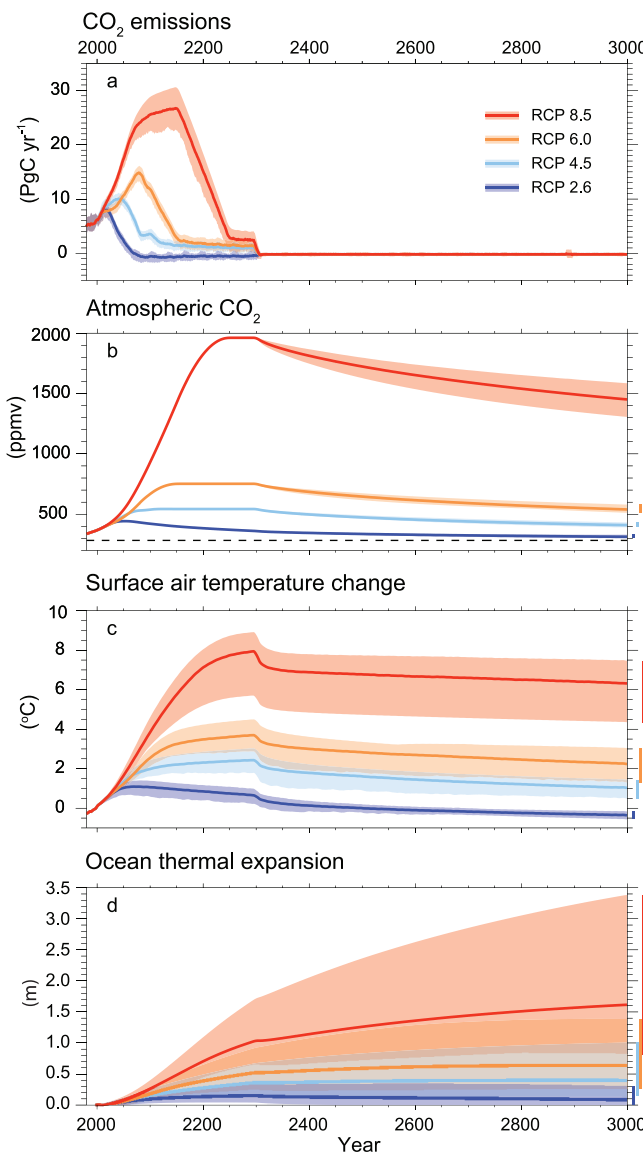


**Figure 12.44 |** (a) Compatible anthropogenic CO<sub>2</sub> emissions up to 2300, followed by zero emissions after 2300, (b) prescribed atmospheric CO<sub>2</sub> concentration up to 2300 followed by projected CO<sub>2</sub> concentration after 2300, (c) global mean surface temperature change and (d) ocean thermal expansion as simulated by Earth System Models of Intermediate Complexity (EMICs) for the four concentration driven RCPs with all forcings included (Zickfeld et al., 2013). A 10-year smoothing was applied. The drop in temperature in 2300 is a result of eliminating all non-CO<sub>2</sub> forcings along with CO<sub>2</sub> emissions. Shadings and bars denote the minimum to maximum range. The dashed line on (b) indicates the pre-industrial CO<sub>2</sub> concentration.

over the course of the millennium. Larger forcings induce longer delays before the Earth system would reach equilibrium. For RCP8.5, by year 3000 (700 years after emissions have ceased) global temperature has decreased only by 1°C to 2°C (relative to its peak value by 2300) and ocean thermal expansion has almost doubled (relative to 2300) and is still increasing (Zickfeld et al., 2013).

The previous paragraph discussed climate change commitment from GHGs that have already been emitted. Another form of commitment refers to climate change associated with heat and carbon that has gone into the land surface and oceans. This would be relevant to the consequences of a one-time removal of all of the excess CO<sub>2</sub> in the atmosphere and is computed by taking a transient simulation and instantaneously setting atmospheric CO<sub>2</sub> concentrations to initial (pre-industrial) values (Cao and Caldeira, 2010). In such an extreme case, there would be a net flux of CO<sub>2</sub> from the ocean and land surface to the atmosphere, releasing an amount of CO<sub>2</sub> representing about 30% of what was removed from the atmosphere, i.e., the airborne fraction applies equally to positive and negative emissions, and it depends on the emissions history. A related form of experiment investigates the consequences of an initial complete removal followed by sustained removal of any CO<sub>2</sub> returned to the atmosphere from the land surface and oceans, and is computed by setting atmospheric CO<sub>2</sub> concentrations to pre-industrial values and maintaining this concentration (Cao and Caldeira, 2010). In this case, only about one-tenth of the pre-existing temperature perturbation persists for more than half of a century. A similar study performed with a GFDL AOGCM where forcing was instantaneously returned to its pre-industrial value, found larger residual warming, up to 30% of the pre-existing warming (Held et al., 2010).

Several studies on commitment to past emissions have demonstrated that the persistence of warming is substantially longer than the lifetime of anthropogenic GHGs themselves, as a result of nonlinear absorption effects as well as the slow heat transfer into and out of the ocean. In much the same way as the warming to a step increase of forcing is delayed, the cooling after setting RF to zero is also delayed. Loss of excess heat from the ocean will lead to a positive surface air temperature anomaly for decades to centuries (Held et al., 2010; Solomon et al., 2010; Bouttes et al., 2013).

A more general form of commitment is the question of how much warming we are committed to as a result of inertia and hence commitments related to the time scales for energy system transitions and other societal, economic and technological aspects (Grubb, 1997; Washington et al., 2009; Davis et al., 2010). For example, Davis et al. (2010) estimated climate commitment of 1.3°C (range 1.1°C to 1.4°C, relative to pre-industrial) from existing CO<sub>2</sub>-emitting devices under specific assumptions regarding their lifetimes. These forms of commitment, however, are strongly based on political, economic and social assumptions that are outside the domain of IPCC WGI and are not further considered here.

### 12.5.3 Forcing and Response, Time Scales of Feedbacks

Equilibrium climate sensitivity (ECS), transient climate response (TCR) and climate feedbacks are useful concepts to characterize the

response of a model to an external forcing perturbation. However, there are limitations to the concept of RF (Joshi et al., 2003; Shine et al., 2003; Hansen et al., 2005b; Stuber et al., 2005), and the separation of forcings and fast (or rapid) responses (e.g., clouds changing almost instantaneously as a result of CO<sub>2</sub>-induced heating rates rather than as a response to the slower surface warming) is sometimes difficult (Andrews and Forster, 2008; Gregory and Webb, 2008). Equilibrium warming also depends on the type of forcing (Stott et al., 2003; Hansen et al., 2005b; Davin et al., 2007). ECS is time or state dependent in some models (Senior and Mitchell, 2000; Gregory et al., 2004; Boer et al., 2005; Williams et al., 2008; Colman and McAvaney, 2009; Colman and Power, 2010), and in some but not all models climate sensitivity from a slab ocean version differs from that of coupled models or the effective climate sensitivity (see Glossary) diagnosed from a transient coupled integration (Gregory et al., 2004; Danabasoglu and Gent, 2009; Li et al., 2013a). The computational cost of coupled AOGCMs is often prohibitively large to run simulations to full equilibrium, and only a few models have performed those (Manabe and Stouffer, 1994; Voss and Mikolajewicz, 2001; Gregory et al., 2004; Danabasoglu and Gent, 2009; Li et al., 2013a). Because of the time dependence of effective climate sensitivity, fitting simple models to AOGCMs over the first few centuries may lead to errors when inferring the response on multi-century time scales. In the HadCM3 case the long-term warming would be underestimated by 30% if extrapolated from the first century (Gregory et al., 2004), in other models the warming of the slab and coupled model is almost identical (Danabasoglu and Gent, 2009). The assumption that the response to different forcings is approximately additive appears to be justified for large-scale temperature changes but limited for other climate variables (Boer and Yu, 2003; Sexton et al., 2003; Gillett et al., 2004; Meehl et al., 2004; Jones et al., 2007). A more complete discussion of the concept of ECS and the limitations is given in Knutti and Hegerl (2008). The CMIP5 model estimates of ECS and TCR are also discussed in Section 9.7. Despite all limitations, the ECS and TCR remain key concepts to characterize the transient and near equilibrium warming as a response to RF on time scales of centuries. Their overall assessment is given in Box 12.2.

A number of recent studies suggest that equilibrium climate sensitivities determined from AOGCMs and recent warming trends may significantly underestimate the true Earth system sensitivity (see Glossary) which is realized when equilibration is reached on millennial time scales (Hansen et al., 2008; Rohling et al., 2009; Lunt et al., 2010; Pagani et al., 2010; Rohling and Members, 2012). The argument is that slow feedbacks associated with vegetation changes and ice sheets have their own intrinsic long time scales and are not represented in most models (Jones et al., 2009). Additional feedbacks are mostly thought to be positive but negative feedbacks of smaller magnitude are also simulated (Swingedouw et al., 2008; Goelzer et al., 2011). The climate sensitivity of a model may therefore not reflect the sensitivity of the full Earth system because those feedback processes are not considered (see also Sections 10.8, 5.3.1 and 5.3.3.2; Box 5.1). Feedbacks determined in very different base state (e.g., the Last Glacial Maximum) differ from those in the current warm period (Rohling and Members, 2012), and relationships between observables and climate sensitivity are model dependent (Crucifix, 2006; Schneider von Deimling et al., 2006; Edwards et al., 2007; Hargreaves et al., 2007, 2012). Estimates of climate sensitivity based on paleoclimate archives (Hansen

## Frequently Asked Questions

**FAQ 12.3 | What Would Happen to Future Climate if We Stopped Emissions Today?**

*Stopping emissions today is a scenario that is not plausible, but it is one of several idealized cases that provide insight into the response of the climate system and carbon cycle. As a result of the multiple time scales in the climate system, the relation between change in emissions and climate response is quite complex, with some changes still occurring long after emissions ceased. Models and process understanding show that as a result of the large ocean inertia and the long lifetime of many greenhouse gases, primarily carbon dioxide, much of the warming would persist for centuries after greenhouse gas emissions have stopped.*

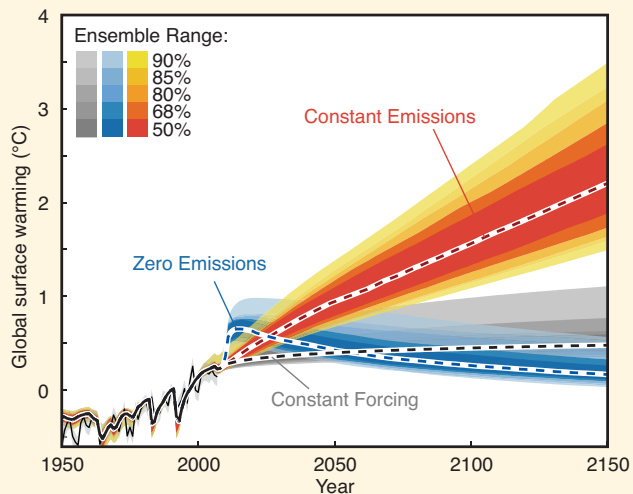
When emitted in the atmosphere, greenhouse gases get removed through chemical reactions with other reactive components or, in the case of carbon dioxide ( $\text{CO}_2$ ), get exchanged with the ocean and the land. These processes characterize the lifetime of the gas in the atmosphere, defined as the time it takes for a concentration pulse to decrease by a factor of e (2.71). How long greenhouse gases and aerosols persist in the atmosphere varies over a wide range, from days to thousands of years. For example, aerosols have a lifetime of weeks, methane ( $\text{CH}_4$ ) of about 10 years, nitrous oxide ( $\text{N}_2\text{O}$ ) of about 100 years and hexafluoroethane ( $\text{C}_2\text{F}_6$ ) of about 10,000 years.  $\text{CO}_2$  is more complicated as it is removed from the atmosphere through multiple physical and biogeochemical processes in the ocean and the land; all operating at different time scales. For an emission pulse of about 1000 PgC, about half is removed within a few decades, but the remaining fraction stays in the atmosphere for much longer. About 15 to 40% of the  $\text{CO}_2$  pulse is still in the atmosphere after 1000 years.

As a result of the significant lifetimes of major anthropogenic greenhouse gases, the increased atmospheric concentration due to past emissions will persist long after emissions are ceased. Concentration of greenhouse gases would not return immediately to their pre-industrial levels if emissions were halted. Methane concentration would return to values close to pre-industrial level in about 50 years,  $\text{N}_2\text{O}$  concentrations would need several centuries, while  $\text{CO}_2$  would essentially never come back to its pre-industrial level on time scales relevant for our society. Changes in emissions of short-lived species like aerosols on the other hand would result in nearly instantaneous changes in their concentrations.

The climate system response to the greenhouse gases and aerosols forcing is characterized by an inertia, driven mainly by the ocean. The ocean has a very large capacity of absorbing heat and a slow mixing between the surface and the deep ocean. This means that it will take several centuries for the whole ocean to warm up and to reach equilibrium with the altered radiative forcing. The surface ocean (and hence the continents) will continue to warm until it reaches a surface temperature in equilibrium with this new radiative forcing. The AR4 showed that if concentration of greenhouse gases were held constant at present day level, the Earth surface would still continue to warm by about  $0.6^\circ\text{C}$  over the 21st century relative to the year 2000. This is the climate commitment to current concentrations (or constant composition commitment), shown in grey in FAQ 12.3, Figure 1. Constant emissions at current levels would further increase the atmospheric concentration and result in much more warming than observed so far (FAQ 12.3, Figure 1, red lines).

Even if anthropogenic greenhouses gas emissions were halted now, the radiative forcing due to these long-lived greenhouse gases concentrations would only slowly decrease in the future, at a rate determined by the lifetime of the gas (see above). Moreover, the

(continued on next page)



**FAQ 12.3, Figure 1 |** Projections based on the energy balance carbon cycle model Model for the Assessment of Greenhouse Gas-Induced Climate Change (MAGICC) for constant atmospheric composition (constant forcing, grey), constant emissions (red) and zero future emissions (blue) starting in 2010, with estimates of uncertainty. Figure adapted from Hare and Meinshausen (2006) based on the calibration of a simple carbon cycle climate model to all Coupled Model Intercomparison Project Phase 3 (CMIP3) and Coupled Climate Carbon Cycle Model Intercomparison Project (C4MIP) models (Meinshausen et al., 2011a; Meinshausen et al., 2011b). Results are based on a full transient simulation starting from pre-industrial and using all radiative forcing components. The thin black line and shading denote the observed warming and uncertainty.

*FAQ 12.3 (continued)*

climate response of the Earth System to that radiative forcing would be even slower. Global temperature would not respond quickly to the greenhouse gas concentration changes. Eliminating CO<sub>2</sub> emissions only would lead to near constant temperature for many centuries. Eliminating short-lived negative forcings from sulphate aerosols at the same time (e.g., by air pollution reduction measures) would cause a temporary warming of a few tenths of a degree, as shown in blue in FAQ 12.3, Figure 1. Setting all emissions to zero would therefore, after a short warming, lead to a near stabilization of the climate for multiple centuries. This is called the commitment from past emissions (or zero future emission commitment). The concentration of GHG would decrease and hence the radiative forcing as well, but the inertia of the climate system would delay the temperature response.

As a consequence of the large inertia in the climate and carbon cycle, the long-term global temperature is largely controlled by total CO<sub>2</sub> emissions that have accumulated over time, irrespective of the time when they were emitted. Limiting global warming below a given level (e.g., 2°C above pre-industrial) therefore implies a given budget of CO<sub>2</sub>, that is, higher emissions earlier implies stronger reductions later. A higher climate target allows for a higher CO<sub>2</sub> concentration peak, and hence larger cumulative CO<sub>2</sub> emissions (e.g., permitting a delay in the necessary emission reduction).

Global temperature is a useful aggregate number to describe the magnitude of climate change, but not all changes will scale linearly with global temperature. Changes in the water cycle for example also depend on the type of forcing (e.g., greenhouse gases, aerosols, land use change), slower components of the Earth system such as sea level rise and ice sheet would take much longer to respond, and there may be critical thresholds or abrupt or irreversible changes in the climate system.

et al., 2008; Rohling et al., 2009; Lunt et al., 2010; Pagani et al., 2010; Schmittner et al., 2011; Rohling and Members, 2012), most but not all based on climate states colder than present, are therefore not necessarily representative for an estimate of climate sensitivity today (see also Sections 5.3.1, 5.3.3.2, Box 5.1). Also it is uncertain on which time scale some of those Earth system feedbacks would become significant.

Equilibrium climate sensitivity undoubtedly remains a key quantity, useful to relate a change in GHGs or other forcings to a global temperature change. But the above caveats imply that estimates based on past climate states very different from today, estimates based on time scales different than those relevant for climate stabilization (e.g., estimates based on climate response to volcanic eruptions), or based on forcings other than GHGs (e.g., spatially non-uniform land cover changes, volcanic eruptions or solar forcing) may differ from the climate sensitivity measuring the climate feedbacks of the Earth system today, and this measure, in turn, may be slightly different from the sensitivity of the Earth in a much warmer state on time scales of millennia. The TCR and the transient climate response to cumulative carbon emissions (TCRE) are often more directly relevant to evaluate short term changes and emission reductions needed for stabilization (see Section 12.5.4).

## 12.5.4 Climate Stabilization and Long-term Climate Targets

This section discusses the relation between emissions and climate targets, in the context of the uncertainties characterizing both the transient and the equilibrium climate responses to emissions. 'Climate targets' considered here are both stabilizing temperature at a specified value and avoiding a warming beyond a predefined threshold.

The latter idea of limiting peak warming is a more general concept than stabilization of temperature or atmospheric CO<sub>2</sub>, and one that is more realistic than an exact climate stabilization which would require perpetual non-zero positive emissions to counteract the otherwise unavoidable long-term slow decrease in global temperature (Matsuno et al., 2012a) (Figure 12.44).

### 12.5.4.1 Background

The concept of stabilization is strongly linked to the ultimate objective of the UNFCCC, which is 'to achieve [...] stabilization of greenhouse gas concentrations in the atmosphere at a level that would prevent dangerous anthropogenic interference with the climate system'. Recent policy discussions focussed on a global temperature increase, rather than on GHG concentrations. The most prominent target currently discussed is the 2°C temperature target, that is, to limit global temperature increase relative to pre-industrial times to below 2°C. The 2°C target has been used first by the European Union as a policy target in 1996 but can be traced further back (Jaeger and Jaeger, 2010; Randalls, 2010). Climate impacts however are geographically diverse (Joshi et al., 2011) and sector specific, and no objective threshold defines when dangerous interference is reached. Some changes may be delayed or irreversible, and some impacts are likely to be beneficial. It is thus not possible to define a single critical threshold without value judgments and without assumptions on how to aggregate current and future costs and benefits. Targets other than 2°C have been proposed (e.g., 1.5°C global warming relative to pre-industrial), or targets based on CO<sub>2</sub> concentration levels, for example, 350 ppm (Hansen et al., 2008). The rate of change may also be important (e.g., for adaptation). This section does not advocate or defend any threshold, nor does it judge

the economic or political feasibility of such goals, but simply assesses the implications of different illustrative climate targets on allowed carbon emissions, based on our current understanding of climate and carbon cycle feedbacks.

#### 12.5.4.2 Constraints on Cumulative Carbon Emissions

The current RF from GHGs maintained indefinitely (i.e., the commitment from constant greenhouse gas concentrations) would correspond to approximately 2°C warming. That, however, does not imply that the commitment from past emissions has already exceeded 2°C. Part of the positive RF from GHGs is currently compensated by negative aerosol forcing, and stopping GHG emissions would lead to a decrease in the GHG forcing. Actively removing CO<sub>2</sub> from the atmosphere, for example by the combined use of biomass energy and carbon capture and storage, would further accelerate the decrease in GHG forcing.

The total amount of anthropogenic CO<sub>2</sub> released in the atmosphere (often termed cumulative carbon emission) is a good indicator of the atmospheric CO<sub>2</sub> concentration and hence of the global warming response to CO<sub>2</sub>. The ratio of global temperature change to total cumulative anthropogenic CO<sub>2</sub> emissions (TCRE) is relatively constant over time and independent of the scenario, but is model dependent as it depends on the model cumulative airborne fraction of CO<sub>2</sub> and ECS/TCR (Matthews and Caldeira, 2008; Allen et al., 2009; Gregory et al., 2009; Matthews et al., 2009; Meinshausen et al., 2009; Zickfeld et al., 2009; Bowerman et al., 2011; Knutti and Plattner, 2012; Zickfeld et al., 2012, 2013). This is consistent with an earlier study indicating that the global warming potential of CO<sub>2</sub> is approximately independent of the scenario (Caldeira and Kasting, 1993). The concept of a constant ratio of cumulative emissions of CO<sub>2</sub> to temperature holds well only until temperatures peak (see Figure 12.45e) and only for smoothly varying cumulative CO<sub>2</sub> emissions (Gillett et al., 2013). It does not hold for stabilization on millennial time scales or for non-CO<sub>2</sub> forcings, and there is limited evidence for its applicability for cumulative emissions exceeding 2000 PgC owing to limited simulations available (Plattner et al., 2008; Hajima et al., 2012; Matsuno et al., 2012b; Gillett et al., 2013; Zickfeld et al., 2013). For non-CO<sub>2</sub> forcings with shorter atmospheric life times than CO<sub>2</sub> the rate of emissions at the time of peak warming is more important than the cumulative emissions over time (Smith et al., 2012).

Assuming constant climate sensitivity and fixed carbon cycle feedbacks, long-term (several centuries to millennium) stabilization of global temperatures requires eventually the stabilization of atmospheric concentrations (or decreasing concentrations if the temperature should be stabilized more quickly). This requires decreasing emissions to near-zero (Jones et al., 2006; Meehl et al., 2007b; Weaver et al., 2007; Matthews and Caldeira, 2008; Plattner et al., 2008; Allen et al., 2009; Matthews et al., 2009; Meinshausen et al., 2009; Zickfeld et al., 2009; Friedlingstein et al., 2011; Gillett et al., 2011; Roeckner et al., 2011; Knutti and Plattner, 2012; Matsuno et al., 2012a).

The relationships between cumulative emissions and temperature for various studies are shown in Figure 12.45. Note that some lines mark the evolution of temperature as a function of emissions over time while other panels show peak temperatures for different simulations.

Also some models prescribe only CO<sub>2</sub> emissions while others use multi-gas scenarios, and the time horizons differ. The warming is usually larger if non-CO<sub>2</sub> forcings are considered, since the net effect of the non-CO<sub>2</sub> forcings is positive in most scenarios (Hajima et al., 2012). Not all numbers are therefore directly comparable. Matthews et al. (2009) estimated the TCRE as 1°C to 2.1°C per 1000 PgC (TtC, or 10<sup>12</sup> metric tonnes of carbon) (5 to 95%) based on the C<sup>4</sup>MIP model range (Figure 12.45a). The ENSEMBLES E1 show a range of 1°C to 4°C per 1000 PgC (scaled from 0.5°C to 2°C for 500 PgC, Figure 12.45d) (Johns et al., 2011). Rogelj et al. (2012) estimate a 5 to 95% range of about 1°C to 2°C per 1000 PgC (Figure 12.45e) based on the MAGICC model calibrated to the C<sup>4</sup>MIP model range and the *likely* range of 2°C to 4.5°C for climate sensitivity given in AR4. Allen et al. (2009) used a simple model and found 1.3°C to 3.9°C per 1000 PgC (5 to 95%) for peak warming (Figure 12.45g) and 1.4°C to 2.5°C for TCRE. The EMICs TCRE simulations suggest a range of about 1.4°C to 2.5°C per 1000 PgC and a mean of 1.9°C per 1000 PgC (Zickfeld et al., 2013) (Figure 12.45h). The results of Meinshausen et al. (2009) confirm the approximate linearity between temperature and CO<sub>2</sub> emissions (Figure 12.45b). Their results are difficult to compare owing to the shorter time period considered, but the model was found to be consistent with that of Allen et al. (2009). Zickfeld et al. (2009), using an EMIC, find a best estimate of about 1.5°C per 1000 PgC. Gillett et al. (2013) find a range of 0.8°C to 2.4°C per 1000 PgC in 15 CMIP5 models and derive an observationally constrained range of 0.7°C to 2.0°C per 1000 PgC. Results from much earlier model studies support the near linear relationship of cumulative emissions and global temperature, even though these studies did not discuss the linear relationship. An example is given in Figure 12.45c based on data shown in IPCC TAR Figure 13.3 (IPCC, 2001) and IPCC AR4 Figure 10.35 (Meehl et al., 2007b). The relationships between cumulative CO<sub>2</sub> emissions and temperature in CMIP5 are shown in Figure 12.45f for the 1% yr<sup>-1</sup> CO<sub>2</sub> increase scenarios and in Figure 12.45i for the RCP8.5 emission driven ESM simulations (Gillett et al., 2013). Compatible emissions from concentration driven CMIP5 ESMs are discussed in Section 6.4.3.3.

Expert judgement based on the available evidence therefore suggests that the TCRE is *likely* between 0.8°C to 2.5°C per 1000 PgC, for cumulative CO<sub>2</sub> emissions less than about 2000 PgC until the time at which temperature peaks. Under these conditions, and for low to medium estimates of climate sensitivity, the TCRE is nearly identical to the peak climate response to cumulative carbon emissions. For high climate sensitivity, strong carbon cycle climate feedbacks or large cumulative emissions, the peak warming can be delayed and the peak response may be different from TCRE, but is often poorly constrained by models and observations. The range of TCRE assessed here is consistent with other recent attempts to synthesize the available evidence (NRC, 2011; Matthews et al., 2012). The results by Schwartz et al. (2010, 2012) imply a much larger warming for the carbon emitted over the historical period and have been questioned by Knutti and Plattner (2012) for neglecting the relevant response time scales and combining a transient airborne fraction with an equilibrium climate sensitivity.

The TCRE can be compared to the temperature response to emissions on a time scale of about 1000 years after emissions cease. This can be estimated from the *likely* range of equilibrium climate sensitivity (1.5°C to 4.5°C) and a cumulative CO<sub>2</sub> airborne fraction after about

1000 years of about  $25 \pm 5\%$  (Archer et al., 2009; Joos et al., 2013). Again combining the extreme values would suggest a range of  $0.6^\circ\text{C}$  to  $2.7^\circ\text{C}$  per 1000 PgC, and  $1.5^\circ\text{C}$  per 1000 PgC for an ECS of  $3^\circ\text{C}$  and a cumulative airborne fraction of 25%. However, this equilibrium estimate is based on feedbacks estimated for the present day climate. Climate and carbon cycle feedbacks may increase substantially on long time scales and for high cumulative CO<sub>2</sub> emissions (see Section 12.5.3), introducing large uncertainties in particular on the upper bound. Based on paleoclimate data and an analytical model, Goodwin et al. (2009) estimate a long term RF of  $1.5 \text{ W m}^{-2}$  for an emission of 1000 PgC. For an equilibrium climate sensitivity of  $3^\circ\text{C}$  this corresponds to a warming of  $1.2^\circ\text{C}$  on millennial time scales, consistent with the climate carbon cycle models results discussed above.

The uncertainty in TCRE is caused by the uncertainty in the physical feedbacks and ocean heat uptake (reflected in TCR) and uncertainties in carbon cycle feedbacks (affecting the cumulative airborne fraction of CO<sub>2</sub>). TCRE only characterizes the warming due to CO<sub>2</sub> emissions, and contributions from non-CO<sub>2</sub> gases need to be considered separately when estimating likelihoods to stay below a temperature limit. Warming as a function of cumulative CO<sub>2</sub> emissions is similar in the four RCP scenarios, and larger than that due to CO<sub>2</sub> alone, since non-CO<sub>2</sub> forcings contribute warming in these scenarios (compare Figure 12.45 f, i) (Hajima et al., 2012).

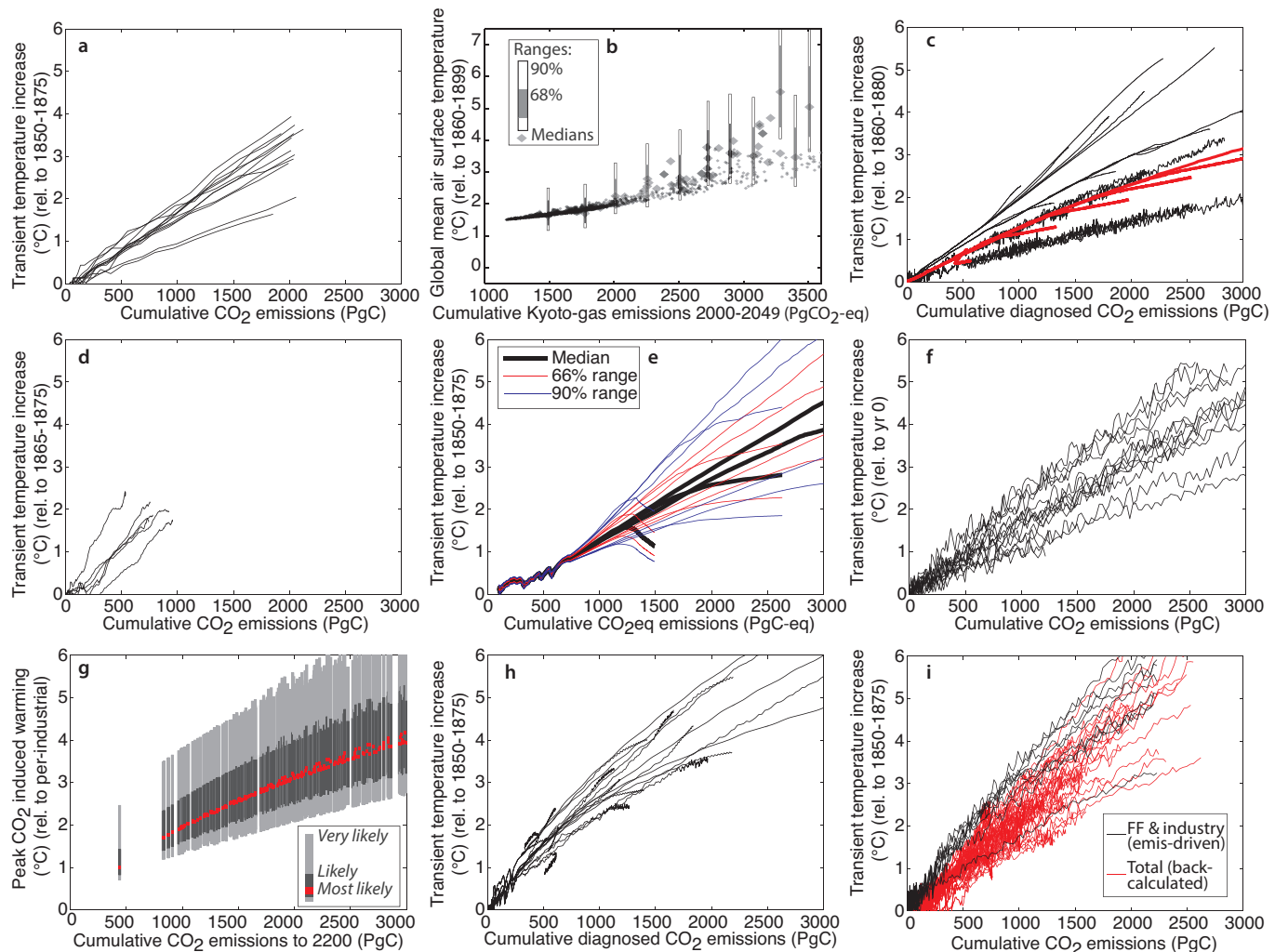
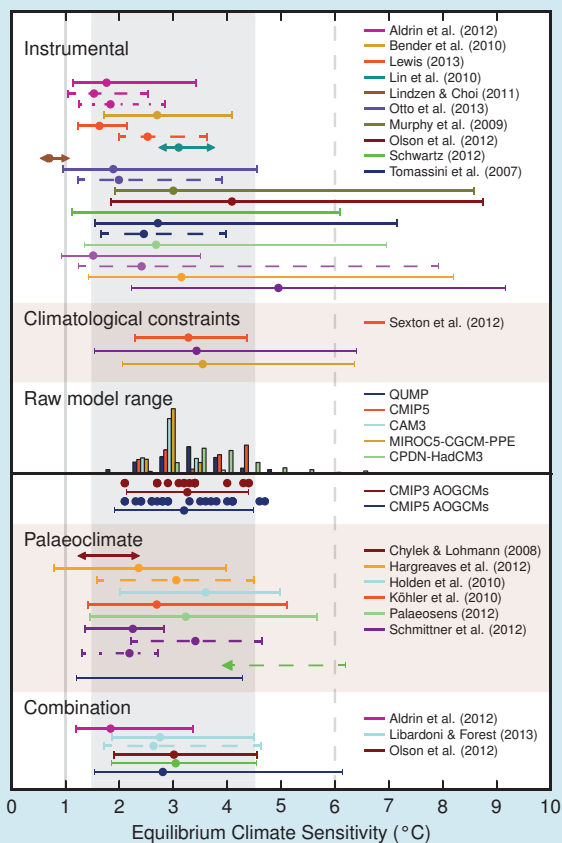


**Figure 12.45 |** Global temperature change vs. cumulative carbon emissions for different scenarios and models. (a) Transient global temperature increase vs. cumulative CO<sub>2</sub> emissions for Coupled Climate Carbon Cycle Model Intercomparison Project (C<sup>4</sup>MIP) (Matthews et al., 2009). (b) Maximum temperature increase until 2100 vs. cumulative Kyoto-gas emissions (CO<sub>2</sub> equivalent; note that all other panels are given in C equivalent) (Meinshausen et al., 2009). (c) Transient temperature increase vs. cumulative CO<sub>2</sub> emissions for IPCC TAR models (red, IPCC TAR Figure 13.3) and IPCC AR4 Earth System Models of Intermediate Complexity (EMICs, black; IPCC AR4 Figure 10.35). (d) As in (a) but for the ENSEMBLES E1 scenario (Johns et al., 2011). (e) Transient temperature increase for the RCP scenarios based on the Model for the Assessment of Greenhouse Gas-Induced Climate Change (MAGICC) model constrained to C<sup>4</sup>MIP, observed warming, and the IPCC AR4 climate sensitivity range (Rogelj et al., 2012). (f) Transient temperature change from the CMIP5 1% yr<sup>-1</sup> concentration driven simulations. (g) Peak CO<sub>2</sub> induced warming vs. cumulative CO<sub>2</sub> emissions to 2200 (Allen et al., 2009; Bowerman et al., 2011). (h) Transient temperature increase from the new EMIC RCP simulations (Zickfeld et al., 2013). (i) Transient temperature change from the CMIP5 historical and RCP8.5 emission driven simulations (black) and transient temperature change in all concentration-driven CMIP5 RCP simulations with back-calculated emissions (red). Note that black lines in panel (i) do not include land use CO<sub>2</sub> and that warming in (i) is higher than in (f) due to additional non-CO<sub>2</sub> forcings.

## Box 12.2 | Equilibrium Climate Sensitivity and Transient Climate Response

Equilibrium climate sensitivity (ECS) and transient climate response (TCR) are useful metrics summarizing the global climate system's temperature response to an externally imposed radiative forcing (RF). ECS is defined as the equilibrium change in annual mean global surface temperature following a doubling of the atmospheric CO<sub>2</sub> concentration (see Glossary), while TCR is defined as the annual mean global surface temperature change at the time of CO<sub>2</sub> doubling following a linear increase in CO<sub>2</sub> forcing over a period of 70 years (see Glossary). Both metrics have a broader application than these definitions imply: ECS determines the eventual warming in response to stabilization of atmospheric composition on multi-century time scales, while TCR determines the warming expected at a given time following any steady increase in forcing over a 50- to 100-year time scale.

ECS and TCR can be estimated from various lines of evidence. The estimates can be based on the values of ECS and TCR diagnosed from climate models (Section 9.7.1; Table 9.5), or they can be constrained by analysis of feedbacks in climate models (see Section 9.7.2), patterns of mean climate and variability in models compared to observations (Section 9.7.3.3), temperature fluctuations as reconstructed from paleoclimate archives (Sections 5.3.1 and 5.3.3.2; Box 5.1), observed and modelled short-term perturbations of the energy balance like those caused by volcanic eruptions (Section 10.8), and the observed surface and ocean temperature trends since pre-industrial (see Sections 10.8.1 and 10.8.2; Figure 10.20). For many applications, the limitations of the forcing-feedback analysis framework and the dependence of feedbacks on time scales and the climate state (see Section 12.5.3) must be kept in mind. Some studies estimate the TCR as the ratio of global mean temperature change to RF (Section 10.8.2.2) (Gregory and Forster, 2008; Padilla et al., 2011; Schwartz, 2012). Those estimates are scaled by the RF of 2 × CO<sub>2</sub> (3.7 W m<sup>-2</sup>; Myhre et al., 1998) to be comparable to TCR in the following discussion.



**Box 12.2, Figure 1 |** Probability density functions, distributions and ranges for equilibrium climate sensitivity, based on Figure 10.20b plus climatological constraints shown in IPCC AR4 (Meehl et al., 2007b; Box 10.2, Figure 1), and results from CMIP5 (Table 9.5). The grey shaded range marks the *likely* 1.5°C to 4.5°C range, and the grey solid line the *extremely unlikely* less than 1°C, the grey dashed line the *very unlikely* greater than 6°C. See Figure 10.20b and Chapter 10 Supplementary Material for full caption and details. Labels refer to studies since AR4. Full references are given in Section 10.8.

Newer studies of constraints based on the observed warming since pre-industrial, analysed using simple and intermediate complexity models, improved statistical methods, and several different and newer data sets, are assessed in detail in Section 10.8.2. Together with results from feedback analysis and paleoclimate constraints (Sections 5.3.1 and 5.3.3.2; Box 5.1), but without considering the CMIP based evidence, these studies show ECS is *likely* between 1.5°C to 4.5°C (*medium confidence*) and *extremely unlikely* less than 1.0°C (see Section 10.8.2). A few studies argued for very low values of climate sensitivity, but many of them have received criticism in the literature (see Section 10.8.2). Estimates based on AOGCMs and feedback analysis indicate a range of 2°C to 4.5°C, with the CMIP5 model mean at 3.2°C, similar to CMIP3. A summary of published ranges and PDFs of ECS is given in Box 12.2, Figure 1. Distributions and ranges for the TCR are shown in Box 12.2, Figure 2.

Simultaneously imposing different constraints from the observed warming trends, volcanic eruptions, model climatology, and paleoclimate, for example, by using a distribution obtained from the Last Glacial Maximum as a prior for the 20th century analysis, yields a more narrow range for climate sensitivity (see Figure 10.20; Section 10.8.2.5) (e.g., Annan and Hargreaves, 2006, 2011b; Hegerl et al., 2006; Aldrin et al., 2012). However, such methods are sensitive to assumptions of independence of the various lines of evidence, which might have shared biases (Lemoine, 2010), and the assumption that each individual line of evidence is unbiased and its uncertainties are captured completely. Expert elicitation for PDFs of climate sensitivity exist (Morgan and Keith, 1995; Zickfeld et al., 2010), but have also received some criticism (Millner et al., 2013). They are not used formally here because the experts base their opinion on the same studies as we assess. The peer-reviewed literature provides no consensus on a

(continued on next page)

## Box 12.2 (continued)

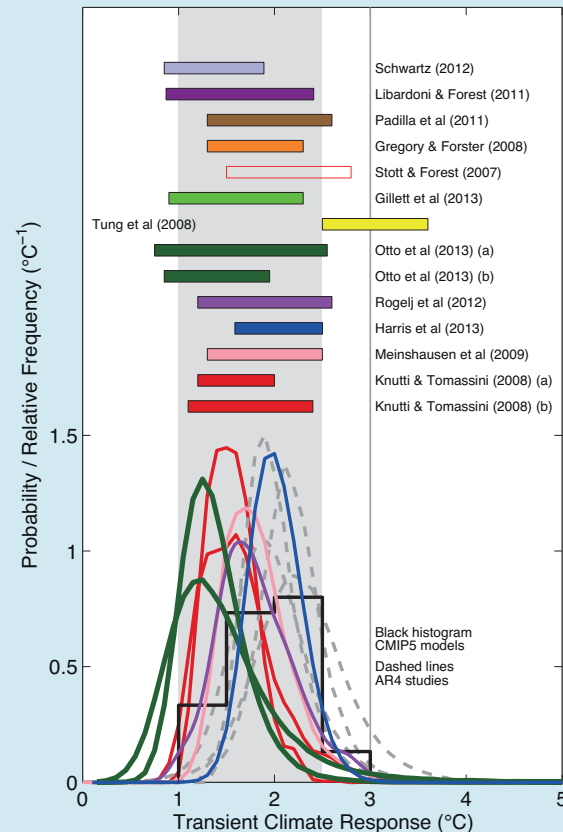
formal statistical method to combine different lines of evidence. All methods in general are sensitive to the assumed prior distributions. These limitations are discussed in detail in Section 10.8.2.

Based on the combined evidence from observed climate change including the observed 20th century warming, climate models, feedback analysis and paleoclimate, ECS is *likely* in the range 1.5°C to 4.5°C with *high confidence*. The combined evidence increases the confidence in this final assessment compared to that based on the observed warming and paleoclimate only. ECS is positive, *extremely unlikely* less than 1°C (*high confidence*), and *very unlikely* greater than 6°C (*medium confidence*). The upper limit of the *likely* range is unchanged compared to AR4. The lower limit of the *likely* range of 1.5°C is less than the lower limit of 2°C in AR4. This change reflects the evidence from new studies of observed temperature change, using the extended records in atmosphere and ocean. These studies suggest a best fit to the observed surface and ocean warming for ECS values in the lower part of the *likely* range. Note that these studies are not purely observational, because they require an estimate of the response to RF from models. In addition, the uncertainty in ocean heat uptake remains substantial (see Section 3.2, Box 13.1). Accounting for short term variability in simple models remains challenging, and it is important not to give undue weight to any short time period that might be strongly affected by internal variability (see Box 9.2). On the other hand, AOGCMs show very good agreement with observed climatology with ECS values in the upper part of the 1.5°C to 4.5°C range (Section 9.7.3.3), but the simulation of key feedbacks like clouds remains challenging in those models. The estimates from the observed warming, paleoclimate, and from climate models are consistent within their uncertainties, each is supported by many studies and multiple data sets, and in combination they provide *high confidence* for the assessed *likely* range. Even though this assessed range is similar to previous reports (Charney, 1979; IPCC, 2001), confidence today is much higher as a result of high quality and longer observational records with a clearer anthropogenic signal, better process understanding, more and better understood evidence from paleoclimate reconstructions, and better climate models with higher resolution that capture many more processes more realistically. Box 12.2 Figure 1 illustrates that all these lines of evidence individually support the assessed *likely* range of 1.5°C to 4.5°C.

The tails of the ECS distribution are now better understood. Multiple lines of evidence provide *high confidence* that an ECS value less than 1°C is *extremely unlikely*. The assessment that ECS is *very unlikely* greater than 6°C is an expert judgment informed by several lines of evidence. First, the comprehensive climate models used in the CMIP5 exercise produce an ECS range of 2.1°C to 4.7°C (Table 9.5), very similar to CMIP3. Second, comparisons of perturbed-physics ensembles against the observed climate find that models with ECS values in the range 3°C to 4°C show the smallest errors for many fields (Section 9.7.3.3). Third, there is increasing evidence that the aerosol RF of the 20th century is not strongly negative, which makes it unlikely that the observed warming was caused by a very large ECS in response to a very small net forcing. Fourth, multiple and at least partly independent observational constraints from the satellite period, instrumental period and palaeoclimate studies continue to yield very low probabilities for ECS larger than 6°C, particularly when including most recent ocean and atmospheric data (see Box 12.2, Figure 1).

Analyses of observations and simulations of the instrumental period are estimating the effective climate sensitivity (a measure of the strengths of the climate feedbacks today, see Glossary), rather than ECS directly. In some climate models ECS tends to be higher than the effective climate sensitivity (see Section 12.5.3), because the feedbacks that are represented in the models (water vapour, lapse

(continued on next page)



**Box 12.2, Figure 2 |** Probability density functions, distributions and ranges (5 to 95%) for the transient climate response from different studies, based on Figure 10.20a, and results from CMIP5 (black histogram; Table 9.5). The grey shaded range marks the *likely* 1°C to 2.5°C range, and the grey solid line marks the *extremely unlikely* greater than 3°C. See Figure 10.20a and Chapter 10 Supplementary Material for full caption and details. Full references are given in Section 10.8.

## Box 12.2 (continued)

rate, albedo and clouds) vary with the climate state. On time scales of many centuries, additional feedbacks with their own intrinsic time scales (e.g., vegetation, ice sheets; see Sections 5.3.3 and 12.5.3) (Jones et al., 2009; Goelzer et al., 2011) may become important but are not usually modelled. The resulting Earth system sensitivity is less well constrained but likely to be larger than ECS (Hansen et al., 2008; Rohling et al., 2009; Lunt et al., 2010; Pagani et al., 2010; Rohling and Members, 2012), implying that lower atmospheric CO<sub>2</sub> concentrations are needed to meet a given temperature target on multi-century time scales. A number of caveats, however, apply to those studies (see Section 12.5.3). Those long-term feedbacks have their own intrinsic time scales, and are less likely to be proportional to global mean temperature change.

For scenarios of increasing RF, TCR is a more informative indicator of future climate than ECS (Frame et al., 2005; Held et al., 2010). This assessment concludes with *high confidence* that the TCR is *likely* in the range 1°C to 2.5°C, close to the estimated 5 to 95% range of CMIP5 (1.2°C to 2.4°C; see Table 9.5), is positive and *extremely unlikely* greater than 3°C. As with the ECS, this is an expert-assessed range, supported by several different and partly independent lines of evidence, each based on multiple studies, models and data sets. TCR is estimated from the observed global changes in surface temperature, ocean heat uptake and RF, the detection/attribution studies identifying the response patterns to increasing GHG concentrations (Section 10.8.1), and the results of CMIP3 and CMIP5 (Section 9.7.1). Estimating TCR suffers from fewer difficulties in terms of state- or time-dependent feedbacks (see Section 12.5.3), and is less affected by uncertainty as to how much energy is taken up by the ocean. Unlike ECS, the ranges of TCR estimated from the observed warming and from AOGCMs agree well, increasing our confidence in the assessment of uncertainties in projections over the 21st century.

Another useful metric relating directly CO<sub>2</sub> emissions to temperature is the transient climate response to cumulative carbon emission (TCRE) (see Sections 12.5.4 and 10.8.4). This metric is useful to determine the allowed cumulative carbon emissions for stabilization at a specific global temperature. TCRE is defined as the annual mean global surface temperature change per unit of cumulated CO<sub>2</sub> emissions, usually 1000 PgC, in a scenario with continuing emissions (see Glossary). It considers physical and carbon cycle feedbacks and uncertainties, but not additional feedbacks associated for example with the release of methane hydrates or large amounts of carbon from permafrost. The assessment based on climate models as well as the observed warming suggests that the TCRE is *likely* between 0.8°C to 2.5°C per 1000 PgC ( $10^{12}$  metric tons of carbon), for cumulative CO<sub>2</sub> emissions less than about 2000 PgC until the time at which temperatures peak. Under these conditions, and for low to medium estimates of climate sensitivity, the TCRE gives an accurate estimate of the peak global mean temperature response to cumulated carbon emissions. TCRE has the advantage of directly relating global mean surface temperature change to CO<sub>2</sub> emissions, but as a result of combining the uncertainty in both TCR and the carbon cycle response, it is more uncertain. It also ignores non-CO<sub>2</sub> forcings and the fact that other components of the climate system (e.g., sea level rise, ice sheets) have their own intrinsic time scales, resulting in climate change not avoided by limiting global temperature change.

#### 12.5.4.3 Conclusions and Limitations

One difficulty with the concepts of climate stabilization and targets is that stabilization of global temperature does not imply stabilization for all aspects of the climate system. For example, some models show significant hysteresis behaviour in the global water cycle, because global precipitation depends on both atmospheric CO<sub>2</sub> and temperature (Wu et al., 2010). Processes related to vegetation changes (Jones et al., 2009) or changes in the ice sheets (Charbit et al., 2008; Ridley et al., 2010) as well as ocean acidification, deep ocean warming and associated sea level rise (Meehl et al., 2005b; Wigley, 2005; Zickfeld et al., 2013) (see Figure 12.44d), and potential feedbacks linking, for example, ocean and the ice sheets (Gillett et al., 2011; Goelzer et al., 2011), have their own intrinsic long time scales. Those will result in significant changes hundreds to thousands of years after global temperature is stabilized. Thermal expansion, in contrast to global mean temperature, also depends on the evolution of surface temperature (Stouffer and Manabe, 1999; Bouttes et al., 2013; Zickfeld et al., 2013).

The simplicity of the concept of a cumulative carbon emission budget makes it attractive for policy (WBGU, 2009). The principal driver of long term warming is the total cumulative emission of CO<sub>2</sub> over time. To limit warming caused by CO<sub>2</sub> emissions to a given temperature target, cumulative CO<sub>2</sub> emissions from all anthropogenic sources therefore need to be limited to a certain budget. Higher emissions in earlier decades simply imply lower emissions by the same amount later on. This is illustrated in the RCP2.6 scenario in Figure 12.46a/b. Two idealized emission pathways with initially higher emissions (even sustained at high level for a decade in one case) eventually lead to the same warming if emissions are then reduced much more rapidly. Even a stepwise emission pathway with levels constant at 2010 and zero near mid-century would eventually lead to a similar warming as they all have identical cumulative emissions.

However, several aspects related to the concept of a cumulative carbon emission budget should be kept in mind. The ratio of global temperature and cumulative carbon is only approximately constant. It is the result of an interplay of several compensating carbon cycle and climate

feedback processes operating on different time scales (a cancellation of variations in the increase in RF per ppm of CO<sub>2</sub>, the ocean heat uptake efficiency and the airborne fraction) (Gregory et al., 2009; Matthews et al., 2009; Solomon et al., 2009). It depends on the modelled climate sensitivity and carbon cycle feedbacks. Thus, the allowed emissions for a given temperature target are uncertain (see Figure 12.45) (Matthews et al., 2009; Zickfeld et al., 2009; Knutti and Plattner, 2012). Nevertheless, the relationship is nearly linear in all models. Most models do not consider the possibility that long term feedbacks (Hansen et al., 2007; Knutti and Hegerl, 2008) may be different (see Section 12.5.3). Despite the fact that stabilization refers to equilibrium, the results assessed here are primarily relevant for the next few centuries and may differ for millennial scales. Notably, many of these limitations apply similarly to other policy targets, for example, stabilizing the atmospheric CO<sub>2</sub> concentration.

Non-CO<sub>2</sub> forcing constituents are important, which requires either assumptions on how CO<sub>2</sub> emission reductions are linked to changes in other forcings (Meinshausen et al., 2006; Meinshausen et al., 2009; McCollum et al., 2013), or separate emission budgets and climate modelling for short-lived and long-lived gases. So far, many studies ignored non-CO<sub>2</sub> forcings altogether. Those that consider them find significant effects, in particular warming of several tenths of a degree for abrupt reductions in emissions of short-lived species, like aerosols (Brasseur and Roeckner, 2005; Hare and Meinshausen, 2006; Zickfeld et al., 2009; Armour and Roe, 2011; Tanaka and Raddatz, 2011) (see also FAQ 12.3). Other studies, which model reductions that explicitly target warming from short-lived non-CO<sub>2</sub> species only, find important short-term cooling benefits shortly after the reduction of these species (Shindell et al., 2012), but do not extend beyond 2030.

The concept of cumulative carbon also implies that higher initial emissions can be compensated by a faster decline in emissions later or by negative emissions. However, in the real world short-term and long-term goals are not independent and mitigation rates are limited by economic constraints and existing infrastructure (Rive et al., 2007; Mignone et al., 2008; Meinshausen et al., 2009; Davis et al., 2010; Friedlingstein et al., 2011; Rogelj et al., 2013). An analysis of 193 published emission pathways with an energy balance model (UNEP, 2010; Rogelj et al., 2011) is shown in Figure 12.46c, d. Those emission pathways that *likely* limit warming below 2°C (above pre-industrial) by 2100 show emissions of about 31 to 46 Pg(CO<sub>2</sub>-eq) yr<sup>-1</sup> and 17 to 23 Pg(CO<sub>2</sub>-eq) yr<sup>-1</sup> by 2020 and 2050, respectively. Median 2010 emissions of all models are 48 Pg(CO<sub>2</sub>-eq) yr<sup>-1</sup>. Note that, as opposed to Figure 12.46a, b, many scenarios still have positive emissions in 2100. As these will not be zero immediately after 2100, they imply that the warming may exceed the target after 2100.

The aspects discussed above do not limit the robustness of the overall scientific assessment, but highlight factors that need to be considered when determining cumulative CO<sub>2</sub> emissions consistent with a given temperature target. In conclusion, taking into account the available information from multiple lines of evidence (observations, models and process understanding), the near linear relationship between cumulative CO<sub>2</sub> emissions and peak global mean temperature is well established in the literature and robust for cumulative total CO<sub>2</sub> emissions up to about 2000 PgC. It is consistent with the relationship inferred

from past cumulative CO<sub>2</sub> emissions and observed warming, is supported by process understanding of the carbon cycle and global energy balance, and emerges as a robust result from the entire hierarchy of models.

Using a best estimate for the TCRE would provide a most likely value for the cumulative CO<sub>2</sub> emissions compatible with stabilization at a given temperature. However, such a budget would imply about 50% probability for staying below the temperature target. Higher probabilities for staying below a temperature or concentration target require significantly lower budgets (Knutti et al., 2005; Meinshausen et al., 2009; Rogelj et al., 2012). Based on the assessment of TCRE (assuming a normal distribution with a ±1 standard deviation range of 0.8–2.5°C per 1000 PgC), limiting the warming caused by anthropogenic CO<sub>2</sub> emissions alone (i.e., ignoring other radiative forcings) to less than 2°C since the period 1861–1880 with a probability of >33%, >50%, and >66%, total CO<sub>2</sub> emissions from all anthropogenic sources would need to be below a cumulative budget of about 1570 PgC, 1210 PgC and 1000 PgC since 1870, respectively. An amount of 515 [445 to 585] PgC was emitted between 1870 and 2011. Accounting for non-CO<sub>2</sub> forcings contributing to peak warming, or requiring a higher likelihood of temperatures remaining below 2°C, both imply lower cumulative CO<sub>2</sub> emissions. A possible release of GHGs from permafrost or methane hydrates, not accounted for in current models, would also further reduce the anthropogenic CO<sub>2</sub> emissions compatible with a given temperature target. When accounting for the non-CO<sub>2</sub> forcings as in the RCP scenarios, compatible carbon emissions since 1870 are reduced to about 900 PgC, 820 PgC and 790 PgC to limit warming to less than 2°C since the period 1861–1880 with a probability of >33%, >50%, and >66%, respectively. These estimates were derived by computing the fraction of CMIP5 ESMs and EMICs that stay below 2°C for given cumulative emissions following RCP8.5, as shown in TFE.8 Figure 1c. The non-CO<sub>2</sub> forcing in RCP8.5 is higher than in RCP2.6. Because all likelihood statements in calibrated IPCC language are open intervals, the provided estimates are thus both conservative and consistent choices valid for non-CO<sub>2</sub> forcings across all RCP scenarios. There is no RCP scenario which limits warming to 2°C with probabilities of >33% or >50%, and which could be used to directly infer compatible cumulative emissions. For a probability of >66% RCP2.6 can be used as a comparison. Combining the average back-calculated fossil fuel carbon emissions for RCP2.6 between 2012 and 2100 (270 PgC) with the average historical estimate of 515 PgC gives a total of 785 PgC, i.e., 790 PgC when rounded to 10 PgC. As the 785 PgC estimate excludes an explicit assessment of future land-use change emissions, the 790 PgC value also remains a conservative estimate consistent with the overall likelihood assessment. The ranges of emissions for these three likelihoods based on the RCP scenarios are rather narrow, as they are based on a single scenario and on the limited sample of models available (TFE.8 Figure 1c). In contrast to TCRE they do not include observational constraints or account for sources of uncertainty not sampled by the models. The concept of a fixed cumulative CO<sub>2</sub> budget holds not just for 2°C, but for any temperature level explored with models so far (up to about 5°C; see Figures 12.44 to 12.46), with higher temperature levels implying larger budgets.

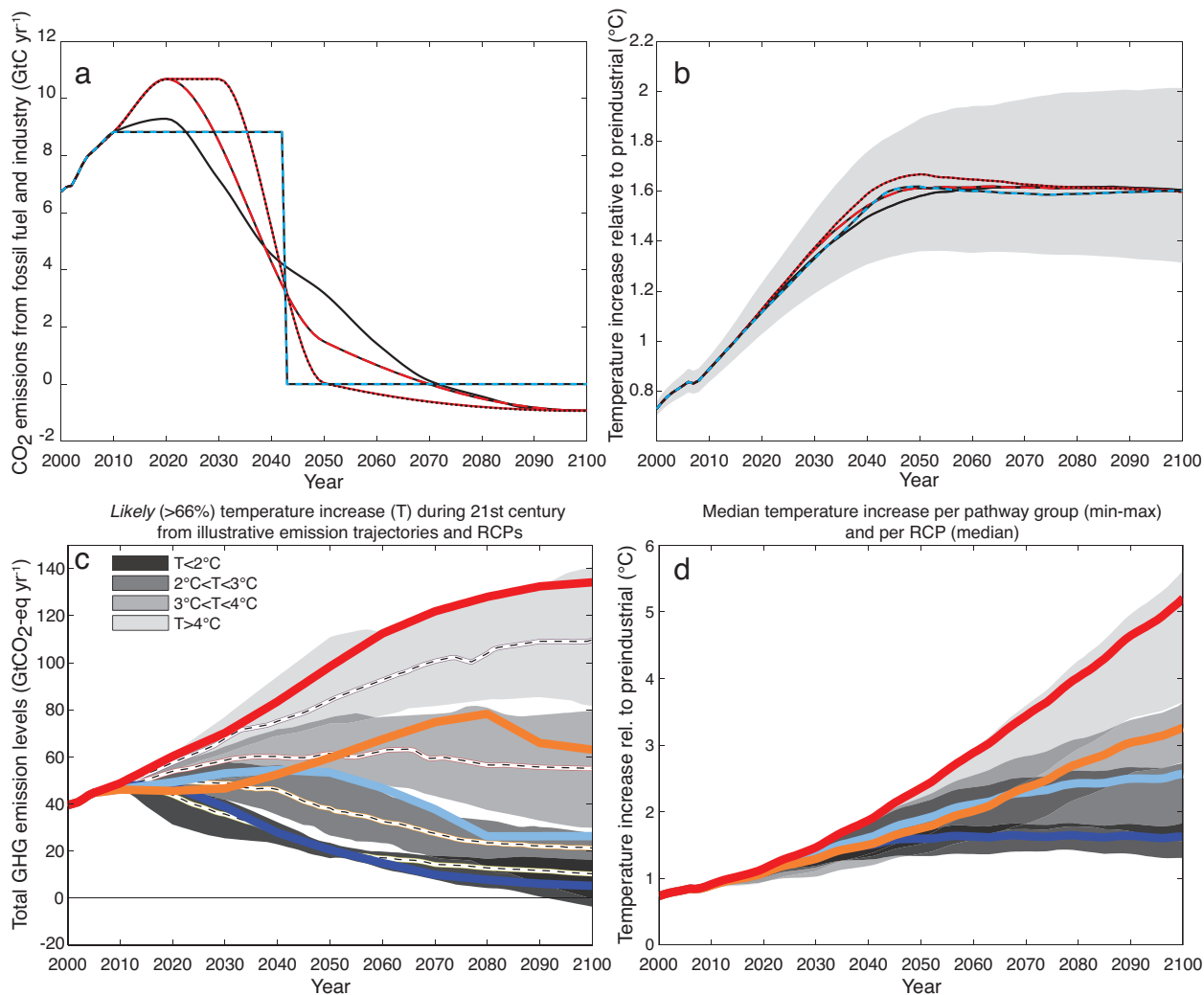


**Figure 12.46 |** (a) CO<sub>2</sub> emissions for the RCP.2.6 scenario (black) and three illustrative modified emission pathways leading to the same warming. (b) Global temperature change relative to pre-industrial for the pathways shown in panel (a). (c) Grey shaded bands show Integrated Assessment Model (IAM) emission pathways over the 21st century. The pathways were grouped based on ranges of *likely* avoided temperature increase in the 21st century. Pathways in the darkest three bands *likely* stay below 2°C, 3°C, 4°C by 2100, respectively (see legend), while those in the lightest grey band are higher than that. Emission corridors were defined by, at each year, identifying the 15th to 85th percentile range of emissions and drawing the corresponding bands across the range. Individual scenarios that follow the upper edge of the bands early on tend to follow the lower edge of the band later on. Black-white lines show median paths per range. (d) Global temperature relative to pre-industrial for the pathways in (c). (Data in (c) and (d) based on Rogelj et al. (2011).) Coloured lines in (c) and (d) denote the four RCP scenarios.

12

## 12.5.5 Potentially Abrupt or Irreversible Changes

### 12.5.5.1 Introduction

This report adopts the definition of abrupt climate change used in Synthesis and Assessment Product 3.4 of the U.S. Climate Change Science Program CCSP (CCSP, 2008b). We define *abrupt climate change* as a large-scale change in the climate system that takes place over a few decades or less, persists (or is anticipated to persist) for at least a few decades, and causes substantial disruptions in human and natural systems (see Glossary). Other definitions of abrupt climate change exist. For example, in the AR4 climate change was defined as abrupt if it occurred faster than the typical time scale of the responsible forcing.

A number of components or phenomena within the Earth system have been proposed as potentially possessing critical thresholds (some-

times referred to as tipping points (Lenton et al., 2008)), beyond which abrupt or nonlinear transitions to a different state ensues. The term irreversibility is used in various ways in the literature. The AR5 report defines a perturbed state as *irreversible* on a given time scale if the recovery time scale from this state due to natural processes is significantly longer than the time it takes for the system to reach this perturbed state (see Glossary). In that context, most aspects of the climate change resulting from CO<sub>2</sub> emissions are irreversible, due to the long residence time of the CO<sub>2</sub> perturbation in the atmosphere and the resulting warming (Solomon et al., 2009). These results are discussed in Sections 12.5.2 to 12.5.4. Here, we also assess aspects of irreversibility in the context of abrupt change, multiple steady states and hysteresis, i.e., the question whether a change (abrupt or not) would be reversible if the forcing was reversed or removed (e.g., Boucher et al., 2012). Irreversibility of ice sheets and sea level rise are also assessed in Chapter 13.

**Table 12.4** Components in the Earth system that have been proposed in the literature as potentially being susceptible to abrupt or irreversible change. Column 2 defines whether or not a potential change can be considered to be abrupt under the AR5 definition. Column 3 states whether or not the process is irreversible in the context of abrupt change, and also gives the typical recovery time scales. Column 4 provides an assessment, if possible, of the likelihood of occurrence of abrupt change in the 21st century for the respective components or phenomena within the Earth system, for the scenarios considered in this chapter.

Change in climate system component	Potentially abrupt (AR5 definition)	Irreversibility if forcing reversed	Projected likelihood of 21st century change in scenarios considered
Atlantic MOC collapse	Yes	Unknown	<i>Very unlikely</i> that the AMOC will undergo a rapid transition ( <i>high confidence</i> )
Ice sheet collapse	No	Irreversible for millennia	<i>Exceptionally unlikely</i> that either Greenland or West Antarctic Ice sheets will suffer near-complete disintegration ( <i>high confidence</i> )
Permafrost carbon release	No	Irreversible for millennia	Possible that permafrost will become a net source of atmospheric greenhouse gases ( <i>low confidence</i> )
Clathrate methane release	Yes	Irreversible for millennia	<i>Very unlikely</i> that methane from clathrates will undergo catastrophic release ( <i>high confidence</i> )
Tropical forests dieback	Yes	Reversible within centuries	<i>Low confidence</i> in projections of the collapse of large areas of tropical forest
Boreal forests dieback	Yes	Reversible within centuries	<i>Low confidence</i> in projections of the collapse of large areas of boreal forest
Disappearance of summer Arctic sea ice	Yes	Reversible within years to decades	<i>Likely</i> that the Arctic Ocean becomes nearly ice-free in September before mid-century under high forcing scenarios such as RCP8.5 ( <i>medium confidence</i> )
Long-term droughts	Yes	Reversible within years to decades	<i>Low confidence</i> in projections of changes in the frequency and duration of megadroughts
Monsoonal circulation	Yes	Reversible within years to decades	<i>Low confidence</i> in projections of a collapse in monsoon circulations

In this section we examine the main components or phenomena within the Earth system that have been proposed in the literature as potentially being susceptible to abrupt or irreversible change (see Table 12.4). Abrupt changes that arise from nonlinearities within the climate system are inherently difficult to assess and their timing, if any, of future occurrences is difficult to predict. Nevertheless, progress is being made exploring the potential existence of early warning signs for abrupt climate change (see e.g., Dakos et al., 2008; Scheffer et al., 2009).

#### 12.5.5.2 The Atlantic Meridional Overturning

EMICs for which the stability has been systematically assessed by suitably designed hysteresis experiments robustly show a threshold beyond which the Atlantic thermohaline circulation cannot be sustained (Rahmstorf et al., 2005). This is also the case for one low-resolution ESM (Hawkins et al., 2011). However, proximity to this threshold is highly model dependent and influenced by factors that are currently poorly understood. There is some indication that the CMIP3 climate models may generally overestimate the stability of the Atlantic Ocean circulation (Hofmann and Rahmstorf, 2009; Drijfhout et al., 2010). In particular, De Vries and Weber (2005), Dijkstra (2007), Weber et al. (2007), Huisman et al. (2010), Drijfhout et al. (2010) and Hawkins et al. (2011) suggest that the sign of net freshwater flux into the Atlantic transported through its southern boundary via the overturning circulation determines whether or not the AMOC is in a mono-stable or bi-stable state. For the pre-industrial control climate of most of the CMIP3 models, Drijfhout et al. (2010) found that the salt flux was negative (implying a positive freshwater flux), indicating that they were in a mono-stable regime. However, this is not the case in the CMIP5 models where Weaver et al. (2012) found that the majority of the models were in a bi-stable regime during RCP integrations. Observations suggest that the present day ocean is in a bi-stable regime, thereby allowing for multiple equilibria and a stable ‘off’ state of the AMOC (Bryden et al., 2011; Hawkins et al., 2011).

In addition to the main threshold for a complete breakdown of the circulation, others may exist that involve more limited changes, such as a cessation of Labrador Sea deep water formation (Wood et al., 1999). Rapid melting of the Greenland ice sheet causes increases in freshwater runoff, potentially weakening the AMOC. None of the CMIP5 simulations include an interactive ice sheet component. However, Jungclaus et al. (2006), Mikolajewicz et al. (2007), Driesschaert et al. (2007) and Hu et al. (2009) found only a slight temporary effect of increased melt water fluxes on the AMOC, that was either small compared to the effect of enhanced poleward atmospheric moisture transport or only noticeable in the most extreme scenarios.

Although many more model simulations have been conducted since the AR4 under a wide range of forcing scenarios, projections of the AMOC behaviour have not changed. Based on the available CMIP5 models, EMICs and the literature, it remains *very likely* that the AMOC will weaken over the 21st century relative to pre-industrial. Best estimates and ranges for the reduction from CMIP5 are 11% (1 to 24%) in RCP2.6 and 34% (12 to 54%) in RCP8.5 (Weaver et al., 2012) (see Section 12.4.7.2, Figure 12.35). But there is *low confidence* in the magnitude of the weakening. Drijfhout et al. (2012) show that the AMOC decrease per degree global mean temperature rise varies from 1.5 to 1.9 Sv ( $10^6 \text{ m}^3 \text{ s}^{-1}$ ) for the CMIP5 multi-model ensemble members they considered depending on the scenario, but that the standard deviation in this regression is almost half the signal.

The FIO-ESM model shows cooling over much of the NH that may be related to a strong reduction of the AMOC in all RCP scenarios (even RCP2.6), but the limited output available from the model precludes an assessment of the response and realism of this response. Hence it is not included the overall assessment of the likelihood of abrupt changes.

It is *unlikely* that the AMOC will collapse beyond the end of the 21st century for the scenarios considered but a collapse beyond the 21st century for large sustained warming cannot be excluded. There is *low confidence* in assessing the evolution of the AMOC beyond the 21st century. Two of the CMIP5 models revealed an eventual slowdown of the AMOC to an off state (Figure 12.35). But this did not occur abruptly.

As assessed by Delworth et al. (2008), for an abrupt transition of the AMOC to occur, the sensitivity of the AMOC to forcing would have to be far greater than seen in current models. Alternatively, significant ablation of the Greenland ice sheet greatly exceeding even the most aggressive of current projections would be required (Swingedouw et al., 2007; Hu et al., 2009). While neither possibility can be excluded entirely, it is *unlikely* that the AMOC will collapse beyond the end of the 21st century because of global warming based on the models and range of scenarios considered.

### 12.5.5.3 Ice Sheets

As detailed in Section 13.4.3, all available modelling studies agree that the Greenland ice sheet will significantly decrease in area and volume in a warmer climate as a consequence of increased melt rates not compensated for by increased snowfall rates and amplified by positive feedbacks. Conversely, the surface mass balance of the Antarctic ice sheet is projected to increase in most projections because increased snowfall rates outweigh melt increase (see Section 13.4.4).

Irreversibility of ice sheet volume and extent changes can arise because of the surface-elevation feedback that operates when a decrease of the elevation of the ice sheet induces a decreased surface mass balance (generally through increased melting), and therefore essentially applies to Greenland. As detailed in Section 13.4.3.3, several stable states of the Greenland ice sheet might exist (Charbit et al., 2008; Ridley et al., 2010; Langen et al., 2012; Robinson et al., 2012; Solgaard and Langen, 2012), and the ice sheet might irreversibly shrink to a stable smaller state once a warming threshold is crossed for a certain amount of time, with the critical duration depending on how far the temperature threshold has been exceeded. Based on the available evidence (see Section 13.4.3.3), an irreversible decrease of the Greenland ice sheet due to surface mass balance changes appears *very unlikely* in the 21st century but *likely* on multi-centennial to millennial time scales in the strongest forcing scenarios.

In theory (Weertman, 1974; Schoof, 2007) ice sheet volume and extent changes can be abrupt because of the grounding line instability that can occur in coastal regions where bedrock is retrograde (i.e., sloping towards the interior of the ice sheet) and below sea level (see Section 4.4.4 and Box 13.2). This essentially applies to West Antarctica, but also to parts of Greenland and East Antarctica. Furthermore, ice shelf decay induced by oceanic or atmospheric warming might lead to abruptly accelerated ice flow further inland (De Angelis and Skvarca, 2003). Because ice sheet growth is usually a slow process, such changes could also be irreversible in the definition adopted here. The available evidence (see Section 13.4) suggests that it is *exceptionally unlikely* that the ice sheets of either Greenland or West Antarctica will suffer a near-complete disintegration during the 21st century. More generally, the potential for abrupt and/or irreversible ice sheet changes (or the

initiation thereof) during the 21st century and beyond is discussed in detail in Sections 13.4.3 and 13.4.4.

### 12.5.5.4 Permafrost Carbon Storage

Since the IPCC AR4, estimates of the amount of carbon stored in permafrost have been significantly revised upwards (Tarnocai et al., 2009), putting the permafrost carbon stock to an equivalent of twice the atmospheric carbon pool (Dolman et al., 2010). Because of low carbon input at high latitudes, permafrost carbon is to a large part of Pleistocene (Zimov et al., 2006) or Holocene (Smith et al., 2004) origin, and its potential vulnerability is dominated by decomposition (Eglin et al., 2010). The conjunction of a long carbon accumulation time scale on one hand and potentially rapid permafrost thawing and carbon decomposition under warmer climatic conditions (Zimov et al., 2006; Schuur et al., 2009; Kuhry et al., 2010) on the other hand suggests potential irreversibility of permafrost carbon decomposition (leading to an increase of atmospheric CO<sub>2</sub> and/or CH<sub>4</sub> concentrations) on time scales of hundreds to thousands of years in a warming climate. Indeed, recent observations (Dorrepaal et al., 2009; Kuhry et al., 2010) suggest that this process, induced by widespread permafrost warming and thawing (Romanovsky et al., 2010), might be already occurring. However, the existing modelling studies of permafrost carbon balance under future warming that take into account at least some of the essential permafrost-related processes (Khvorostyanov et al., 2008; Wania et al., 2009; Koven et al., 2011; Schaefer et al., 2011; MacDougall et al., 2012; Schneider von Deimling et al., 2012) do not yield coherent results beyond the fact that present-day permafrost might become a net emitter of carbon during the 21st century under plausible future warming scenarios (*low confidence*). This also reflects an insufficient understanding of the relevant soil processes during and after permafrost thaw, including processes leading to stabilization of unfrozen soil carbon (Schmidt et al., 2011), and precludes a firm assessment of the amplitude of irreversible changes in the climate system potentially related to permafrost degassing and associated global feedbacks at this stage (see also Sections 6.4.3.4 and 6.4.7.2 and FAQ 6.1).

### 12.5.5.5 Atmospheric Methane from Terrestrial and Oceanic Clathrates

Model simulations (Fyke and Weaver, 2006; Reagan and Moridis, 2007; Lamarque, 2008; Reagan and Moridis, 2009) suggest that clathrate deposits in shallow regions (in particular at high latitude regions and in the Gulf of Mexico) are susceptible to destabilization via ocean warming. However, concomitant sea level rise due to changes in ocean mass enhances clathrate stability in the ocean (Fyke and Weaver, 2006). A recent assessment of the potential for a future abrupt release of methane was undertaken by the U.S. Climate Change Science Program (Synthesis and Assessment Product 3.4 see Brooke et al., 2008). They concluded that it was *very unlikely* that such a catastrophic release would occur this century. However, they argued that anthropogenic warming will *very likely* lead to enhanced methane emissions from both terrestrial and oceanic clathrates (Brooke et al., 2008). Although difficult to formally assess, initial estimates of the 21st century positive feedback from methane clathrate destabilization are small but not insignificant (Fyke and Weaver, 2006; Archer, 2007; Lamarque, 2008). Nevertheless, on multi-millennial time scales, the positive feedback to anthropogenic

warming of such methane emissions is potentially larger (Archer and Buffett, 2005; Archer, 2007; Brooke et al., 2008). Once more, due to the difference between release and accumulation time scales, such emissions are irreversible. See also FAQ 6.1.

### 12.5.5.6 Tropical and Boreal Forests

#### 12.5.5.6.1 Tropical forests

In today's climate, the strongest growth in the Amazon rainforest occurs during the dry season when strong insolation is combined with water drawn from underground aquifers that store the previous wet season's rainfall (Huete et al., 2006). AOGCMs do not agree about how the dry season length in the Amazon may change in the future under the SRES A1 scenario (Bombardi and Carvalho, 2009), but simulations with coupled regional climate/potential vegetation models are consistent in simulating an increase in dry season length, a 70% reduction in the areal extent of the rainforest by the end of the 21st century using the SRES A2 scenario, and an eastward expansion of the Caatinga vegetation (Cook and Vizy, 2008; Sorensson et al., 2010). In addition, some models have demonstrated the existence of multiple equilibria of the tropical South American climate–vegetation system (e.g., Oyama and Nobre, 2003). The transition could be abrupt when the dry season becomes too long for the vegetation to survive, although the resilience of the vegetation to a longer dry period may be increased by the CO<sub>2</sub> fertilization effect (Zelazowski et al., 2011). Deforestation may also increase dry season length (Costa and Pires, 2010) and drier conditions increase the likelihood of wildfires that, combined with fire ignition associated with human activity, can undermine the forest's resiliency to climate change (see also Section 6.4.8.1). If climate change brings drier conditions closer to those supportive of seasonal forests rather than rainforest, fire can act as a trigger to abruptly and irreversibly change the ecosystem (Malhi et al., 2009). However, the existence of refugia is an important determinant of the potential for the re-emergence of the vegetation (Walker et al., 2009).

Analysis of projected change in the climate–biome space of current vegetation distributions suggest that the risk of Amazonian forest die-back is small (Malhi et al., 2009), a finding supported by modelling when strong carbon dioxide fertilization effects on Amazonian vegetation are assumed (Rammig et al., 2010). However, the strength of CO<sub>2</sub> fertilization on tropical vegetation is poorly known (see Box 6.3). Uncertainty concerning the existence of critical thresholds in the Amazonian and other tropical rainforests purely driven by climate change therefore remains high, and so the possibility of a critical threshold being crossed in precipitation volume cannot be ruled out (Nobre and Borma, 2009; Good et al., 2011b, 2011c). Nevertheless, there is still some question as to whether a transition of the Amazonian or other tropical rainforests into a lower biomass state could result from the combined effects of limits to carbon fertilization, climate warming, potential precipitation decline in interaction with the effects of human land use.

#### 12.5.5.6.2 Boreal forest

Evidence from field observations and biogeochemical modelling make it scientifically conceivable that regions of the boreal forest could tip into a different vegetation state under climate warming, but uncertainties

on the likelihood of this occurring are very high (Lenton et al., 2008; Allen et al., 2010). This is mainly due to large gaps in knowledge concerning relevant ecosystemic and plant physiological responses to warming (Niinemets, 2010). The main response is a potential advancement of the boreal forest northward and the potential transition from a forest to a woodland or grassland state on its dry southern edges in the continental interiors, leading to an overall increase in herbaceous vegetation cover in the affected parts of the boreal zone (Lucht et al., 2006). The proposed potential mechanisms for decreased forest growth and/or increased forest mortality are: increased drought stress under warmer summer conditions in regions with low soil moisture (Barber et al., 2000; Dulamsuren et al., 2009, 2010); desiccation of saplings with shallow roots due to summer drought periods in the top soil layers, causing suppression of forest reproduction (Hogg and Schwarz, 1997); leaf tissue damage due to high leaf temperatures during peak summer temperatures under strong climate warming; and increased insect, herbivory and subsequent fire damage in damaged or struggling stands (Dulamsuren et al., 2008). The balance of effects controlling standing biomass, fire type and frequency, permafrost thaw depth, snow volume and soil moisture remains uncertain. Although the existence of, and the thresholds controlling, a potential critical threshold in the boreal forest are extremely uncertain, its existence cannot at present be ruled out.

#### 12.5.5.7 Sea Ice

Several studies based on observational data or model hindcasts suggest that the rapidly declining summer Arctic sea ice cover might reach or might already have passed a tipping point (Lindsay and Zhang, 2005; Wadhams, 2012; Livina and Lenton, 2013). Identifying Arctic sea ice tipping points from the short observational record is difficult due to high interannual and decadal variability. In some climate projections, the decrease in summer Arctic sea ice areal coverage is not gradual but is instead punctuated by 5- to 10-year periods of strong ice loss (Holland et al., 2006; Vavrus et al., 2012; Dööscher and Koenigk, 2013). Still, these abrupt reductions do not necessarily require the existence of a tipping point in the system or further imply an irreversible behaviour (Amstrup et al., 2010; Lenton, 2012). The 5- to 10-year events discussed by Holland et al. (2006) arise when large natural climate variability in the Arctic reinforces the anthropogenically-forced change (Holland et al., 2008). Positive trends on the same time scale also occur when internal variability counteracts the forced change until the middle of the 21st century (Holland et al., 2008; Kay et al., 2011; Vavrus et al., 2012).

Further work using single-column energy-balance models (Merryfield et al., 2008; Eisenman and Wettlaufer, 2009; Abbot et al., 2011) yielded mixed results about the possibility of tipping points and bifurcations in the transition from perennial to seasonal sea ice cover. Thin ice and snow covers promote strong longwave radiative loss to space and high ice growth rates (e.g., Bitz and Roe, 2004; Notz, 2009; Eisenman, 2012). These stabilizing negative feedbacks can be large enough to overcome the positive surface–albedo feedback and/or cloud feedback, which act to amplify the forced sea ice response. In such low-order models, the emergence of multiple stable states with increased climate forcing is a parameter-dependent feature (Abbot et al., 2011; Eisenman, 2012). For example, Eisenman (2012) showed with a single-column energy-balance model that certain parameter choices that cause thicker ice or warmer ocean under a given climate forcing make the model more prone to bifurcations and hence irreversible behaviour.

The reversibility of sea ice loss with respect to global or hemispheric mean surface temperature change has been directly assessed in AOGCMs/ESMs by first raising the CO<sub>2</sub> concentration until virtually all sea ice disappears year-round and then lowering the CO<sub>2</sub> level at the same rate as during the ramp-up phase until it reaches again the initial value (Armour et al., 2011; Boucher et al., 2012; Ridley et al., 2012; Li et al., 2013b). None of these studies show evidence of a bifurcation leading to irreversible changes in Arctic sea ice. AOGCMs have also been used to test summer Arctic sea ice recovery after either sudden or very rapid artificial removal, and all had sea ice return within a few years (Schröder and Connolley, 2007; Sedláček et al., 2011; Tietsche et al., 2011). In the Antarctic, as a result of the strong coupling between the Southern Ocean's surface and the deep ocean, the sea ice areal coverage in some of the models integrated with ramp-up and ramp-down atmospheric CO<sub>2</sub> concentration exhibits a significant lag relative to the global or hemispheric mean surface temperature (Ridley et al., 2012; Li et al., 2013b), so that its changes may be considered irreversible on centennial time scales.

Diagnostic analyses of a few global climate models have shown abrupt sea ice losses in the transition from seasonal to year-round Arctic ice-free conditions after raising CO<sub>2</sub> to very high levels (Winton, 2006b; Ridley et al., 2008; Li et al., 2013b), but without evidence for irreversible changes. Winton (2006b, 2008) hypothesized that the small ice cap instability (North, 1984) could cause such an abrupt transition. With a low-order Arctic sea ice model, Eisenman and Wettlaufer (2009) also found an abrupt change behaviour in the transition from seasonal ice to year-round ice-free conditions, accompanied by an irreversible bifurcation to a new stable, annually ice-free state. They concluded that the cause is a loss of the stabilizing effect of sea ice growth when the ice season shrinks in time. The Arctic sea ice may thus experience a sharp transition to annually ice-free conditions, but the irreversible nature of this transition seems to depend on the model complexity and structure.

In conclusion, rapid summer Arctic sea ice losses are *likely* to occur in the transition to seasonally ice-free conditions. These abrupt changes might have consequences throughout the climate system as noted by Vavrus et al. (2011) for cloud cover and Lawrence et al. (2008b) for the high-latitude ground state. Furthermore, the interannual-to-decadal variability in the summer Arctic sea ice extent is projected to increase in response to global warming (Holland et al., 2008; Goosse et al., 2009). These studies suggest that large anomalies in Arctic sea ice areal coverage, like the ones that occurred in 2007 and 2012, might become increasingly frequent. However, there is little evidence in global climate models of a tipping point (or critical threshold) in the transition from a perennially ice-covered to a seasonally ice-free Arctic Ocean beyond which further sea ice loss is unstoppable and irreversible.

### 12.5.5.8 Hydrologic Variability: Long-Term Droughts and Monsoonal Circulation

#### 12.5.5.8.1 Long-term Droughts

As noted in Section 5.5.5, long-term droughts (often called megadroughts, see Glossary) are a recurring feature of Holocene paleoclimate records in North America, East and South Asia, Europe, Africa and India. The transitions into and out of the long-term droughts take many

years. Because the long-term droughts all ended, they are not irreversible. Nonetheless transitions over years to a decade into a state of long-term drought would have impacts on human and natural systems.

AR4 climate model projections (Milly et al., 2008) and CMIP5 ensembles (Figure 12.23) both suggest widespread drying and drought across most of southwestern North America and many other subtropical regions by the mid to late 21st century (see Section 12.4.5), although without abrupt change. Some studies suggest that this subtropical drying may have already begun in southwestern North America (Seager et al., 2007; Seidel and Randel, 2007; Barnett et al., 2008; Pierce et al., 2008). More recent studies (Hoerling et al., 2010; Seager and Vecchi, 2010; Dai, 2011; Seager and Naik, 2012) suggest that regional reductions in precipitation are due primarily to internal variability and that the anthropogenic forced trends are currently weak in comparison.

While previous long-term droughts in southwest North America arose from natural causes, climate models project that this region will undergo progressive aridification as part of a general drying and poleward expansion of the subtropical dry zones driven by rising GHGs (Held and Soden, 2006; Seager et al., 2007; Seager and Vecchi, 2010). The models project the aridification to intensify steadily as RF and global warming progress without abrupt changes. Because of the very long lifetime of the anthropogenic atmospheric CO<sub>2</sub> perturbation, such drying induced by global warming would be largely irreversible on millennium time scale (Solomon et al., 2009; Frölicher and Joos, 2010; Gillett et al., 2011) (see Sections 12.5.2 and 12.5.4). For example, Solomon et al. (2009) found in a simulation where atmospheric CO<sub>2</sub> increases to 600 ppm followed by zero emissions, that the 15% reduction in precipitation in areas such as southwest North America, southern Europe and western Australia would persist long after emissions ceased. This, however, is largely a consequence of the warming persisting for centuries after emissions cease rather than an irreversible behaviour of the water cycle itself.

#### 12.5.5.8.2 Monsoonal circulation

Climate model simulations and paleo-reconstructions provide evidence of past abrupt changes in Saharan vegetation, with the 'green Sahara' conditions (Hoelzmann et al., 1998) of the African Humid Period (AHP) during the mid-Holocene serving as the most recent example. However, Mitchell (1990) and Claussen et al. (2003) note that the mid-Holocene is not a direct analogue for future GHG-induced climate change since the forcings are different: a increased shortwave forcing in the NH summer versus a globally and seasonally uniform atmospheric CO<sub>2</sub> increase, respectively. Paleoclimate examples suggest that a strong radiative or SST forcing is needed to achieve a rapid climate change, and that the rapid changes are reversible when the forcing is withdrawn. Both the abrupt onset and termination of the AHP were triggered when northern African summer insolation was 4.2% higher than present day, representing a local increase of about 19 W m<sup>-2</sup> (deMenocal et al., 2000). Note that the globally averaged radiative anthropogenic forcing from 1750 to 2011 (Table 8.6) is small compared to this local increase in insolation. A rapid Saharan greening has been simulated in a climate model of intermediate complexity forced by a rapid increase in atmospheric CO<sub>2</sub>, with the overall extent of greening depending on the equilibrium atmospheric CO<sub>2</sub> level reached (Claussen et al., 2003).

Abrupt Saharan vegetation changes of the Younger Dryas are linked with a rapid AMOC weakening which is considered *very unlikely* during the 21st century and *unlikely* beyond that as a consequence of global warming.

Studies with conceptual models (Zickfeld et al., 2005; Levermann et al., 2009) have shown that the Indian summer monsoon can operate in two stable regimes: besides the ‘wet’ summer monsoon, a stable state exists which is characterized by low precipitation over India. These studies suggest that any perturbation of the radiative budget that tends to weaken the driving pressure gradient has the potential to induce abrupt transitions between these two regimes.

Numerous studies with coupled ocean–atmosphere models have explored the potential impact of anthropogenic forcing on the Indian monsoon (see also Section 14.2). When forced with anticipated increases in GHG concentrations, the majority of these studies show an intensification of the rainfall associated with the Indian summer monsoon (Meehl and Washington, 1993; Kitoh et al., 1997; Douville et al., 2000; Hu et al., 2000; May, 2002; Ueda et al., 2006; Kripalani et al., 2007; Stowasser et al., 2009; Cherchi et al., 2010). Despite the intensification of precipitation, several of these modelling studies show a weakening of the summer monsoon circulation (Kitoh et al., 1997; May, 2002; Ueda et al., 2006; Kripalani et al., 2007; Stowasser et al., 2009; Cherchi et al., 2010). The net effect is nevertheless an increase of precipitation due to enhanced moisture transport into the Asian monsoon region (Ueda et al., 2006). In recent years, studies with GCMs have also explored the direct effect of aerosol forcing on the Indian monsoon (Lau et al., 2006; Meehl et al., 2008; Randles and Ramaswamy, 2008; Collier and Zhang, 2009). Considering absorbing aerosols (black carbon) only, Meehl et al. (2008) found an increase in pre-monsoonal precipitation, but a decrease in summer monsoon precipitation over parts of South Asia. In contrast, Lau et al. (2006) found an increase in May–June–July precipitation in that region. If an increase in scattering aerosols only is considered, the monsoon circulation weakens and precipitation is inhibited (Randles and Ramaswamy, 2008). More recently, Bollasina et al. (2011) showed that anthropogenic aerosols played a fundamental role in driving the recent observed weakening of the summer monsoon. Given that the effect of increased atmospheric regional loading of aerosols is opposed by the concomitant increases in GHG concentrations, it is *unlikely* that an abrupt transition to the dry summer monsoon regime will be triggered in the 21st century.

## Acknowledgements

We especially acknowledge the input of Contributing Authors Urs Beyerle for maintaining the database of CMIP5 output, Jan Sedláček for producing a large number of CMIP5 figures, and Joeri Rogelj for preparing synthesis figures. Chapter technical assistants Oliver Stebler, Franziska Gerber and Barbara Aellig, provided great help in assembling the chapter and Sébastien Denvil and Jérôme Raciazek provided technical assistance in downloading the CMIP5 data.

## References

- Abbot, D. S., M. Silber, and R. T. Pierrehumbert, 2011: Bifurcations leading to summer Arctic sea ice loss. *J. Geophys. Res.*, **116**, D19120.
- Abe, M., H. Shioigama, T. Nozawa, and S. Emori, 2011: Estimation of future surface temperature changes constrained using the future-present correlated modes in inter-model variability of CMIP3 multimodel simulations. *J. Geophys. Res.*, **116**, D18104.
- Adachi, Y., et al., 2013: Basic performance of a new earth system model of the Meteorological Research Institute (MRI-ESM1). *Papers Meteorol. Geophys.*, doi:10.2467/mrpapers.64.
- Adams, P. J., J. H. Seinfeld, D. Koch, L. Mickley, and D. Jacob, 2001: General circulation model assessment of direct radiative forcing by the sulfate-nitrate-ammonium-water inorganic aerosol system. *J. Geophys. Res.*, **106**, 1097–1111.
- Adler, R. F., G. J. Gu, J. J. Wang, G. J. Huffman, S. Curtis, and D. Bolvin, 2008: Relationships between global precipitation and surface temperature on interannual and longer timescales (1979–2006). *J. Geophys. Res.*, **113**, D22104.
- Aldrin, M., M. Holden, P. Guttorp, R. B. Skeie, G. Myhre, and T. K. Berntsen, 2012: Bayesian estimation of climate sensitivity based on a simple climate model fitted to observations of hemispheric temperatures and global ocean heat content. *Environmetrics*, **23**, 253–271.
- Alexander, L. V., and J. M. Arblaster, 2009: Assessing trends in observed and modelled climate extremes over Australia in relation to future projections. *Int. J. Climatol.*, **29**, 417–435.
- Alexander, L. V., et al., 2006: Global observed changes in daily climate extremes of temperature and precipitation. *J. Geophys. Res.*, **111**, D05109.
- Alexeev, V., and C. Jackson, 2012: Polar amplification: Is atmospheric heat transport important? *Clim. Dyn.*, doi:10.1007/s00382-012-1601-z.
- Alexeev, V., D. Nicolsky, V. Romanovsky, and D. Lawrence, 2007: An evaluation of deep soil configurations in the CLM3 for improved representation of permafrost. *Geophys. Res. Lett.*, **34**, L09502.
- Alexeev, V. A., P. L. Langen, and J. R. Bates, 2005: Polar amplification of surface warming on an aquaplanet in “ghost forcing” experiments without sea ice feedbacks. *Clim. Dyn.*, **24**, 655–666.
- Allan, R., and B. Soden, 2008: Atmospheric warming and the amplification of precipitation extremes. *Science*, **321**, 1481–1484.
- Allan, R. P., 2012: Regime dependent changes in global precipitation. *Clim. Dyn.*, doi:10.1007/s00382-011-1134-x.
- Allen, C., et al., 2010: A global overview of drought and heat-induced tree mortality reveals emerging climate change risks for forests. *Forest Ecol. Manage.*, **259**, 660–684.
- Allen, M. R., and W. J. Ingram, 2002: Constraints on future changes in climate and the hydrologic cycle. *Nature*, **419**, 224–232.
- Allen, M. R., D. J. Frame, C. Huntingford, C. D. Jones, J. A. Lowe, M. Meinshausen, and N. Meinshausen, 2009: Warming caused by cumulative carbon emissions towards the trillionth tonne. *Nature*, **458**, 1163–1166.
- Allen, R. J., and S. C. Sherwood, 2008: Warming maximum in the tropical upper troposphere deduced from thermal winds. *Nature Geosci.*, **1**, 399–403.
- Allen, R. J., and S. C. Sherwood, 2010: Aerosol-cloud semi-direct effect and land-sea temperature contrast in a GCM. *Geophys. Res. Lett.*, **37**, L07702.
- Allen, R. J., S. C. Sherwood, J. R. Norris, and C. S. Zender, 2012: Recent Northern Hemisphere tropical expansion primarily driven by black carbon and tropospheric ozone. *Nature*, **485**, 350–354.
- Amstrup, S., E. DeWeaver, D. Douglas, B. Marcot, G. Durner, C. Bitz, and D. Bailey, 2010: Greenhouse gas mitigation can reduce sea-ice loss and increase polar bear persistence. *Nature*, **468**, 955–958.
- Andrews, T., and P. M. Forster, 2008: CO<sub>2</sub> forcing induces semi-direct effects with consequences for climate feedback interpretations. *Geophys. Res. Lett.*, **35**, L04802.
- Andrews, T., P. M. Forster, and J. M. Gregory, 2009: A surface energy perspective on climate change. *J. Clim.*, **22**, 2557–2570.
- Andrews, T., P. Forster, O. Boucher, N. Bellouin, and A. Jones, 2010: Precipitation, radiative forcing and global temperature change. *Geophys. Res. Lett.*, **37**, L14701.
- Annan, J. D., and J. C. Hargreaves, 2006: Using multiple observationally-based constraints to estimate climate sensitivity. *Geophys. Res. Lett.*, **33**, L06704.
- Annan, J. D., and J. C. Hargreaves, 2010: Reliability of the CMIP3 ensemble. *Geophys. Res. Lett.*, **37**, L02703.
- Annan, J. D., and J. C. Hargreaves, 2011a: Understanding the CMIP3 multi-model ensemble. *J. Clim.*, **24**, 4529–4538.
- Annan, J. D., and J. C. Hargreaves, 2011b: On the generation and interpretation of probabilistic estimates of climate sensitivity. *Clim. Change*, **104**, 423–436.
- Arblaster, J. M., G. A. Meehl, and D. J. Karoly, 2011: Future climate change in the Southern Hemisphere: Competing effects of ozone and greenhouse gases. *Geophys. Res. Lett.*, **38**, L02701.
- Archer, D., 2007: Methane hydrate stability and anthropogenic climate change. *Biogeosciences*, **4**, 521–544.
- Archer, D., and B. Buffett, 2005: Time-dependent response of the global ocean clathrate reservoir to climatic and anthropogenic forcing. *Geochem. Geophys. Geosyst.*, **6**, Q03002.
- Archer, D., et al., 2009: Atmospheric lifetime of fossil fuel carbon dioxide. *Annu. Rev. Earth Planet. Sci.*, **37**, 117–134.
- Armour, K., and G. Roe, 2011: Climate commitment in an uncertain world. *Geophys. Res. Lett.*, **38**, L01707.
- Armour, K., I. Eisenman, E. Blanchard-Wrigglesworth, K. McCusker, and C. Bitz, 2011: The reversibility of sea ice loss in a state-of-the-art climate model. *Geophys. Res. Lett.*, **38**, L16705.
- Arora, V. K., et al., 2011: Carbon emission limits required to satisfy future representative concentration pathways of greenhouse gases. *Geophys. Res. Lett.*, **38**, L05805.
- Arzel, O., T. Fichefet, and H. Goosse, 2006: Sea ice evolution over the 20th and 21st centuries as simulated by current AOGCMs. *Ocean Model.*, **12**, 401–415.
- Augustsson, T., and V. Ramanathan, 1977: Radiative-convective model study of CO<sub>2</sub> climate problem. *J. Atmos. Sci.*, **34**, 448–451.
- Bala, G., K. Caldeira, and R. Nemani, 2010: Fast versus slow response in climate change: Implications for the global hydrological cycle. *Clim. Dyn.*, **35**, 423–434.
- Baldwin, M. P., M. Dameris, and T. G. Shepherd, 2007: Atmosphere—How will the stratosphere affect climate change? *Science*, **316**, 1576–1577.
- Ballester, J., F. Giorgi, and X. Rodo, 2010a: Changes in European temperature extremes can be predicted from changes in PDF central statistics. *Clim. Change*, **98**, 277–284.
- Ballester, J., X. Rodo, and F. Giorgi, 2010b: Future changes in Central Europe heat waves expected to mostly follow summer mean warming. *Clim. Dyn.*, **35**, 1191–1205.
- Banks, H. T., and J. M. Gregory, 2006: Mechanisms of ocean heat uptake in a coupled climate model and the implications for tracer based predictions of ocean heat uptake. *Geophys. Res. Lett.*, **33**, L07608.
- Bao, Q., et al., 2013: The Flexible Global Ocean-Atmosphere-Land system model, Spectral Version 2: FGOALS-s2. *Adv. Atmos. Sci.*, **30**, 561–576.
- Barber, V., G. Juday, and B. Finney, 2000: Reduced growth of Alaskan white spruce in the twentieth century from temperature-induced drought stress. *Nature*, **405**, 668–673.
- Barnes, E. A., and L. M. Polvani, 2013: Response of the midlatitude jets and of their variability to increased greenhouse gases in the CMIP5 models. *J. Clim.*, doi:10.1175/JCLI-D-12-00536.1.
- Barnett, D. N., S. J. Brown, J. M. Murphy, D. M. H. Sexton, and M. J. Webb, 2006: Quantifying uncertainty in changes in extreme event frequency in response to doubled CO<sub>2</sub> using a large ensemble of GCM simulations. *Clim. Dyn.*, **26**, 489–511.
- Barnett, T., and D. Pierce, 2008: When will Lake Mead go dry? *Water Resour. Res.*, **44**, W03201.
- Barnett, T. P., et al., 2008: Human-induced changes in the hydrology of the western United States. *Science*, **319**, 1080–1083.
- Barriopedro, D., E. M. Fischer, J. Luterbacher, R. Trigo, and R. Garcia-Herrera, 2011: The hot summer of 2010: Redrawing the temperature record map of Europe. *Science*, **332**, 220–224.
- Bekryaev, R. V., I. V. Polyakov, and V. A. Alexeev, 2010: Role of polar amplification in long-term surface air temperature variations and modern Arctic warming. *J. Clim.*, **23**, 3888–3906.
- Bellouin, N., J. Rae, A. Jones, C. Johnson, J. Haywood, and O. Boucher, 2011: Aerosol forcing in the Hadley Centre CMIP5 simulations and the role of ammonium nitrate. *J. Geophys. Res.*, **116**, D20206.
- Bengtsson, L., K. I. Hodges, and E. Roeckner, 2006: Storm tracks and climate change. *J. Clim.*, **19**, 3518–3543.

- Bengtsson, L., K. I. Hodges, and N. Keenlyside, 2009: Will extratropical storms intensify in a warmer climate? *J. Clim.*, **22**, 2276–2301.
- Berg, P., J. O. Haerter, P. Thejll, C. Piani, S. Hagemann, and J. H. Christensen, 2009: Seasonal characteristics of the relationship between daily precipitation intensity and surface temperature. *J. Geophys. Res.*, **114**, D18102.
- Beets, R., et al., 2007: Projected increase in continental runoff due to plant responses to increasing carbon dioxide. *Nature*, **448**, 1037–1041.
- Bitz, C., and G. Roe, 2004: A mechanism for the high rate of sea ice thinning in the Arctic Ocean. *J. Clim.*, **17**, 3623–3632.
- Bitz, C., and Q. Fu, 2008: Arctic warming aloft is data set dependent. *Nature*, **455**, E3–E4.
- Bitz, C. M., 2008: Some aspects of uncertainty in predicting sea ice thinning. In: *Arctic Sea Ice Decline: Observations, Projections, Mechanisms, and Implications* [E. T. DeWeaver, C. M. Bitz and L. B. Tremblay (eds.)]. American Geophysical Union, Washington, DC, pp. 63–76.
- Bitz, C. M., J. K. Ridley, M. M. Holland, and H. Cattle, 2012: Global climate models and 20th and 21st century Arctic climate change. In: *Arctic Climate Change – The ACSYS Decade and Beyond* [P. Lemke (ed.)]. Springer Science+Business Media, Dordrecht, Netherlands, pp. 405–436.
- Boberg, F., P. Berg, P. Thejll, W. Gutowski, and J. Christensen, 2010: Improved confidence in climate change projections of precipitation evaluated using daily statistics from the PRUDENCE ensemble. *Clim. Dyn.*, **35**, 1097–1106.
- Boé, J., and L. Terray, 2008: Uncertainties in summer evapotranspiration changes over Europe and implications for regional climate change. *Geophys. Res. Lett.*, **35**, L05702.
- Boé, J., A. Hall, and X. Qu, 2009a: Current GCMs' unrealistic negative feedback in the Arctic. *J. Clim.*, **22**, 4682–4695.
- Boé, J. L., A. Hall, and X. Qu, 2009b: September sea-ice cover in the Arctic Ocean projected to vanish by 2100. *Nature Geosci.*, **2**, 341–343.
- Boer, G. J., 1993: Climate change and the regulation of the surface moisture and energy budgets. *Clim. Dyn.*, **8**, 225–239.
- Boer, G. J., 2011: The ratio of land to ocean temperature change under global warming. *Clim. Dyn.*, **37**, 2253–2270.
- Boer, G. J., and B. Yu, 2003: Climate sensitivity and response. *Clim. Dyn.*, **20**, 415–429.
- Boer, G. J., K. Hamilton, and W. Zhu, 2005: Climate sensitivity and climate change under strong forcing. *Clim. Dyn.*, **24**, 685–700.
- Ballasina, M. A., Y. Ming, and V. Ramaswamy, 2011: Anthropogenic aerosols and the weakening of the South Asian summer monsoon. *Science*, **334**, 502–505.
- Bombardi, R., and L. Carvalho, 2009: IPCC global coupled model simulations of the South America monsoon system. *Clim. Dyn.*, **33**, 893–916.
- Böning, C., A. Dispert, M. Visbeck, S. Rintoul, and F. Schwarzkopf, 2008: The response of the Antarctic Circumpolar Current to recent climate change. *Nature Geosci.*, **1**, 864–869.
- Bony, S., and J. L. Dufresne, 2005: Marine boundary layer clouds at the heart of tropical cloud feedback uncertainties in climate models. *Geophys. Res. Lett.*, **32**, L20806.
- Bony, S., G. Bellon, D. Klocke, S. Sherwood, S. Fermeipin, and S. Denvil, 2013: Robust direct effect of carbon dioxide on tropical circulation and regional precipitation. *Nature Geosci.*, doi:10.1038/ngeo1799.
- Bony, S., et al., 2006: How well do we understand and evaluate climate change feedback processes? *J. Clim.*, **19**, 3445–3482.
- Booth, B. B., et al., 2012: High sensitivity of future global warming to land carbon cycle processes. *Environ. Res. Lett.*, **7**, 024002.
- Boucher, O., et al., 2012: Reversibility in an Earth System model in response to CO<sub>2</sub> concentration changes. *Environ. Res. Lett.*, **7**, 024013.
- Bouttes, N., J. M. Gregory, and J. A. Lowe, 2013: The reversibility of sea level rise. *J. Clim.*, **26**, 2502–2513.
- Bowman, N., D. Frame, C. Huntingford, J. Lowe, and M. Allen, 2011: Cumulative carbon emissions, emissions floors and short-term rates of warming: Implications for policy. *Philos. Trans. R. Soc. A*, **369**, 45–66.
- Bracegirdle, T., and D. Stephenson, 2012: Higher precision estimates of regional polar warming by ensemble regression of climate model projections. *Clim. Dyn.*, **39**, 2805–2821.
- Bracegirdle, T., W. Connolley, and J. Turner, 2008: Antarctic climate change over the twenty first century. *J. Geophys. Res.*, **113**, D03103.
- Bracegirdle, T. J., et al., 2013: Assessment of surface winds over the Atlantic, Indian, and Pacific Ocean sectors of the Southern Ocean in CMIP5 models: Historical bias, forcing response, and state dependence. *J. Geophys. Res.*, **118**, 547–562.
- Brasseur, G., and E. Roeckner, 2005: Impact of improved air quality on the future evolution of climate. *Geophys. Res. Lett.*, **32**, L23704.
- Brient, F., and S. Bony, 2013: Interpretation of the positive low-cloud feedback predicted by a climate model under global warming. *Clim. Dyn.*, **40**, 2415–2431.
- Brierley, C. M., M. Collins, and A. J. Thorpe, 2010: The impact of perturbations to ocean-model parameters on climate and climate change in a coupled model. *Clim. Dyn.*, **34**, 325–343.
- Bromwich, D. H., J. P. Nicolas, A. J. Monaghan, M. A. Lazzara, L. M. Keller, G. A. Weidner, and A. B. Wilson, 2013: Central West Antarctica among the most rapidly warming regions on Earth. *Nature Geosci.*, **6**, 139–145.
- Brooke, E., D. Archer, E. Dlugokencky, S. Frolking, and D. Lawrence, 2008: Potential for abrupt changes in atmospheric methane. *Abrupt Climate Change: A Report by the U.S. Climate Change Science Program and the Subcommittee on Global Change Research*. U.S. Geological Survey, Washington, DC, pp. 163–201.
- Brooks, H. E., 2009: Proximity soundings for severe convection for Europe and the United States from reanalysis data. *Atmos. Res.*, **93**, 546–553.
- Brooks, H. E., 2013: Severe thunderstorms and climate change. *Atmos. Res.*, **123**, 129–138.
- Brooks, H. E., J. W. Lee, and J. P. Craven, 2003: The spatial distribution of severe thunderstorm and tornado environments from global reanalysis data. *Atmos. Res.*, **67–68**, 73–94.
- Brovkin, V., et al., 2013: Effect of anthropogenic land-use and land cover changes on climate and land carbon storage in CMIP5 projections for the 21st century. *J. Clim.*, doi:10.1175/JCLI-D-12-00623.1.
- Brown, R., and P. Mote, 2009: The response of Northern Hemisphere snow cover to a changing climate. *J. Clim.*, **22**, 2124–2145.
- Brown, R. D., and D. A. Robinson, 2011: Northern Hemisphere spring snow cover variability and change over 1922–2010 including an assessment of uncertainty. *Cryosphere*, **5**, 219–229.
- Brutel-Vuilmet, C., M. Menegoz, and G. Krinner, 2013: An analysis of present and future seasonal Northern Hemisphere land snow cover simulated by CMIP5 coupled climate models. *Cryosphere*, **7**, 67–80.
- Bryan, K., F. G. Komro, S. Manabe, and M. J. Spelman, 1982: Transient climate response to increasing atmospheric carbon-dioxide. *Science*, **215**, 56–58.
- Bryden, H. L., B. A. King, and G. D. McCarthy, 2011: South Atlantic overturning circulation at 24S. *J. Mar. Res.*, **69**, 38–55.
- Burke, E., and S. Brown, 2008: Evaluating uncertainties in the projection of future drought. *J. Hydrometeorol.*, **9**, 292–299.
- Burke, E. J., C. D. Jones, and C. D. Koven, 2012: Estimating the permafrost-carbon-climate response in the CMIP5 climate models using a simplified approach. *J. Clim.*, doi:10.1175/JCLI-D-12-00550.1.
- Buser, C. M., H. R. Kunsch, D. Luthi, M. Wild, and C. Schär, 2009: Bayesian multi-model projection of climate: Bias assumptions and interannual variability. *Clim. Dyn.*, **33**, 849–868.
- Butchart, N., and A. A. Scaife, 2001: Removal of chlorofluorocarbons by increased mass exchange between the stratosphere and troposphere in a changing climate. *Nature*, **410**, 799–802.
- Butchart, N., et al., 2006: Simulations of anthropogenic change in the strength of the Brewer-Dobson circulation. *Clim. Dyn.*, **27**, 727–741.
- Butchart, N., et al., 2010: Chemistry-climate model simulations of twenty-first century stratospheric climate and circulation changes. *J. Clim.*, **23**, 5349–5374.
- Butler, A. H., D. W. J. Thompson, and R. Heikes, 2010: The steady-state atmospheric circulation response to climate change-like thermal forcings in a simple General Circulation Model. *J. Clim.*, **23**, 3474–3496.
- Cabré, M. F., S. A. Solman, and M. N. Nunez, 2010: Creating regional climate change scenarios over southern South America for the 2020's and 2050's using the pattern scaling technique: Validity and limitations. *Clim. Change*, **98**, 449–469.
- Caesar, J., and J. A. Lowe, 2012: Comparing the impacts of mitigation versus non-intervention scenarios on future temperature and precipitation extremes in the HadGEM2 climate model. *J. Geophys. Res.*, **117**, D15109.
- Cagnazzo, C., E. Manzini, P. G. Fogli, M. Vichi, and P. Davini, 2013: Role of stratospheric dynamics in the ozone–carbon connection in the Southern Hemisphere. *Clim. Dyn.*, doi:10.1007/s00382-013-1745-5.
- Cai, M., 2005: Dynamical amplification of polar warming. *Geophys. Res. Lett.*, **32**, L22710.
- Caldeira, K., and J. F. Kasting, 1993: Insensitivity of global warming potentials to carbon-dioxide emission scenarios. *Nature*, **366**, 251–253.
- Caldwell, P., and C. S. Bretherton, 2009: Response of a subtropical stratocumulus-capped mixed layer to climate and aerosol changes. *J. Clim.*, **22**, 20–38.

- Calvo, N., and R. R. Garcia, 2009: Wave forcing of the tropical upwelling in the lower stratosphere under increasing concentrations of greenhouse gases. *J. Atmos. Sci.*, **66**, 3184–3196.
- Calvo, N., R. R. Garcia, D. R. Marsh, M. J. Mills, D. E. Kinnison, and P. J. Young, 2012: Reconciling modeled and observed temperature trends over Antarctica. *Geophys. Res. Lett.*, **39**, L16803.
- Cao, L., and K. Caldeira, 2010: Atmospheric carbon dioxide removal: Long-term consequences and commitment. *Environ. Res. Lett.*, **5**, 024011.
- Cao, L., G. Bala, and K. Caldeira, 2012: Climate response to changes in atmospheric carbon dioxide and solar irradiance on the time scale of days to weeks. *Environ. Res. Lett.*, **7**, 034015.
- Capotondi, A., M. Alexander, N. Bond, E. Curchitser, and J. Scott, 2012: Enhanced upper ocean stratification with climate change in the CMIP3 models. *J. Geophys. Res.*, **117**, C04031.
- Caroli, D., and H. Teyssedre, 2007: A revised linear ozone photochemistry parameterization for use in transport and general circulation models: Multi-annual simulations. *Atmos. Chem. Phys.*, **7**, 2183–2196.
- Carslaw, K., O. Boucher, D. Spracklen, G. Mann, J. Rae, S. Woodward, and M. Kulmala, 2010: A review of natural aerosol interactions and feedbacks within the Earth system. *Atmos. Chem. Phys.*, **10**, 1701–1737.
- Catto, J. L., L. C. Shaffrey, and K. I. Hodges, 2011: Northern Hemisphere extratropical cyclones in a warming climate in the HiGEM high-resolution climate model. *J. Clim.*, **24**, 5336–5352.
- CCSP, 2008a: *Weather and Climate Extremes in a Changing Climate: A Report by the U.S. Climate Change Science Program and the Subcommittee on Global Change Research*. Department of Commerce, NOAA's National Climatic Data Center, College Park, MD, 164 pp.
- CCSP, 2008b: *Abrupt Climate Change. A Report by the U.S. Climate Change Science Program and the Subcommittee on Global Change Research*. U.S. Geological Survey, Washington, DC, 459 pp.
- Cess, R., et al., 1990: Intercomparison and interpretation of climate feedback processes in 19 atmospheric general-circulation models. *J. Geophys. Res.*, **95**, 16601–16615.
- Chadwick, R., I. Boulle, and G. Martin, 2012: Spatial patterns of precipitation change in CMIP5: Why the rich don't get richer in the Tropics. *J. Clim.*, doi:10.1175/JCLI-D-12-00543.1.
- Chadwick, R., P. Wu, P. Good, and T. Andrews, 2013: Asymmetries in tropical rainfall and circulation patterns in idealised CO<sub>2</sub> removal experiments. *Clim. Dyn.*, **40**, 295–316.
- Chang, E. K. M., Y. Guo, and X. Xia, 2012a: CMIP5 multimodel ensemble projection of storm track change under global warming. *J. Geophys. Res.*, **117**, D23118.
- Chang, E. K. M., Y. Guo, X. Xia, and M. Zheng, 2012b: Storm track activity in IPCC AR4/CMIP3 model simulations. *J. Clim.*, **26**, 246–260.
- Chapin, F., et al., 2005: Role of land-surface changes in Arctic summer warming. *Science*, **310**, 657–660.
- Charbit, S., D. Paillard, and G. Ramstein, 2008: Amount of CO<sub>2</sub> emissions irreversibly leading to the total melting of Greenland. *Geophys. Res. Lett.*, **35**, L12503.
- Charney, J. G., 1979: *Carbon Dioxide and Climate: A Scientific Assessment*. National Academies of Science Press, Washington, DC, 22 pp.
- Chen, C. T., and T. Knutson, 2008: On the verification and comparison of extreme rainfall indices from climate models. *J. Clim.*, **21**, 1605–1621.
- Chen, G., J. Lu, and D. M. W. Frierson, 2008: Phase speed spectra and the latitude of surface westerlies: Interannual variability and global warming trend. *J. Clim.*, **21**, 5942–5959.
- Cherchi, A., A. Alessandri, S. Masina, and A. Navarra, 2010: Effect of increasing CO<sub>2</sub> levels on monsoons. *Clim. Dyn.*, **37**, 83–101.
- Choi, D. H., J. S. Kug, W. T. Kwon, F. F. Jin, H. J. Baek, and S. K. Min, 2010: Arctic Oscillation responses to greenhouse warming and role of synoptic eddy feedback. *J. Geophys. Res. Atmos.*, **115**, D17103.
- Chou, C., and J. D. Neelin, 2004: Mechanisms of global warming impacts on regional tropical precipitation. *J. Clim.*, **17**, 2688–2701.
- Chou, C., and C. Chen, 2010: Depth of convection and the weakening of tropical circulation in global warming. *J. Clim.*, **23**, 3019–3030.
- Chou, C., and C.-W. Lan, 2012: Changes in the annual range of precipitation under global warming. *J. Clim.*, **25**, 222–235.
- Chou, C., J. D. Neelin, J. Y. Tu, and C. T. Chen, 2006: Regional tropical precipitation change mechanisms in ECHAM4/OPYC3 under global warming. *J. Clim.*, **19**, 4207–4223.
- Chou, C., J. D. Neelin, C. A. Chen, and J. Y. Tu, 2009: Evaluating the "Rich-Get-Richer" mechanism in tropical precipitation change under global warming. *J. Clim.*, **22**, 1982–2005.
- Chou, C., C. Chen, P.-H. Tan, and K.-T. Chen, 2012: Mechanisms for global warming impacts on precipitation frequency and intensity. *J. Clim.*, **25**, 3291–3306.
- Chou, C., J. C. H. Chiang, C.-W. Lan, C.-H. Chung, Y.-C. Liao, and C.-J. Lee, 2013: Increase in the range between wet and dry season precipitation. *Nature Geosci.*, **6**, 263–267.
- Christensen, J. H., F. Boberg, O. B. Christensen, and P. Lucas-Picher, 2008: On the need for bias correction of regional climate change projections of temperature and precipitation. *Geophys. Res. Lett.*, **35**, L20709.
- Christensen, J. H., et al., 2007: Regional climate projections. In: *Climate Change 2007: The Physical Science Basis. Contribution of Working Group I to the Fourth Assessment Report of the Intergovernmental Panel on Climate Change* [Solomon, S., D. Qin, M. Manning, Z. Chen, M. Marquis, K. B. Averyt, M. Tignor and H. L. Miller (eds.)] Cambridge University Press, Cambridge, United Kingdom and New York, NY, USA, pp. 847–940.
- Christensen, N., and D. Lettenmaier, 2007: A multimodel ensemble approach to assessment of climate change impacts on the hydrology and water resources of the Colorado River Basin. *Hydrol. Earth Syst. Sci.*, **11**, 1417–1434.
- Cionni, I., et al., 2011: Ozone database in support of CMIP5 simulations: Results and corresponding radiative forcing. *Atmos. Chem. Phys.*, **11**, 11267–11292.
- Clark, R. T., S. J. Brown, and J. M. Murphy, 2006: Modeling Northern Hemisphere summer heat extreme changes and their uncertainties using a physics ensemble of climate sensitivity experiments. *J. Clim.*, **19**, 4418–4435.
- Clark, R. T., J. M. Murphy, and S. J. Brown, 2010: Do global warming targets limit heatwave risk? *Geophys. Res. Lett.*, **37**, L17703.
- Claussen, M., V. Brovkin, A. Ganopolski, C. Kubatzki, and V. Petoukhov, 2003: Climate change in northern Africa: The past is not the future. *Clim. Change*, **57**, 99–118.
- Colle, B. A., Z. Zhang, K. A. Lombardo, E. Chang, P. Liu, and M. Zhang, 2013: Historical evaluation and future prediction of eastern North America and western Atlantic extratropical cyclones in the CMIP5 models during the cool season. *J. Clim.*, doi:10.1175/JCLI-D-12-00498.1.
- Collier, J., and G. Zhang, 2009: Aerosol direct forcing of the summer Indian monsoon as simulated by the NCAR CAM3. *Clim. Dyn.*, **32**, 313–332.
- Collins, M., C. M. Brierley, M. MacVean, B. B. B. Booth, and G. R. Harris, 2007: The sensitivity of the rate of transient climate change to ocean physics perturbations. *J. Clim.*, **20**, 2315–2320.
- Collins, M., B. B. B. Booth, G. Harris, J. M. Murphy, D. M. H. Sexton, and M. J. Webb, 2006a: Towards quantifying uncertainty in transient climate change. *Clim. Dyn.*, **27**, 127–147.
- Collins, M., R. E. Chandler, P. M. Cox, J. M. Huthnance, J. Rougier, and D. B. Stephenson, 2012: Quantifying future climate change. *Nature Clim. Change*, **2**, 403–409.
- Collins, M., B. Booth, B. Bhaskaran, G. Harris, J. Murphy, D. Sexton, and M. Webb, 2011: Climate model errors, feedbacks and forcings: A comparison of perturbed physics and multi-model ensembles. *Clim. Dyn.*, **36**, 1737–1766.
- Collins, M., et al., 2010: The impact of global warming on the tropical Pacific ocean and El Niño. *Nature Geosci.*, **3**, 391–397.
- Collins, W. D., et al., 2006b: Radiative forcing by well-mixed greenhouse gases: Estimates from climate models in the Intergovernmental Panel on Climate Change (IPCC) Fourth Assessment Report (AR4). *J. Geophys. Res.*, **111**, D14317.
- Colman, R., and B. McAvaney, 2009: Climate feedbacks under a very broad range of forcing. *Geophys. Res. Lett.*, **36**, L01702.
- Colman, R., and S. Power, 2010: Atmospheric radiative feedbacks associated with transient climate change and climate variability. *Clim. Dyn.*, **34**, 919–933.
- Comiso, J. C., and F. Nishio, 2008: Trends in the sea ice cover using enhanced and compatible AMSR-E, SSM/I, and SMMR data. *J. Geophys. Res.*, **113**, C02S07.
- Cook, K., and E. Vizy, 2008: Effects of twenty-first-century climate change on the Amazon rain forest. *J. Clim.*, **21**, 542–560.
- Costa, M., and G. Pires, 2010: Effects of Amazon and Central Brazil deforestation scenarios on the duration of the dry season in the arc of deforestation. *Int. J. Climatol.*, **30**, 1970–1979.
- Crook, J. A., P. M. Forster, and N. Stuber, 2011: Spatial patterns of modeled climate feedback and contributions to temperature response and polar amplification. *J. Clim.*, **24**, 3575–3592.
- Crucifix, M., 2006: Does the Last Glacial Maximum constrain climate sensitivity? *Geophys. Res. Lett.*, **33**, L18701.

- Cruz, F. T., A. J. Pitman, J. L. McGregor, and J. P. Evans, 2010: Contrasting regional responses to increasing leaf-level atmospheric carbon dioxide over Australia. *J. Hydrometeorol.*, **11**, 296–314.
- Dai, A., 2011: Drought under global warming: A review. *WIREs Clim. Change*, **2**, 45–65.
- Dai, A., 2013: Increasing drought under global warming in observations and models. *Nature Clim. Change*, **3**, 52–58.
- Dakos, V., M. Scheffer, E. H. van Nes, V. Brovkin, V. Petoukhov, and H. Held, 2008: Slowing down as an early warning signal for abrupt climate change. *Proc. Natl. Acad. Sci. U.S.A.*, **105**, 14308–14312.
- Danabasoglu, G., and P. Gent, 2009: Equilibrium climate sensitivity: Is it accurate to use a slab ocean model? *J. Clim.*, **22**, 2494–2499.
- Davin, E. L., N. de Noblet-Ducoudre, and P. Friedlingstein, 2007: Impact of land cover change on surface climate: Relevance of the radiative forcing concept. *Geophys. Res. Lett.*, **34**, L13702.
- Davis, S., K. Caldeira, and H. Matthews, 2010: Future CO<sub>2</sub> emissions and climate change from existing energy infrastructure. *Science*, **329**, 1330–1333.
- Davis, S. M., and K. H. Rosenlof, 2012: A multidagnostic intercomparison of tropical-width time series using reanalyses and satellite observations. *J. Clim.*, **25**, 1061–1078.
- De Angelis, H., and P. Skvarca, 2003: Glacier surge after ice shelf collapse. *Science*, **299**, 1560–1562.
- de Vries, H., R. J. Haarsma, and W. Hazeleger, 2012: Western European cold spells in current and future climate. *Geophys. Res. Lett.*, **39**, L04706.
- de Vries, P., and S. Weber, 2005: The Atlantic freshwater budget as a diagnostic for the existence of a stable shut down of the meridional overturning circulation. *Geophys. Res. Lett.*, **32**, L09606.
- Del Genio, A. D., M.-S. Yao, and J. Jonas, 2007: Will moist convection be stronger in a warmer climate? *Geophys. Res. Lett.*, **34**, L16703.
- Delisle, G., 2007: Near-surface permafrost degradation: How severe during the 21st century? *Geophys. Res. Lett.*, **34**, L09503.
- Delworth, T. L., et al., 2008: The potential for abrupt change in the Atlantic meridional overturning circulation. In: *Abrupt Climate Change: A Report by the U.S. Climate Change Science Program and the Subcommittee on Global Change Research*, U.S. Geological Survey, Washington, DC, pp. 258–359.
- deMenocal, P., J. Ortiz, T. Guilderson, J. Adkins, M. Sarnthein, L. Baker, and M. Yarusinsky, 2000: Abrupt onset and termination of the African Humid Period: Rapid climate responses to gradual insolation forcing. *Quaternary Science Reviews*, **19**, 347–361.
- Deser, C., A. Phillips, V. Bourdette, and H. Teng, 2012a: Uncertainty in climate change projections: The role of internal variability. *Clim. Dyn.*, **38**, 527–546.
- Deser, C., R. Knutti, S. Solomon, and A. S. Phillips, 2012b: Communication of the role of natural variability in future North American climate. *Nature Clim. Change*, **2**, 775–779.
- Dessai, S., X. F. Lu, and M. Hulme, 2005: Limited sensitivity analysis of regional climate change probabilities for the 21st century. *J. Geophys. Res. Atmos.*, **110**, D19108.
- Diffenbaugh, N. S., and M. Ashfaq, 2010: Intensification of hot extremes in the United States. *Geophys. Res. Lett.*, **37**, L15701.
- Diffenbaugh, N. S., J. S. Pal, F. Giorgi, and X. J. Gao, 2007: Heat stress intensification in the Mediterranean climate change hotspot. *Geophys. Res. Lett.*, **34**, L11706.
- Dijkstra, H., 2007: Characterization of the multiple equilibria regime in a global ocean model. *Tellus A*, **59**, 695–705.
- DiNezio, P. N., A. C. Clement, G. A. Vecchi, B. J. Soden, and B. P. Kirtman, 2009: Climate response of the equatorial Pacific to global warming. *J. Clim.*, **22**, 4873–4892.
- Dirmeyer, P. A., Y. Jin, B. Singh, and X. Yan, 2013: Evolving land-atmosphere interactions over North America from CMIP5 simulations. *J. Clim.*, doi:10.1175/JCLI-D-12-00454.1.
- Dix, M., et al., 2013: The ACCESS Coupled Model: Documentation of core CMIP5 simulations and initial results. *Aust. Meteorol. Oceanogr. J.*, **63**, 83–199.
- Dole, R., et al., 2011: Was there a basis for anticipating the 2010 Russian heat wave? *Geophys. Res. Lett.*, **38**, L06702.
- Dolman, A., G. van der Werf, M. van der Molen, G. Ganssen, J. Erisman, and B. Strengers, 2010: A carbon cycle science update since IPCC AR-4. *Ambio*, **39**, 402–412.
- Donat, M. G., et al., 2013: Updated analyses of temperature and precipitation extreme indices since the beginning of the twentieth century: The HadEX2 dataset. *J. Geophys. Res.*, **118**, 2098–2118.
- Dong, B. W., J. M. Gregory, and R. T. Sutton, 2009: Understanding land-sea warming contrast in response to increasing greenhouse gases. Part I: Transient adjustment. *J. Clim.*, **22**, 3079–3097.
- Dorrepaal, E., S. Toet, R. van Logtestijn, E. Swart, M. van de Weg, T. Callaghan, and R. Aerts, 2009: Carbon respiration from subsurface peat accelerated by climate warming in the subarctic. *Nature*, **460**, 616–619.
- Döscher, R., and T. Koenigk, 2013: Arctic rapid sea ice loss events in regional coupled climate scenario experiments. *Ocean Sci.*, **9**, 217–248.
- Doutriaux-Boucher, M., M. J. Webb, J. M. Gregory, and O. Boucher, 2009: Carbon dioxide induced stomatal closure increases radiative forcing via a rapid reduction in low cloud. *Geophys. Res. Lett.*, **36**, L02703.
- Douville, H., J. F. Royer, J. Polcher, P. Cox, N. Gedney, D. B. Stephenson, and P. J. Valdes, 2000: Impact of CO<sub>2</sub> doubling on the Asian summer monsoon: Robust versus model-dependent responses. *J. Meteorol. Soc. Jpn.*, **78**, 421–439.
- Dowdy, A. J., G. A. Mills, B. Timbal, and Y. Wang, 2013: Changes in the risk of extratropical cyclones in Eastern Australia. *J. Clim.*, **26**, 1403–1417.
- Downes, S., A. Budnick, J. Sarmiento, and R. Farneti, 2011: Impacts of wind stress on the Antarctic Circumpolar Current fronts and associated subduction. *Geophys. Res. Lett.*, **38**, L11605.
- Downes, S. M., and A. M. Hogg, 2013: Southern Ocean circulation and eddy compensation in CMIP5 models. *J. Clim.*, doi:10.1175/JCLI-D-12-00504.1.
- Downes, S. M., N. L. Bindoff, and S. R. Rintoul, 2010: Changes in the subduction of Southern Ocean water masses at the end of the twenty-first century in eight IPCC models. *J. Clim.*, **23**, 6526–6541.
- Driesschaert, E., et al., 2007: Modeling the influence of Greenland ice sheet melting on the Atlantic meridional overturning circulation during the next millennia. *Geophys. Res. Lett.*, **34**, L10707.
- Drijfhout, S., G. J. van Oldenborgh, and A. Cimatoribus, 2012: Is a decline of AMOC causing the warming hole above the North Atlantic in observed and modeled warming patterns? *J. Clim.*, **25**, 8373–8379.
- Drijfhout, S. S., S. Weber, and E. van der Swaluw, 2010: The stability of the MOC as diagnosed from the model projections for the pre-industrial, present and future climate. *Clim. Dyn.*, **37**, 1575–1586.
- Dufresne, J.-L., et al., 2013: Climate change projections using the IPSL-CM5 Earth system model: From CMIP3 to CMIP5. *Clim. Dyn.*, **40**, 2123–2165.
- Dufresne, J., J. Quaas, O. Boucher, S. Denavit, and L. Fairhead, 2005: Contrasts in the effects on climate of anthropogenic sulfate aerosols between the 20th and the 21st century. *Geophys. Res. Lett.*, **32**, L21703.
- Dufresne, J. L., and S. Bony, 2008: An assessment of the primary sources of spread of global warming estimates from coupled atmosphere-ocean models. *J. Clim.*, **21**, 5135–5144.
- Dulamsuren, C., M. Hauck, and M. Muhlenberg, 2008: Insect and small mammal herbivores limit tree establishment in northern Mongolian steppe. *Plant Ecol.*, **195**, 143–156.
- Dulamsuren, C., M. Hauck, and C. Leuschner, 2010: Recent drought stress leads to growth reductions in *Larix sibirica* in the western Khentey, Mongolia. *Global Change Biol.*, **16**, 3024–3035.
- Dulamsuren, C., et al., 2009: Water relations and photosynthetic performance in *Larix sibirica* growing in the forest-steppe ecotone of northern Mongolia. *Tree Physiol.*, **29**, 99–110.
- Dunne, J. P., R. J. Stouffer, and J. G. John, 2013: Reductions in labour capacity from heat stress under climate warming. *Nature Clim. Change*, doi:10.1038/nclimate1827.
- Durack, P., and S. Wijffels, 2010: Fifty-year trends in global ocean salinities and their relationship to broad-scale warming. *J. Clim.*, **23**, 4342–4362.
- Durack, P. J., S. E. Wijffels, and R. J. Matear, 2012: Ocean salinities reveal strong global water cycle intensification during 1950 to 2000. *Science*, **336**, 455–458.
- Eby, M., K. Zickfeld, A. Montenegro, D. Archer, K. Meissner, and A. Weaver, 2009: Lifetime of anthropogenic climate change: Millennial time scales of potential CO<sub>2</sub> and surface temperature perturbations. *J. Clim.*, **22**, 2501–2511.
- Edwards, T., M. Crucifix, and S. Harrison, 2007: Using the past to constrain the future: How the palaeorecord can improve estimates of global warming. *Prog. Phys. Geogr.*, **31**, 481–500.
- Eglin, T., et al., 2010: Historical and future perspectives of global soil carbon response to climate and land-use changes. *Tellus B*, **62**, 700–718.
- Eisenman, I., 2012: Factors controlling the bifurcation structure of sea ice retreat. *J. Geophys. Res.*, **117**, D01111.
- Eisenman, I., and J. Wetzlaufer, 2009: Nonlinear threshold behavior during the loss of Arctic sea ice. *Proc. Natl. Acad. Sci. U.S.A.*, **106**, 28–32.

- Eisenman, I., T. Schneider, D. S. Battisti, and C. M. Bitz, 2011: Consistent changes in the sea ice seasonal cycle in response to global warming. *J. Clim.*, **24**, 5325–5335.
- Eliseev, A., P. Demchenko, M. Arzhanov, and I. Mokhov, 2013: Transient hysteresis of near-surface permafrost response to external forcing. *Clim. Dyn.*, doi:10.1007/s00382-013-1672-5.
- Emori, S., and S. Brown, 2005: Dynamic and thermodynamic changes in mean and extreme precipitation under changed climate. *Geophys. Res. Lett.*, **32**, L17706.
- Eyring, V., et al., 2005: A strategy for process-oriented validation of coupled chemistry-climate models. *Bull. Am. Meteorol. Soc.*, **86**, 1117–1133.
- Eyring, V., et al., 2013: Long-term ozone changes and associated climate impacts in CMIP5 simulations. *J. Geophys. Res.*, doi:10.1002/jgrd.50316.
- Falloon, P. D., R. Dankers, R. A. Betts, C. D. Jones, B. B. Booth, and F. H. Lambert, 2012: Role of vegetation change in future climate under the A1B scenario and a climate stabilisation scenario, using the HadCM3C Earth system model. *Biogeosciences*, **9**, 4739–4756.
- Farneti, R., and P. Gent, 2011: The effects of the eddy-induced advection coefficient in a coarse-resolution coupled climate model. *Ocean Model.*, **39**, 135–145.
- Farneti, R., T. Delworth, A. Rosati, S. Griffies, and F. Zeng, 2010: The role of mesoscale eddies in the rectification of the Southern Ocean response to climate change. *J. Phys. Oceanogr.*, **40**, 1539–1557.
- Fasullo, J. T., 2010: Robust land-ocean contrasts in energy and water cycle feedbacks. *J. Clim.*, **23**, 4677–4693.
- Favre, A., and A. Gershunov, 2009: North Pacific cyclonic and anticyclonic transients in a global warming context: Possible consequences for Western North American daily precipitation and temperature extremes. *Clim. Dyn.*, **32**, 969–987.
- Finnis, J., M. M. Holland, M. C. Serreze, and J. J. Cassano, 2007: Response of Northern Hemisphere extratropical cyclone activity and associated precipitation to climate change, as represented by the Community Climate System Model. *J. Geophys. Res.*, **112**, G04S42.
- Fischer, E. M., and C. Schär, 2009: Future changes in daily summer temperature variability: Driving processes and role for temperature extremes. *Clim. Dyn.*, **33**, 917–935.
- Fischer, E. M., and C. Schär, 2010: Consistent geographical patterns of changes in high-impact European heatwaves. *Nature Geosci.*, **3**, 398–403.
- Fischer, E. M., and R. Knutti, 2013: Robust projections of combined humidity and temperature extremes. *Nature Clim. Change*, **3**, 126–130.
- Fischer, E. M., D. M. Lawrence, and B. M. Sanderson, 2011: Quantifying uncertainties in projections of extremes—A perturbed land surface parameter experiment. *Clim. Dyn.*, **37**, 1381–1398.
- Fischer, E. M., J. Rajczak, and C. Schär, 2012a: Changes in European summer temperature variability revisited. *Geophys. Res. Lett.*, **39**, L19702.
- Fischer, E. M., K. W. Oleson, and D. M. Lawrence, 2012b: Contrasting urban and rural heat stress responses to climate change. *Geophys. Res. Lett.*, **39**, L03705.
- Flannery, B. P., 1984: Energy-balance models incorporating transport of thermal and latent energy. *J. Atmos. Sci.*, **41**, 414–421.
- Forest, C. E., P. H. Stone, and A. P. Sokolov, 2006: Estimated PDFs of climate system properties including natural and anthropogenic forcings. *Geophys. Res. Lett.*, **33**, L01705.
- Forest, C. E., P. H. Stone, and A. P. Sokolov, 2008: Constraining climate model parameters from observed 20th century changes. *Tellus A*, **60**, 911–920.
- Forster, P., and K. Taylor, 2006: Climate forcings and climate sensitivities diagnosed from coupled climate model integrations. *J. Clim.*, **19**, 6181–6194.
- Forster, P. M., T. Andrews, P. Good, J. M. Gregory, L. S. Jackson, and M. Zelinka, 2013: Evaluating adjusted forcing and model spread for historical and future scenarios in the CMIP5 generation of climate models. *J. Geophys. Res.*, **118**, 1139–1150.
- Fowler, H., M. Ekstrom, S. Blenkinsop, and A. Smith, 2007a: Estimating change in extreme European precipitation using a multimodel ensemble. *J. Geophys. Res.*, **112**, D18104.
- Fowler, H. J., S. Blenkinsop, and C. Tebaldi, 2007b: Linking climate change modelling to impacts studies: Recent advances in downscaling techniques for hydrological modelling. *Int. J. Climatol.*, **27**, 1547–1578.
- Frame, D., B. Booth, J. Kettleborough, D. Stainforth, J. Gregory, M. Collins, and M. Allen, 2005: Constraining climate forecasts: The role of prior assumptions. *Geophys. Res. Lett.*, **32**, L09702.
- Frederiksen, C. S., J. S. Frederiksen, J. M. Sisson, and S. L. Osbrough, 2011: Australian winter circulation and rainfall changes and projections. *Int. J. Clim. Change Strat. Manage.*, **3**, 170–188.
- Friedlingstein, P., and S. Solomon, 2005: Contributions of past and present human generations to committed warming caused by carbon dioxide. *Proc. Natl. Acad. Sci. U.S.A.*, **102**, 10832–10836.
- Friedlingstein, P., S. Solomon, G. Plattner, R. Knutti, P. Ciais, and M. Raupach, 2011: Long-term climate implications of twenty-first century options for carbon dioxide emission mitigation. *Nature Clim. Change*, **1**, 457–461.
- Friedlingstein, P., et al., 2006: Climate-carbon cycle feedback analysis: Results from the C4MIP model intercomparison. *J. Clim.*, **19**, 3337–3353.
- Frieler, K., M. Meinshausen, M. Mengel, N. Braun, and W. Hare, 2012: A scaling approach to probabilistic assessment of regional climate. *J. Clim.*, **25**, 3117–3144.
- Frierson, D., J. Lu, and G. Chen, 2007: Width of the Hadley cell in simple and comprehensive general circulation models. *Geophys. Res. Lett.*, **34**, L18804.
- Frölicher, T., and F. Joos, 2010: Reversible and irreversible impacts of greenhouse gas emissions in multi-century projections with the NCAR global coupled carbon cycle-climate model. *Clim. Dyn.*, **35**, 1439–1459.
- Fu, Q., C. M. Johanson, J. M. Wallace, and T. Reichler, 2006: Enhanced mid-latitude tropospheric warming in satellite measurements. *Science*, **312**, 1179–1179.
- Fyfe, J., O. Saenko, K. Zickfeld, M. Eby, and A. Weaver, 2007: The role of poleward intensifying winds on Southern Ocean warming. *J. Clim.*, **20**, 5391–5400.
- Fyfe, J., and A. Weaver, 2006: The effect of potential future climate change on the marine methane hydrate stability zone. *J. Clim.*, **19**, 5903–5917.
- Garcia, R. R., and W. J. Randel, 2008: Acceleration of the Brewer-Dobson circulation due to increases in greenhouse gases. *J. Atmos. Sci.*, **65**, 2731–2739.
- Gastineau, G., and B. J. Soden, 2009: Model projected changes of extreme wind events in response to global warming. *Geophys. Res. Lett.*, **36**, L10810.
- Gastineau, G., H. Le Treut, and L. Li, 2008: Hadley circulation changes under global warming conditions indicated by coupled climate models. *Tellus A*, **60**, 863–884.
- Gastineau, G., L. Li, and H. Le Treut, 2009: The Hadley and Walker circulation changes in global warming conditions described by idealized atmospheric simulations. *J. Clim.*, **22**, 3993–4013.
- Gent, P. R., et al., 2011: The Community Climate System Model Version 4. *J. Clim.*, **24**, 4973–4991.
- Georgescu, M., D. Lobell, and C. Field, 2011: Direct climate effects of perennial bioenergy crops in the United States. *Proc. Natl. Acad. Sci. U.S.A.*, **109**, 4307–4312.
- Gerber, E. P., et al., 2012: Assessing and understanding the impact of stratospheric dynamics and variability on the Earth system. *Bull. Am. Meteorol. Soc.*, **93**, 845–859.
- Gillett, N., M. Wehner, S. Tett, and A. Weaver, 2004: Testing the linearity of the response to combined greenhouse gas and sulfate aerosol forcing. *Geophys. Res. Lett.*, **31**, L14201.
- Gillett, N. P., and P. A. Stott, 2009: Attribution of anthropogenic influence on seasonal sea level pressure. *Geophys. Res. Lett.*, **36**, L23709.
- Gillett, N. P., V. K. Arora, D. Matthews, and M. R. Allen, 2013: Constraining the ratio of global warming to cumulative CO<sub>2</sub> emissions using CMIP5 simulations. *J. Clim.*, doi:10.1175/JCLI-D-12-00476.1.
- Gillett, N. P., V. K. Arora, K. Zickfeld, S. J. Marshall, and A. J. Merryfield, 2011: Ongoing climate change following a complete cessation of carbon dioxide emissions. *Nature Geosci.*, **4**, 83–87.
- Giorgi, F., 2008: A simple equation for regional climate change and associated uncertainty. *J. Clim.*, **21**, 1589–1604.
- Gleckler, P. J., K. AchutaRao, J. M. Gregory, B. D. Santer, K. E. Taylor, and T. M. L. Wigley, 2006: Krakatoa lives: The effect of volcanic eruptions on ocean heat content and thermal expansion. *Geophys. Res. Lett.*, **33**, L17702.
- Goelzer, H., P. Huybrechts, M. Loutre, H. Goosse, T. Fichefet, and A. Mouchet, 2011: Impact of Greenland and Antarctic ice sheet interactions on climate sensitivity. *Clim. Dyn.*, **37**, 1005–1018.
- Good, P., J. M. Gregory, and J. A. Lowe, 2011a: A step-response simple climate model to reconstruct and interpret AOGCM projections. *Geophys. Res. Lett.*, **38**, L01703.
- Good, P., J. M. Gregory, J. A. Lowe, and T. Andrews, 2013: Abrupt CO<sub>2</sub> experiments as tools for predicting and understanding CMIP5 representative concentration pathway projections. *Clim. Dyn.*, **40**, 1041–1053.
- Good, P., C. Jones, J. Lowe, R. Betts, B. Booth, and C. Huntingford, 2011b: Quantifying environmental drivers of future tropical forest extent. *J. Clim.*, **24**, 1337–1349.
- Good, P., et al., 2012: A step-response approach for predicting and understanding non-linear precipitation changes. *Clim. Dyn.*, **39**, 2789–2803.

- Good, P., et al., 2011c: A review of recent developments in climate change science. Part I: Understanding of future change in the large-scale climate system. *Prog. Phys. Geogr.*, **35**, 281–296.
- Goodwin, P., R. Williams, A. Ridgwell, and M. Follows, 2009: Climate sensitivity to the carbon cycle modulated by past and future changes in ocean chemistry. *Nature Geosci.*, **2**, 145–150.
- Gossoe, H., O. Arzel, C. Bitz, A. de Montety, and M. Vancoppenolle, 2009: Increased variability of the Arctic summer ice extent in a warmer climate. *Geophys. Res. Lett.*, **36**, L23702.
- Goubanova, K., and L. Li, 2007: Extremes in temperature and precipitation around the Mediterranean basin in an ensemble of future climate scenario simulations. *Global Planet. Change*, **57**, 27–42.
- Gouttevin, I., G. Krinner, P. Ciais, J. Polcher, and C. Legout, 2012: Multi-scale validation of a new soil freezing scheme for a land-surface model with physically-based hydrology. *Cryosphere*, **6**, 407–430.
- Granier, C., et al., 2011: Evolution of anthropogenic and biomass burning emissions at global and regional scales during the 1980–2010 period. *Clim. Change*, **109**, 163–190.
- Grant, A., S. Brönnimann, and L. Haimberger, 2008: Recent Arctic warming vertical structure contested. *Nature*, **455**, E2–E3.
- Graversen, R., and M. Wang, 2009: Polar amplification in a coupled climate model with locked albedo. *Clim. Dyn.*, **33**, 629–643.
- Graversen, R., T. Mauritsen, M. Tjernstrom, E. Kallen, and G. Svensson, 2008: Vertical structure of recent Arctic warming. *Nature*, **541**, 53–56.
- Gregory, J., and M. Webb, 2008: Tropospheric adjustment induces a cloud component in CO<sub>2</sub> forcing. *J. Clim.*, **21**, 58–71.
- Gregory, J., and P. Forster, 2008: Transient climate response estimated from radiative forcing and observed temperature change. *J. Geophys. Res.*, **113**, D23105.
- Gregory, J. M., 2010: Long-term effect of volcanic forcing on ocean heat content. *Geophys. Res. Lett.*, **37**, L22701.
- Gregory, J. M., and J. F. B. Mitchell, 1995: Simulation of daily variability of surface-temperature and precipitation over Europe in the current and 2xCO<sub>2</sub> climates using the UKMO climate model. *Q. J. R. Meteorol. Soc.*, **121**, 1451–1476.
- Gregory, J. M., and R. Tailleux, 2011: Kinetic energy analysis of the response of the Atlantic meridional overturning circulation to CO<sub>2</sub>-forced climate change. *Clim. Dyn.*, **37**, 893–914.
- Gregory, J. M., C. D. Jones, P. Cadule, and P. Friedlingstein, 2009: Quantifying carbon cycle feedbacks. *J. Clim.*, **22**, 5232–5250.
- Gregory, J. M., et al., 2004: A new method for diagnosing radiative forcing and climate sensitivity. *Geophys. Res. Lett.*, **31**, L03205.
- Gregory, J. M., et al., 2005: A model intercomparison of changes in the Atlantic thermohaline circulation in response to increasing atmospheric CO<sub>2</sub> concentration. *Geophys. Res. Lett.*, **32**, L12703.
- Grubb, M., 1997: Technologies, energy systems and the timing of CO<sub>2</sub> emissions abatement—An overview of economic issues. *Energy Policy*, **25**, 159–172.
- Gumpenberger, M., et al., 2010: Predicting pan-tropical climate change induced forest stock gains and losses—Implications for REDD. *Environ. Res. Lett.*, **5**, 014013.
- Gutowski, W., K. Kozak, R. Arritt, J. Christensen, J. Patton, and E. Takle, 2007: A possible constraint on regional precipitation intensity changes under global warming. *J. Hydrometeorol.*, **8**, 1382–1396.
- Haarsma, R. J., F. Selten, and G. J. van Oldenborgh, 2013: Anthropogenic changes of the thermal and zonal flow structure over Western Europe and Eastern North Atlantic in CMIP3 and CMIP5 models. *Clim. Dyn.*, doi:10.1007/s00382-013-1734-8.
- Haarsma, R. J., F. Selten, B. V. Hurk, W. Hazeleger, and X. L. Wang, 2009: Drier Mediterranean soils due to greenhouse warming bring easterly winds over summertime central Europe. *Geophys. Res. Lett.*, **36**, L04705.
- Hajima, T., T. Ise, K. Tachiri, E. Kato, S. Watanabe, and M. Kawamiya, 2012: Climate change, allowable emission, and Earth system response to representative concentration pathway scenarios. *J. Meteorol. Soc. Jpn.*, **90**, 417–433.
- Hall, A., 2004: The role of surface albedo feedback in climate. *J. Clim.*, **17**, 1550–1568.
- Hall, A., X. Qu, and J. Neelin, 2008: Improving predictions of summer climate change in the United States. *Geophys. Res. Lett.*, **35**, L01702.
- Hansen, J., M. Sato, P. Kharecha, and K. von Schuckmann, 2011: Earth's energy imbalance and implications. *Atmos. Chem. Phys.*, **11**, 13421–13449.
- Hansen, J., G. Russell, A. Lacis, I. Fung, D. Rind, and P. Stone, 1985: Climate response-times—Dependence on climate sensitivity and ocean mixing. *Science*, **229**, 857–859.
- Hansen, J., M. Sato, P. Kharecha, G. Russell, D. Lea, and M. Siddall, 2007: Climate change and trace gases. *Philos. Trans. R. Soc. A*, **365**, 1925–1954.
- Hansen, J., et al., 1984: Climate sensitivity: Analysis of feedback mechanisms. In: *Climate Processes and Climate Sensitivity* [J. Hansen and T. Takahashi (eds.)]. American Geophysical Union, Washington, DC, pp. 130–163.
- Hansen, J., et al., 1988: Global climate changes as forecast by Goddard Institute for Space Studies 3-dimensional model. *J. Geophys. Res. Atmos.*, **93**, 9341–9364.
- Hansen, J., et al., 2008: Target atmospheric CO<sub>2</sub>: Where should humanity aim? *Open Atmos. Sci. J.*, **2**, 217–231.
- Hansen, J., et al., 2005a: Earth's energy imbalance: Confirmation and implications. *Science*, **308**, 1431–1435.
- Hansen, J., et al., 2005b: Efficacy of climate forcings. *J. Geophys. Res.*, **110**, D18104.
- Hardiman, S., N. Butchart, T. Hinton, S. Osprey, and L. Gray, 2012: The effect of a well resolved stratosphere on surface climate: Differences between CMIP5 simulations with high and low top versions of the Met Office climate model. *J. Clim.*, **35**, 7083–7099.
- Hare, B., and M. Meinshausen, 2006: How much warming are we committed to and how much can be avoided? *Clim. Change*, **75**, 111–149.
- Hargreaves, J. C., A. Abe-Ouchi, and J. D. Annan, 2007: Linking glacial and future climates through an ensemble of GCM simulations. *Clim. Past*, **3**, 77–87.
- Hargreaves, J. C., J. D. Annan, M. Yoshimori, and A. Abe-Ouchi, 2012: Can the Last Glacial Maximum constrain climate sensitivity? *Geophys. Res. Lett.*, **39**, L24702.
- Harris, G. R., M. Collins, D. M. H. Sexton, J. M. Murphy, and B. B. B. Booth, 2010: Probabilistic projections for 21st century European climate. *Nat. Hazards Earth Syst. Sci.*, **10**, 2009–2020.
- Harris, G. R., D. M. H. Sexton, B. B. B. Booth, M. Collins, J. M. Murphy, and M. J. Webb, 2006: Frequency distributions of transient regional climate change from perturbed physics ensembles of general circulation model simulations. *Clim. Dyn.*, **27**, 357–375.
- Hartmann, D. L., and K. Larson, 2002: An important constraint on tropical cloud-climate feedback. *Geophys. Res. Lett.*, **29**, 1951.
- Harvey, B. J., L. C. Shaffrey, T. J. Woollings, G. Zappa, and K. I. Hodges, 2012: How large are projected 21st century storm track changes? *Geophys. Res. Lett.*, **39**, L18707.
- Haugen, J., and T. Iversen, 2008: Response in extremes of daily precipitation and wind from a downscaled multi-model ensemble of anthropogenic global climate change scenarios. *Tellus A*, **60**, 411–426.
- Hawkins, E., and R. Sutton, 2009: The potential to narrow uncertainty in regional climate predictions. *Bull. Am. Meteorol. Soc.*, **90**, 1095–1107.
- Hawkins, E., and R. Sutton, 2011: The potential to narrow uncertainty in projections of regional precipitation change. *Clim. Dyn.*, **37**, 407–418.
- Hawkins, E., R. Smith, L. Allison, J. Gregory, T. Woollings, H. Pohlmann, and B. de Cuevas, 2011: Bistability of the Atlantic overturning circulation in a global climate model and links to ocean freshwater transport. *Geophys. Res. Lett.*, **38**, L16699.
- Hazeleger, W., et al., 2013: Multiyear climate predictions using two initialisation strategies. *Geophys. Res. Lett.*, doi:10.1002/grl.50355.
- Hegerl, G., T. Crowley, W. Hyde, and D. Frame, 2006: Climate sensitivity constrained by temperature reconstructions over the past seven centuries. *Nature*, **440**, 1029–1032.
- Hegerl, G. C., F. W. Zwiers, P. A. Stott, and V. V. Kharin, 2004: Detectability of anthropogenic changes in annual temperature and precipitation extremes. *J. Clim.*, **17**, 3683–3700.
- Held, I., and B. Soden, 2006: Robust responses of the hydrological cycle to global warming. *J. Clim.*, **19**, 5686–5699.
- Held, I. M., M. Winton, K. Takahashi, T. Delworth, F. R. Zeng, and G. K. Vallis, 2010: Probing the fast and slow components of global warming by returning abruptly to preindustrial forcing. *J. Clim.*, **23**, 2418–2427.
- Hellmer, H. H., F. Kauker, R. Timmermann, J. Determann, and J. Rae, 2012: Twenty-first-century warming of a large Antarctic ice-shelf cavity by a redirected coastal current. *Nature*, **484**, 225–228.
- Henderson-Sellers, A., P. Irannejad, and K. McGuffie, 2008: Future desertification and climate change: The need for land-surface system evaluation improvement. *Global and Planetary Change*, **64**, 129–138.
- Hibbard, K. A., G. A. Meehl, P. A. Cox, and P. Friedlingstein, 2007: A strategy for climate change stabilization experiments. *EOS Transactions AGU*, **88**, 217–221.
- Hirschi, M., et al., 2011: Observational evidence for soil-moisture impact on hot extremes in southeastern Europe. *Nature Geosci.*, **4**, 17–21.

- Ho, C. K., D. B. Stephenson, M. Collins, C. A. T. Ferro, and S. J. Brown, 2012: Calibration strategies: A source of additional uncertainty in climate change projections. *Bull. Am. Meteorol. Soc.*, **93**, 21–26.
- Hodson, D. L. R., S. P. E. Keeley, A. West, J. Ridley, E. Hawkins, and H. T. Hewitt, 2012: Identifying uncertainties in Arctic climate change projections. *Clim. Dyn.*, doi:10.1007/s00382-012-1512-z.
- Hoelzmann, P., D. Jolly, S. Harrison, F. Laarif, R. Bonnefille, and H. Pachur, 1998: Mid-Holocene land-surface conditions in northern Africa and the Arabian Peninsula: A data set for the analysis of biogeophysical feedbacks in the climate system. *Global Biogeochem. Cycles*, **12**, 35–51.
- Hoerling, M., J. Eischeid, and J. Perlitz, 2010: Regional precipitation trends: Distinguishing natural variability from anthropogenic forcing. *J. Clim.*, **23**, 2131–2145.
- Hoerling, M. P., J. K. Eischeid, X.-W. Quan, H. F. Diaz, R. S. Webb, R. M. Dole, and D. R. Easterling, 2012: Is a transition to semipermanent drought conditions imminent in the US Great Plains? *J. Clim.*, **25**, 8380–8386.
- Hofmann, M., and S. Rahmstorf, 2009: On the stability of the Atlantic meridional overturning circulation. *Proc. Natl. Acad. Sci. U.S.A.*, **106**, 20584–20589.
- Hogg, E., and A. Schwarz, 1997: Regeneration of planted conifers across climatic moisture gradients on the Canadian prairies: Implications for distribution and climate change. *J. Biogeogr.*, **24**, 527–534.
- Holden, P. B., and N. R. Edwards, 2010: Dimensionally reduced emulation of an AOGCM for application to integrated assessment modelling. *Geophys. Res. Lett.*, **37**, L21707.
- Holland, M., C. Bitz, and B. Tremblay, 2006: Future abrupt reductions in the summer Arctic sea ice. *Geophys. Res. Lett.*, **33**, L23503.
- Holland, M., M. Serreze, and J. Stroeve, 2010: The sea ice mass budget of the Arctic and its future change as simulated by coupled climate models. *Clim. Dyn.*, **34**, 185–200.
- Holland, M. M., and C. M. Bitz, 2003: Polar amplification of climate change in coupled models. *Clim. Dyn.*, **21**, 221–232.
- Holland, M. M., C. M. Bitz, B. Tremblay, and D. A. Bailey, 2008: The role of natural versus forced change in future rapid summer Arctic ice loss. In: *Arctic Sea Ice Decline: Observations, Projections, Mechanisms, and Implications* [E. T. DeWeaver, C. M. Bitz and L. B. Tremblay (eds.)]. American Geophysical Union, Washington, DC, pp. 133–150.
- Hu, A., G. Meehl, W. Han, and J. Yin, 2009: Transient response of the MOC and climate to potential melting of the Greenland ice sheet in the 21st century. *Geophys. Res. Lett.*, **36**, L10707.
- Hu, Y., and Q. Fu, 2007: Observed poleward expansion of the Hadley circulation since 1979. *Atmos. Chem. Phys.*, **7**, 5229–5236.
- Hu, Z.-Z., M. Latif, E. Roeckner, and L. Bengtsson, 2000: Intensified Asian summer monsoon and its variability in a coupled model forced by increasing greenhouse gas concentrations. *Geophys. Res. Lett.*, **27**, 2681–2684.
- Hu, Z. Z., A. Kumar, B. Jha, and B. H. Huang, 2012: An analysis of forced and internal variability in a warmer climate in CCSM3. *J. Clim.*, **25**, 2356–2373.
- Huang, P., S.-P. Xie, K. Hu, G. Huang, and R. Huang, 2013: Patterns of the seasonal response of tropical rainfall to global warming. *Nature Geosci.*, **6**, 357–361.
- Huete, A. R., et al., 2006: Amazon rainforests green-up with sunlight in dry season. *Geophys. Res. Lett.*, **33**, L06405.
- Huisman, S., M. den Toom, H. Dijkstra, and S. Drijfhout, 2010: An indicator of the multiple equilibria regime of the Atlantic meridional overturning circulation. *J. Phys. Oceanogr.*, **40**, 551–567.
- Huntingford, C., and P. M. Cox, 2000: An analogue model to derive additional climate change scenarios from existing GCM simulations. *Clim. Dyn.*, **16**, 575–586.
- Huntingford, C., J. Lowe, B. Booth, C. Jones, G. Harris, L. Gohar, and P. Meir, 2009: Contributions of carbon cycle uncertainty to future climate projection spread. *Tellus B*, **61**, 355–360.
- Huntingford, C., et al., 2008: Towards quantifying uncertainty in predictions of Amazon 'dieback'. *Philos. Trans. R. Soc. B*, **363**, 1857–1864.
- Huntingford, C., et al., 2013: Simulated resilience of tropical rainforests to CO<sub>2</sub>-induced climate change. *Nature Geosci.*, **6**, 268–273.
- Hurtt, G., et al., 2011: Harmonization of land-use scenarios for the period 1500–2100: 600 years of global gridded annual land-use transitions, wood harvest, and resulting secondary lands. *Clim. Change*, **109**, 117–161.
- Hwang, Y.-T., D. M. W. D.M.W. Frierson, B. J. Soden, and I. M. Held, 2011: Corrigendum for Held and Soden (2006). *J. Clim.*, **24**, 1559–1560.
- IPCC, 2000: *IPCC Special Report on Emissions Scenarios. Prepared by Working Group III of the Intergovernmental Panel on Climate Change*. Cambridge University Press, Cambridge, United Kingdom, and New York, NY, USA.
- IPCC, 2001: *Climate Change 2001: The Scientific Basis. Contribution of Working Group I to the Third Assessment Report of the Intergovernmental Panel on Climate Change* [J. T. Houghton, Y. Ding, D. J. Griggs, M. Noquer, P. J. van der Linden, X. Dai, K. Maskell and C. A. Johnson (eds.)]. Cambridge University Press, Cambridge, United Kingdom and New York, NY, USA, 881 pp.
- IPCC, 2007: *Climate Change 2007: The Physical Science Basis. Contribution of Working Group I to the Fourth Assessment Report of the Intergovernmental Panel on Climate Change* [Solomon, S., D. Qin, M. Manning, Z. Chen, M. Marquis, K. B. Averyt, M. Tignor and H. L. Miller (eds.)]. Cambridge University Press, Cambridge, United Kingdom and New York, NY, USA, 996 pp.
- Ishizaki, Y., et al., 2012: Temperature scaling pattern dependence on representative concentration pathway emission scenarios. *Clim. Change*, **112**, 535–546.
- Iversen, T., et al., 2013: The Norwegian Earth System Model, NorESM1–M – Part 2: Climate response and scenario projections. *Geosci. Model Dev.*, **6**, 389–415.
- Jackson, C. S., M. K. Sen, G. Huerta, Y. Deng, and K. P. Bowman, 2008: Error reduction and convergence in climate prediction. *J. Clim.*, **21**, 6698–6709.
- Jaeger, C., and J. Jaeger, 2010: Three views of two degrees. *Clim. Change Econ.*, **3**, 145–166.
- Jiang, X., S. J. Eichelberger, D. L. Hartmann, R. Shia, and Y. L. Yung, 2007: Influence of doubled CO<sub>2</sub> on ozone via changes in the Brewer-Dobson circulation. *J. Atmos. Sci.*, **64**, 2751–2755.
- Johanson, C. M., and Q. Fu, 2009: Hadley Cell widening: Model simulations versus observations. *J. Clim.*, **22**, 2713–2725.
- Johns, T. C., et al., 2011: Climate change under aggressive mitigation: The ENSEMBLES multi-model experiment. *Clim. Dyn.*, **37**, 1975–2003.
- Johnson, N. C., and S.-P. Xie, 2010: Changes in the sea surface temperature threshold for tropical convection. *Nature Geosci.*, **3**, 842–845.
- Jones, A., J. Haywood, and O. Boucher, 2007: Aerosol forcing, climate response and climate sensitivity in the Hadley Centre climate model. *J. Geophys. Res.*, **112**, D20211.
- Jones, C., P. Cox, and C. Huntingford, 2006: Climate-carbon cycle feedbacks under stabilization: Uncertainty and observational constraints. *Tellus B*, **58**, 603–613.
- Jones, C., J. Lowe, S. Liddicoat, and R. Betts, 2009: Committed terrestrial ecosystem changes due to climate change. *Nature Geosci.*, **2**, 484–487.
- Jones, C. D., et al., 2013: 21st Century compatible CO<sub>2</sub> emissions and airborne fraction simulated by CMIP5 Earth System models under 4 Representative Concentration Pathways. *J. Clim.*, doi:10.1175/JCLI-D-12-00554.1.
- Jones, C. D., et al., 2011: The HadGEM2–ES implementation of CMIP5 centennial simulations. *Geosci. Model Dev.*, **4**, 543–570.
- Joos, F., et al., 2013: Carbon dioxide and climate impulse response functions for the computation of greenhouse gas metrics: A multi-model analysis. *Atmos. Chem. Phys.*, **13**, 2793–2825.
- Joshi, M., E. Hawkins, R. Sutton, J. Lowe, and D. Frame, 2011: Projections of when temperature change will exceed 2°C above pre-industrial levels. *Nature Clim. Change*, **1**, 407–412.
- Joshi, M., K. Shine, M. Ponater, N. Stuber, R. Sausen, and L. Li, 2003: A comparison of climate response to different radiative forcings in three general circulation models: Towards an improved metric of climate change. *Clim. Dyn.*, **20**, 843–854.
- Joshi, M. M., F. H. Lambert, and M. J. Webb, 2013: An explanation for the difference between twentieth and twenty-first century land-sea warming ratio in climate models. *Clim. Dyn.*, doi:10.1007/s00382-013-1664-5.
- Joshi, M. M., M. J. Webb, A. C. Maycock, and M. Collins, 2010: Stratospheric water vapour and high climate sensitivity in a version of the HadSM3 climate model. *Atmos. Chem. Phys.*, **10**, 7161–7167.
- Joshi, M. M., J. M. Gregory, M. J. Webb, D. M. H. Sexton, and T. C. Johns, 2008: Mechanisms for the land/sea warming contrast exhibited by simulations of climate change. *Clim. Dyn.*, **30**, 455–465.
- Jun, M., R. Knutti, and D. W. Nychka, 2008: Spatial analysis to quantify numerical model bias and dependence: How many climate models are there? *J. Am. Stat. Assoc. Appl. Case Stud.*, **103**, 934–947.
- Jungclaus, J., H. Haak, M. Esch, E. Röckner, and J. Marotzke, 2006: Will Greenland melting halt the thermohaline circulation? *Geophys. Res. Lett.*, **33**, L17708.
- Kang, S. M., and I. M. Held, 2012: Tropical precipitation, SSTs and the surface energy budget: A zonally symmetric perspective. *Clim. Dyn.*, **38**, 1917–1924.
- Kang, S. M., L. M. Polvani, J. C. Fyfe, and M. Sigmond, 2011: Impact of polar ozone depletion on subtropical precipitation. *Science*, **332**, 951–954.

- Karpechko, A. Y., and E. Manzini, 2012: Stratospheric influence on tropospheric climate change in the Northern Hemisphere. *J. Geophys. Res.*, **117**, D05133.
- Kattenberg, A., et al., 1996: Climate models—Projections of future climate. In: *Climate Change 1995: The Science of Climate Change. Contribution of WGI to the Second Assessment Report of the Intergovernmental Panel on Climate Change* [J. T. Houghton, L. G. Meira . A. Callander, N. Harris, A. Kattenberg and K. Maskell (eds.)]. Cambridge University Press, Cambridge, United Kingdom, and New York, NY, USA, pp. 285–357.
- Kawase, H., T. Nagashima, K. Sudo, and T. Nozawa, 2011: Future changes in tropospheric ozone under Representative Concentration Pathways (RCPs). *Geophys. Res. Lett.*, **38**, L05801.
- Kay, J., M. Holland, and A. Jahn, 2011: Inter-annual to multi-decadal Arctic sea ice extent trends in a warming world. *Geophys. Res. Lett.*, **38**, L15708.
- Kay, J. E., M. M. Holland, C. Bitz, E. Blanchard-Wrigglesworth, A. Gettelman, A. Conley, and D. Bailey, 2012: The influence of local feedbacks and northward heat transport on the equilibrium Arctic climate response to increased greenhouse gas forcing in coupled climate models. *J. Clim.*, **25**, 5433–5450.
- Kaye, N., A. Hartley, and D. Hemming, 2012: Mapping the climate: Guidance on appropriate techniques to map climate variables and their uncertainty. *Geosci. Model Dev.*, **5**, 245–256.
- Kellomaki, S., M. Maajarvi, H. Strandman, A. Kilpelainen, and H. Peltola, 2010: Model computations on the climate change effects on snow cover, soil moisture and soil frost in the boreal conditions over Finland. *Silva Fennica*, **44**, 213–233.
- Kendon, E., D. Rowell, and R. Jones, 2010: Mechanisms and reliability of future projected changes in daily precipitation. *Clim. Dyn.*, **35**, 489–509.
- Kendon, E., D. Rowell, R. Jones, and E. Buonomo, 2008: Robustness of future changes in local precipitation extremes. *J. Clim.*, **17**, 4280–4297.
- Kharin, V.V., F.W. Zwiers, X. B. Zhang, and G.C. Hegerl, 2007: Changes in temperature and precipitation extremes in the IPCC ensemble of global coupled model simulations. *J. Clim.*, **20**, 1419–1444.
- Kharin, V. V., F. W. Zwiers, X. Zhang, and M. Wehner, 2013: Changes in temperature and precipitation extremes in the CMIP5 ensemble. *Clim. Change*, doi:10.1007/s10584-013-0705-8.
- Khvorostyanov, D., P. Ciais, G. Krinner, and S. Zimov, 2008: Vulnerability of east Siberia's frozen carbon stores to future warming. *Geophys. Res. Lett.*, **35**, L10703.
- Kidston, J., and E. P. Gerber, 2010: Intermodel variability of the poleward shift of the austral jet stream in the CMIP3 integrations linked to biases in 20th century climatology. *Geophys. Res. Lett.*, **37**, L09708.
- Kienzle, S., M. Nemeth, J. Byrne, and R. MacDonald, 2012: Simulating the hydrological impacts of climate change in the upper North Saskatchewan River basin, Alberta, Canada. *J. Hydrol.*, **412**, 76–89.
- Kirkevåg, K., et al., 2013: Aerosol–climate interactions in the Norwegian Earth System Model – NorESM1–M. *Geosci. Model Dev.*, **6**, 207–244.
- Kitoh, A., S. Yukimoto, A. Noda, and T. Motoi, 1997: Simulated changes in the Asian summer monsoon at times of increased atmospheric CO<sub>2</sub>. *J. Meteorol. Soc. Jpn.*, **75**, 1019–1031.
- Kjellstrom, E., L. Barring, D. Jacob, R. Jones, G. Lenderink, and C. Schär, 2007: Modelling daily temperature extremes: Recent climate and future changes over Europe. *Clim. Change*, **81**, 249–265.
- Knutti, R., 2010: The end of model democracy? *Clim. Change*, **102**, 395–404.
- Knutti, R., and G. C. Hegerl, 2008: The equilibrium sensitivity of the Earth's temperature to radiation changes. *Nature Geosci.*, **1**, 735–743.
- Knutti, R., and L. Tomassini, 2008: Constraints on the transient climate response from observed global temperature and ocean heat uptake. *Geophys. Res. Lett.*, **35**, L09701.
- Knutti, R., and G.-K. Plattner, 2012: Comment on 'Why hasn't Earth warmed as much as expected?' by Schwartz et al. 2010. *J. Clim.*, **25**, 2192–2199.
- Knutti, R., and J. Sedláček, 2013: Robustness and uncertainties in the new CMIP5 climate model projections. *Nature Clim. Change*, **3**, 369–373.
- Knutti, R., D. Masson, and A. Gettelman, 2013: Climate model genealogy: Generation CMIP5 and how we got there. *Geophys. Res. Lett.*, **40**, 1194–1199.
- Knutti, R., S. Krähenmann, D. Frame, and M. Allen, 2008a: Comment on "Heat capacity, time constant, and sensitivity of Earth's climate system" by S. E. Schwartz. *J. Geophys. Res.*, **113**, D15103.
- Knutti, R., F. Joos, S. Müller, G. Plattner, and T. Stocker, 2005: Probabilistic climate change projections for CO<sub>2</sub> stabilization profiles. *Geophys. Res. Lett.*, **32**, L20707.
- Knutti, R., R. Furrer, C. Tebaldi, J. Cermak, and G. A. Meehl, 2010a: Challenges in combining projections from multiple climate models. *J. Clim.*, **23**, 2739–2758.
- Knutti, R., G. Abramowitz, M. Collins, V. Eyring, P. J. Gleckler, B. Hewitson, and L. Mearns, 2010b: Good practice guidance paper on assessing and combining multi model climate projections. *Meeting Report of the Intergovernmental Panel on Climate Change Expert Meeting on Assessing and Combining Multi-Model Climate Projections*. IPCC Working Group I Technical Support Unit, University of Bern, Bern, Switzerland.
- Knutti, R., et al., 2008b: A review of uncertainties in global temperature projections over the twenty-first century. *J. Clim.*, **21**, 2651–2663.
- Kodra, E., K. Steinhäuser, and A. R. Ganguly, 2011: Persisting cold extremes under 21st-century warming scenarios. *Geophys. Res. Lett.*, **38**, L08705.
- Kolomyts, E., and N. Surova, 2010: Predicting the impact of global warming on soil water resources in marginal forests of the middle Volga region. *Water Resour.*, **37**, 89–101.
- Komuro, Y., et al., 2012: Sea-ice in twentieth-century simulations by new MIROC coupled models: A comparison between models with high resolution and with ice thickness distribution. *J. Meteorol. Soc. Jpn.*, **90A**, 213–232.
- Körper, J., et al., 2013: The effects of aggressive mitigation on steric sea level rise and sea ice changes. *Clim. Dyn.*, **40**, 531–550.
- Koster, R., Z. Guo, R. Yang, P. Dirmeyer, K. Mitchell, and M. Puma, 2009a: On the nature of soil moisture in land surface models. *J. Clim.*, **22**, 4322–4335.
- Koster, R., et al., 2006: GLACE: The Global Land-Atmosphere Coupling Experiment. Part I: Overview. *J. Hydrometeorol.*, **7**, 590–610.
- Koster, R. D., S. D. Schubert, and M. J. Suarez, 2009b: Analyzing the concurrence of meteorological droughts and warm periods, with implications for the determination of evaporative regime. *J. Clim.*, **22**, 3331–3341.
- Koster, R. D., H. L. Wang, S. D. Schubert, M. J. Suarez, and S. Mahanama, 2009c: Drought-induced warming in the continental United States under different SST regimes. *J. Clim.*, **22**, 5385–5400.
- Koven, C., P. Friedlingstein, P. Ciais, D. Khvorostyanov, G. Krinner, and C. Tarnocai, 2009: On the formation of high-latitude soil carbon stocks: Effects of cryoturbation and insulation by organic matter in a land surface model. *Geophys. Res. Lett.*, **36**, L21501.
- Koven, C. D., W. J. Riley, and A. Stern, 2013: Analysis of permafrost thermal dynamics and response to climate change in the CMIP5 Earth system models. *J. Clim.*, **26**, 1877–1900.
- Koven, C. D., et al., 2011: Permafrost carbon-climate feedbacks accelerate global warming. *Proc. Natl. Acad. Sci. U.S.A.*, **108**, 14769–14774.
- Kripalani, R., J. Oh, A. Kulkarni, S. Sabade, and H. Chaudhari, 2007: South Asian summer monsoon precipitation variability: Coupled climate model simulations and projections under IPCC AR4. *Theor. Appl. Climatol.*, **90**, 133–159.
- Kug, J., D. Choi, F. Jin, W. Kwon, and H. Ren, 2010: Role of synoptic eddy feedback on polar climate responses to the anthropogenic forcing. *Geophys. Res. Lett.*, **37**, L14704.
- Kuhry, P., E. Dorrepaal, G. Hugelius, E. Schuur, and C. Tarnocai, 2010: Potential remobilization of belowground permafrost carbon under future global warming. *Permafro. Periglac. Process.*, **21**, 208–214.
- Kumar, A., et al., 2010: Contribution of sea ice loss to Arctic amplification. *Geophys. Res. Lett.*, **37**, L21701.
- Kunkel, K. E., T. R. Karl, D. R. Easterling, K. Redmond, J. Young, X. Yin, and P. Hennon, 2013: Probable Maximum Precipitation (PMP) and climate change. *Geophys. Res. Lett.*, **40**, 1402–1408.
- Kysely, J., and R. Beranova, 2009: Climate-change effects on extreme precipitation in central Europe: Uncertainties of scenarios based on regional climate models. *Theor. Appl. Climatol.*, **95**, 361–374.
- Lamarque, J.-F., et al., 2011: Global and regional evolution of short-lived radiatively-active gases and aerosols in the Representative Concentration Pathways. *Clim. Change*, **109**, 191–212.
- Lamarque, J., 2008: Estimating the potential for methane clathrate instability in the 1%-CO<sub>2</sub> IPCC AR-4 simulations. *Geophys. Res. Lett.*, **35**, L19806.
- Lamarque, J., et al., 2010: Historical (1850–2000) gridded anthropogenic and biomass burning emissions of reactive gases and aerosols: Methodology and application. *Atmos. Chem. Phys.*, **10**, 7017–7039.
- Lamarque, J. F., et al., 2013: The Atmospheric Chemistry and Climate Model Intercomparison Project (ACCMIP): Overview and description of models, simulations and climate diagnostics. *Geosci. Model Dev.*, **6**, 179–206.

- Lambert, F., and M. Webb, 2008: Dependency of global mean precipitation on surface temperature. *Geophys. Res. Lett.*, **35**, L16706.
- Lambert, F. H., and J. C. H. Chiang, 2007: Control of land-ocean temperature contrast by ocean heat uptake. *Geophys. Res. Lett.*, **34**, L13704.
- Lambert, F. H., M. J. Webb, and M. J. Joshi, 2011: The relationship between land-ocean surface temperature contrast and radiative forcing. *J. Clim.*, **24**, 3239–3256.
- Lambert, F. H., N. P. Gillett, D. A. Stone, and C. Huntingford, 2005: Attribution studies of observed land precipitation changes with nine coupled models. *Geophys. Res. Lett.*, **32**, L18704.
- Lambert, F. H., G. R. Harris, M. Collins, J. M. Murphy, D. M. H. Sexton, and B. B. Booth, 2012: Interactions between perturbations to different Earth system components simulated by a fully-coupled climate model. *Clim. Dyn.*, doi:10.1007/s00382-012-1618-3.
- Langen, P. L., and V. A. Alexeev, 2007: Polar amplification as a preferred response in an idealized aquaplanet GCM. *Clim. Dyn.*, **29**, 305–317.
- Langen, P. L., A. M. Solgaard, and C. S. Hvidberg, 2012: Self-inhibiting growth of the Greenland Ice Sheet. *Geophys. Res. Lett.*, **39**, L12502.
- Lapola, D. M., M. D. Oyama, and C. A. Nobre, 2009: Exploring the range of climate biome projections for tropical South America: The role of CO<sub>2</sub> fertilization and seasonality. *Global Biogeochem. Cycles*, **23**, GB3003.
- Lau, K., M. Kim, and K. Kim, 2006: Asian summer monsoon anomalies induced by aerosol direct forcing: The role of the Tibetan Plateau. *Clim. Dyn.*, **26**, 855–864.
- Lawrence, D., and A. Slater, 2010: The contribution of snow condition trends to future ground climate. *Clim. Dyn.*, **34**, 969–981.
- Lawrence, D., A. Slater, and S. Swenson, 2012: Simulation of present-day and future permafrost and seasonally frozen ground conditions in CCSM4. *J. Clim.*, **25**, 2207–2225.
- Lawrence, D., A. Slater, V. Romanovsky, and D. Nicolsky, 2008a: Sensitivity of a model projection of near-surface permafrost degradation to soil column depth and representation of soil organic matter. *J. Geophys. Res. Earth Surface*, **113**, F02011.
- Lawrence, D., A. Slater, R. Tomas, M. Holland, and C. Deser, 2008b: Accelerated Arctic land warming and permafrost degradation during rapid sea ice loss. *Geophys. Res. Lett.*, **35**, L11506.
- Lean, J., and D. Rind, 2009: How will Earth's surface temperature change in future decades? *Geophys. Res. Lett.*, **36**, L15708.
- Lee, S., T. Gong, N. Johnson, S. B. Feldstein, and D. Pollard, 2011: On the possible link between tropical convection and the Northern Hemisphere Arctic surface air temperature change between 1958 and 2001. *J. Clim.*, **24**, 4350–4367.
- Lefebvre, W., and H. Goosse, 2008: Analysis of the projected regional sea-ice changes in the Southern Ocean during the twenty-first century. *Clim. Dyn.*, **30**, 59–76.
- Lemoine, D. M., 2010: Climate sensitivity distributions dependence on the possibility that models share biases. *J. Clim.*, **23**, 4395–4415.
- Lenderink, G., and E. Van Meijgaard, 2008: Increase in hourly precipitation extremes beyond expectations from temperature changes. *Nature Geosci.*, **1**, 511–514.
- Lenderink, G., A. van Ulden, B. van den Hurk, and E. van Meijgaard, 2007: Summertime inter-annual temperature variability in an ensemble of regional model simulations: Analysis of the surface energy budget. *Clim. Change*, **81**, 233–247.
- Lenton, T., H. Held, E. Kriegler, J. Hall, W. Lucht, S. Rahmstorf, and H. Schellnhuber, 2008: Tipping elements in the Earth's climate system. *Proc. Natl. Acad. Sci. U.S.A.*, **105**, 1786–1793.
- Lenton, T. M., 2012: Arctic climate tipping points. *Ambio*, **41**, 10–22.
- Leslie, L. M., M. Leplastrier, and B. W. Buckley, 2008: Estimating future trends in severe hailstorms over the Sydney Basin: A climate modelling study. *Atmos. Res.*, **87**, 37–51.
- Levermann, A., J. Schewe, V. Petoukhov, and H. Held, 2009: Basic mechanism for abrupt monsoon transitions. *Proc. Natl. Acad. Sci. U.S.A.*, **106**, 20572–20577.
- Levitus, S., J. Antonov, and T. Boyer, 2005: Warming of the world ocean, 1955–2003. *Geophys. Res. Lett.*, **32**, L02604.
- Levitus, S., et al., 2012: World ocean heat content and thermosteric sea level change (0–2000 m), 1955–2010. *Geophys. Res. Lett.*, **39**, L10603.
- Levy II, H., L. W. Horowitz, M. D. Schwarzkopf, Y. Ming, J.-C. Golaz, V. Naik, and V. Ramaswamy, 2013: The roles of aerosol direct and indirect effects in past and future climate change. *J. Geophys. Res.*, doi:10.1002/jgrd.50192.
- Li, C., J. S. von Storch, and J. Marotzke, 2013a: Deep-ocean heat uptake and equilibrium climate response. *Clim. Dyn.*, **40**, 1071–1086.
- Li, C., D. Notz, S. Tietsche, and J. Marotzke, 2013b: The transient versus the equilibrium response of sea ice to global warming. *J. Clim.*, doi:10.1175/JCLI-D-12-00492.1.
- Li, F., J. Austin, and J. Wilson, 2008: The strength of the Brewer-Dobson circulation in a changing climate: Coupled chemistry-climate model simulations. *J. Clim.*, **21**, 40–57.
- Li, F., W. Collins, M. Wehner, D. Williamson, J. Olson, and C. Algieri, 2011a: Impact of horizontal resolution on simulation of precipitation extremes in an aqua-planet version of Community Atmospheric Model (CAM3). *Tellus*, **63**, 884–892.
- Li, L., X. Jiang, M. Chahine, E. Olsen, E. Fetzer, L. Chen, and Y. Yung, 2011b: The recycling rate of atmospheric moisture over the past two decades (1988–2009). *Environ. Res. Lett.*, **6**, 034018.
- Li, L. J., et al., 2013c: The Flexible Global Ocean-Atmosphere-Land System Model: Grid-point Version 2: FGOALS-g2. *Adv. Atmos. Sci.*, **30**, 543–560.
- Liepert, B. G., and M. Previdi, 2009: Do models and observations disagree on the rainfall response to global warming? *J. Clim.*, **22**, 3156–3166.
- Liepert, B. G., and M. Previdi, 2012: Inter-model variability and biases of the global water cycle in CMIP3 coupled climate models. *Environ. Res. Lett.*, **7**, 014006.
- Lim, E. P., and I. Simmonds, 2009: Effect of tropospheric temperature change on the zonal mean circulation and SH winter extratropical cyclones. *Clim. Dyn.*, **33**, 19–32.
- Lindsay, R., and J. Zhang, 2005: The thinning of Arctic sea ice, 1988–2003: Have we passed a tipping point? *J. Clim.*, **18**, 4879–4894.
- Liu, Z., S. J. Vavrus, F. He, N. Wen, and Y. Zhong, 2005: Rethinking tropical ocean response to global warming: The enhanced equatorial warming. *J. Clim.*, **18**, 4684–4700.
- Livina, V. N., and T. M. Lenton, 2013: A recent tipping point in the Arctic sea-ice cover: Abrupt and persistent increase in the seasonal cycle since 2007. *Cryosphere*, **7**, 275–286.
- Loarie, S. R., D. B. Lobell, G. P. Asner, Q. Z. Mu, and C. B. Field, 2011: Direct impacts on local climate of sugar-cane expansion in Brazil. *Nature Clim. Change*, **1**, 105–109.
- Loeb, N. G., et al., 2009: Toward optimal closure of the Earth's Top-of-Atmosphere radiation budget. *J. Clim.*, **22**, 748–766.
- Long, M. C., K. Lindsay, S. Peacock, J. K. Moore, and S. C. Doney, 2013: Twentieth-century oceanic carbon uptake and storage in CESM1(BGC). *J. Clim.*, doi:10.1175/JCLI-D-12-00184.1.
- Lorenz, D. J., and E. T. DeWeaver, 2007: Tropopause height and zonal wind response to global warming in the IPCC scenario integrations. *J. Geophys. Res. Atmos.*, **112**, D10119.
- Lowe, J., C. Huntingford, S. Raper, C. Jones, S. Liddicoat, and L. Gohar, 2009: How difficult is it to recover from dangerous levels of global warming? *Environ. Res. Lett.*, **4**, 014012.
- Lowe, J. A., and J. M. Gregory, 2006: Understanding projections of sea level rise in a Hadley Centre coupled climate model. *J. Geophys. Res.*, **111**, C11014.
- Lu, J., and M. Cai, 2009: Seasonality of polar surface warming amplification in climate simulations. *Geophys. Res. Lett.*, **36**, L16704.
- Lu, J., G. Vecchi, and T. Reichler, 2007: Expansion of the Hadley cell under global warming. *Geophys. Res. Lett.*, **34**, L06805.
- Lu, J., G. Chen, and D. Frierson, 2008: Response of the zonal mean atmospheric circulation to El Niño versus global warming. *J. Clim.*, **21**, 5835–5851.
- Lucht, W., S. Schaphoff, T. Ebrecht, U. Heyder, and W. Cramer, 2006: Terrestrial vegetation redistribution and carbon balance under climate change. *Carbon Balance Manage.*, **1**, 1–6.
- Lunt, D., A. Haywood, G. Schmidt, U. Salzmann, P. Valdes, and H. Dowsett, 2010: Earth system sensitivity inferred from Pliocene modelling and data. *Nature Geosci.*, **3**, 60–64.
- Luo, J. J., W. Sasaki, and Y. Masumoto, 2012: Indian Ocean warming modulates Pacific climate change. *Proc. Natl. Acad. Sci. U.S.A.*, **109**, 18701–18706.
- Lustenberger, A., R. Knutti, and E. M. Fischer, 2013: The potential of pattern scaling for projecting temperature-related extreme indices. *Int. J. Climatol.*, doi:10.1002/joc.3659.
- Ma, J., and S.-P. Xie, 2013: Regional patterns of sea surface temperature change: A source of uncertainty in future projections of precipitation and atmospheric circulation. *J. Clim.*, **26**, 2482–2501.
- Ma, J., S.-P. Xie, and Y. Kosaka, 2012: Mechanisms for tropical tropospheric circulation change in response to global warming. *J. Clim.*, **25**, 2979–2994.
- MacDougall, A. H., C. A. Avis, and A. J. Weaver, 2012: Significant contribution to climate warming from the permafrost carbon feedback. *Nature Geosci.*, **5**, 719–721.
- Mahlstein, I., and R. Knutti, 2011: Ocean heat transport as a cause for model uncertainty in projected Arctic warming. *J. Clim.*, **24**, 1451–1460.

- Mahlstein, I., and R. Knutti, 2012: September Arctic sea ice predicted to disappear near 2°C global warming above present. *J. Geophys. Res.*, **117**, D06104.
- Mahlstein, I., R. Knutti, S. Solomon, and R. W. Portmann, 2011: Early onset of significant local warming in low latitude countries. *Environ. Res. Lett.*, **6**, 034009.
- Mahlstein, I., R. W. Portmann, J. S. Daniel, S. Solomon, and R. Knutti, 2012: Perceptible changes in regional precipitation in a future climate. *Geophys. Res. Lett.*, **39**, L05701.
- Maksym, T., S. E. Stammerjohn, S. Ackley, and R. Massom, 2012: Antarctic sea ice—A polar opposite? *Oceanography*, **25**, 140–151.
- Malhi, Y., et al., 2009: Exploring the likelihood and mechanism of a climate-change-induced dieback of the Amazon rainforest. *Proc. Natl. Acad. Sci. U.S.A.*, **106**, 20610–20615.
- Manabe, S., and R. Stouffer, 1980: Sensitivity of a global climate model to an increase of CO<sub>2</sub> concentration in the atmosphere. *J. Geophys. Res.*, **85**, 5529–5554.
- Manabe, S., and R. T. Wetherald, 1980: Distribution of climate change resulting from an increase in CO<sub>2</sub> content of the atmosphere. *J. Atmos. Sci.*, **37**, 99–118.
- Manabe, S., and R. Stouffer, 1994: Multiple-century response of a coupled ocean-atmosphere model to an increase of atmospheric carbon-dioxide. *J. Clim.*, **7**, 5–23.
- Manabe, S., K. Bryan, and M. J. Spelman, 1990: Transient-response of a global ocean atmosphere model to a doubling of atmospheric carbon-dioxide. *J. Phys. Oceanogr.*, **20**, 722–749.
- Manabe, S., R. J. Stouffer, M. J. Spelman, and K. Bryan, 1991: Transient responses of a coupled ocean atmosphere model to gradual changes of atmospheric CO<sub>2</sub>. Part I: Annual mean response. *J. Clim.*, **4**, 785–818.
- Marsh, P. T., H. E. Brooks, and D. J. Karoly, 2009: Preliminary investigation into the severe thunderstorm environment of Europe simulated by the Community Climate System Model 3. *Atmos. Res.*, **93**, 607–618.
- Maslowski, W., J. C. Kinney, M. Higgins, and A. Roberts, 2012: The future of Arctic sea ice. In: *Annual Review of Earth and Planetary Sciences* [R. Jeanloz (ed.)]. Annual Reviews, Palo Alto, CA, USA, pp. 625–654.
- Masson, D., and R. Knutti, 2011: Climate model genealogy. *Geophys. Res. Lett.*, **38**, L08703.
- Massonnet, F., T. Fichefet, H. Goosse, C. M. Bitz, G. Philippon-Berthier, M. Holland, and P. Y. Barriat, 2012: Constraining projections of summer Arctic sea ice. *Cryosphere*, **6**, 1383–1394.
- Matsuno, T., K. Maruyama, and J. Tsutsui, 2012a: Stabilization of atmospheric carbon dioxide via zero emissions-An alternative way to a stable global environment. Part 1: Examination of the traditional stabilization concept. *Proc. Jpn. Acad. B*, **88**, 368–384.
- Matsuno, T., K. Maruyama, and J. Tsutsui, 2012b: Stabilization of atmospheric carbon dioxide via zero emissions-An alternative way to a stable global environment. Part 2: A practical zero-emissions scenario. *Proc. Jpn. Acad. B*, **88**, 385–395.
- Matthews, H., and K. Caldeira, 2008: Stabilizing climate requires near-zero emissions. *Geophys. Res. Lett.*, **35**, L04705.
- Matthews, H., N. Gillett, P. Stott, and K. Zickfeld, 2009: The proportionality of global warming to cumulative carbon emissions. *Nature*, **459**, 829–832.
- Matthews, H. D., and K. Zickfeld, 2012: Climate response to zeroed emissions of greenhouse gases and aerosols. *Nature Clim. Change*, **2**, 338–341.
- Matthews, H. D., S. Solomon, and R. Pierrehumbert, 2012: Cumulative carbon as a policy framework for achieving climate stabilization. *Philos. Trans. R. Soc. A*, **370**, 4365–4379.
- May, W., 2002: Simulated changes of the Indian summer monsoon under enhanced greenhouse gas conditions in a global time-slice experiment. *Geophys. Res. Lett.*, **29**, 1118.
- May, W., 2008a: Climatic changes associated with a global “2°C-stabilization” scenario simulated by the ECHAM5/MPI-OM coupled climate model. *Clim. Dyn.*, **31**, 283–313.
- May, W., 2008b: Potential future changes in the characteristics of daily precipitation in Europe simulated by the HIRHAM regional climate model. *Clim. Dyn.*, **30**, 581–603.
- May, W., 2012: Assessing the strength of regional changes in near-surface climate associated with a global warming of 2°C. *Clim. Change*, **110**, 619–644.
- McCabe, G., and D. Wolock, 2007: Warming may create substantial water supply shortages in the Colorado River basin. *Geophys. Res. Lett.*, **34**, L22708.
- McCollum, D., V. Krey, K. Riahi, P. Kolp, A. Grubler, M. Makowski, and N. Nakicenovic, 2013: Climate policies can help resolve energy security and air pollution challenges. *Clim. Change*, doi:10.1007/s10584-013-0710-y.
- McLandress, C., and T. G. Shepherd, 2009: Simulated anthropogenic changes in the Brewer-Dobson circulation, including its extension to high latitudes. *J. Clim.*, **22**, 1516–1540.
- McLandress, C., T. G. Shepherd, J. F. Scinocca, D. A. Plummer, M. Sigmond, A. I. Jonsson, and M. C. Reader, 2011: Separating the dynamical effects of climate change and ozone depletion. Part II: Southern Hemisphere troposphere. *J. Clim.*, **24**, 1850–1868.
- Meehl, G., and W. Washington, 1993: South Asian summer monsoon variability in a model with doubled atmospheric carbon-dioxide concentration. *Science*, **260**, 1101–1104.
- Meehl, G., J. Arblaster, and C. Tebaldi, 2005a: Understanding future patterns of increased precipitation intensity in climate model simulations. *Geophys. Res. Lett.*, **32**, L18719.
- Meehl, G., J. Arblaster, and W. Collins, 2008: Effects of black carbon aerosols on the Indian monsoon. *J. Clim.*, **21**, 2869–2882.
- Meehl, G., et al., 2012: Climate system response to external forcings and climate change projections in CCSM4. *J. Clim.*, **25**, 3661–3683.
- Meehl, G. A., and C. Tebaldi, 2004: More intense, more frequent, and longer lasting heat waves in the 21st century. *Science*, **305**, 994–997.
- Meehl, G. A., G. J. Boer, C. Covey, M. Latif, and R. J. Stouffer, 2000: The Coupled Model Intercomparison Project (CMIP). *Bull. Am. Meteorol. Soc.*, **81**, 313–318.
- Meehl, G. A., C. Tebaldi, G. Walton, D. Easterling, and L. McDaniel, 2009: Relative increase of record high maximum temperatures compared to record low minimum temperatures in the U. S. *Geophys. Res. Lett.*, **36**, L23701.
- Meehl, G. A., W. M. Washington, C. M. Ammann, J. M. Arblaster, T. M. L. Wigley, and C. Tebaldi, 2004: Combinations of natural and anthropogenic forcings in twentieth-century climate. *J. Clim.*, **17**, 3721–3727.
- Meehl, G. A., et al., 2005b: How much more global warming and sea level rise? *Science*, **307**, 1769–1772.
- Meehl, G. A., et al., 2007a: The WCRP CMIP3 multimodel dataset - A new era in climate change research. *Bull. Am. Meteorol. Soc.*, **88**, 1383–1394.
- Meehl, G. A., et al., 2006: Climate change projections for the twenty-first century and climate change commitment in the CCSM3. *J. Clim.*, **19**, 2597–2616.
- Meehl, G. A., et al., 2013: Climate change projections in CESM1(CAM5) compared to CCSM4. *J. Clim.*, doi:10.1175/JCLI-D-12-00572.1.
- Meehl, G. A., et al., 2007b: Global climate projections. In: *Climate Change 2007: The Physical Science Basis. Contribution of Working Group I to the Fourth Assessment Report of the Intergovernmental Panel on Climate Change* [Solomon, S., D. Qin, M. Manning, Z. Chen, M. Marquis, K. B. Averyt, M. Tignor and H. L. Miller (eds.)] Cambridge University Press, Cambridge, United Kingdom and New York, NY, USA, pp. 747–846.
- Meijers, A. J. S., E. Shuckburgh, N. Bruneau, J.-B. Sallee, T. J. Bracegirdle, and Z. Wang, 2012: Representation of the Antarctic Circumpolar Current in the CMIP5 climate models and future changes under warming scenarios. *J. Geophys. Res.*, **117**, C12008.
- Meinshausen, M., S. Raper, and T. Wigley, 2011a: Emulating coupled atmosphere-ocean and carbon cycle models with a simpler model, MAGICC6—Part 1: Model description and calibration. *Atmos. Chem. Phys.*, **11**, 1417–1456.
- Meinshausen, M., T. Wigley, and S. Raper, 2011b: Emulating atmosphere-ocean and carbon cycle models with a simpler model, MAGICC6—Part 2: Applications. *Atmos. Chem. Phys.*, **11**, 1457–1471.
- Meinshausen, M., B. Hare, T. Wigley, D. Van Vuuren, M. Den Elzen, and R. Swart, 2006: Multi-gas emissions pathways to meet climate targets. *Clim. Change*, **75**, 151–194.
- Meinshausen, M., et al., 2009: Greenhouse-gas emission targets for limiting global warming to 2°C. *Nature*, **458**, 1158–1162.
- Meinshausen, M., et al., 2011c: The RCP greenhouse gas concentrations and their extensions from 1765 to 2300. *Clim. Change*, **109**, 213–241.
- Merrifield, M. A., 2011: A shift in western tropical Pacific sea level trends during the 1990s. *J. Clim.*, **24**, 4126–4138.
- Merryfield, W. J., M. M. Holland, and A. H. Monahan, 2008: Multiple equilibria and abrupt transitions in Arctic summer sea ice extent. In: *Arctic Sea Ice Decline: Observations, Projections, Mechanisms, and Implications*. American Geophysical Union, Washington, DC, pp. 151–174.
- Mignone, B., R. Socolow, J. Sarmiento, and M. Oppenheimer, 2008: Atmospheric stabilization and the timing of carbon mitigation. *Clim. Change*, **88**, 251–265.
- Mikolajewicz, U., M. Vizcaino, J. Jungclaus, and G. Schurgers, 2007: Effect of ice sheet interactions in anthropogenic climate change simulations. *Geophys. Res. Lett.*, **34**, L18706.

- Millner, A., R. Calel, D. A. Stainforth, and G. MacKerron, 2013: Do probabilistic expert elicitations capture scientists' uncertainty about climate change? *Clim. Change*, **116**, 427–436.
- Milly, P., J. Betancourt, M. Falkenmark, R. Hirsch, Z. Kundzewicz, D. Lettenmaier, and R. Stouffer, 2008: Stationarity is dead: Whither water management? *Science*, **319**, 573–574.
- Min, S., X. Zhang, F. Zwiers, and G. Hegerl, 2011: Human contribution to more intense precipitation extremes. *Nature*, **470**, 378–381.
- Ming, Y., V. Ramaswamy, and G. Persad, 2010: Two opposing effects of absorbing aerosols on global-mean precipitation. *Geophys. Res. Lett.*, **37**, L13701.
- Mitas, C., and A. Clement, 2006: Recent behavior of the Hadley cell and tropical thermodynamics in climate models and reanalyses. *Geophys. Res. Lett.*, **33**, L01810.
- Mitchell, J. F. B., 1990: Is the Holocene a good analogue for greenhouse warming? *J. Clim.*, **3**, 1177–1192.
- Mitchell, J. F. B., C. A. Wilson, and W. M. Cunningham, 1987: On CO<sub>2</sub> climate sensitivity and model dependence of results. *Q. J. R. Meteorol. Soc.*, **113**, 293–322.
- Mitchell, J. F. B., T. C. Johns, W. J. Ingram, and J. A. Lowe, 2000: The effect of stabilising atmospheric carbon dioxide concentrations on global and regional climate change. *Geophys. Res. Lett.*, **27**, 2977–2980.
- Mitchell, J. F. B., T. C. Johns, M. Eagles, W. J. Ingram, and R. A. Davis, 1999: Towards the construction of climate change scenarios. *Clim. Change*, **41**, 547–581.
- Mitchell, T. D., 2003: Pattern scaling - An examination of the accuracy of the technique for describing future climates. *Clim. Change*, **60**, 217–242.
- Mizuta, R., 2012: Intensification of extratropical cyclones associated with the polar jet change in the CMIP5 global warming projections. *Geophys. Res. Lett.*, **39**, L19707.
- Monaghan, A., D. Bromwich, and D. Schneider, 2008: Twentieth century Antarctic air temperature and snowfall simulations by IPCC climate models. *Geophys. Res. Lett.*, **35**, L07502.
- Montenegro, A., V. Brovkin, M. Eby, D. Archer, and A. Weaver, 2007: Long term fate of anthropogenic carbon. *Geophys. Res. Lett.*, **34**, L19707.
- Morgan, M. G., and D. W. Keith, 1995: Climate-change - Subjective judgments by climate experts. *Environ. Sci. Technol.*, **29**, A468–A476.
- Moss, R. H., et al., 2010: The next generation of scenarios for climate change research and assessment. *Nature*, **463**, 747–756.
- Moss, R. H., et al., 2008: Towards new scenarios for analysis of emissions, climate change, impacts, and response strategies. In: *IPCC Expert Meeting Report: Towards New Scenarios*. Intergovernmental Panel on Climate Change, Geneva, Switzerland, 132 pp.
- Muller, C. J., and P. A. O'Gorman, 2011: An energetic perspective on the regional response of precipitation to climate change. *Nature Clim. Change*, **1**, 266–271.
- Murphy, D. M., S. Solomon, R. W. Portmann, K. H. Rosenlof, P. M. Forster, and T. Wong, 2009: An observationally based energy balance for the Earth since 1950. *J. Geophys. Res.*, **114**, D17107.
- Murphy, J., D. Sexton, D. Barnett, G. Jones, M. Webb, and M. Collins, 2004: Quantification of modelling uncertainties in a large ensemble of climate change simulations. *Nature*, **430**, 768–772.
- Murphy, J. M., B. B. Booth, M. Collins, G. R. Harris, D. M. H. Sexton, and M. J. Webb, 2007: A methodology for probabilistic predictions of regional climate change from perturbed physics ensembles. *Philos. Trans. R. Soc. A*, **365**, 1993–2028.
- Myhre, G., E. Highwood, K. Shine, and F. Stordal, 1998: New estimates of radiative forcing due to well mixed greenhouse gases. *Geophys. Res. Lett.*, **25**, 2715–2718.
- Neelin, J. D., C. Chou, and H. Su, 2003: Tropical drought regions in global warming and El Niño teleconnections. *Geophys. Res. Lett.*, **30**, 2275.
- Neelin, J. D., M. Munnich, H. Su, J. E. Meyerson, and C. E. Holloway, 2006: Tropical drying trends in global warming models and observations. *Proc. Natl. Acad. Sci. U.S.A.*, **103**, 6110–6115.
- Nelson, F., and S. Outcalt, 1987: A computational method for prediction and regionalization of permafrost. *Arct. Alpine Res.*, **19**, 279–288.
- Newlands, N. K., G. Espino-Hernández, and R. S. Erickson, 2012: Understanding crop response to climate variability with complex agroecosystem models. *Int. J. Ecol.*, **2012**, 756242.
- Niall, S., and K. Walsh, 2005: The impact of climate change on hailstorms in southeastern Australia. *Int. J. Climatol.*, **25**, 1933–1952.
- Nikolksy, D., V. Romanovsky, V. Alexeev, and D. Lawrence, 2007: Improved modeling of permafrost dynamics in a GCM land-surface scheme. *Geophys. Res. Lett.*, **34**, L08501.
- Niinemets, U., 2010: Responses of forest trees to single and multiple environmental stresses from seedlings to mature plants: Past stress history, stress interactions, tolerance and acclimation. *Forest Ecol. Manage.*, **260**, 1623–1639.
- Nikulin, G., E. Kjellstrom, U. Hansson, G. Strandberg, and A. Ullerstig, 2011: Evaluation and future projections of temperature, precipitation and wind extremes over Europe in an ensemble of regional climate simulations. *Tellus A*, **63**, 41–55.
- Nobre, C., and L. Borma, 2009: 'Tipping points' for the Amazon forest. *Curr. Opin. Environ. Sustain.*, **1**, 28–36.
- North, G., 1984: The small ice cap instability in diffuse climate models. *J. Atmos. Sci.*, **41**, 3390–3395.
- Notaro, M., 2008: Statistical identification of global hot spots in soil moisture feedbacks among IPCC AR4 models. *J. Geophys. Res.*, **113**, D09101.
- Notz, D., 2009: The future of ice sheets and sea ice: Between reversible retreat and unstoppable loss. *Proc. Natl. Acad. Sci. U.S.A.*, **106**, 20590–20595.
- NRC, 2011: *Climate Stabilization Targets: Emissions, Concentrations, and Impacts over Decades to Millennia*. National Academies Press, Washington, DC, 298 pp.
- O'Connor, F., et al., 2010: Possible role of wetlands, permafrost, and methane hydrates in the methane cycle under future climate change: A review. *Rev. Geophys.*, **48**, RG4005.
- O'Gorman, P., and T. Schneider, 2009a: Scaling of precipitation extremes over a wide range of climates simulated with an idealized GCM. *J. Clim.*, **22**, 5676–5685.
- O'Gorman, P., and T. Schneider, 2009b: The physical basis for increases in precipitation extremes in simulations of 21st-century climate change. *Proc. Natl. Acad. Sci. U.S.A.*, **106**, 14773–14777.
- O'Gorman, P., R. Allan, M. Byrne, and M. Previdi, 2012: Energetic constraints on precipitation under climate change. *Surv. Geophys.*, **33**, 585–608.
- O'Gorman, P. A., 2010: Understanding the varied response of the extratropical storm tracks to climate change. *Proc. Natl. Acad. Sci. U.S.A.*, **107**, 19176–19180.
- O'Gorman, P. A., and C. J. Muller, 2010: How closely do changes in surface and column water vapor follow Clausius-Clapeyron scaling in climate change simulations? *Environ. Res. Lett.*, **5**, 025207.
- Orlowsky, B., and S. I. Seneviratne, 2012: Global changes in extreme events: Regional and seasonal dimension. *Clim. Change*, **110**, 669–696.
- Otto, A., et al., 2013: Energy budget constraints on climate response. *Nature Geosci.*, **6**, 415–416.
- Overland, J. E., and M. Wang, 2013: When will the summer Arctic be nearly sea ice free? *Geophys. Res. Lett.*, doi:10.1002/grl.50316.
- Overland, J. E., M. Wang, N. A. Bond, J. E. Walsh, V. M. Kattsov, and W. L. Chapman, 2011: Considerations in the selection of global climate models for regional climate projections: The Arctic as a case study. *J. Clim.*, **24**, 1583–1597.
- Oyama, M. D., and C. A. Nobre, 2003: A new climate-vegetation equilibrium state for Tropical South America. *Geophys. Res. Lett.*, **30**, 2199.
- Padilla, L., G. Vallis, and C. Rowley, 2011: Probabilistic estimates of transient climate sensitivity subject to uncertainty in forcing and natural variability. *J. Clim.*, **24**, 5521–5537.
- Paeth, H., and F. Pollinger, 2010: Enhanced evidence in climate models for changes in extratropical atmospheric circulation. *Tellus A*, **62**, 647–660.
- Pagani, M., Z. Liu, J. LaRiviere, and A. Ravelo, 2010: High Earth-system climate sensitivity determined from Pliocene carbon dioxide concentrations. *Nature Geosci.*, **3**, 27–30.
- Pall, P., M. Allen, and D. Stone, 2007: Testing the Clausius-Clapeyron constraint on changes in extreme precipitation under CO<sub>2</sub> warming. *Clim. Dyn.*, **28**, 351–363.
- Pennell, C., and T. Reichler, 2011: On the effective number of climate models. *J. Clim.*, **24**, 2358–2367.
- Perkins, S. E., L. V. Alexander, and J. R. Nairn, 2012: Increasing frequency, intensity and duration of observed global heatwaves and warm spells. *Geophys. Res. Lett.*, **39**, L20714.
- Perrie, W., Y. H. Yao, and W. Q. Zhang, 2010: On the impacts of climate change and the upper ocean on midlatitude northwest Atlantic landfalling cyclones. *J. Geophys. Res.*, **115**, D23110.
- Piani, C., D. J. Frame, D. A. Stainforth, and M. R. Allen, 2005: Constraints on climate change from a multi-thousand member ensemble of simulations. *Geophys. Res. Lett.*, **32**, L23825.
- Pierce, D., et al., 2008: Attribution of declining Western US snowpack to human effects. *J. Clim.*, **21**, 6425–6444.
- Pinto, J. G., U. Ulbrich, G. C. Leckebusch, T. Spangehl, M. Reyers, and S. Zacharias, 2007: Changes in storm track and cyclone activity in three SRES ensemble experiments with the ECHAM5/MPI-OM1 GCM. *Clim. Dyn.*, **29**, 195–210.

- Pitman, A., et al., 2009: Uncertainties in climate responses to past land cover change: First results from the LUCID intercomparison study. *Geophys. Res. Lett.*, **36**, L14814.
- Plattner, G.-K., et al., 2008: Long-term climate commitments projected with climate-carbon cycle models. *J. Clim.*, **21**, 2721–2751.
- Polvani, L. M., M. Previdi, and C. Deser, 2011: Large cancellation, due to ozone recovery, of future Southern Hemisphere atmospheric circulation trends. *Geophys. Res. Lett.*, **38**, L04707.
- Pongratz, J., C. Reick, T. Raddatz, and M. Claussen, 2010: Biogeophysical versus biogeochemical climate response to historical anthropogenic land cover change. *Geophys. Res. Lett.*, **37**, L08702.
- Port, U., V. Brovkin, and M. Claussen, 2012: The influence of vegetation dynamics on anthropogenic climate change. *Earth Syst. Dyn.*, **3**, 233–243.
- Power, S., and G. Kociuba, 2011a: The impact of global warming on the Southern Oscillation Index. *Clim. Dyn.*, **37**, 1745–1754.
- Power, S., F. Delage, R. Colman, and A. Moise, 2012: Consensus on twenty-first-century rainfall projections in climate models more widespread than previously thought. *J. Clim.*, **25**, 3792–3809.
- Power, S. B., and G. Kociuba, 2011b: What caused the observed twentieth-century weakening of the Walker circulation? *J. Clim.*, **24**, 6501–6514.
- Previdi, M., 2010: Radiative feedbacks on global precipitation. *Environ. Res. Lett.*, **5**, 025211.
- Rahmstorf, S., et al., 2005: Thermohaline circulation hysteresis: A model intercomparison. *Geophys. Res. Lett.*, **32**, L23605.
- Räisänen, J., 2007: How reliable are climate models? *Tellus A*, **59**, 2–29.
- Räisänen, J., 2008: Warmer climate: Less or more snow? *Clim. Dyn.*, **30**, 307–319.
- Räisänen, J., and L. Ruokolainen, 2006: Probabilistic forecasts of near-term climate change based on a resampling ensemble technique. *Tellus A*, **58**, 461–472.
- Räisänen, J., and J. S. Ylhäisi, 2011: Cold months in a warming climate. *Geophys. Res. Lett.*, **38**, L22704.
- Ramanathan, V., P. J. Crutzen, J. T. Kiehl, and D. Rosenfeld, 2001: Aerosols, climate, and the hydrologic cycle. *Science*, **294**, 2119–2124.
- Ramaswamy, V., et al., 2001: Radiative forcing of climate change. In: *Climate Change 2001: The Scientific Basis. Contribution of Working Group I to the Third Assessment Report of the Intergovernmental Panel on Climate Change* [J. T. Houghton, Y. Ding, D. J. Griggs, M. Noquer, P. J. van der Linden, X. Dai, K. Maskell and C. A. Johnson (eds.)]. Cambridge University Press, Cambridge, United Kingdom and New York, NY, USA pp. 349–416.
- Rammig, A., et al., 2010: Estimating the risk of Amazonian forest dieback. *New Phytologist*, **187**, 694–706.
- Randall, D. A., et al., 2007: Climate models and their evaluation. In: *Climate Change 2007: The Physical Science Basis. Contribution of Working Group I to the Fourth Assessment Report of the Intergovernmental Panel on Climate Change* [Solomon, S., D. Qin, M. Manning, Z. Chen, M. Marquis, K. B. Averyt, M. Tignor and H. L. Miller (eds.)]. Cambridge University Press, Cambridge, United Kingdom and New York, NY, USA, pp. 589–662.
- Randalls, S., 2010: History of the 2°C climate target. *WIREs Climate Change*, **1**, 598–605.
- Randel, W., and F. Wu, 2007: A stratospheric ozone profile data set for 1979–2005: Variability, trends, and comparisons with column ozone data. *J. Geophys. Res.*, **112**, D06313.
- Randel, W. J., M. Park, F. Wu, and N. Livesey, 2007: A large annual cycle in ozone above the tropical tropopause linked to the Brewer-Dobson circulation. *J. Atmos. Sci.*, **64**, 4479–4488.
- Randles, C., and V. Ramaswamy, 2008: Absorbing aerosols over Asia: A Geophysical Fluid Dynamics Laboratory general circulation model sensitivity study of model response to aerosol optical depth and aerosol absorption. *J. Geophys. Res.*, **113**, D21203.
- Reagan, M., and G. Moridis, 2007: Oceanic gas hydrate instability and dissociation under climate change scenarios. *Geophys. Res. Lett.*, **34**, L22709.
- Reagan, M., and G. Moridis, 2009: Large-scale simulation of methane hydrate dissociation along the West Spitsbergen Margin. *Geophys. Res. Lett.*, **36**, L23612.
- Ridley, J., J. Lowe, and D. Simonin, 2008: The demise of Arctic sea ice during stabilisation at high greenhouse gas concentrations. *Clim. Dyn.*, **30**, 333–341.
- Ridley, J., J. Lowe, C. Brierley, and G. Harris, 2007: Uncertainty in the sensitivity of Arctic sea ice to global warming in a perturbed parameter climate model ensemble. *Geophys. Res. Lett.*, **34**, L19704.
- Ridley, J., J. Gregory, P. Huybrechts, and J. Lowe, 2010: Thresholds for irreversible decline of the Greenland ice sheet. *Clim. Dyn.*, **35**, 1049–1057.
- Ridley, J. K., J. A. Lowe, and H. T. Hewitt, 2012: How reversible is sea ice loss? *Cryosphere*, **6**, 193–198.
- Riley, W. J., et al., 2011: Barriers to predicting changes in global terrestrial methane fluxes: Analyses using CLM4ME, a methane biogeochemistry model integrated in CESM. *Biogeosciences*, **8**, 1925–1953.
- Rind, D., 1987: The doubled CO<sub>2</sub> climate - Impact of the sea-surface temperature gradient. *J. Atmos. Sci.*, **44**, 3235–3268.
- Rinke, A., P. Kuhry, and K. Dethloff, 2008: Importance of a soil organic layer for Arctic climate: A sensitivity study with an Arctic RCM. *Geophys. Res. Lett.*, **35**, L13709.
- Rive, N., A. Torvanger, T. Berntsen, and S. Kallbekken, 2007: To what extent can a long-term temperature target guide near-term climate change commitments? *Clim. Change*, **82**, 373–391.
- Robinson, A., R. Calov, and A. Ganopolski, 2012: Multistability and critical thresholds of the Greenland ice sheet. *Nature Clim. Change*, **2**, 429–432.
- Roeckner, E., M. A. Giorgetta, T. Crucifix, M. Esch, and J. Pongratz, 2011: Historical and future anthropogenic emission pathways derived from coupled climate-carbon cycle simulations. *Clim. Change*, **105**, 91–108.
- Roehrig, R., D. Bouniol, F. Guichard, F. Hourdin, and J.-L. Redelsperger, 2013: The present and future of the West African monsoon: A process-oriented assessment of CMIP5 simulations along the AMMA transect. *J. Clim.*, doi:10.1175/JCLI-D-12-00505.1.
- Roesch, A., 2006: Evaluation of surface albedo and snow cover in AR4 coupled climate models. *J. Geophys. Res.*, **111**, D15111.
- Rogelj, J., M. Meinshausen, and R. Knutti, 2012: Global warming under old and new scenarios using IPCC climate sensitivity range estimates. *Nature Clim. Change*, **2**, 248–253.
- Rogelj, J., D. L. McCollum, B. C. O'Neill, and K. Riahi, 2013: 2020 emissions levels required to limit warming to below 2°C. *Nature Clim. Change*, **3**, 405–412.
- Rogelj, J., et al., 2011: Emission pathways consistent with a 2°C global temperature limit. *Nature Clim. Change*, **1**, 413–418.
- Rohling, E., and P. P. Members, 2012: Making sense of palaeoclimate sensitivity. *Nature*, **491**, 683–691.
- Rohling, E., K. Grant, M. Bolshaw, A. Roberts, M. Siddall, C. Hemleben, and M. Kucera, 2009: Antarctic temperature and global sea level closely coupled over the past five glacial cycles. *Nature Geosci.*, **2**, 500–504.
- Romanovsky, V. E., S. L. Smith, and H. H. Christiansen, 2010: Permafrost thermal state in the polar Northern Hemisphere during the international polar year 2007–2009: A synthesis. *Permafrost Periglac. Process.*, **21**, 106–116.
- Rotstayn, L. D., S. J. Jeffrey, M. A. Collier, S. M. Dravitzki, A. C. Hirst, J. I. Syktus, and K. K. Wong, 2012: Aerosol- and greenhouse gas-induced changes in summer rainfall and circulation in the Australasian region: A study using single-forcing climate simulations. *Atmos. Chem. Phys.*, **12**, 6377–6404.
- Rougier, J., 2007: Probabilistic inference for future climate using an ensemble of climate model evaluations. *Clim. Change*, **81**, 247–264.
- Rougier, J., D. M. H. Sexton, J. M. Murphy, and D. Stainforth, 2009: Analyzing the climate sensitivity of the HadSM3 climate model using ensembles from different but related experiments. *J. Clim.*, **22**, 3540–3557.
- Rowell, D. P., 2012: Sources of uncertainty in future changes in local precipitation. *Clim. Dyn.*, doi:10.1007/s00382-011-1210-2.
- Rowlands, D. J., et al., 2012: Broad range of 2050 warming from an observationally constrained large climate model ensemble. *Nature Geosci.*, **5**, 256–260.
- Ruosteenoja, K., H. Tuomenvirta, and K. Jylha, 2007: GCM-based regional temperature and precipitation change estimates for Europe under four SRES scenarios applying a super-ensemble pattern-scaling method. *Clim. Change*, **81**, 193–208.
- Saenko, O. A., A. S. Gupta, and P. Spence, 2012: On challenges in predicting bottom water transport in the Southern Ocean. *J. Clim.*, **25**, 1349–1356.
- Saito, K., M. Kimoto, T. Zhang, K. Takata, and S. Emori, 2007: Evaluating a high-resolution climate model: Simulated hydrothermal regimes in frozen ground regions and their change under the global warming scenario. *J. Geophys. Res.*, **112**, F02S11.
- Sallée, J.-B., E. Shuckburgh, N. Bruneau, A. J. S. Meijers, T. Bracegirdle, and Z. Wang, 2013a: Assessment of Southern Ocean mixed-layer depths in CMIP5 models: Historical bias and forcing response. *J. Geophys. Res.*, doi:10.1002/jgrc.20157.
- Sallée, J.-B., E. Shuckburgh, N. Bruneau, A. J. S. Meijers, T. J. Bracegirdle, Z. Wang, and T. Roy, 2013b: Assessment of Southern Ocean water mass circulation and characteristics in CMIP5 models: Historical bias and forcing response. *J. Geophys. Res.*, doi:10.1002/jgrc.20135.

- Sanchez-Gomez, E., S. Somot, and A. Mariotti, 2009: Future changes in the Mediterranean water budget projected by an ensemble of regional climate models. *Geophys. Res. Lett.*, **36**, L21401.
- Sanderson, B. M., 2011: A multimodel study of parametric uncertainty in predictions of climate response to rising greenhouse gas concentrations. *J. Clim.*, **25**, 1362–1377.
- Sanderson, B. M., 2013: On the estimation of systematic error in regression-based predictions of climate sensitivity. *Clim. Change*, doi:10.1007/s10584-012-0671-6.
- Sanderson, B. M., and R. Knutti, 2012: On the interpretation of constrained climate model ensembles. *Geophys. Res. Lett.*, **39**, L16708.
- Sanderson, B. M., K. M. Shell, and W. Ingram, 2010: Climate feedbacks determined using radiative kernels in a multi-thousand member ensemble of AOGCMs. *Clim. Dyn.*, **35**, 1219–1236.
- Sanderson, B. M., et al., 2008: Constraints on model response to greenhouse gas forcing and the role of subgrid-scale processes. *J. Clim.*, **21**, 2384–2400.
- Sanderson, M. G., D. L. Hemming, and R. A. Betts, 2011: Regional temperature and precipitation changes under high-end ( $\geq 4^{\circ}\text{C}$ ) global warming. *Philos. Trans. R. Soc. A*, **369**, 85–98.
- Sanso, B., and C. Forest, 2009: Statistical calibration of climate system properties. *J. R. Stat. Soc. C*, **58**, 485–503.
- Sanso, B., C. E. Forest, and D. Zantedeschi, 2008: Inferring climate system properties using a computer model. *Bayes. Anal.*, **3**, 1–37.
- Sansom, P. G., D. B. Stephenson, C. A. T. Ferro, G. Zappa, and L. Shaffrey, 2013: Simple uncertainty frameworks for selecting weighting schemes and interpreting multi-model ensemble climate change experiments. *J. Clim.*, doi:10.1175/JCLI-D-12-00462.1.
- Santer, B. D., T. M. L. Wigley, M. E. Schlesinger, and J. F. B. Mitchell, 1990: *Developing Climate Scenarios from Equilibrium GCM Results*. Max-Planck-Institut für-Meteorologie Report. Max-Planck-Institut-für-Meteorologie, Hamburg, Germany, 29 pp.
- Scaife, A. A., et al., 2012: Climate change projections and stratosphere-troposphere interaction. *Clim. Dyn.*, **38**, 2089–2097.
- Schaefer, K., T. Zhang, L. Bruhwiler, and A. Barrett, 2011: Amount and timing of permafrost carbon release in response to climate warming. *Tellus B*, **63**, 165–180.
- Schär, C., P. L. Vidale, D. Lüthi, C. Frei, C. Häberli, M. A. Liniger, and C. Appenzeller, 2004: The role of increasing temperature variability in European summer heatwaves. *Nature*, **427**, 332–336.
- Scheff, J., and D. M. W. Frierson, 2012: Robust future precipitation declines in CMIP5 largely reflect the poleward expansion of model subtropical dry zones. *Geophys. Res. Lett.*, **39**, L18704.
- Scheffer, M., et al., 2009: Early-warning signals for critical transitions. *Nature*, **461**, 53–59.
- Schlesinger, M., 1986: Equilibrium and transient climatic warming induced by increased atmospheric CO<sub>2</sub>. *Clim. Dyn.*, **1**, 35–51.
- Schlesinger, M., et al., 2000: Geographical distributions of temperature change for scenarios of greenhouse gas and sulfur dioxide emissions. *Technol. Forecast. Soc. Change*, **65**, 167–193.
- Schmidt, M. W. I., et al., 2011: Persistence of soil organic matter as an ecosystem property. *Nature*, **478**, 49–56.
- Schmittner, A., et al., 2011: Climate sensitivity estimated from temperature reconstructions of the Last Glacial Maximum. *Science*, **334**, 1385–1388.
- Schneider von Deimling, T., H. Held, A. Ganopolski, and S. Rahmstorf, 2006: Climate sensitivity estimated from ensemble simulations of glacial climate. *Clim. Dyn.*, **27**, 149–163.
- Schneider von Deimling, T., M. Meinshausen, A. Levermann, V. Huber, K. Frieler, D. Lawrence, and V. Brovkin, 2012: Estimating the near-surface permafrost-carbon feedback on global warming. *Biogeosciences*, **9**, 649–665.
- Schoof, C., 2007: Ice sheet grounding line dynamics: Steady states, stability, and hysteresis. *J. Geophys. Res.*, **112**, F03S28.
- Schröder, D., and W. M. Connolley, 2007: Impact of instantaneous sea ice removal in a coupled general circulation model. *Geophys. Res. Lett.*, **34**, L14502.
- Schuenemann, K. C., and J. J. Cassano, 2010: Changes in synoptic weather patterns and Greenland precipitation in the 20th and 21st centuries: 2. Analysis of 21st century atmospheric changes using self-organizing maps. *J. Geophys. Res.*, **115**, D05108.
- Schuur, E., J. Vogel, K. Crummer, H. Lee, J. Sickman, and T. Osterkamp, 2009: The effect of permafrost thaw on old carbon release and net carbon exchange from tundra. *Nature*, **459**, 556–559.
- Schwalm, C. R., et al., 2012: Reduction in carbon uptake during turn of the century drought in western North America. *Nature Geosci.*, **5**, 551–556.
- Schwartz, S., R. Charlson, R. Kahn, J. Ogren, and H. Rodhe, 2010: Why hasn't Earth warmed as much as expected? *J. Clim.*, **23**, 2453–2464.
- Schwartz, S., R. Charlson, R. Kahn, J. Ogren, and H. Rodhe, 2012: Reply to "Comments on 'Why hasn't Earth warmed as much as expected?'". *J. Clim.*, **25**, 2200–2204.
- Schwartz, S. E., 2012: Determination of Earth's transient and equilibrium climate sensitivities from observations over the twentieth century: Strong dependence on assumed forcing. *Surv. Geophys.*, **33**, 745–777.
- Schweiger, A., R. Lindsay, J. Zhang, M. Steele, H. Stern, and R. Kwok, 2011: Uncertainty in modeled Arctic sea ice volume. *J. Geophys. Res.*, **116**, C00D06.
- Screen, J., and I. Simmonds, 2010: The central role of diminishing sea ice in recent Arctic temperature amplification. *Nature*, **464**, 1334–1337.
- Screen, J. A., N. P. Gillett, A. Y. Karpechko, and D. P. Stevens, 2010: Mixed layer temperature response to the Southern Annular Mode: Mechanisms and model representation. *J. Clim.*, **23**, 664–678.
- Seager, R., and G. A. Vecchi, 2010: Greenhouse warming and the 21st century hydroclimate of the southwestern North America. *Proc. Natl. Acad. Sci. U.S.A.*, **107**, 21277–21282.
- Seager, R., and N. Naik, 2012: A mechanisms-based approach to detecting recent anthropogenic hydroclimate change. *J. Clim.*, **25**, 236–261.
- Seager, R., N. Naik, and G. A. Vecchi, 2010: Thermodynamic and dynamic mechanisms for large-scale changes in the hydrological cycle in response to global warming. *J. Clim.*, **23**, 4651–4668.
- Seager, R., et al., 2007: Model projections of an imminent transition to a more arid climate in southwestern North America. *Science*, **316**, 1181–1184.
- Sedláček, J., R. Knutti, O. Martius, and U. Beyerle, 2011: Impact of a reduced Arctic sea ice cover on ocean and atmospheric properties. *J. Clim.*, **25**, 307–319.
- Seidel, D., and W. Randel, 2007: Recent widening of the tropical belt: Evidence from tropopause observations. *J. Geophys. Res.*, **112**, D20113.
- Seidel, D. J., Q. Fu, W. J. Randel, and T. J. Reichler, 2008: Widening of the tropical belt in a changing climate. *Nature Geosci.*, **1**, 21–24.
- Sen Gupta, A., A. Santoso, A. Taschetto, C. Ummenhofer, J. Trevena, and M. England, 2009: Projected changes to the Southern Hemisphere ocean and sea ice in the IPCC AR4 climate models. *J. Clim.*, **22**, 3047–3078.
- Seneviratne, S. I., D. Lüthi, M. Litschi, and C. Schär, 2006: Land-atmosphere coupling and climate change in Europe. *Nature*, **443**, 205–209.
- Seneviratne, S. I., et al., 2010: Investigating soil moisture-climate interactions in a changing climate: A review. *Earth Sci. Rev.*, **99**, 125–161.
- Seneviratne, S. I., et al., 2012: Changes in climate extremes and their impacts on the natural physical environment. In: *Managing the Risks of Extreme Events and Disasters to Advance Climate Change Adaptation. A Special Report of Working Groups I and II of the Intergovernmental Panel on Climate Change (IPCC)* [C. B. Field, et al. (eds.)]. Cambridge University Press, Cambridge, United Kingdom, and New York, NY, USA, pp. 109–230.
- Senior, C. A., and J. F. B. Mitchell, 2000: The time-dependence of climate sensitivity. *Geophys. Res. Lett.*, **27**, 2685–2688.
- Serreze, M., A. Barrett, J. Stroeve, D. Kindig, and M. Holland, 2009: The emergence of surface-based Arctic amplification. *Cryosphere*, **3**, 11–19.
- Serreze, M. C., and J. A. Francis, 2006: The Arctic amplification debate. *Clim. Change*, **76**, 241–264.
- Sexton, D., H. Grubb, K. Shine, and C. Folland, 2003: Design and analysis of climate model experiments for the efficient estimation of anthropogenic signals. *J. Clim.*, **16**, 1320–1336.
- Sexton, D. M. H., and J. M. Murphy, 2012: Multivariate probabilistic projections using imperfect climate models. Part II: Robustness of methodological choices and consequences for climate sensitivity. *Clim. Dyn.*, **40**, 2543–2558.
- Sexton, D. M. H., J. M. Murphy, M. Collins, and M. J. Webb, 2012: Multivariate probabilistic projections using imperfect climate models. Part I: Outline of methodology. *Clim. Dyn.*, **40**, 2513–2542.
- Shepherd, T. G., and C. McLandress, 2011: A robust mechanism for strengthening of the Brewer-Dobson circulation in response to climate change: Critical-layer control of subtropical wave breaking. *J. Atmos. Sci.*, **68**, 784–797.
- Sherwood, S. C., 2010: Direct versus indirect effects of tropospheric humidity changes on the hydrologic cycle. *Environ. Res. Lett.*, **5**, 025206.

- Sherwood, S. C., and M. Huber, 2010: An adaptability limit to climate change due to heat stress. *Proc. Natl. Acad. Sci. U.S.A.*, **107**, 9552–9555.
- Sherwood, S. C., W. Ingram, Y. Tsubisha, M. Satoh, M. Roberts, P. L. Vidale, and P. A. O’Gorman, 2010: Relative humidity changes in a warmer climate. *J. Geophys. Res.*, **115**, D09104.
- Shindell, D., et al., 2012: Simultaneously mitigating near-term climate change and improving human health and food security. *Science*, **335**, 183–189.
- Shindell, D. T., et al., 2006: Simulations of preindustrial, present-day, and 2100 conditions in the NASA GISS composition and climate model G-PUCCINI. *Atmos. Chem. Phys.*, **6**, 4427–4459.
- Shindell, D. T., et al., 2013a: Interactive ozone and methane chemistry in GISS-E2 historical and future climate simulations. *Atmos. Chem. Phys.*, **13**, 2653–2689.
- Shindell, D. T., et al., 2013b: Radiative forcing in the ACCMIP historical and future climate simulations. *Atmos. Chem. Phys.*, **13**, 2939–2974.
- Shine, K. P., J. Cook, E. J. Highwood, and M. M. Joshi, 2003: An alternative to radiative forcing for estimating the relative importance of climate change mechanisms. *Geophys. Res. Lett.*, **30**, 2047.
- Shiogama, H., S. Emori, K. Takahashi, T. Nagashima, T. Ogura, T. Nozawa, and T. Takemura, 2010a: Emission scenario dependency of precipitation on global warming in the MIROC3.2 model. *J. Clim.*, **23**, 2404–2417.
- Shiogama, H., et al., 2010b: Emission scenario dependencies in climate change assessments of the hydrological cycle. *Clim. Change*, **99**, 321–329.
- Shkolnik, I., E. Nadyozhina, T. Pavlova, E. Molkentin, and A. Semioshina, 2010: Snow cover and permafrost evolution in Siberia as simulated by the MGO regional climate model in the 20th and 21st centuries. *Environ. Res. Lett.*, **5**, 015005.
- Shongwe, M. E., G. J. van Oldenborgh, B. van den Hurk, and M. van Aalst, 2011: Projected changes in mean and extreme precipitation in Africa under global warming. Part II: East Africa. *J. Clim.*, **24**, 3718–3733.
- Siegenthaler, U., and H. Oeschger, 1984: Transient temperature changes due to increasing CO<sub>2</sub> using simple models. *Ann. Glaciol.*, **5**, 153–159.
- Sigmond, M., P. C. Siegmund, E. Manzini, and H. Kelder, 2004: A simulation of the separate climate effects of middle-atmosphere and tropospheric CO<sub>2</sub> doubling. *J. Clim.*, **17**, 2352–2367.
- Sillmann, J., and E. Roeckner, 2008: Indices for extreme events in projections of anthropogenic climate change. *Clim. Change*, **86**, 83–104.
- Sillmann, J., and M. Croci-Maspoli, 2009: Present and future atmospheric blocking and its impact on European mean and extreme climate. *Geophys. Res. Lett.*, **36**, L10702.
- Sillmann, J., V. V. Kharin, F. W. Zwiers, X. Zhang, and D. Branaugh, 2013: Climate extremes indices in the CMIP5 multimodel ensemble: Part 2. Future climate projections. *J. Geophys. Res.*, **118**, 2473–2493.
- Simmons, A. J., K. M. Willett, P. D. Jones, P. W. Thorne, and D. P. Dee, 2010: Low-frequency variations in surface atmospheric humidity, temperature, and precipitation: Inferences from reanalyses and monthly gridded observational data sets. *J. Geophys. Res.*, **115**, D01110.
- Simpkins, G. R., and A. Y. Karpechko, 2012: Sensitivity of the southern annular mode to greenhouse gas emission scenarios. *Clim. Dyn.*, **38**, 563–572.
- Slater, A. G., and D. M. Lawrence, 2013: Diagnosing present and future permafrost from climate models. *J. Clim.*, doi:10.1175/JCLI-D-12-00341.1.
- Smeets, E. M. W., L. F. Bouwman, E. Stehfest, D. P. van Vuuren, and A. Postuma, 2009: Contribution of N<sub>2</sub>O to the greenhouse gas balance of first-generation biofuels. *Global Change Biol.*, **15**, 1–23.
- Smith, L., Y. Sheng, G. MacDonald, and L. Hinzman, 2005: Disappearing Arctic lakes. *Science*, **308**, 1429–1429.
- Smith, L., et al., 2004: Siberian peatlands a net carbon sink and global methane source since the early Holocene. *Science*, **303**, 353–356.
- Smith, R. L., C. Tebaldi, D. Nychka, and L. O. Mearns, 2009: Bayesian modeling of uncertainty in ensembles of climate models. *J. Am. Stat. Assoc.*, **104**, 97–116.
- Smith, S. J., J. van Aardenne, Z. Klimont, R. J. Andres, A. Volke, and S. Delgado Arias, 2011: Anthropogenic sulfur dioxide emissions: 1850–2005. *Atmos. Chem. Phys.*, **11**, 1101–1116.
- Smith, S. M., J. A. Lowe, N. H. A. Bowerman, L. K. Gohar, C. Huntingford, and M. R. Allen, 2012: Equivalence of greenhouse-gas emissions for peak temperature limits. *Nature Clim. Change*, **2**, 535–538.
- Sobel, A. H., and S. J. Camargo, 2011: Projected future seasonal changes in tropical summer climate. *J. Clim.*, **24**, 473–487.
- Soden, B., I. Held, R. Colman, K. Shell, J. Kiehl, and C. Shields, 2008: Quantifying climate feedbacks using radiative kernels. *J. Clim.*, **21**, 3504–3520.
- Soden, B. J., and I. M. Held, 2006: An assessment of climate feedbacks in coupled ocean-atmosphere models. *J. Clim.*, **19**, 3354–3360.
- Soden, B. J., and G. A. Vecchi, 2011: The vertical distribution of cloud feedback in coupled ocean-atmosphere models. *Geophys. Res. Lett.*, **38**, L12704.
- Sohn, B. J., and S.-C. Park, 2010: Strengthened tropical circulations in past three decades inferred from water vapor transport. *J. Geophys. Res.*, **115**, D15112.
- Sokolov, A. P., et al., 2009: Probabilistic forecast for twenty-first-century climate based on uncertainties in emissions (without policy) and climate parameters. *J. Clim.*, **23**, 2230–2231.
- Solgaard, A. M., and P. L. Langen, 2012: Multistability of the Greenland ice sheet and the effects of an adaptive mass balance formulation. *Clim. Dyn.*, **39**, 1599–1612.
- Solomon, S., G. Plattner, R. Knutti, and P. Friedlingstein, 2009: Irreversible climate change due to carbon dioxide emissions. *Proc. Natl. Acad. Sci. U.S.A.*, **106**, 1704–1709.
- Solomon, S., J. Daniel, T. Sanford, D. Murphy, G. Plattner, R. Knutti, and P. Friedlingstein, 2010: Persistence of climate changes due to a range of greenhouse gases. *Proc. Natl. Acad. Sci. U.S.A.*, **107**, 18354–18359.
- Solomon, S., et al., 2007: Technical Summary. In: *Climate Change 2007: The Physical Science Basis. Contribution of Working Group I to the Fourth Assessment Report of the Intergovernmental Panel on Climate Change* [Solomon, S., D. Qin, M. Manning, Z. Chen, M. Marquis, K. B. Averyt, M. Tignor and H. L. Miller (eds.)] Cambridge University Press, Cambridge, United Kingdom and New York, NY, USA, pp. 19–92.
- Son, S. W., et al., 2010: Impact of stratospheric ozone on Southern Hemisphere circulation change: A multimodel assessment. *J. Geophys. Res.*, **115**, D00M07.
- Sorensson, A., C. Menendez, R. Ruscica, P. Alexander, P. Samuelsson, and U. Willen, 2010: Projected precipitation changes in South America: A dynamical downscaling within CLARIS. *Meteorol. Z.*, **19**, 347–355.
- Spence, P., O. A. Saenko, C. O. Dufour, J. Le Sommer, and M. H. England, 2012: Mechanisms maintaining Southern Ocean meridional heat transport under projected wind forcing. *J. Phys. Oceanogr.*, **42**, 1923–1931.
- St. Clair, S., J. Hillier, and P. Smith, 2008: Estimating the pre-harvest greenhouse gas costs of energy crop production. *Biomass Bioenerg.*, **32**, 442–452.
- Stachnik, J. P., and C. Schumacher, 2011: A comparison of the Hadley circulation in modern reanalyses. *J. Geophys. Res.*, **116**, D22102.
- Stephenson, D. B., M. Collins, J. C. Rougier, and R. E. Chandler, 2012: Statistical problems in the probabilistic prediction of climate change. *Environmetrics*, **23**, 364–372.
- Sterl, A., et al., 2008: When can we expect extremely high surface temperatures? *Geophys. Res. Lett.*, **35**, L14703.
- Stott, P., G. Jones, and J. Mitchell, 2003: Do models underestimate the solar contribution to recent climate change? *J. Clim.*, **16**, 4079–4093.
- Stott, P., P. Good, G. A. Jones, N. Gillett, and E. Hawkins, 2013: The upper end of climate model temperature projections is inconsistent with past warming. *Environ. Res. Lett.*, **8**, 014024.
- Stouffer, R., 2004: Time scales of climate response. *J. Clim.*, **17**, 209–217.
- Stouffer, R. J., and S. Manabe, 1999: Response of a coupled ocean-atmosphere model to increasing atmospheric carbon dioxide: Sensitivity to the rate of increase. *J. Clim.*, **12**, 2224–2237.
- Stowasser, M., H. Annamalai, and J. Hafner, 2009: Response of the South Asian summer monsoon to global warming: Mean and synoptic systems. *J. Clim.*, **22**, 1014–1036.
- Stroeve, J., M. Holland, W. Meier, T. Scambos, and M. Serreze, 2007: Arctic sea ice decline: Faster than forecast. *Geophys. Res. Lett.*, **34**, L09501.
- Stroeve, J. C., V. Kattsov, A. Barrett, M. Serreze, T. Pavlova, M. Holland, and W. N. Meier, 2012: Trends in Arctic sea ice extent from CMIP5, CMIP3 and observations. *Geophys. Res. Lett.*, **39**, L16502.
- Stuber, N., M. Ponater, and R. Sausen, 2005: Why radiative forcing might fail as a predictor of climate change. *Clim. Dyn.*, **24**, 497–510.
- Sudo, K., M. Takahashi, and H. Akimoto, 2003: Future changes in stratosphere-troposphere exchange and their impacts on future tropospheric ozone simulations. *Geophys. Res. Lett.*, **30**, 2256.
- Sugiyama, M., H. Shiogama, and S. Emori, 2010: Precipitation extreme changes exceeding moisture content increases in MIROC and IPCC climate models. *Proc. Natl. Acad. Sci. U.S.A.*, **107**, 571–575.
- Sun, Y., S. Solomon, A. Dai, and R. W. Portmann, 2007: How often will it rain? *J. Clim.*, **20**, 4801–4818.

- Sutton, R. T., B. W. Dong, and J. M. Gregory, 2007: Land/sea warming ratio in response to climate change: IPCC AR4 model results and comparison with observations. *Geophys. Res. Lett.*, **34**, L02701.
- Swann, A. L., I. Y. Fung, S. Lewis, G. B. Bonan, and S. C. Doney, 2010: Changes in Arctic vegetation amplify high-latitude warming through the greenhouse effect. *Proc. Natl. Acad. Sci. U.S.A.*, **107**, 1295–1300.
- Swart, N. C., and J. C. Fyfe, 2012: Observed and simulated changes in the Southern Hemisphere surface westerly wind-stress. *Geophys. Res. Lett.*, **39**, L16711.
- Swingedouw, D., P. Braconnot, P. Delecluse, E. Guilyardi, and O. Marti, 2007: Quantifying the AMOC feedbacks during a  $2\times\text{CO}_2$  stabilization experiment with land-ice melting. *Clim. Dyn.*, **29**, 521–534.
- Swingedouw, D., T. Fichefet, P. Huybrechts, H. Goosse, E. Driesschaert, and M. Loutre, 2008: Antarctic ice-sheet melting provides negative feedbacks on future climate warming. *Geophys. Res. Lett.*, **35**, L17705.
- Szopa, S., et al., 2013: Aerosol and ozone changes as forcing for climate evolution between 1850 and 2100. *Clim. Dyn.*, **40**, 2223–2250.
- Takahashi, K., 2009a: Radiative constraints on the hydrological cycle in an idealized radiative-convective equilibrium model. *J. Atmos. Sci.*, **66**, 77–91.
- Takahashi, K., 2009b: The global hydrological cycle and atmospheric shortwave absorption in climate models under  $\text{CO}_2$  forcing. *J. Clim.*, **22**, 5667–5675.
- Tanaka, K., and T. Raddatz, 2011: Correlation between climate sensitivity and aerosols forcing and its implication for the “climate trap”. *Clim. Change*, **109**, 815–825.
- Tarnocai, C., J. Canadell, E. Schuur, P. Kuhry, G. Mazhitova, and S. Zimov, 2009: Soil organic carbon pools in the northern circumpolar permafrost region. *Global Biogeochem. Cycles*, **23**, GB2023.
- Taylor, K. E., R. J. Stouffer, and G. A. Meehl, 2012: A summary of the CMIP5 experiment design. *Bull. Am. Meteorol. Soc.*, **93**, 485–498.
- Tebaldi, C., and R. Knutti, 2007: The use of the multi-model ensemble in probabilistic climate projections. *Philos. Trans. R. Soc. A*, **365**, 2053–2075.
- Tebaldi, C., and D. B. Lobell, 2008: Towards probabilistic projections of climate change impacts on global crop yields. *Geophys. Res. Lett.*, **35**, L08705.
- Tebaldi, C., and B. Sanso, 2009: Joint projections of temperature and precipitation change from multiple climate models: A hierarchical Bayesian approach. *J. R. Stat. Soc. A*, **172**, 83–106.
- Tebaldi, C., J. M. Arblaster, and R. Knutti, 2011: Mapping model agreement on future climate projections. *Geophys. Res. Lett.*, **38**, L23701.
- Tebaldi, C., K. Hayhoe, J. M. Arblaster, and G. A. Meehl, 2006: Going to the extremes. *Clim. Change*, **79**, 185–211.
- Terray, L., L. Corre, S. Cravatte, T. Delcroix, G. Reverdin, and A. Ribes, 2012: Near-surface salinity as nature’s rain gauge to detect human influence on the tropical water cycle. *J. Clim.*, **25**, 958–977.
- Thorne, P., 2008: Arctic tropospheric warming amplification? *Nature*, **455**, E1–E2.
- Tietsche, S., D. Notz, J. H. Jungclaus, and J. Marotzke, 2011: Recovery mechanisms of Arctic summer sea ice. *Geophys. Res. Lett.*, **38**, L02707.
- Tjiputra, J. F., et al., 2013: Evaluation of the carbon cycle components in the Norwegian Earth System Model (NorESM). *Geosci. Model Dev.*, **6**, 301–325.
- Tokinaga, H., S.-P. Xie, C. Deser, Y. Kosaka, and Y. M. Okumura, 2012: Slowdown of the Walker circulation driven by tropical Indo-Pacific warming. *Nature*, **491**, 439–443.
- Trapp, R. J., N. S. Diffenbaugh, and A. Gluhovsky, 2009: Transient response of severe thunderstorm forcing to elevated greenhouse gas concentrations. *Geophys. Res. Lett.*, **36**, L01703.
- Trapp, R. J., N. S. Diffenbaugh, H. E. Brooks, M. E. Baldwin, E. D. Robinson, and J. S. Pal, 2007: Changes in severe thunderstorm environment frequency during the 21st century caused by anthropogenically enhanced global radiative forcing. *Proc. Natl. Acad. Sci. U.S.A.*, **104**, 19719–19723.
- Trenberth, K. E., and D. J. Shea, 2005: Relationships between precipitation and surface temperature. *Geophys. Res. Lett.*, **32**, L14703.
- Trenberth, K. E., and J. T. Fasullo, 2009: Global warming due to increasing absorbed solar radiation. *Geophys. Res. Lett.*, **36**, L07706.
- Trenberth, K. E., and J. T. Fasullo, 2010: Simulation of present-day and twenty-first-century energy budgets of the Southern Oceans. *J. Clim.*, **23**, 440–454.
- Turner, J., T. J. Bracegirdle, T. Phillips, G. J. Marshall, and J. S. Hosking, 2013: An initial assessment of Antarctic sea ice extent in the CMIP5 models. *J. Clim.*, **26**, 1473–1484.
- Ueda, H., A. Iwai, K. Kuwako, and M. Hori, 2006: Impact of anthropogenic forcing on the Asian summer monsoon as simulated by eight GCMs. *Geophys. Res. Lett.*, **33**, L06703.
- Ulbrich, U., G. C. Leckebusch, and J. G. Pinto, 2009: Extra-tropical cyclones in the present and future climate: A review. *Theor. Appl. Climatol.*, **96**, 117–131.
- Ulbrich, U., et al., 2013: Are greenhouse gas signals of Northern Hemisphere winter extra-tropical cyclone activity dependent on the identification and tracking algorithm? *Meteorol. Z.*, **22**, 61–68.
- UNEP, 2010: The emissions gap report: Are the Copenhagen Accord pledges sufficient to limit global warming to  $2^\circ\text{C}$  or  $1.5^\circ\text{C}$ ? , 55 pp.
- Utsumi, N., S. Seto, S. Kanae, E. E. Maeda, and T. Oki, 2011: Does higher surface temperature intensify extreme precipitation? *Geophys. Res. Lett.*, **38**, L16708.
- Vaks, A., et al., 2013: Speleothems reveal 500,000-year history of Siberian permafrost. *Science*, **340**, 183–186.
- Van Klooster, S. L., and P. J. Roebber, 2009: Surface-based convective potential in the contiguous United States in a business-as-usual future climate. *J. Clim.*, **22**, 3317–3330.
- van Vuuren, D. P., et al., 2011: RCP3-PD: Exploring the possibilities to limit global mean temperature change to less than  $2^\circ\text{C}$ . *Clim. Change*, **109**, 95–116.
- Vavrus, S., M. Holland, and D. Bailey, 2011: Changes in Arctic clouds during intervals of rapid sea ice loss. *Clim. Dyn.*, **36**, 1475–1489.
- Vavrus, S. J., M. M. Holland, A. Jahn, D. A. Bailey, and B. A. Blazey, 2012: Twenty-first-century Arctic climate change in CCSM4. *J. Clim.*, **25**, 2696–2710.
- Vecchi, G. A., and B. J. Soden, 2007: Global warming and the weakening of the tropical circulation. *Bull. Am. Meteorol. Soc.*, **88**, 1529–1530.
- Vecchi, G. A., B. J. Soden, A. T. Wittenberg, I. M. Held, A. Leetmaa, and M. J. Harrison, 2006: Weakening of tropical Pacific atmospheric circulation due to anthropogenic forcing. *Nature*, **441**, 73–76.
- Vial, J., J.-L. Dufresne, and S. Bony, 2013: On the interpretation of inter-model spread in CMIP5 climate sensitivity estimates. *Clim. Dyn.*, doi:10.1007/s00382-013-1725-9.
- Vidale, P. L., D. Lüthi, R. Wegmann, and C. Schär, 2007: European summer climate variability in a heterogeneous multi-model ensemble. *Clim. Change*, **81**, 209–232.
- Volodire, A., et al., 2013: The CNRM-CM5.1 global climate model: Description and basic evaluation. *Clim. Dyn.*, **40**, 2091–2121.
- Voss, R., and U. Mikolajewicz, 2001: Long-term climate changes due to increased  $\text{CO}_2$  concentration in the coupled atmosphere-ocean general circulation model ECHAM3/LSG. *Clim. Dyn.*, **17**, 45–60.
- Wadhams, P., 2012: Arctic ice cover, ice thickness and tipping points. *Ambio*, **41**, 23–33.
- Walker, R., et al., 2009: Protecting the Amazon with protected areas. *Proc. Natl. Acad. Sci. U.S.A.*, **106**, 10582–10586.
- Wang, M., and J. Overland, 2009: A sea ice free summer Arctic within 30 years? *Geophys. Res. Lett.*, **36**, L07502.
- Wang, M., and J. E. Overland, 2012: A sea ice free summer Arctic within 30 years: An update from CMIP5 models. *Geophys. Res. Lett.*, **39**, L18501.
- Wania, R., I. Ross, and I. Prentice, 2009: Integrating peatlands and permafrost into a dynamic global vegetation model: 2. Evaluation and sensitivity of vegetation and carbon cycle processes. *Global Biogeochem. Cycles*, **23**, GB3015.
- Washington, W., et al., 2009: How much climate change can be avoided by mitigation? *Geophys. Res. Lett.*, **36**, L08703.
- Watanabe, S., et al., 2011: MIROC-ESM 2010: Model description and basic results of CMIP5-20c3m experiments. *Geosci. Model Dev.*, **4**, 845–872.
- Watterson, I. G., 2008: Calculation of probability density functions for temperature and precipitation change under global warming. *J. Geophys. Res.*, **113**, D12106.
- Watterson, I. G., 2011: Calculation of joint PDFs for climate change with properties matching recent Australian projections. *Aust. Meteorol. Oceanogr. J.*, **61**, 211–219.
- Watterson, I. G., and P. H. Whetton, 2011a: Joint PDFs for Australian climate in future decades and an idealized application to wheat crop yield. *Aust. Meteorol. Oceanogr. J.*, **61**, 221–230.
- Watterson, I. G., and P. H. Whetton, 2011b: Distributions of decadal means of temperature and precipitation change under global warming. *J. Geophys. Res.*, **116**, D07101.
- Watterson, I. G., J. L. McGregor, and K. C. Nguyen, 2008: Changes in extreme temperatures of Australasian summer simulated by CCAM under global warming, and the roles of winds and land-sea contrasts. *Aust. Meteorol. Mag.*, **57**, 195–212.
- WBGU, 2009: Solving the Climate Dilemma: The Budget Approach. German Advisory Council on Global Change, Berlin, 59 pp.

- Weaver, A., K. Zickfeld, A. Montenegro, and M. Eby, 2007: Long term climate implications of 2050 emission reduction targets. *Geophys. Res. Lett.*, **34**, L19703.
- Weaver, A. J., et al., 2012: Stability of the Atlantic meridional overturning circulation: A model intercomparison. *Geophys. Res. Lett.*, **39**, L20709.
- Webb, M., et al., 2006: On the contribution of local feedback mechanisms to the range of climate sensitivity in two GCM ensembles. *Clim. Dyn.*, **27**, 17–38.
- Webb, M. J., F. H. Lambert, and J. M. Gregory, 2013: Origins of differences in climate sensitivity, forcing and feedback in climate models. *Clim. Dyn.*, **40**, 677–707.
- Weber, S., et al., 2007: The modern and glacial overturning circulation in the Atlantic Ocean in PMIP coupled model simulations. *Clim. Past*, **3**, 51–64.
- Weertman, J., 1974: Stability of the junction of an ice sheet and an ice shelf. *J. Glaciol.*, **13**, 3–11.
- Wehner, M., D. Easterling, J. Lawrimore, R. Heim, R. Vose, and B. Santer, 2011: Projections of future drought in the continental United States and Mexico. *J. Hydrometeorol.*, **12**, 1359–1377.
- Weigel, A., R. Knutti, M. Liniger, and C. Appenzeller, 2010: Risks of model weighting in multimodel climate projections. *J. Clim.*, **23**, 4175–4191.
- Wentz, F., L. Ricciardulli, K. Hilburn, and C. Mears, 2007: How much more rain will global warming bring? *Science*, **317**, 233–235.
- Wetherald, R., and S. Manabe, 1988: Cloud feedback processes in a General-Circulation Model. *J. Atmos. Sci.*, **45**, 1397–1415.
- Wetherald, R. T., R. J. Stouffer, and K. W. Dixon, 2001: Committed warming and its implications for climate change. *Geophys. Res. Lett.*, **28**, 1535–1538.
- Wigley, T. M. L., 2005: The climate change commitment. *Science*, **307**, 1766–1769.
- Wilcox, L. J., A. J. Charlton-Perez, and L. J. Gray, 2012: Trends in Austral jet position in ensembles of high- and low-top CMIP5 models. *J. Geophys. Res.*, **117**, D13115.
- Willett, K., and S. Sherwood, 2012: Exceedance of heat index thresholds for 15 regions under a warming climate using the wet-bulb globe temperature. *Int. J. Climatol.*, **32**, 161–177.
- Williams, J. W., S. T. Jackson, and J. E. Kutzbach, 2007: Projected distributions of novel and disappearing climates by 2100 AD. *Proc. Natl. Acad. Sci. U.S.A.*, **104**, 5738–5742.
- Williams, K. D., W. J. Ingram, and J. M. Gregory, 2008: Time variation of effective climate sensitivity in GCMs. *J. Clim.*, **21**, 5076–5090.
- Winton, M., 2006a: Amplified Arctic climate change: What does surface albedo feedback have to do with it? *Geophys. Res. Lett.*, **33**, L03701.
- Winton, M., 2006b: Does the Arctic sea ice have a tipping point? *Geophys. Res. Lett.*, **33**, L23504.
- Winton, M., 2008: Sea ice-albedo feedback and nonlinear Arctic climate change. In: *Arctic Sea Ice Decline: Observations, Projections, Mechanisms, and Implications* [E. T. DeWeaver, C. M. Bitz and L. B. Tremblay (eds.)]. American Geophysical Union, Washington, DC, pp. 111–131.
- Winton, M., 2011: Do climate models underestimate the sensitivity of Northern Hemisphere sea ice cover? *J. Clim.*, **24**, 3924–3934.
- WMO, 2007: Scientific assessment of ozone depletion. In: *2006, Global Ozone Research and Monitoring Project*. World Meteorological Organization, Geneva, Switzerland, 572 pp.
- Wood, R., A. Keen, J. Mitchell, and J. Gregory, 1999: Changing spatial structure of the thermohaline circulation in response to atmospheric CO<sub>2</sub> forcing in a climate model. *Nature*, **399**, 572–575.
- Woollings, T., 2008: Vertical structure of anthropogenic zonal-mean atmospheric circulation change. *Geophys. Res. Lett.*, **35**, L19702.
- Woollings, T., and M. Blackburn, 2012: The North Atlantic jet stream under climate change and its relation to the NAO and EA patterns. *J. Clim.*, **25**, 886–902.
- Woollings, T., J. M. Gregory, J. G. Pinto, M. Reyers, and D. J. Brayshaw, 2012: Response of the North Atlantic storm track to climate change shaped by ocean-atmosphere coupling. *Nature Geosci.*, **5**, 313–317.
- Wu, P., R. Wood, J. Ridley, and J. Lowe, 2010: Temporary acceleration of the hydrological cycle in response to a CO<sub>2</sub> rampdown. *Geophys. Res. Lett.*, **37**, L12705.
- Wu, P., L. Jackson, A. Pardaens, and N. Schaller, 2011a: Extended warming of the northern high latitudes due to an overshoot of the Atlantic meridional overturning circulation. *Geophys. Res. Lett.*, **38**, L24704.
- Wu, T., et al., 2013: Global carbon budgets simulated by the Beijing Climate Center Climate System Model for the last century. *J. Geophys. Res.*, doi:10.1002/jgrd.50320.
- Wu, Y., M. Ting, R. Seager, H.-P. Huang, and M. A. Cane, 2011b: Changes in storm tracks and energy transports in a warmer climate simulated by the GFDL CM2.1 model. *Clim. Dyn.*, **37**, 53–72.
- Wyant, M. C., et al., 2006: A comparison of low-latitude cloud properties and their response to climate change in three AGCMs sorted into regimes using mid-tropospheric vertical velocity. *Clim. Dyn.*, **27**, 261–279.
- Xie, P., and G. Vallis, 2012: The passive and active nature of ocean heat uptake in idealized climate change experiments. *Clim. Dyn.*, **38**, 667–684.
- Xie, S. P., C. Deser, G. A. Vecchi, J. Ma, H. Y. Teng, and A. T. Wittenberg, 2010: Global warming pattern formation: Sea surface temperature and rainfall. *J. Clim.*, **23**, 966–986.
- Xin, X., L. Zhang, J. Zhang, T. Wu, and Y. Fang, 2013a: Climate change projections over East Asia with BCC\_CSM1.1 climate model under RCP scenarios. *J. Meteorol. Soc. Jpn.*, **4**, 413–429.
- Xin, X., T. Wu, J. Li, Z. Wang, W. Li, and F. Wu, 2013b: How well does BCC\_CSM1.1 reproduce the 20th century climate change in China? *Atmos. Ocean. Sci. Lett.*, **6**, 21–26.
- Yang, F. L., A. Kumar, M. E. Schlesinger, and W. Q. Wang, 2003: Intensity of hydrological cycles in warmer climates. *J. Clim.*, **16**, 2419–2423.
- Yin, J., J. Overpeck, S. Griffies, A. Hu, J. Russell, and R. Stouffer, 2011: Different magnitudes of projected subsurface ocean warming around Greenland and Antarctica. *Nature Geosci.*, **4**, 524–528.
- Yokohata, T., M. Webb, M. Collins, K. Williams, M. Yoshimori, J. Hargreaves, and J. Annan, 2010: Structural similarities and differences in climate responses to CO<sub>2</sub> increase between two perturbed physics ensembles. *J. Clim.*, **23**, 1392–1410.
- Yokohata, T., J. D. Annan, M. Collins, C. S. Jackson, M. Tobis, M. Webb, and J. C. Hargreaves, 2012: Reliability of multi-model and structurally different single-model ensembles. *Clim. Dyn.*, **39**, 599–616.
- Young, P. J., K. H. Rosenlof, S. Solomon, S. C. Sherwood, Q. Fu, and J.-F. Lamarque, 2012: Changes in stratospheric temperatures and their implications for changes in the Brewer Dobson circulation, 1979–2005. *J. Clim.*, **25**, 1759–1772.
- Yukimoto, S., et al., 2012: A new global climate model of the Meteorological Research Institute: MRI-CGCM3—Model description and basic performance. *J. Meteorol. Soc. Jpn.*, **90A**, 23–64.
- Zappa, G., L. C. Shaffrey, K. I. Hodges, P. G. Sansom, and D. B. Stephenson, 2013: A multi-model assessment of future projections of North Atlantic and European extratropical cyclones in the CMIP5 climate models. *J. Clim.*, doi:10.1175/JCLI-D-12-00573.1.
- Zelazowski, P., Y. Malhi, C. Huntingford, S. Sitch, and J. Fisher, 2011: Changes in the potential distribution of humid tropical forests on a warmer planet. *Philos. Trans. R. Soc. A*, **369**, 137–160.
- Zelinka, M., and D. Hartmann, 2010: Why is longwave cloud feedback positive? *J. Geophys. Res.*, **115**, D16117.
- Zelinka, M., S. Klein, and D. Hartmann, 2012: Computing and partitioning cloud feedbacks using Cloud property histograms. Part II: Attribution to changes in cloud amount, altitude, and optical depth. *J. Clim.*, **25**, 3736–3754.
- Zhang, M., and H. Song, 2006: Evidence of deceleration of atmospheric vertical overturning circulation over the tropical Pacific. *Geophys. Res. Lett.*, **33**, L12701.
- Zhang, M. H., and C. Bretherton, 2008: Mechanisms of low cloud-climate feedback in idealized single-column simulations with the Community Atmospheric Model, version 3 (CAM3). *J. Clim.*, **21**, 4859–4878.
- Zhang, R., 2010a: Northward intensification of anthropogenically forced changes in the Atlantic meridional overturning circulation (AMOC). *Geophys. Res. Lett.*, **37**, L24603.
- Zhang, T., 2005: Influence of the seasonal snow cover on the ground thermal regime: An overview. *Rev. Geophys.*, **43**, RG4002.
- Zhang, T., J. A. Heginbottom, R. G. Barry, and J. Brown, 2000: Further statistics on the distribution of permafrost and ground ice in the Northern Hemisphere 1. *Polar Geogr.*, **24**, 126–131.
- Zhang, X., 2010b: Sensitivity of Arctic summer sea ice coverage to global warming forcing: Towards reducing uncertainty in arctic climate change projections. *Tellus A*, **62**, 220–227.
- Zhang, X., and J. Walsh, 2006: Toward a seasonally ice-covered Arctic Ocean: Scenarios from the IPCC AR4 model simulations. *J. Clim.*, **19**, 1730–1747.
- Zhang, X. B., et al., 2007: Detection of human influence on twentieth-century precipitation trends. *Nature*, **448**, 461–U464.
- Zhou, L. M., R. E. Dickinson, P. Dirmeyer, A. Dai, and S. K. Min, 2009: Spatiotemporal patterns of changes in maximum and minimum temperatures in multi-model simulations. *Geophys. Res. Lett.*, **36**, L02702.

- Zhuang, Q., et al., 2004: Methane fluxes between terrestrial ecosystems and the atmosphere at northern high latitudes during the past century: A retrospective analysis with a process-based biogeochemistry model. *Global Biogeochem. Cycles*, **18**, GB3010.
- Zickfeld, K., V. K. Arora, and N. P. Gillett, 2012: Is the climate response to CO<sub>2</sub> emissions path dependent? *Geophys. Res. Lett.*, **39**, L05703.
- Zickfeld, K., B. Knopf, V. Petoukhov, and H. Schellnhuber, 2005: Is the Indian summer monsoon stable against global change? *Geophys. Res. Lett.*, **32**, L15707.
- Zickfeld, K., M. Eby, H. Matthews, and A. Weaver, 2009: Setting cumulative emissions targets to reduce the risk of dangerous climate change. *Proc. Natl. Acad. Sci. U.S.A.*, **106**, 16129–16134.
- Zickfeld, K., M. Morgan, D. Frame, and D. Keith, 2010: Expert judgments about transient climate response to alternative future trajectories of radiative forcing. *Proc. Natl. Acad. Sci. U.S.A.*, **107**, 12451–12456.
- Zickfeld, K., et al., 2013: Long-term climate change commitment and reversibility: An EMIC intercomparison. *J. Clim.*, doi:10.1175/JCLI-D-12-00584.1.
- Zimov, S., S. Davydov, G. Zimova, A. Davydova, E. Schuur, K. Dutta, and F. Chapin, 2006: Permafrost carbon: Stock and decomposability of a globally significant carbon pool. *Geophys. Res. Lett.*, **33**, L20502.
- Zunz, V., H. Goosse, and F. Massonnet, 2013: How does internal variability influence the ability of CMIP5 models to reproduce the recent trend in Southern Ocean sea ice extent? *Cryosphere*, **7**, 451–468.